Durham E-Theses

Some heavy doping effects in silicon

Saunderson, P.A.

How to cite:

Saunderson, P.A. (1983) *Some heavy doping effects in silicon*, Durham theses, Durham University. Available at Durham E-Theses Online: http://etheses.dur.ac.uk/7229/

SOME HEAVY DOPING EFFECTS IN SILICON.

by

P. A. Saunderson BSc. (Dunelm)

A thesis submitted for the degree of Doctor of Philosophy

in the University of Durham.

September 1983.

Thesis
1983/SAV

To my Wife

Joanna.

ACKNOWLEDGEMENTS

ABSTRACT

In this thesis the theoretical and experimental concentration and temperature dependent band gap narrowing in uncompensated n-type silicon is studied. Electron-electron and electron-impurity interaction energies are used to calculate the theoretical band gap narrowing in the plasmon-pole approximation. These reveal an increase of 14 meV in the band gap narrowing at 300 K for a donor concentration of 3.10^{19} cm^{-3} above the zero temperature value of 95 meV. For higher concentrations the degeneracy deepens and the zero and finite temperature band gap narrowing curves converge. Localized states in the band gap resulting from local fluctuations in the electron-impurity interaction, a result of the random position of the impurities, are also considered. When the analysis includes the effect on the host band of the electron-impurity interactions calculated above the resulting density of states in the band tail of uncompensated silicon is found to be ten times smaller than is usually imagined.

Using published values for the minority carrier mobility both the band gap narrowing and the minority carrier lifetime are experimentally determined in the buried n-type layer of an Integrated Injection Logic transistor. The transport factor in the base of a parasitic pnp transistor formed by the p-type substrate, buried layer and p-type Integrated Injection Logic transistors base region is calculated by monitoring the substrate current density and minority carrier injection into the buried layer. A range of temperatures from 200 K to 400 K are used to determine the temperature dependence of the minority carrier mobility in the buried layer (T^0). A band gap narrowing of (100 ± 15) meV and minority carrier lifetime of (30 ± 10) ns are measured for the buried layer ($2.4.10^{19}$ cm^{-3}).

LIST OF CONTENTS

LIST OF FIGURES

CHAPTER 1

1.0   INTRODUCTION.

Semiconductor bipolar devices depend for their operation on the minority carriers. The emitter efficiency of bipolar transistors is defined for example by the ratio of emitted majority current to the total emitter current that is formed by the sum of majority and minority currents at the emitter base junction (Sze 1981). This ratio is large when the minority current is small. To increase this ratio and hence also the common emitter current gain the device designer decreases the equilibrium minority carrier concentration in the emitter by increasing the emitter concentration whilst decreasing the base concentration and width. This thesis concentrates on the theoretical calculation and experimental measurement of the reduction in silicon's band gap caused by the presence of a large number of shallow level impurities. Minority carrier concentrations are significantly increased by such band gap narrowing, giving corresponding decreases in the emitter efficiency.

The band gap is by no means the only important parameter of interest to the device physicist. However by limiting the scope of the thesis it is possible to make a valuable contribution to one area of current interest (for recent reviews see Abram et al 1978 and Mertens 1981). The scope of the thesis is further limited to un-compensated n-type silicon which is easier to model conceptually since the impurities in the simplest model are all hydrogen like with a positive centre surrounded by an easily ionisable impurity electron. The theories developed here may be extended to cover a wider range of materials however this is beyond the scope of the present work. Most theoretical workers to date have

concentrated on the zero temperature limit for their calculations. In the present work however the principal results are extended to finite temperature so that a more informed value for the band gap narrowing of use to experimentalists is presented.

The following brief description of the changes of state that occur as increasing numbers of donor impurities are added to a semiconductor serves to introduce the most basic parameters used in this thesis. Appendix A contains numerical values for these and other parameters for silicon. At low concentrations (N_d < 10^{17} cm^{-3}) the shallow impurities are well separated in the bulk of the host semiconductor. The positive cores of the simple impurities considered form potential wells that allow the impurity electrons to occupy states in the band gap. These donor impurities have hydrogen like orbits modified by the semiconductor dielectric constant (ϵ_r=11.8) characterised by an effective Bohr radius (a_{eff}=1.91.10^{-7} cm) and effective Rydberg energy (R_{eff}=32 meV). At finite temperatures Boltzmann statistics are usually valid and the impurities are easily ionised. However as the donor concentration increases the Bohr orbitals begin to overlap. This results in the impurity levels splitting and eventually the formation of a band. As the concentration is increased this impurity band becomes more extensive and eventually merges with the host conduction band. The detailed structure of this impurity band is of interest in the concentration region close to this transition. One model for this impurity band of particular use in compensated semiconductors is named after Hubbard (1963, 1964). In the lower Hubbard band the localized impurity states are hydrogen like (H). In the upper Hubbard band the impurities would have two electrons (H$^-$). When the semiconductor is slightly compensated those impurity sites that lose electrons to the acceptors are available for impurity band conduction or hopping.

The presence of the impurity band changes the statistics required to analyse carrier concentrations. In the first place the Fermi level approaches the impurity energy. In the second place the semiconductor becomes degenerate and Fermi Dirac statistics have to be used. Heasell (1979) and Popovic (1979) have developed statistics where a partially ionised impurity band is considered. Indeed by choosing an appropriate degeneracy factor their model may effectively model . the effective band gap reduction in doped silicon up to 10^{19} cm^{-3}. However the calculations of this thesis show that there is a physical band gap reduction in heavily doped semiconductors.

At a sufficiently high concentration the impurity band becomes metal like and the impurity electrons are free to move throughout the semiconductor. A transition has then occurred from an insulating state ($N_d < 10^{18}$ cm^{-3}), at zero temperature, to a conducting or metal like state. The transition from metal to insulator is characterised by the Mott critical density (N_c). There are transitions in other parameters at the Mott critical density including the magnetic susceptibility, the zero temperature resistivity, the Hall coefficient and the specific heat capacity (Mott 1978, Mott 1974).

The Mott transition provides a lower bound to the validity of calculations in the chapters to follow. The Mott metal insulator transition may be investigated simply by considering first the metallic side of the transition. On this side of the transition the impurity electron wavefunctions are extended throughout space. This electron gas acts to screen any coulombic interactions in the semiconductor. A simple model for this electron screening used in metals is the Thomas Fermi screened potential characterised by the Thomas Fermi screening length

$(\lambda = 1/\kappa,$ Fistul 1969)

$$V(r) = \frac{e^2}{4\pi \epsilon \epsilon_r r} e^{-\kappa r} \qquad (100.01)$$

This may be used to give a qualitative description of the band structure in heavily doped silicon. The inverse Thomas Fermi screening length is then defined by (see Appendix A)

$$\kappa = 2 \left(\frac{3}{\pi}\right)^{1/6} \frac{M_c^{1/3}}{\sqrt{a_{eff}}} N_d^{1/6} = 8.2549.10^3 \, N_d^{1/6} \, cm^{-1} \qquad (100.02)$$

As the concentration of impurity centres is decreased so the screening length (λ) increases (see Fig 2.4, 7.2). At some point the screening becomes so small that orbitals bound to the positively charged impurity centres are possible characterised by the effective Bohr radius (a_{eff}).

Thus the ratio (a_{eff}/λ) provides a convenient measure of the extent of this localization. For example with $a_{eff}/\lambda = 2$ the exponential in Eq. 100.01 at $r=a_{eff}$ is 0.13 thus the potential (Eq. 100.01) is reduced to a tenth of the unscreened coulombic potential. If the ratio were any greater than this screening would be greater and bound states even less likely. Using Eq. 100.02 for the inverse screening length $(\lambda = 1/\kappa)$ the impurity concentration associated with this ratio is $4.10^{18} \, cm^{-3}$. The results of the more detailed calculations of Berggren et al (1979) for this Mott critical concentration N_c are presented in Fig 2.4.

The conduction and valence bands are also affected by the presence of the extra screening due to the impurity electrons. At a sufficiently high concentration the impurity band merges with the conduction band. It is this very high density regime that is of interest in this thesis. The study of the concentration region about the metal insulator transition (N_c) is left to other workers. Chapters 2 to 6 are concerned with the theoretical estimation of the change in the band gap due to the presence of

the impurities at zero temperature. In Chapter 7 these theories are extended to describe the change in the band gap at finite temperature. Chapter 8 deals with an experimental measurements of the transport parameters in heavily doped n-type silicon. Finally chapter 9 summarizes the most important results.

The change in the band structure of intrinsic silicon (introduced in chapter 2) due to the introduction of the impurities may be divided into two parts. That due to the extra electron-electron (ee) and that due to electron-impurity (ei) interactions. If the change in the conduction (valence) band bottom (top) is given by ΔE_c (ΔE_v) then the change in the band gap is given by

$$\Delta E_g(N_d) = \Delta E_c - \Delta E_v = \Delta E_c^{ee} + \Delta E_c^{ei} - \Delta E_v^{ee} - \Delta E_v^{ei} \quad (100.03)$$

The electron-electron contributions to the band gap reduction are dealt with in chapters 2 and 3. In chapters 4, 5 and 6 the electron-impurity interactions are considered.

The change in the band edges is determined from the change in the exchange or self energies (Σ). In chapter 2 the electron-electron self energy is derived. In this thesis the electron screening used to evaluate the self energy is derived in the plasmon pole approximation (derived in chapter 2). This is more accurate than the Thomas Fermi screened potential mentioned above which is only strictly valid at very high impurity concentrations where the electron wavefunctions are close to being plane waves.

The self energy describes the exchange energy of an electron in a particular band. For example in the conduction band it is made up of exchange energies between electrons in the same band (Σ^{ee}_{cc}) and exchange between the electrons in different bands (Σ^{ee}_{cv})

$$\Sigma_c^{ee} = \Sigma_{cc}^{ee} + \Sigma_{cv}^{ee} \qquad (100.04)$$

However as Inkson (1976) points out it is the change in the band energies that is of interest. This is derived from the difference between this self energy and that present in the intrinsic semiconductor (Σ^{int}_c). Thus the change in the conduction band energy is defined by

$$\Delta\Sigma_c^{ee} = \Sigma_{cc}^{ee} + \Sigma_{cv}^{ee} - \Sigma_{cc}^{int} - \Sigma_{cv}^{int} = \Sigma_{cc}^{ee} = \Delta E_c^{ee} \qquad (100.05)$$

In this thesis (chapter 3) as in work by other authors (Berggren and Sernelius 1981, Abram et al 1978) it is assumed that the exchange between electrons in the conduction and valence band is unchanged by the presence of the extra electrons in the conduction band. The intrinsic exchange of the conduction band electrons with themselves (Σ^{int}_{cc}) is clearly zero, since the intrinsic conduction band is calculated on a one electron model. A similar expression may be derived for the valence band

$$\Delta\Sigma_v^{ee} = \Sigma_{vc}^{ee} + \Sigma_{vv}^{ee} - \Sigma_{vc}^{int} - \Sigma_{vv}^{int} = \Sigma_{vv}^{ee} - \Sigma_{vv}^{int} = \Delta E_v^{ee} \qquad (100.06)$$

However in this case the intrinsic valence band has a self energy since it is full of electrons in contrast to the intrinsic conduction band. This Hartree Fock energy must be subtracted from the valence band contribution. Chapter 4 is concerned with the ensemble averaged electron-impurity self energy

$$\langle\Delta\Sigma_g^{ei}\rangle = \langle\Delta\Sigma_c^{ei}\rangle - \langle\Delta\Sigma_v^{ei}\rangle = \langle\Delta E_g^{ei}\rangle \qquad (100.07)$$

This shift in the band energies is due to the average impurity concentration. Local fluctuations in the impurity concentration are taken into account in chapter 5. These local fluctuations in the impurity concentration are responsible for a band tail forming on the host bands

density of states. Several approaches have been made to this problem in the past (Parameter (1955), Kane (1963), Halperin and Lax (1966), Lloyd and Best (1979), Samathiyakanit (1979)). In this thesis the most useful theories of Halperin and Lax and Lloyd Best are considered and improved. Both use the Thomas Fermi approximation to the electron screening.

The above chapters define the three major areas of interest in this thesis describing the electron-electron, the electron-impurity shifts in the band edges and finally the formation of localized states within the band gap resulting in a tail on the density of states. In chapter 6 an alternative approach to the electron-impurity problem is presented. Where the former chapters (4, 5) treat a random array of impurity centres superimposed on the host lattice, chapter 6 deals with a regular arrangement of impurities. However where in the former chapters an approximation to the electron screening is used, in chapter 6 the electron screening is determined self consistently using the calculated electron wavefunctions.

The final theory section, chapter 7, extends the most useful theories of chapter 2 to chapter 4 to finite temperature so that a comparison between the experimental results of chapter 8 and the theory is possible in chapter 9. In chapter 8 a novel use of the pnp parisitic transistor in an Integrated Injection Logic transistor provides the means of studying the transport parameters in the heavily n-type doped buried layer (the emitter of the Integrated Injection Logic device).

CHAPTER 2

GENERALIZED ELECTRON SELF ENERGY FOR SILICON.

2.0   INTRODUCTION.

Introduced in this chapter are expressions that will be used throughout the thesis.   A brief outline of the salient properties of silicon's conduction and valence bands is presented in section 2.1. Section 2.2 contains a derivation of the electron-electron self energy, taking the detailed nature of silicon's band structure into account.   In section 2.3 the Lindhard and plasmon pole approximations to the electron dielectric function are derived for silicon and the justification for the use of the plasmon pole approximation in this thesis is presented.   Finally in section 2.4 a brief summary of the results of this chapter are presented.

2.1   BAND STRUCTURE OF SILICON.

Crystalline silicon has a face centre cubic spatial lattice with a body centred cubic reciprocal lattice.   The well known (see for example Kittel 1976) shape of the first Brillouin zone is shown in Fig 2.1 with all the important symmetry labels.   Where in a free electron gas the electron wavefunctions would be given by plane waves, in silicon these wavefunctions may be expressed in terms of Bloch functions.   The relationship between energy and wavevector becomes more complicated than that of a free electron gas.   The resulting band diagrams for silicon in reduced zone, calculated by Herman et al 1967, are also drawn in Fig 2.1.
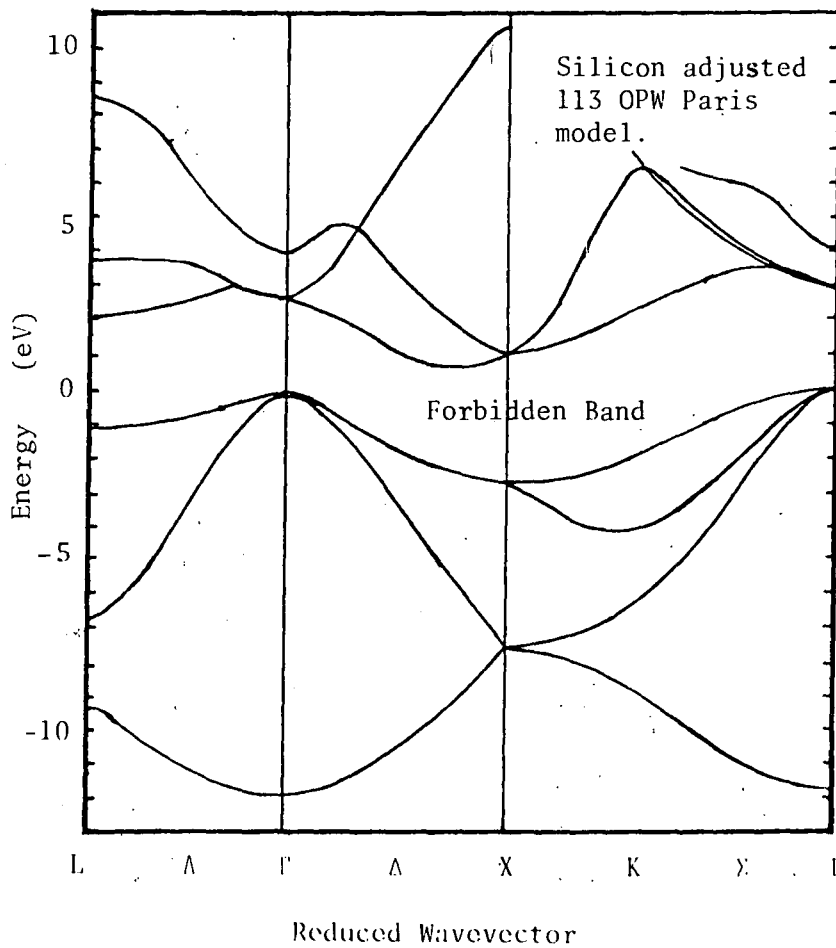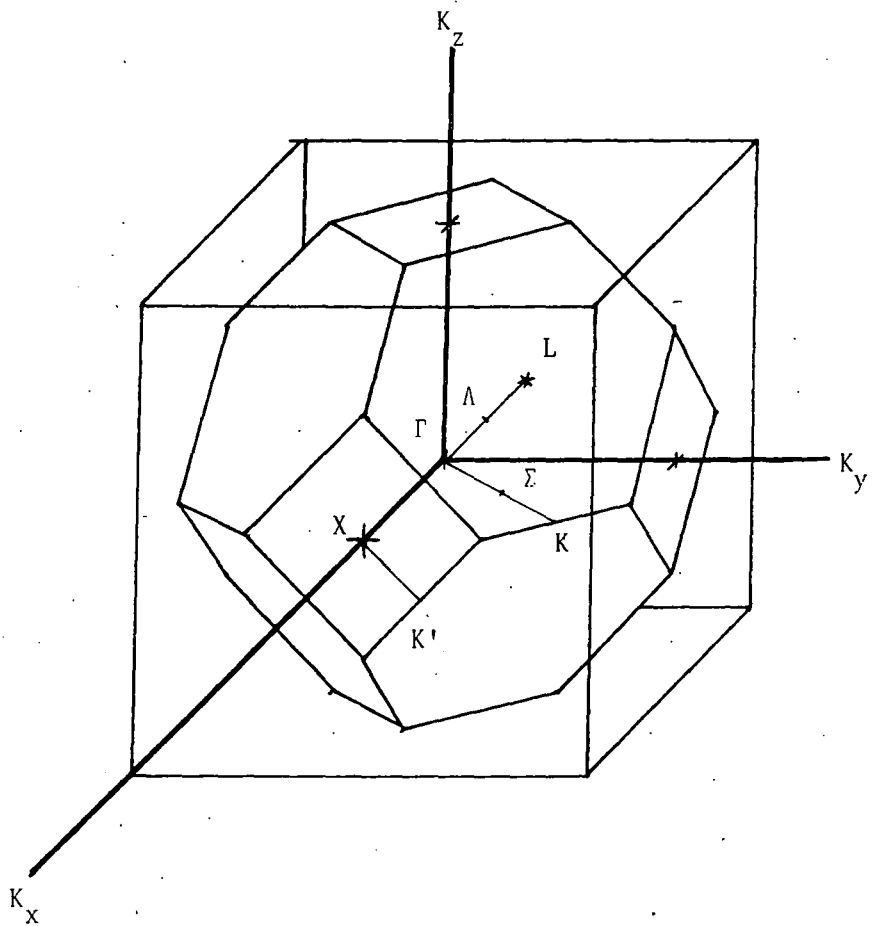
Fig 2.1.   First Brillouin Zone of silicon showing the principle points of symmetry, and the energy bands for silicon between those points. (Herman et al 1967)

From Fig 2.1 it is possible to see that the bottom of the conduction band forms about 75% of the way from the zone centre to the point X. There will then be six of these valleys, two each along the three axes k_x, k_y and k_z. Constant energy surfaces for these six valleys, shown in Fig 2.2, may be approximated for energies close to the band edge by ellipsoids characterized by a longitudinal mass m_l ($m_l = 0.98m_o$) and two equal transverse masses m_t ($m_t = 0.19m_o$, see Appendix A). Considering just one of these ellipsoids at k_i, a new set of axes (k') centred on that ellipsoid with the k'_x axis orientated longitudinally can be defined. The energy of that valley may be written

$$\epsilon_{ck}^{0} = E_c + (\hbar^2/2) \ (k'^2_x/m_l + (k'^2_y + k'^2_z)/m_t) \qquad (210.01)$$

$$k'^2 = (k_x - k_{ix})^2 + (k_y - k_{iy})^2 + (k_z - k_{iz})^2$$

where E_c is the conduction band energy. Frequently, for example when calculating the density of states, this approximation to silicon's conduction band is used, accounting for the six valleys by multiplying the answer for one valley by the number of valleys (M_c) at the end of the calculation.

Silicon's valence band has been found to be more complex than the conduction band (for a good summary see Blakemore 1962). It consists of three bands centred at the origin of the Brillouin zone, a schematic diagram of these three may be found in Fig 2.3 (a). The upper two bands (J=3/2) are known as the heavy and light hole bands and are degenerate at (000) whilst the lower (J=1/2) is separated from these by the spin-orbit interaction (see for example Kane 1982) and is known as the spin-split-off band. The situation is further complicated by the lack of isotropy of light and heavy hole bands (see Fig 2.3 (b)). Dresselhaus et al 1955 have developed an expression for the wavevector dependence of the holes in the
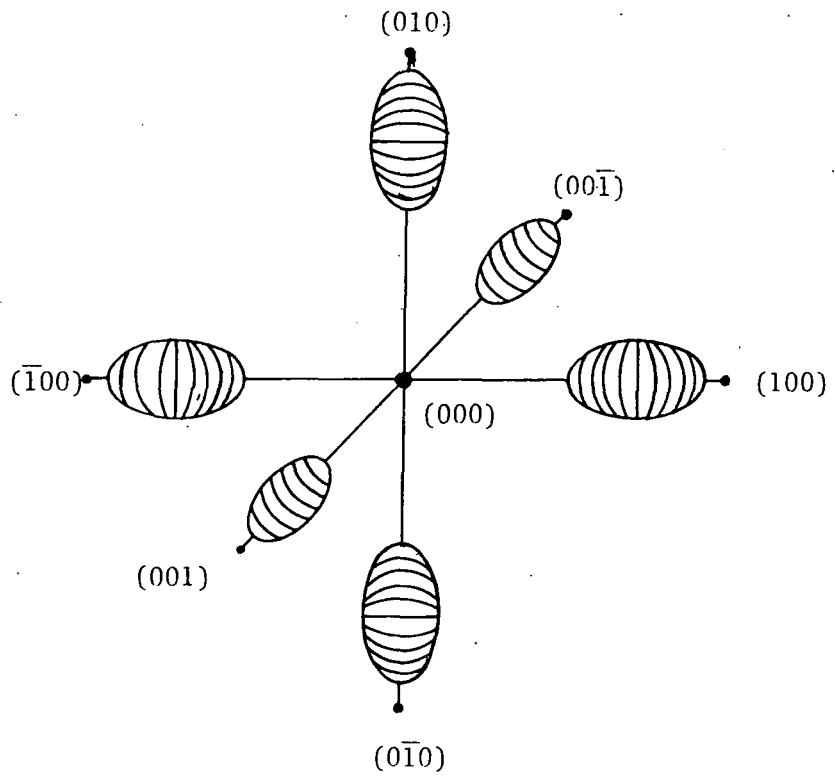
Fig 2.2   The surface of constant energy in k-space for
            an energy just above the bottom of the conduction
            band in silicon.

(a)

k^2 (atomic units) in [111]
direction.
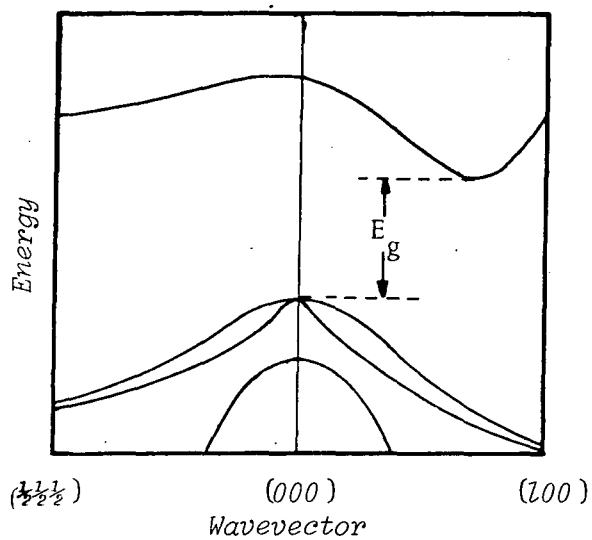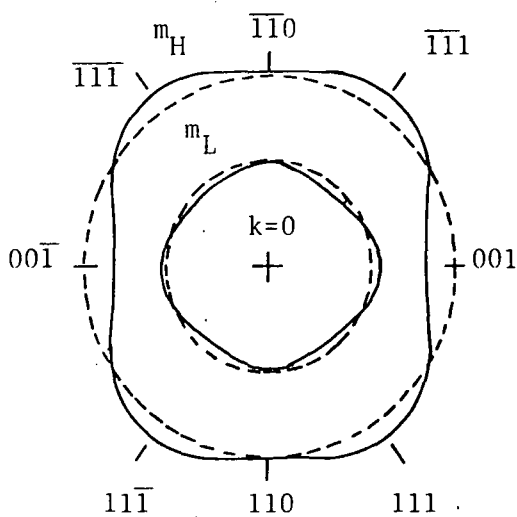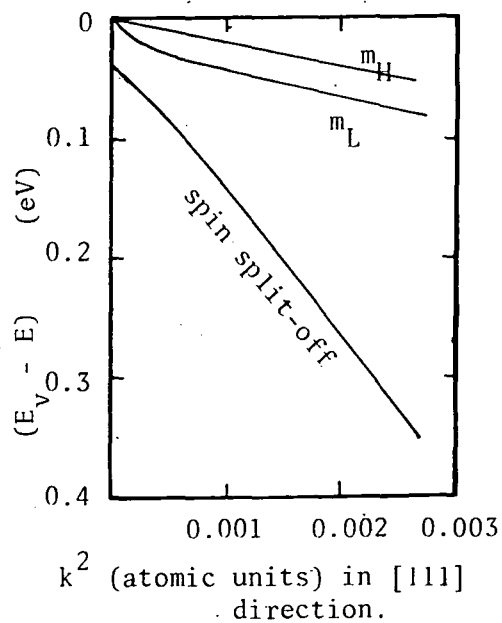
(b)   (c)

Fig 2.3   (a)   Schematic diagram of silicon's conduction and
                    valence bands.

            (b)   Contours of constant energy for the light and
                    heavy hole bands showing warping.   (Lax 1958)

            (c)   Showing the deviation from parabolicity of the
                    light, heavy and spin split-off bands.   (Kane 1956)

upper bands in terms of constants A, B and C

$$\epsilon_{vk}^0 = E_v - \frac{\hbar^2}{2m_o}(Ak^2 \pm (B^2k^4 + C^2(k_x^2k_y^2 + k_x^2k_z^2 + k_y^2k_z^2))^{1/2})$$

(210.02)

where E_v is the valence band edge and the plus sign refers to the light hole band and the minus sign to the heavy holes. Whilst the energy of the spin split off band may be expressed as

$$\epsilon_{vk}^0 = E_v - \Delta - \frac{A\hbar^2k^2}{2m_o}$$

(210.03)

where Δ for silicon is only 44 meV. Kane 1956 has shown that this small separation between upper and lower bands results in the light hole band becoming non-parabolic over a small region of k (see Fig 2.3 (c)) that for large k results in the two bands being characterized by the same mass $(0.5.m_0)$. However for simplicity the light and heavy hole bands may be approximated by parabolic isotropic bands with effective masses m_H and m_L ($m_H=0.5m_0$, $m_L=0.16m_0$, Appendix A). Indeed for the calculations in chapter 5 and 6 the situation is still further simplified by taking but one parabolic band with density of states effective mass given by

$$m_v = (m_L^{3/2} + m_H^{3/2})^{2/3} m_o = 0.55 \, m_o$$

(210.04)

The presence of the spin split off band is ignored in all of the following calculations to simplify an already complex situation. This is consistent with the above parabolic assumption since this also fails at about 50 meV below the bands edge. In p-type silicon the presence of impurity states close to the valence band (only 45 meV for boron in silicon) might be expected to be affected significantly by the spin split off band as is the light hole band. A full description of p-type heavily doped silicon would require the spin split off band to be included.

2.2 GENERALIZED ELECTRON SELF ENERGY IN HEAVILY DOPED SILICON.

The development of the self energy for semiconductor electrons has a strong similarity with those for a free electron gas (Hedin and Lundqvist 1969). For this reason the theory in this section is based on that for the free electron gas (see for example Fetter and Walecka 1971) whilst pointing out the major differences between this and our problem. In section 2.2.1 Dyson's equation is derived analytically for heavily doped silicon and a justification for the importance of the self energy is given. In section 2.2.2 this derivation is complemented by the use of Feynman diagrams. Finally in section 2.2.3 an expression for the self energy in terms of the Green's function and screened interaction is derived that will be used in later chapters of this thesis.

2.2.1   Dyson's Equation.

Motion of electrons between two positions (x and y) and times (t_1 and t_2) and may conveniently be described by there Green's functions $G(xt_1, yt_2)$, where the spin indices are omitted for simplicity. As might be expected this Green's function may be expanded as a series in terms of the unscattered or free particle propagator $G^0(xt_1, yt_2)$. The equation that generates this expansion is called Dyson's equation after F.J. Dyson (1949a, b).

$$G(x,y) = G^0(x,y) + \iint G^0(x,x_1) \, \Sigma(x_1,x_2) \, G(x_2,y) \, d^4x_1 d^4x_2$$

(221.01)

Where an abbreviation for xt_1 and yt_2 has been made. $\Sigma(xt_1, x_2t_2)$ is the irreducible or proper self energy of the particle, its approximate evaluation in subsequent sections will enable us to calculate the change in

energy of the bands due to the presence of many electrons in the conduction band.

When the electrons in the conduction band are considered to be smoothly spread throughout the whole of the heavily doped silicon Dyson's equation simplifies because the interaction is invariant under translations and the system is spatially uniform. As a first step in showing this more exactly the Fourier time transform of the Green's function is taken

$$G^0(xt_1, yt_2) = (1/2\pi) \int G^0(x,y,\omega) \, e^{i\omega(t_1 - t_2)} \, d\omega \qquad (221.02)$$

Then in analogy with the free electron derivation the wavevector (k) dependent Green's function for the unperturbed electron in the band n is defined

$$G^0(n;k,\omega) = \frac{1}{(\omega - \omega_{nk}^0 + i\delta\,sgn(\omega_{nk}^0 - \omega_f^0))} \qquad (221.03)$$

where ω_f is the Fermi angular frequency and the electrons are considered to fill the band up to this Fermi energy $(\hbar\omega_f)$. calculated as if there were no exchange energy

$$\hbar\omega_f = \frac{\hbar^2 k_f^2}{2m} \qquad (221.04a)$$

with Fermi wavevector in one valley given by (see Fig 2.4)

$$k_f = \left(\frac{3\pi^2 N_d}{M_c}\right)^{1/3} \qquad (221.04b)$$

Writing the spatial Green's function as and expansion of this in terms of the complete set of orthogonal functions $\phi_{nk}(x)$ that describe the unperturbed electrons of the band n (Hedin and Lundqvist 1969)

$$G^0(x,y,\omega) = \sum_{nk} \frac{\phi_{nk}(x)\,\phi^*_{nk}(y)}{(\omega - \omega_{nk}^0 + i\delta\,sgn(\omega_{nk}^0 - \omega_f^0))} \qquad (221.05)$$

where the wavevector k is confined to the first Brillouin zone of silicon
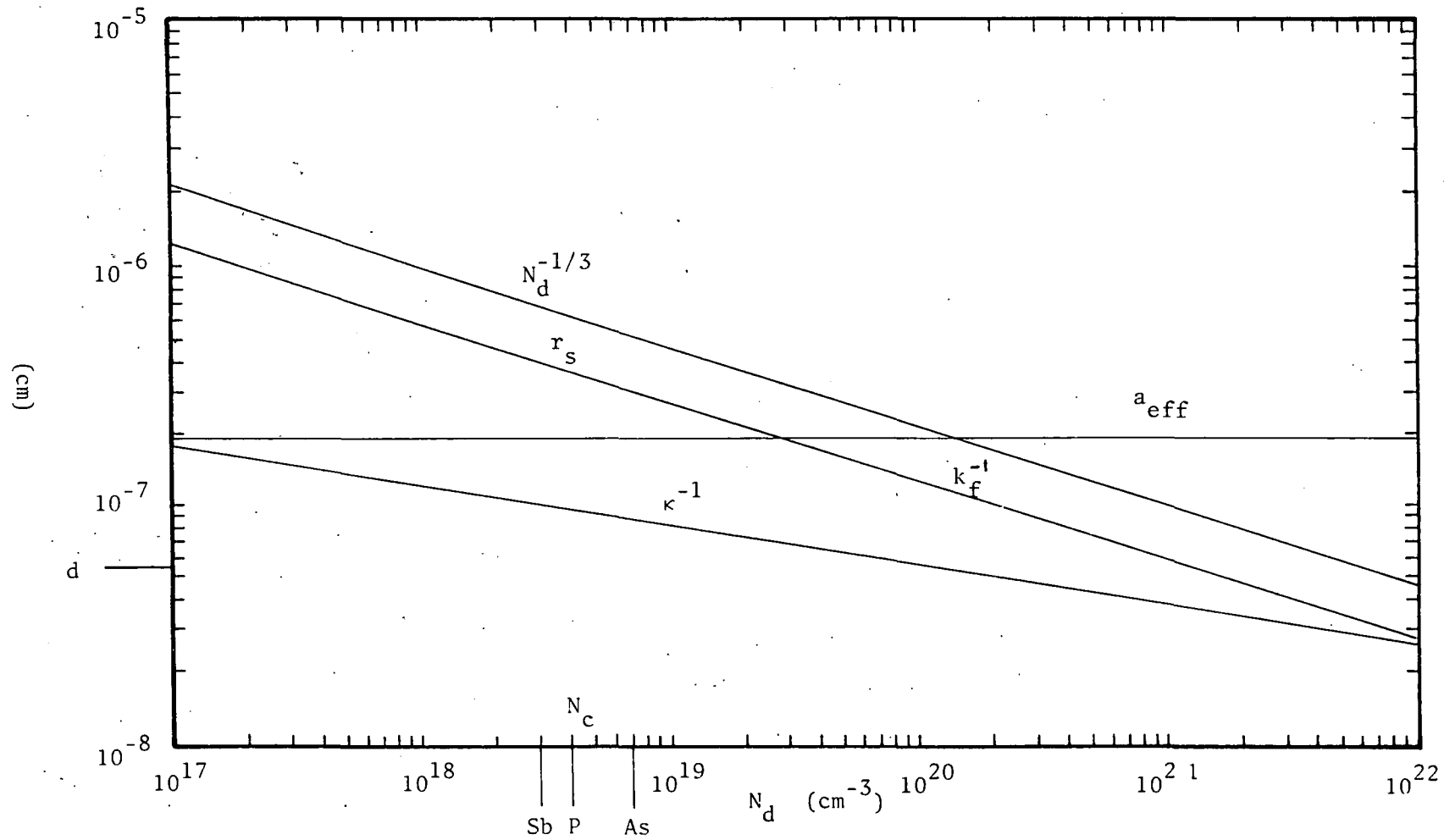
Fig 2.4   Thomas Fermi screening length (κ^{-1}), Fermi wavevector k_f^{-1}, $N_d^{-1/3}$, r_s and a_{eff} in silicon at 0K.

and the index n represents the band. As a small digression if the wavefunctions $\phi_{nk}(x)$ are replaced by the normalised plane waves

$$\phi_k(x) = 1/(2\pi)^{3/2} e^{ik \cdot x}$$

then the spacial Green's function reduces to the Fourier expansion of the wavevector Green's function used when dealing with a free electron gas.

When dealing with interactions between bands matrix elements like

$$G^0(n;k,m;q,\omega) = \iint \phi_{nk}^*(x) G^0(x,y,\omega) \phi_{mq}(y) \, d^3x \, d^3y \quad (221.06)$$

have to be solved where the Green's function (self energy) is expanded in terms of the wavefunctions of two different bands. When Eq. 221.05 is substituted for the Green's function $G^0(x,y,\omega)$ two similar overlap integrals, one in x the other in y, are found. These are evaluated over all space by invoking the orthogonality of the functions

$$I = \int \phi_{nk}^*(x) \, \phi_{mq}(x) \, d^3x = \delta_{n,m} \delta(k-q) \quad (221.07)$$

so that

$$G^0(n;k,m;q,\omega) = \sum_{n'q'} \delta_{n,n'} \delta(q'-k) \delta_{n',m} \delta(q-q') G^0(n';q',\omega)$$

$$(221.08)$$

$$G^0(n;k,m;q,\omega) = \frac{\delta_{n,m} \, \delta(k-q)}{(\omega - \omega_{nk}^0 + i\delta \text{sgn}(\omega_{nk}^0 - \omega_f^0))}$$

A similar process can be performed for the self energy with the result that Dyson's equation (Eq. 221.01) reduces to an algebraic equation in momentum space as in the free electron gas

$$G(n;k,\omega) = G^0(n;k,\omega) + G^0(n;k,\omega) \Sigma(n;k,\omega) G(n;k,\omega) \quad (221.09)$$

Whilst for the electron-electron calculations the above uniformity of the electron distribution is to a large extent a reality, for electron-impurity interactions the impurities certainly do not merge into a uniform positive continuum. However, as will be shown in the electron-impurity self energy chapter (chapter 4) an equivalent Dyson like equation for an ensemble averaged Green's function is obtained in that case also.

Having now derived an expression for the unperturbed Green's function in wavevector space (Eq. 221.08) Dyson's equation (Eq. 221.09) may be rewritten resulting in a straight forward expression for the total Green's function

$$G(n;k,\omega) = \frac{1}{(\omega - \omega_{nk}^0 - \Sigma(n;k,\omega) + i\delta sgn(\omega_{nk}^0 - \omega_f))} \qquad (221.10)$$

as with the free propagator the poles in this Green's function give us the energy of the particles represented by that function

$$\omega = \omega_{nk}^0 + Re(\Sigma(n;k,\omega)) = \epsilon_{nk}/\hbar \qquad (221.11)$$

The real part of the self energy Σ then gives the energy of the quasi particles represented by the total Green's function. It is this energy that is to be calculated in this thesis. The remainder of this chapter is devoted to finding an expression for the wavevector dependent self energy in Eq. 221.11.

The total Green's function has then the same form as the free particle propagator but represents a particle, called the quasi particle, with different energy and lifetime (Mattuck 1976, Fetter and Walecka 1971). Since the effective mass is give by the second derivative of the energy with respect to wavevector this change in the ϵ-k relationship results in an effective mass different from the intrinsic effective mass. Abram et al

(1978) calculate this mass explicitly and find that it is only the conduction band effective mass that is affected and then by only a few percent. This difference in the effective mass is ignored in what follows. It is clear that the total Green's function represents a new particle that has different mass and energy from the unperturbed electrons. This new particle is the result of groups of the electrons moving through the semiconductor in clusters. These clusters or quasi-particles, as they are often called, are continually gaining and losing members so that a lifetime may be ascribed to them. When k=0 the resulting expressions describe the particles at the band edge. The self energy then gives the shift of this band edge relative to its unperturbed position (Eq. 221.11) which then justifies our interest in calculations of the self energy. The remainder of this section will be devoted to finding an approximation for the self energy that is used in later chapters.

2.2.2   Feynman Diagram representation of Dyson's Equation.

An equivalent more lucid method of representing Dyson's equations is presented in this section. Working in k space and omitting the band indices for simplicity, an expression for the self energy is derived in terms of Feynman Diagrams. In section 2.2.3 the resulting expression for silicon is developed.

Dyson's equation for the total Green's function may be written (Mattuck 1976)

$$\text{[diagram]}\ k,\omega = \text{[diagram]}\ k,\omega + \text{[diagram }\Sigma\text{]} \qquad (222.01)$$
$$k,\omega$$

[diagram] k,ω represents the total Green's function $iG(k,\omega)$

[diagram] k,ω represents the free particle Green's function $iG^0(k,\omega)$

[diagram Σ] represents the irreducible self energy $\qquad -i\Sigma(k,\omega)$

Dyson's Equation may be expanded to several orders of approximation to give the total Green's function as series in the self energy

$$\text{[diagram]}^1 = \text{[diagram]} + \text{[diagram }\Sigma\text{]}$$

$$\text{[diagram]}^2 = \text{[diagram]} + \text{[diagram }\Sigma\text{]}_1 \qquad (222.02)$$

$$\text{[diagram]} = \text{[diagram]} + \text{[diagram]} + \text{[diagram]} + \text{[diagram]} + \text{[diagram]} +$$

The irreducible self energy is now defined as

$$\left(\Sigma\right) = \text{[diagram } k,\omega\text{]} + \text{[diagram } k,\omega\text{]} \qquad (222.03)$$

[diagram] k,ω represents the screened interaction that contains all

irreducible polarization parts $-iW_{eff}(k,\omega)$

[diagram]   represents the dressed or irreducible vertices

In common with other work (Hedin and Lundqvist 1969) the so called vertex corrections are omitted. Taking only the most divergent irreducible polarization parts, that corresponds to working in the Random Phase Approximation, and approximating the total Green's function by the free particle propagator the approximate self energy (here after just called the self energy) becomes

$$\left(\Sigma\right) = \text{[diagram RPA]} + \text{[diagram RPA]} \qquad (222.04)$$

where the approximate effective interaction (here after just called the screened potential) is given by the series

$$\text{[diagram RPA]} = \text{[diagram]} + \text{[diagram]} + \text{[diagram]} + \text{[diagram]} + .. (222.05)$$

[diagram]   represents the unscreened interaction $-iW^0(q)$.

The first term in the self energy (Eq. 222.04) is just the average electron-electron interaction that cancels with the average

electron-impurity interaction as will be discussed in more detail in chapter 4

$$0 \quad = \quad \text{\large\(\bigcirc\)} \quad + \quad \text{\large X} \quad (222.06)$$

The second term on the right hand side of Eq. 222.04 may be reduced to functional form using the appropriate rules (see for example Mattuck 1967, Mahan 1981, Fetter and Walecka 1971)

$$i\Sigma(k,\omega) = 1/(2\pi)^4 \int i G^0(k-q,\omega-\nu)(-i W_{eff}(q,\nu)) d^3 q d\nu \quad (222.07)$$

where the summation over spin states ($m_s = \pm 1/2$) has been included.

2.2.3   Derivation of the self energy in heavily doped silicon.

The self energy for heavily doped silicon may be derived by returning to the implicit spacial form of Eq. 222.07

$$\Sigma(x,y,\omega) = - i/2\pi \int G^0(x,y,\omega-\nu) \, W_{eff}(x,y,\nu) \, d\nu \quad (223.01)$$

This reduces to the former expression when the Fourier transforms of both sides are taken.   To achieve and expression for the self energy to substitute into Eq. 221.11 for the quasi particle energy in heavily doped silicon the Green's function and self energy must be expanded in terms of the complete set of orthogonal functions $\phi_{nk}(x)$ that describe the unperturbed electrons in the nth band with k the wavevector restricted to the first Brillouin zone.   The wavevector self energy is then written

$$\Sigma(n;k,\omega) = \iint \phi_{nk}^*(x) \, \Sigma(x,y,\omega) \, \phi_{nk}(y) \, d^3x d^3y \quad (223.02)$$

whilst the unperturbed Green's function (from Eq. 221.03 and Eq. 221.05)

may be written as

$$G^0(x,y,\omega-\nu) = \sum_{mq} \phi_{mq}(x) G^0(m;q,\omega-\nu) \phi_{mq}^*(y) \qquad (223.03)$$

On substituting for $\Sigma(x,y,\omega)$ from Eq. 223.01 and $G^0(x,y,\omega-\nu)$ from Eq. 223.03 the wavevector dependent self energy Eq. 223.02 becomes

$$\Sigma(n;k,\omega) = 1/2\pi \sum_m \iint W(nk,mq,\nu) G^0(m;q,\omega-\nu) \, d\nu d^3q \qquad (223.04)$$

where the interaction matrix is given by

$$W(n;k,m;q,\nu) = \iint \phi_{nk}^*(x) \phi_{mq}^*(y) W_{eff}(x,y,\nu) \phi_{mq}(x) \phi_{nk}(y) d^3x d^3y$$
$$(223.05)$$

The above integral may be solved by taking the Fourier transform for the potential

$$W_{eff}(x,y,\nu) = 1/(2\pi)^3 \int W_{eff}(1,\nu) e^{il\cdot(x-y)} d^3l \qquad (223.06)$$

on substitution into Eq. 223.05 this gives

$$W(n;k,m;q,\nu) = 1/(2\pi)^3 \int I^* I \, W_{eff}(1,\nu) \, d^3l \qquad (223.07a)$$

where the overlap integrals, one in x the other in y, are given by

$$I = \int \phi_{nk}^*(x) e^{il\cdot x} \phi_{mq}(x) \, d^3x \qquad (223.07b)$$

where n and m are the band indices. These overlap integrals are now calculated explicitly for the valence and conduction bands:

a)   The conduction band overlap integral.

To evaluate the overlap integral for the conduction band (n=c) the unperturbed wavefunctions are expanded in terms of their associated Bloch function $u_{nk}(x)$

$$\phi_{nk}(x) = u_{nk}(x) \ e^{ikx} \qquad\qquad (223.08)$$

where the u_{nk} only vary slowly with k.   Expanding the periodic u's in a Fourier series in the reciprocal lattice vector g

$$u_{nk}^{*}(x) u_{mq}(x) = \sum_{g} c_{g} \ e^{igx} \qquad\qquad (223.09a)$$

where

$$c_{g} = 1/(2\pi)^{3} \int u_{nk}^{*}(x) u_{mq}(x) \ e^{-igx} \ d^{3}x \qquad\qquad (223.09b)$$

so that the overlap integral (Eq. 233.07b) becomes

$$I = \sum_{g} \delta(q-k+1+g) \int u_{nk}^{*}(x) u_{mq}(x) \ e^{-igx} \ d^{3}x \qquad (223.10a)$$

Since the wavevectors q, k and l are only defined within the first Brillouin zone and only extend over a small volume in reciprocal space only the first zone need be considered

$$I = \delta(q-k+1) \int u_{nk}^{*}(x) u_{mq}(x) \ d^{3}x \qquad\qquad (223.10b)$$

The Bloch integral may then be written

$$I^{*}I = \delta(q-k+1) \ \delta_{nm} \qquad\qquad (223.10c)$$

where the coupling between conduction and valence bands has been ignored. This coupling is dealt with in more detail in section 3.1.

b)   The valence band overlap integral.

When considering the valence band the coupling between the heavy (n=H) and light (n=L) hole bands (J=3/2) is included. However the spin split off band (J=1/2) is ignored (see section 2.1 for justification). Rather than choosing the simple Bloch functions of the previous section Combescot and Nozieres (1972) expand the wavefunctions ϕ in terms of the complete set of orthonormal functions used by Luttinger and Kohn (1955)

$$\phi_{k\nu}(x) = \sum_{\alpha} C_{\nu\alpha}(k) \, u_{o\alpha}(x) \, e^{ik\cdot x} \qquad (223.11)$$

where the C's are constants and the spin index α is only allowed to scan through the heavy and light hole bands (ie $m_J = \pm 3/2, \pm 1/2$). The wavefunction are then constructed from the k=0 unperturbed Bloch function $u_{o\alpha}$. The overlap integral (Eq. 223.07) may now be rewritten in terms of these basis functions

$$I = \int \sum_{\alpha} C_{\nu\alpha}^{*}(k) u_{o\alpha}^{*}(x) e^{-ik\cdot x} e^{il\cdot x} \sum_{\alpha'} C_{\nu'\alpha'}(q) u_{o\alpha'}(x) e^{-iq\cdot x} \, d^3x \qquad (223.12a)$$

where the bands have been specified by their total orbital angular momentum quantum numbers (m_J) denoted by ν and ν', rather than the band indices used previously (Eq. 223.7 n and m). Invoking the orthogonality of the k=0 Bloch functions the valence band overlap integral becomes

$$I = \sum_{\alpha} C_{\nu\alpha}^{*}(k) \, C_{\nu'\alpha}(q) \int e^{-i(k-q-1)\cdot x} \, d^3x \qquad (223.12b)$$

and performing the integration over all space

$$I = \delta(k-q-1) \sum_{\alpha} C_{\nu\alpha}^{*}(k) \, C_{\nu'\alpha}(q) \qquad (223.12c)$$

In this special case where the summation over m is restricted to just the heavy and light hole bands Combescot and Nozieres showed that

the constants, $C_{\nu\alpha}(k)$, were just the elements of the rotation matrix that rotates the function in the J=3/2 representation bringing k in line with the z axis (see also Bir and Pikus 1974, pp 255). Thus if the function Ψ_{Jm} (J = 3/2, m = m_{Jz} = ±3/2, or ±1/2) describes an eigenstate in the coordinate system x,y,z and the function $\Psi_{Jm'}$, the same eigenstate but in the different coordinate system x',y',z' obtained by rotating about the origin, with m'=$m_{Jz'}$ then the rotation matrix $d^J_{m'm}$ relates these two functions

$$\Psi_{Jm} = \sum_{m'} e^{im'\gamma} d^J_{m'm}(\beta) \; e^{im\alpha} \quad \Psi_{Jm'} \qquad (223.13a)$$

where the Euler angles α, β and γ define the rotation between the two coordinate systems (see for example Arfken 1970 pp 220). The rotation matrix in the J=3/2 representation is given by (see for example Edmonds 1957)

$$d^{3/2}_{m'm}(\beta) = \begin{matrix} & m' \setminus \ ^m \\ \end{matrix} \begin{pmatrix} d_1 & d_2 & -d_3 & -d_4 \\ -d_2 & d_5 & d_6 & -d_3 \\ -d_3 & -d_6 & d_5 & d_2 \\ d_4 & -d_3 & -d_2 & d_1 \end{pmatrix} \qquad (223.13b)$$

with the six constant given by

$$d_1 = 1/4 \; (\cos 3\beta/2 + 3\cos\beta/2)$$

$$d_2 = \sqrt{3}/4 \; (\sin 3\beta/2 + \sin\beta/2)$$

$$d_3 = \sqrt{3}/4 \; (\cos 3\beta/2 - \cos\beta/2)$$

$$d_4 = 1/4 \; (\sin 3\beta/2 - 3\sin\beta/2)$$

$$d_5 = 1/4 \; (3\cos 3\beta/2 + \cos\beta/2)$$

$$d_6 = 1/4 \; (3\sin 3\beta/2 - \sin\beta/2)$$

$$(223.13c)$$

In particular choosing k parallel to the z axis so that

$$C_{\nu\alpha}(k) = d_{\nu\alpha}^{3/2}(0) = \delta_{\nu\alpha} \qquad (223.14)$$

the constants $C_{\nu'\nu}(q)$ are defined by the angle (θ) between the z axis, (or k) and q

$$C_{\nu\nu'}(q) = d_{\nu\nu'}^{3/2}(\theta) \qquad (223.15)$$

The overlap integral (Eq. 223.12c) may then be rewritten

$$I = d_{\nu'\nu}^{3/2}(\theta) \; \delta(k-q-1) \qquad (223.16)$$

But in Eq. 223.04 the summation is over just two bands, either the light hole band (m=L) of the heavy hole band (m=H). Thus to be consistent with Eq. 223.04 a partial summation over the various spin angular momenta ν' associated with the band m must be performed. Since the square of the overlap integral is required (as shown in Eq. 223.07a) it is convenient to define the function Λ used by Combescot and Nozieres (1972), Rice (1977), Berggren and Sernelius (1981)

$$\Lambda_{HH} = \Lambda_{LL} = d_{3/2,3/2}(\theta)d_{3/2,3/2}(\theta)$$
$$+ d_{-3/2,3/2}(\theta)d_{-3/2,3/2}(\theta) \qquad (223.17a)$$

that is interpreted using Eq. 223.13

$$d_1^* d_1 + d_4^* d_4 = d_5 d_5 + d_6 d_6 = 1/4 \; (1 + 3\cos^2\theta) \qquad (223.17b)$$

and

$$\Lambda_{HL} = \Lambda_{LH} = d_{3/2,1/2}(\theta)d_{3/2,1/2}(\theta)$$
$$+ d_{-3/2,1/2}(\theta)d_{-3/2,1/2}(\theta) \qquad (223.17c)$$

given by

$$d_2^* d_2 + d_3^* d_3 = 3/4 \; \sin^2\theta \qquad (223.17d)$$

Notice also that if there were no coupling potential ($I = 0$) the overlap integral (Eq. 223.12c) becomes

$$\int \phi_{nk}^{*}(x) \, \phi_{mq}(x) \, d^3x = \delta(q-k) \sum_{\alpha} d_{\nu\alpha}(0) d_{\nu \cdot \alpha}(0) = \delta(q-k) \delta_{nm}$$

a trivial result used in deriving the wavevector Dyson's equation Eq. 221.09, that shows that the ϕ are indeed orthogonal.

Returning now to the evaluation of the self energy (Eq. 223.04) the overlap integrals for the conduction (Eq. 223.10) and valence bands (Eq. 223.17) have just been calculated. These have to be substituted into Eq. 223.07a and Eq. 223.04. For completeness the definition of Λ is extended to include the conduction band overlap integral

$$I^{*}I = \delta(q-k+l) \, \Lambda_{nm} \qquad\qquad (223.18)$$

$\Lambda_{nm} = \delta_{nm}$ n and m belonging to conduction band

$\qquad\quad \delta_{nm}$ n belonging to conduction band, m belonging to valence band or visa versa (see section 3.1)

$\qquad\quad 1/4 \ (1 + 3\cos^2\theta)$ n and m belonging to the same valence band

$\qquad\quad 3/4 \ \sin^2\theta$ n and m belonging to different valence bands

With the aid of this function the self energy (Eq. 223.04) is written using the interaction (Eq. 223.07) as

$$\Sigma(n;k,\omega) = i/(2\pi)^4 \sum_{m} \iint \Lambda_{nm} \, W_{eff}(q,\nu) \, G^0(m;k-q,\omega-\nu) \, d\nu d^3q$$

$$\Sigma(n;k,\omega) = \frac{i}{(2\pi)^4} \sum_{m} \iint \frac{e^{i\eta(\omega-\nu)}}{(\omega-\nu - \omega_{m(k-q)}^0 + i\delta sgn(\omega_{m(k-q)} - \omega_f))} \Lambda_{nm} W_{eff}(q,\omega) \, d^3q d\nu \qquad (223.19)$$

Where the unperturbed Green's function contains an exponential convergence factor with infinitesimal η. The essential difference between this and the equivalent free electron-gas expression is the inclusion of the vertex function (Λ_{nm}) to describe the coupling between the bands (n,m). In a more

exact calculation these overlap integrals would have to be calculated numerically between all the semiconductor bands. For the present calculations the above expression is used. In the next section an expression for the screened interaction $W_{eff}(q,\omega)$ is derived to complete the expressions needed to calculate the self energy used to predict the change in the band energy (Eq. 221.11).

2.3   COULOMBIC POTENTIAL SCREENED BY CONDUCTION BAND ELECTRONS.

To complete the derivation of a useful expression for the self energy (Eq. 223.19) in heavily doped silicon, the effective interaction $(W_{eff}(q,\omega))$ has to be evaluated. This represents the screening of the impurity potential due to the presence of all the extra carriers in the conduction band of the heavily doped silicon as outlined in section 2.2.2. Only the conduction band electrons need be considered since the valence band will have no extra carriers. Whilst deriving the expressions for the conduction band the inter-valley scattering that has been found to play an important part at high concentrations in an ordered lattice of impurities (Selloni and Pantelides 1982) is ignored. The six conduction band ellipsoidal energy surfaces are then considered to be independent. When considering a p-type semiconductor the corresponding expressions would contain the extra complications of the valence band. The calculation of this screened potential is performed in section 2.3.1 in the Random Phase approximation as outlined in section 2.2.2. In section 2.3.2 the resulting Lindhard Dielectric function is approximated in the plasmon pole approximation used throughout this thesis. In section 2.3.3 a brief comparison of the inverse Lindhard and plasmon pole approximations is made that indicates the power of the plasmon pole approximation.

2.3.1   <u>Derivation of the Lindhard dielectric function in silicon.</u>

As can be seen from the diagrams in Eq. 222.05 the screened potential is just a geometric progression and may be summed to infinite order.

$$\text{RPA} = \frac{\overbrace{}}{1 - \bigotimes}$$

$$= \frac{-iW^0(q)}{1 + W^0(q)\,\pi^0(q,\omega)} = -iW_{RPA}(q,\omega) \qquad (231.01)$$

where the ring diagram

$$q+k,\omega+\nu \quad \bigobot \quad k,\nu$$

is represented by $-i\pi^0(q,\omega)$ where the 0 superscript indicates that the polarization insert has been taken to zeroth order. The effective electron dielectric function $\epsilon(k,\omega)$ is defined by the expression

$$W_{RPA}(q,\omega) = W^0(q) \ / \ (1 + W^0(q)\ \pi^0(q,\omega)) = W^0(q)\ /\ \epsilon(q,\omega)$$
$$(231.02)$$

All that remains is to evaluate the polarization insertion $\pi^0(q,\omega)$,   for this the ring diagram is expanded in its functional form (Mahan 1981, Fetter and Walecka (1971), Mattuck (1976)). The sum over spins ($m_s = \pm 1/2$) is also performed giving

$$-i\pi^0(q,\omega) = (2s+1)(-1)\ \hbar^{-1}\ (2\pi)^{-4}\ \iint iG^0(k,\nu)$$

$$iG^0(k+q,\omega+\nu)\ d^3k d\nu \qquad (231.03)$$

On substituting for the two Green's functions from Eq. 221.03 this gives

$$-i\pi^0(q,\omega) = \frac{-2}{(2\pi)^4\hbar}\ \iint \frac{i}{(\nu - \omega_k^0 + i\delta\,\text{sgn}(k-k_f))}$$

$$(231.04)$$

$$\frac{i}{(\omega + \nu - \omega_{k+q}^0 \pm i\delta\,\text{sgn}(|k+q|-k_f))}\ d^3k d\nu$$

The integrals are perform in two parts, first the frequency integral, then the wavevector integral.

a) Frequency integral.

The integral over the angular frequency ν may be carried out by complex integration taking the integral over a semicircular contour in the upper half plane (see Fig 2.5). The integrand is divided into four parts defined by the relative sizes of k, $k+q$, and k_f using the step function $\theta(x)$. Only two of these have poles above the real axis, they occur when angular frequency ν is given by

$$\nu = \omega_k^0 + i\delta \qquad \text{and} \qquad \nu = \omega_{k+q}^0 - \omega + i\delta$$

when $k > k_f$ and $|k+q| > k_f$ the poles are both below the real axis at

$$\nu = \omega_k^0 - i\delta \qquad \text{and} \qquad \nu = \omega_{k+q}^0 - \omega - i\delta$$

they do not contribute to the integral. The integrand of Eq. 231.04 has then a residue of

$$\frac{\theta(k_f-k)\,\theta(|k+q|-k_f)}{(\omega + (\omega_k^0 + i\delta) - \omega_{k+q}^0 + i\delta)} + \frac{\theta(k-k_f)\,\theta(k_f-|k+q|)}{((\omega_{k+q}^0 - \omega + i\delta) - \omega_k^0 + i\delta)}$$

which may be re-written, by changing the variable from k to $-(k+q)$ in the second term so that

$$-i\pi^0(q,\omega) = \frac{2i}{(2\pi)^3 \hbar} \int \theta(k_f-k)\,\theta(|k+q|-k_f)\left(\frac{1}{(\omega+\omega_k^0-\omega_{k+q}^0+i\delta)}\right.$$

$$\left. - \frac{1}{(\omega-\omega_k^0+\omega_{k+q}^0-i\delta)}\right)\, d^3k \qquad (231.05)$$
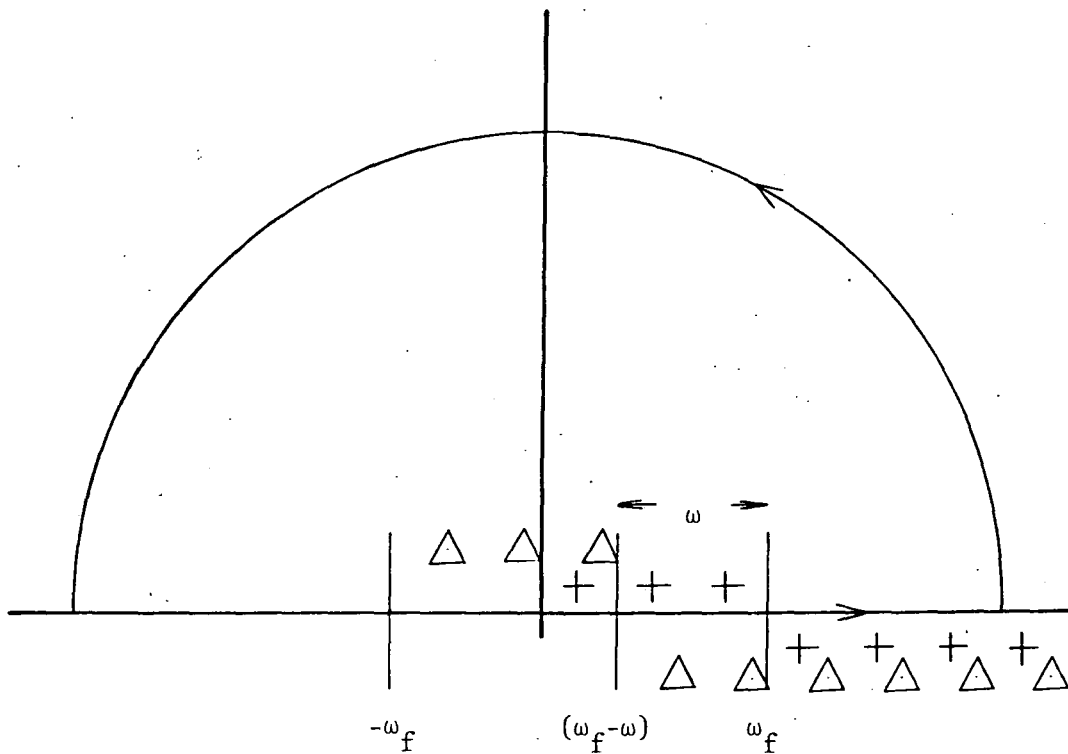
△   poles in the Green's function $G^0(k+q,\omega+\nu)$

+   poles in the Green's function $G^0(k,\nu)$

Fig 2.5   Poles in the Green's function defining the electron dielectric function in the complex angular frequency (ν) plane.

b)   Conduction band wavevector integral for silicon.

To perform the wavevector integral in silicon's non-spherical conduction band the usual substitution for k and q have to be made (section 2.1). Having calculated the polarization for one valley the result is multiplied by the number of valleys (M_c) to find the polarization due to electrons in all the valleys.

The substitution for k and q is

$$k_x'^2 = k_x^2 \, m_{de}/m_l \; ; \; k_y'^2 = k_y^2 \, m_{de}/m_t \; ; \; k_z'^2 = k_z^2 \, m_{de}/m_t$$

(231.06a)

where the density of states effective mass for one valley is given by

$$m_{de} = (m_l m_t^2)^{1/3}$$

(231.06b)

It is justified to make a similar substitution for q since the polarisation $\pi^0(q,\omega)$ is to be integrated over the conduction band states with respect to q in the self energy expressions (Eq. 223.19). The integrals now have the same form as those for a semiconductor with a spherical constant energy surface with mass equal to the density of states effective mass. Dropping the primes and letting

$$\omega_{k+q}^0 - \omega_k^0 = \hbar/2m_{de} \; (|k+q|^2 - k^2)$$
$$= \hbar/2m_{de} \; (2kq\cos\theta + q^2)$$

(231.06c)

and

$$a = q(\epsilon_q - \hbar\omega)/\epsilon_q \quad \text{and} \quad b = q(\epsilon_q + \hbar\omega)/\epsilon_q$$

(231.06d)

where $\epsilon_q = \hbar^2 q^2/2m_{de}$

and θ is the angle between the vectors k and q. The polarization of the

conduction band electron gas becomes

$$\pi^0(q,\omega) = \frac{-2qM_c}{(2\pi)^3 \epsilon_q} \int_0^\infty \int_0^\pi \theta(k_f - k)\,\theta(|k+q| - k_f)\left(\frac{1}{(-a - 2k\cos\theta + i\delta)}\right.$$

$$\left. - \frac{1}{(b + 2k\cos\theta - i\delta)}\right) 2\pi k^2 \sin\theta\, d\theta\, dk \qquad (231.07)$$

where to get the total polarization of conduction band electrons the result for one valley has been multiplied the number of equivalent conduction band valleys (M_c). The real part of this integral gives (Fetter and Walecka 1971)

$$Re(\pi^0(q,\omega)) = \frac{2m_{de}k_f M_c}{(2\pi)^2 \hbar^2}\left\{ 1 + \frac{k_f}{2q}\left[f\left(\frac{k_f(\epsilon_q - \hbar\omega)}{\epsilon_f q}\right)\right.\right.$$

$$\left.\left. + f\left(\frac{k_f(\epsilon_q + \hbar\omega)}{\epsilon_f q}\right) \right]\right\} \qquad (231.08a)$$

where $f(x) = (1 - x^2/4)\ln\left|\frac{(x+2)}{(x-2)}\right|$

Whilst the imaginary part is given by

$$Im(\pi^0(q,\omega)) = \begin{cases} (M_c q/8\pi)(2m_{de}/\hbar^2)(k_f/q)^2(1 - a^2/4) & \text{I} \\ (M_c q/8\pi)(2m_{de}/\hbar^2)(\hbar\omega/\epsilon_q) & \text{II} \\ 0 & \text{III IV} \end{cases}$$

$$(231.08b)$$

with the four regions, shown in Fig 2.6, bounded by the following lines

I $\quad \hbar\omega = 2\epsilon_f q/k_f - \epsilon_q$ and the q axis

II $\quad \hbar\omega = \epsilon_q - 2\epsilon_f q/k_f, \quad \hbar\omega = \epsilon_q + 2\epsilon_f q/k_f$ and $\hbar\omega = 2\epsilon_f q/k_f - \epsilon_q$

III $\quad \hbar\omega = \epsilon_q + 2\epsilon_f q/k_f$ and the ω axis

IV $\quad \hbar\omega = \epsilon_q - 2\epsilon_f q/k_f$ and the q axis
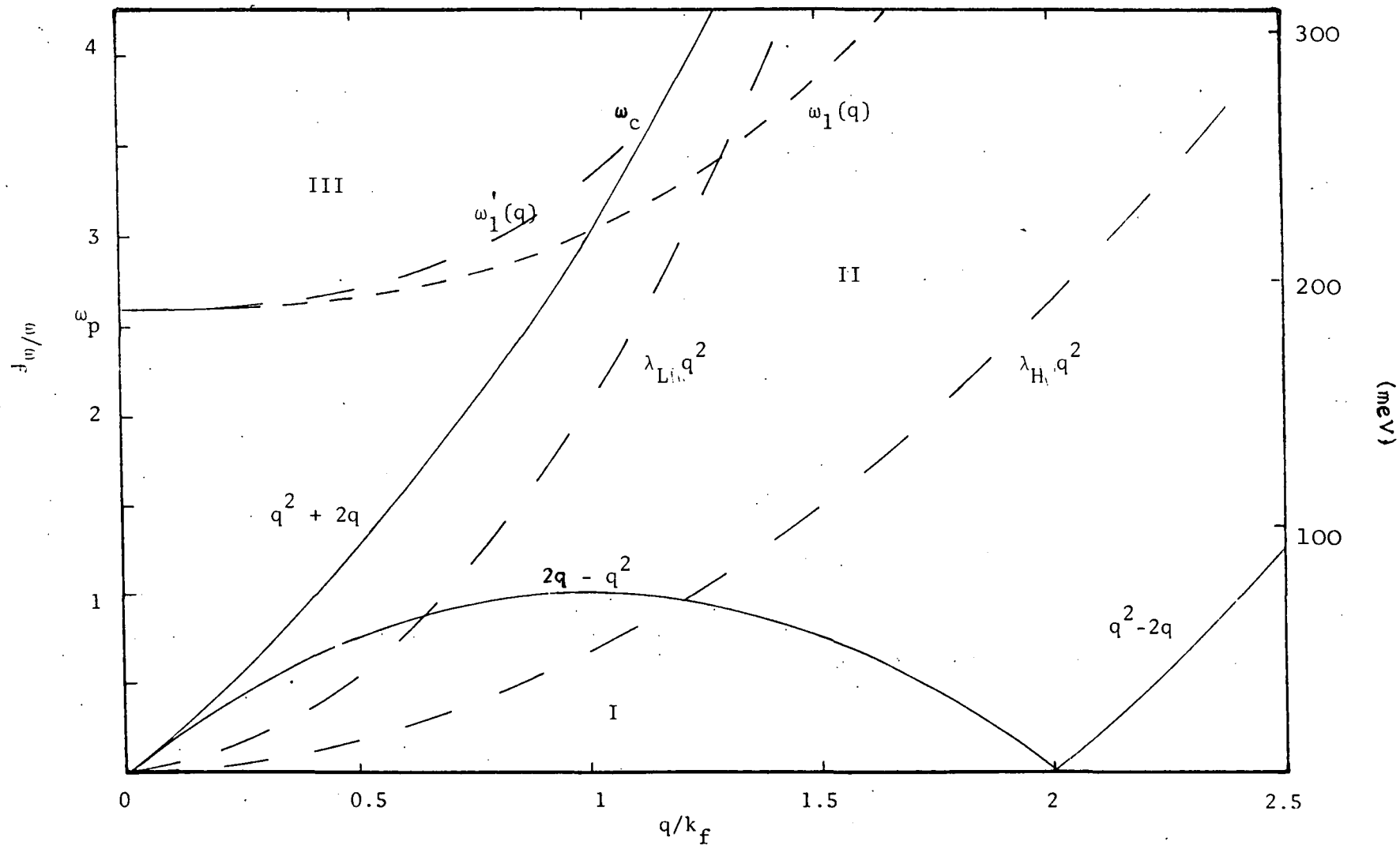
Fig 2.6   Plasmon dispersion curve $(\omega_1'(q))$ and the model used in this thesis $(\omega_1(q))$ for an electron concentration of 10^{20} cm^{-3}. Also shown is the intersection of the light band ($\lambda_L q^2$) with the plasmon dispersion curve $(\omega_1(q))$ above the critical frequency (ω_c).

The real and imaginary parts of this polarization may be combined to give

$$\pi^0(q,\omega) = \frac{2m_{de}k_f M_c}{(2\pi)^2 \hbar^2} \left\{ 1 + \frac{k_f}{2q} \left[f\left(\frac{k_f(\epsilon_q - \hbar(\omega+i\delta))}{\epsilon_f q}\right) \right.\right.$$
$$\left.\left. + f\left(\frac{k_f(\epsilon_q + \hbar(\omega+i\delta))}{\epsilon_f q}\right) \right] \right\} \qquad (231.09)$$

The dielectric function may then be derived from Eq. 231.02 using this expression for the polarization. However in the above derivation a substitution (Eq. 231.06a) was made for q so that the energy difference (Eq. 231.06c) could be defined in the conduction band. The substitution for the wavevector q (Eq. 231.06a) was justified at the time by noticing that $W(q,\omega)$ and hence $\pi^0(q,\omega)$ is to be integrated over the conduction band states in the self energy expression (Eq. 223.19). When this substitution is made in $W^0(q)$

$$W^0(q) = \frac{m_{de} e^2}{\epsilon \epsilon_r (m_1 q'^2_x + m_t q'^2_y + m_t q'^2_z)} \qquad (231.10)$$

Dropping the primes and making a crude adjustment for the complicated denominator this gives

$$W^0(q) = (m_{de}/m_{op}) e^2/\epsilon \epsilon_r q^2 \qquad (231.11a)$$

where the optical effective mass is given by

$$m_{op}^{-1} = 1/3 (1/m_1 + 2/m_t) \qquad (231.11b)$$

The electron dielectric function is then given by

$$\epsilon(q,\omega) = 1 + W^0(q) \, \pi^0(q,\omega) \qquad (231.11c)$$

Identifying the prefactor from the second term on the right hand side of Eq. 231.11c with the inverse Thomas Fermi screening length κ (see Fig 2.4

for values of this function)

$$\kappa^2 = \frac{2m_{de}k_f M_c e^2}{((2\pi)^2 \hbar^2 \epsilon \epsilon_r)} = 4 \left(\frac{3}{\pi}\right) \frac{M_c^{3/2}}{a_{eff}} N_d^{1/3} \qquad (231.12)$$

the electron dielectric function (Eq. 231.11 and Eq. 231.09) may be written

$$\epsilon(q,\omega) = 1 + \frac{m_{de}\kappa^2}{2m_{op}q^2} \left\{ 1 + \frac{k_f}{2q} \left[f\left(\frac{k_f(\epsilon_q - \hbar(\omega+i\delta))}{\epsilon_f q}\right) \right.\right.$$

$$\left.\left. + f\left(\frac{k_f(\epsilon_q + \hbar(\omega+i\delta))}{\epsilon_f q}\right) \right] \right\} \qquad (231.13)$$

where $f(x)$ is defined in Eq. 231.08a. On setting m_{op} equal to the conduction band density of states mass this reduces to the Lindhard dielectric function used by Berggren and Sernelius (1981). The inclusion of m_{op} in the prefactor of Eq. 231.13 justifies the use of m_{op} in the plasma frequency (ω_p Eq. 232.05) used in the next section.

2.3.2   The plasmon pole approximation.

In this thesis the plasmon pole approximation to the above Lindhard function is used. This has been found to be quite adequate for the present calculations and because of its simplicity has the advantage of being easily extended to finite temperature. In this section the plasmon pole approximation is derived from a series expansion of the Lindhard function derived above.

The Lindhard dielectric function (Eq. 231.13) may be written in its real and imaginary parts

$$\epsilon(q,\omega) = \epsilon_1(q,\omega) + i\epsilon_2(q,\omega)$$

$$\epsilon_1(q,\omega) = 1 + \frac{m_{de}\kappa^2}{m_{op}2q^2}\left\{ 1 + \frac{k_f}{2q}\left[f\left(\frac{k_f(\epsilon_q - \hbar\omega)}{\epsilon_f q}\right) \right.\right.$$

$$\left.\left. + f\left(\frac{k_f(\epsilon_q + \hbar\omega)}{\epsilon_f q}\right) \right]\right\} \qquad (232.01a)$$

$$\epsilon_2(q,\omega) = \begin{cases} (M_c/a_{eff}q)\ (\hbar\omega/\epsilon_q) & \text{I} \\ (M_c/a_{eff}q)\ (k_f/q)^2\ (1 - a^2/4) & \text{II} \\ 0 & \text{III} \quad \text{IV} \end{cases} \qquad (232.01b)$$

$$a = q(\epsilon_q - \hbar\omega)/\epsilon_q$$

where the four regions and the function $f(x)$ are those defined in Eq.231.08 and shown in Fig 2.6. The imaginary part of the dielectric function is then only non-zero in regions I and II, where it has the values defined above. Whilst the real part of the dielectric function is given by one expression throughout $q-\omega$ space. In the self energy calculation (Eq. 223.19) it is not simply the dielectric function that is required but rather the inverse dielectric function. Clearly this also has real and imaginary parts given by

$$\frac{1}{\epsilon(q,\omega)} = \frac{\epsilon_1(q,\omega) - i\epsilon_2(q,\omega)}{\epsilon_1(q,\omega)^2 + \epsilon_2(q,\omega)^2} \qquad (232.02)$$

The inverse dielectric function will have poles at values of q and ω when the denominator of this expression is zero. However in region III of Fig 2.6 this amounts to zeros in the real part of the dielectric function since the imaginary part is zero throughout III. Whilst in region II where q is large $\epsilon_2(q,\omega)$ is proportional to the inverse cube of q, so again the imaginary part may be quite small. Taking first large ω and q whilst ignoring $\epsilon_2(q,\omega)$ the poles in the inverse dielectric function may be

calculated by finding the zeros in the real part of the dielectric function.

a)   For large ω the arguments of the logarithmic functions become large so the real part of the dielectric function (Eq. 232.01) may be re-written

$$\epsilon_1(q,\omega) = 1 + \frac{4m_{de}\kappa^2}{3m_{op}q^2}\left(\frac{\epsilon_f\epsilon_q}{(\epsilon_q^2 - (\hbar\omega)^2)}\right)$$
$$+ \frac{16m_{de}\kappa^2\epsilon_f^3(\epsilon_q^3 + 3\epsilon_q(\hbar\omega)^2)}{15m_{op}q^2k_f^2 \ (\epsilon_q^2 - (\hbar\omega)^2)^3} + \ldots \ldots \quad (232.03)$$

To a first approximation the zeros in this function are given by

$$\epsilon_1(q,\omega) = 1 + \frac{4m_{de}\kappa^2}{3m_{op}q^2}\left(\frac{\epsilon_f\epsilon_q}{(\epsilon_q^2 - (\hbar\omega)^2)}\right) = 0$$

or   (232.04)

$$(\hbar\omega)^2 = (\hbar\omega_1(q))^2 = (\hbar\omega_p)^2 + \epsilon_q^2$$

where the plasma frequency ω_p

$$(\hbar\omega_p)^2 = \frac{4m_{de}\kappa^2\epsilon_f^2}{3m_{op}k_f^2} = \frac{N_d e^2}{\epsilon\epsilon_0 m_{op}} \quad (232.05)$$

has been identified and $\omega_1(q)$ is known as the dispersion frequency. The real part of the dielectric function may be re-written

$$\epsilon_1(q,\omega) = 1 + \frac{(\hbar\omega_p)^2}{(\epsilon_q^2 - (\hbar\omega)^2)} = 1 + \frac{\omega_p^2}{(\omega_1(q))^2 - \omega_p^2 - \omega^2}$$
$$(232.06)$$

The Cauchy principle part of the inverse dielectric function is just

$$\frac{1}{\epsilon_1(q,\omega)} = \frac{(\omega_1(q))^2 - (\omega)^2 - (\omega_p)^2}{(\omega_1(q))^2 - (\omega)^2} \quad (232.07a)$$

Whilst the imaginary part of the inverse dielectric function is given by

the delta function

$$\text{Im}(\epsilon^{-1}(q,\omega)) = - \frac{\pi \, \omega_p^2}{2 \, \omega_1(q)} \, \delta(\omega - \omega_1(q)) \qquad (232.07b)$$

A second approximation to the dispersion relationship may be obtained from Eq. 232.03 by substituting for ω from Eq. 232.04

$$0 = (\epsilon_q^2 - (\hbar\omega_1(q))^2) + (\hbar\omega_p)^2 + \frac{4\epsilon_f(\hbar\omega_p)^2(\epsilon_q^3 + 3\epsilon_q(\hbar\omega)^2)}{5 \quad q^2 \quad (\epsilon_q^2 - (\hbar\omega)^2)^2}$$

$$+ \ldots \ldots$$

ie $\qquad\qquad\qquad\qquad\qquad\qquad\qquad\qquad\qquad (232.08)$

$$(\hbar\omega)^2 = (\hbar\omega_1(q))^2 = (\hbar\omega_p)^2 + (12/5)\epsilon_q\epsilon_f + \epsilon_q^2$$

The above derivation of the dispersion relationship illustrates the importance of the q^4 term as pointed out by Lundqvist (1967). Higher approximations to the dispersion relation may be found in Ferrell 1957.

b) In the static ($\omega=0$) limit as q tends towards zero the Thomas Fermi limit

$$\frac{1}{\epsilon_1(q)} = \frac{q^2}{q^2 + \kappa^2} = 1 - \frac{\omega_p^2}{\omega_1(q)^2}$$

$$(\hbar\omega_1(q))^2 = (\hbar\omega_p)^2 + (4/3)\epsilon_q\epsilon_f \qquad (232.09)$$

is obtained from Eq. 232.01. Thus in order that the correct Thomas Fermi limit is obtained for small q the following dispersion relationship is used in this thesis (see Fig 2.6)

$$(\hbar\omega_1(q))^2 = (\hbar\omega_p)^2 + (4/3)\epsilon_q\epsilon_f + \epsilon_q^2 \qquad (232.10)$$

where the factor in front of the q^2 term has been adjusted from that in Eq. 232.08 to give the correct Thomas Fermi limit. Other workers have used a variety of forms for the second term in Eq. 232.10. Mahan (1980) uses

$$\frac{4}{3} \epsilon_q\epsilon_f$$

whilst Berggren and Sernelius (1981) use

$$\frac{4}{3} \frac{m_{de}}{m_{op}} \epsilon_q \epsilon_f$$

in their calculations in the plasmon pole approximation. The additional term in the ratio of the conduction band effective mass (m_{de}) to the optical mass (m_{op}) makes only a small correction to the final result $(r=1.26)$.

The inverse dielectric function in the plasmon pole approximation may now be written

$$\epsilon^{-1}(q,\omega) = 1 + \frac{\omega_p^2}{2\omega_1(q)}(\frac{1}{\omega - \omega_1(q) + i\delta} - \frac{1}{\omega + \omega_1(q) - i\delta})$$

$$(232.11)$$

The peak in the imaginary part of this function indicates a frequency at which with no external electric field an oscillation of the electron gas may exist. These longitudinal oscillations of the electron gas are called plasmons. Although the above definition of the inverse dielectric function is only strictly valid within region III up to the critical wavenumber (q_c) and frequency $(\omega_c$ see Fig 2.6), where the plasmons are undamped, provided the modified dispersion relationship (Eq. 232.10) is used it gives a good approximation to the full Lindhard function.

2.3.3 Detailed comparison of plasmon pole and Lindhard functions.

In order to compare the plasmon pole approximation derived above with the full Lindhard function we introduce the form of the energy variable ω used later in the thesis

$$\hbar\omega = \hbar\omega_{nq}^0 = \lambda_n \epsilon_q^0 = \lambda_n \hbar^2 q^2 / 2m_{de} \qquad (233.01)$$

where $\hbar\omega^0_{nq}$ defines the $\epsilon - k$ relationship for the band n. In the valence band λ_H and λ_L define the heavy and light hole bands. Fig 2.6 shows the two valence band curves defined by 233.01. In Fig 2.7 and Fig 2.8 the magnitude of the inverse Lindhard (Eq. 231.13) and plasmon pole (Eq. 232.11) dielectric functions are plotted for the light hole band (Fig 2.7) and heavy hole band (Fig 2.8). In Fig 2.8 it can be seen that for the heavy hole band (λ_H) the Lindhard and plasmon pole dielectric functions agree very well. However in the light hole band (Fig 2.7) although the plasmon frequency is predicted well the precise nature of the plasmon peak is not identical. The light hole dispersion relationship bisects $\omega_1(q)$ (shown in Fig 2.6) above the critical frequency. Thus the true or Lindhard peak in Fig 2.7 is damped whilst the plasmon pole approximation predicts a pole at

$$\omega^0_{nq} = \omega_1(q) \qquad (233.02)$$

This is a clear indication that use of the plasmon pole approximation for any similar ω–q curve where the dispersion curve is intersected will give erroneous results. However as will be shown in subsequent sections this problem is overcome in the present calculations.

A more fundamental problem arises from the exact nature of the valence band (Fig 2.3c). From the $\epsilon - k$ curve for the light hole band (Fig 2.3c) the effective mass m_L can be seen to change from a low value for small energies to a value little different from m_H at about 30 meV below the band top. From Fig 2.6 the plasmon peak (Fig 2.7) occurs at some hundreds of meV below the valence band top. Thus the light hole mass should have increased long before this point and the plasmon peak (Fig 2.7) would never occur. A more detailed description of the valence band self energies would require the inclusion of these effects.
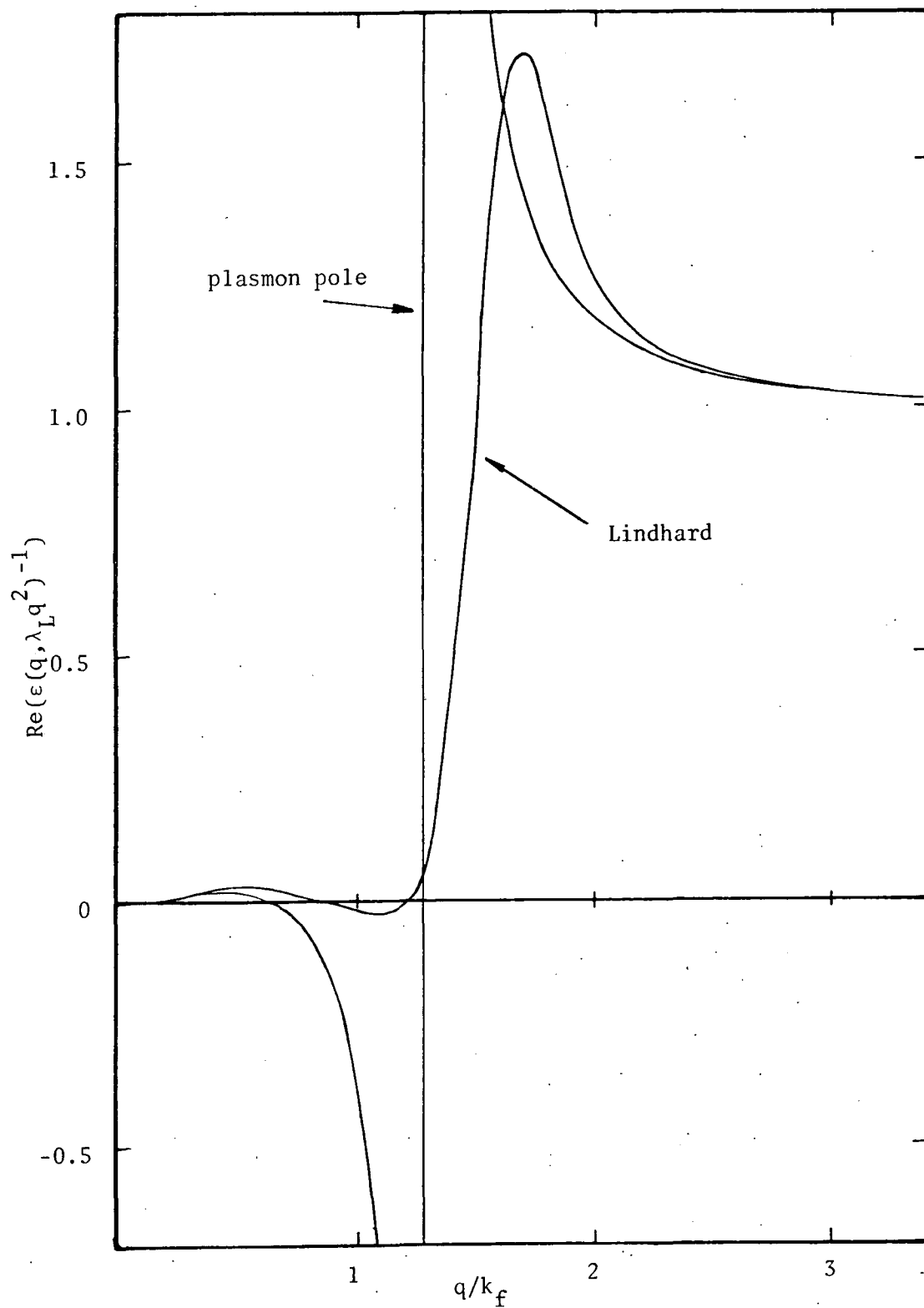
Fig 2.7   The magnitude of the inverse Lindhard and plasmon pole dielectric functions for an electron concentration of 10^{20} cm^{-3}.
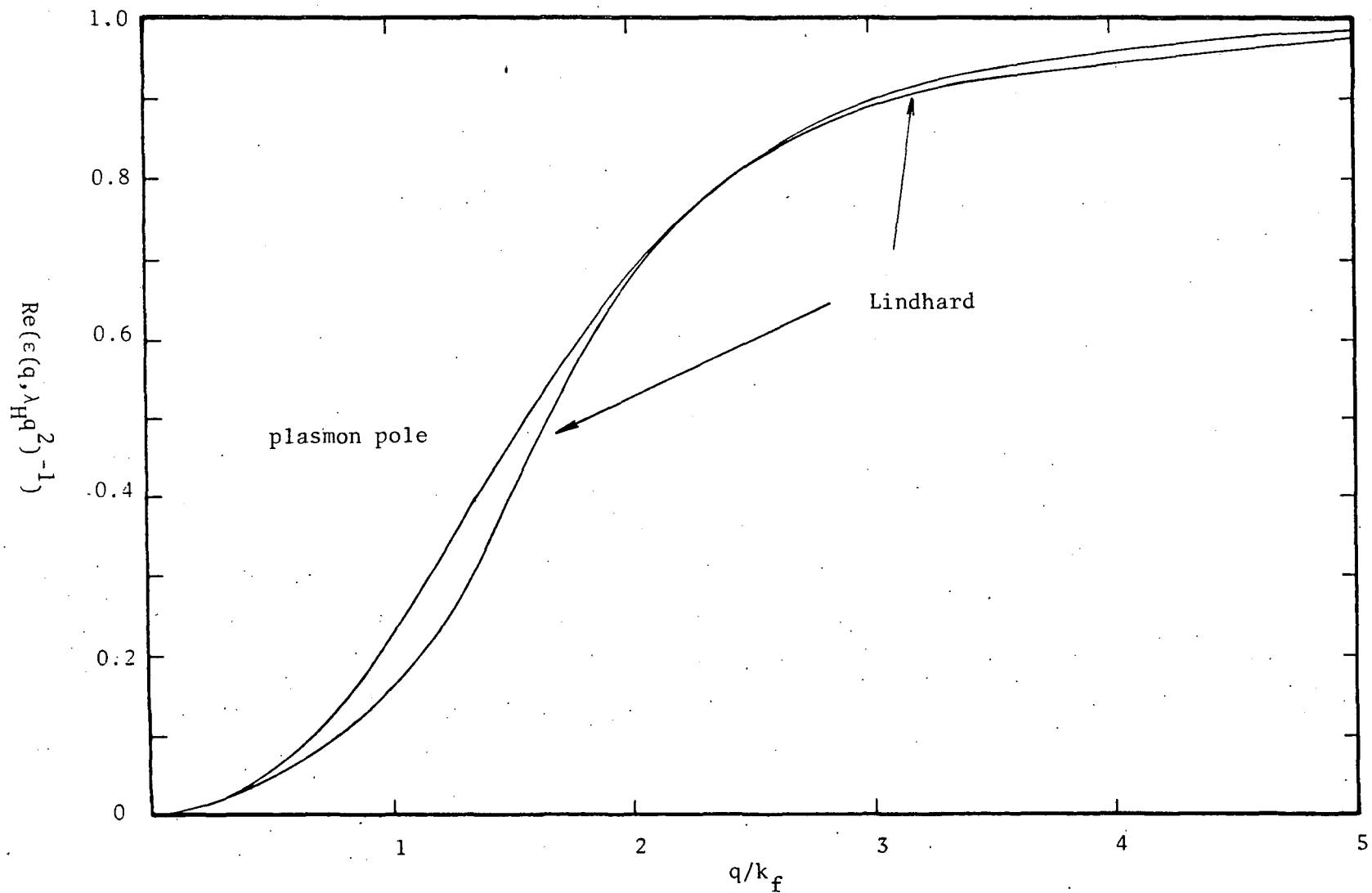
Fig 2.8   Inverse Lindhard and plasmon pole dielectric functions in the Heavy hole band. $N_d \tilde{} 10^{20} cm^{-3}$.

2.4 SUMMARY.

In summary the electrons and holes in the band (n) of heavily doped silicon can no longer be described by the unperturbed Green's function

$$G^0(n;k,\omega) = \frac{1}{(\omega - \omega_{nk}^0 + i\delta sgn(\omega_{nk}^0 - \omega_f))} \qquad (240.01)$$

with unperturbed energy (for details see Eq. 210.01 and Eq. 210.02)

$$\epsilon_{nk}^0 = \hbar\omega_{nk}^0 \qquad (240.02)$$

but rather the total Green's functions that describes the properties of the quasi-particles is used (with ω_f the zero temperature Fermi frequency)

$$G(n;k,\omega) = 1 / (\omega - \omega_{nk}^0 - \Sigma^{ee}(n;k,\omega) + i\delta sgn(\omega_{nk}^0 - \omega_f)) \qquad (240.03)$$

where the poles in the Green's function give us an iterative solution for the wavevector dependent energy (ϵ_{nk}) of these quasi particles

$$\omega_{nk} = \omega_{nk}^0 + Re(\Sigma^{ee}(n;k,\omega_{nk})) \qquad (240.04)$$

To a first approximation this gives

$$\epsilon_{nk} = \hbar\omega_{nk} \approx \hbar\omega_{nk}^0 + hRe(\Sigma^{ee}(n;k,\omega_{nk}^0)) = \hbar\omega_{nk}^0 + \hbar Re(\Sigma_n^{ee}(k)) \qquad (240.05)$$

The self energy (Σ) gives the change in band position compared to its unperturbed position it is represented by $\Delta E^{ee}_n(k)$ where n represents the band index and the super-script indicates that this is the electron-electron contribution to the movement of the band.

$$\Delta E_n^{ee}(k) \approx \hbar\, Re(\Sigma^{ee}(n;k,\omega_{nk}^0)) = \hbar\, Re(\Sigma_n^{ee}(k)) \qquad (240.06)$$

The form of the self energy is given by the following set of equations.

First the self energy (Eq. 223.19)

$$\hbar\Sigma^{ee}(n;k,\omega) = \frac{i}{(2\pi)^4} \sum_m \iint \frac{e^{i\eta(\omega-\nu)}}{(\omega-\nu - \omega^0_{m(k-q)} + i\delta\,\mathrm{sgn}(\omega^0_{m(k-q)} - \omega_f))}$$

$$\Lambda_{nm}W_{eff}(q,\nu)\ d^3q\,d\nu \qquad (240.07a)$$

where the screened interaction $W_{eff}(q,\omega)$ used is defined in Eq. 231.02

$$W_{eff}(q,\omega) = e^2 / \epsilon\epsilon_r q^2 \epsilon(q,\omega) \qquad (240.07b)$$

In this thesis the plasmon pole approximation to the electron dielectric function is used $(\epsilon(q,\omega))$. This is given by (Eq. 232.11)

$$\epsilon^{-1}(q,\omega) = 1 + \frac{\omega_p^2}{2\omega_1(q)} \left(\frac{1}{\omega - \omega_1(q) + i\delta} - \frac{1}{\omega + \omega_1(q) - i\delta} \right)$$

or after a small amount of rearranging

$$\epsilon^{-1}(q,\omega) = 1 - \left(\frac{\omega_p^2}{(\omega_1(q) - i\delta)^2 - \omega^2} \right) \qquad (240.07c)$$

with dispersion relationship (Eq. 232.10), where a term in q^4 is included to give better large q agreement with the Lindhard function

$$\omega_1(q)^2 = \omega_p^2 + \omega_p^2 q^2 / \kappa^2 + \epsilon_q^2/\hbar^2$$

$$= \omega_p^2 \left(1 + \frac{q^2}{\kappa^2} + \frac{3m_{op}}{4m_{de}} \frac{q^4}{k_f^2 \kappa^2} \right) \qquad (240.07d)$$

The plasma frequency is given by Eq. 232.05

$$(\hbar\omega_p)^2 = \frac{4m_{de}\kappa^2\epsilon_f^2}{3m_{op}k_f^2} = \frac{N_d e^2}{\epsilon\epsilon_r m_{op}} \qquad (240.07e)$$

and the Thomas Fermi screening length by (see Fig 2.4)

$$\kappa^2 = \frac{2m_{de}k_f M_c e^2}{((2\pi)^2\hbar^2\epsilon\epsilon_r)} = 4 \left(\frac{3}{\pi}\right)^{1/3} \frac{M_c^{3/2}}{a_{eff}} N_d^{1/3} \qquad (240.07f)$$

whilst the Fermi wavevector is given by (see Fig 2.4)

$$k_f = \left(\frac{3\pi^2 N_d}{M_c}\right)^{1/3}$$ (240.07g)

Finally the Lamda function Λ_{nm}, where n and m represent the different bands (c conduction, v valence) was defined by (Eq. 223.18)

$$\Lambda_{nm} = \Lambda_{mn}$$

$$\Lambda_{cm} = \delta_{cm}$$ (240.07h)

$$\Lambda_{vc} = 0 \qquad \Lambda_{LH} = 3/4 \, \sin^2\theta \qquad \Lambda_{HH} = 1/4 \, (1+3\cos^2\theta)$$

Where H represents the heavy hole band and L represents the light hole band and θ is the angle between wavevectors k and q in Eq. 240.07a.

In summary a first approximation to the self energy has been derived that: ignores the vertex corrections; uses the free particle propagator; contains the screened interaction potential which itself has been approximated by only considering the plasmon pole; ignores inter-valley scattering. To improve the approximations made it would be possible to extend the calculation of the electron self energy to include the vertex functions or use the Lindhard function in the interaction. It would also be possible to combine the electron-electron calculations with the electron impurity calculations as Ghazali and Serre (1982) have done (see chapter 4) but using the plasmon pole approximation, rather than the Thomas Fermi approximation that Ghazali and Serre use.

By comparison with Berggren and Sernelius's work (1981) the chapters to follow show that the plasmon pole approximation to the Lindhard dielectric function has acceptable accuracy. Indeed it has been found that with the aid of this simpler plasmon pole approximation to the above dielectric function an approximation to the self energy at finite temperature may easily be derived (chapter 7). The self energy defined in Eq. 240.07 is then used in this thesis to describe the change in energy of the conduction and valence bands.

CHAPTER 3

ELECTRON-ELECTRON EXCHANGE ENERGIES.

3.0   INTRODUCTION.

In the previous chapter an expression for the exchange or self energy of electrons (holes) in the conduction (valence) band has been defined (Eq. 240.07a) using the plasmon pole approximation to the electron dielectric function.   In this chapter this expression will be used to evaluate the change in the conduction and valence band states as a result of the extra electrons present in the conduction band.   This extra concentration (N_d) of conduction band electrons may be present because of a population inversion, as present in a laser, or may result from impurities in the silicon each providing an easily ionised donor electron to the conduction band.   In the latter example the assumption is made that the conduction and impurity bands have merged which is true at concentrations greater that the Mott metal insulator transition discussed in the chapter 1 and shown in Fig 2.4 to occur in silicon at about 3.10^{18} cm^{-3} depending upon the type of impurity.

The real part of the self energy expression (Eq. 240.07a) describes the exchange energy of an electron in the band n. This is made up of several parts characterised by the summation over band index m. Thus the self energy contribution to the conduction band is made up of exchange energies between electrons in the same band (Σ^{ee}_{cc}) and exchange between the electrons in the conduction band and the valence band (Σ^{ee}_{cv})

$$\Sigma^{ee}_{c} = \Sigma^{ee}_{cc} + \Sigma^{ee}_{cv} \qquad\qquad (300.01)$$

However as Inkson (1976) points out it is the change in the band energies

that is of interest. This is derived from the difference between this self energy and that present in the intrinsic semiconductor (Σ^{int}_n). Thus the change in the conduction band energy is defined by

$$\Delta\Sigma^{ee}_c = \Sigma^{ee}_{cc} + \Sigma^{ee}_{cv} - \Sigma^{int}_{cc} - \Sigma^{int}_{cv} = \Sigma^{ee}_{cc} = \Delta E^{ee}_c \qquad (300.02)$$

In this thesis as in work by other authors (Berggren and Sernelius 1981, Abram et al 1978) it is assumed that the exchange between electrons in the conduction and valence band is unchanged by the presence of the extra electrons in the conduction band (see section 3.1). The intrinsic exchange of the conduction band electrons with themselves (Σ^{int}_{cc}) is clearly zero, since the intrinsic conduction band is calculated on a one electron model. A similar expression may be derived for the valence band

$$\Delta\Sigma^{ee}_v = \Sigma^{ee}_{vc} + \Sigma^{ee}_{vv} - \Sigma^{int}_{vc} - \Sigma^{int}_{vv} = \Sigma^{ee}_{vv} - \Sigma^{int}_{vv} = \Delta E^{ee}_v \qquad (300.03)$$

However in this case the intrinsic valence band has a self energy since it is full of electrons in contrast to the intrinsic conduction band. This Hartree Fock energy must be subtracted from the valence band contribution.

Hedin (1965) and Hedin and Lundqvist (1969) have shown that the self energy (Eq. 240.07a) may be split up into two distinct parts:

a) screened dynamic exchange terms denoted by the superscript sx that are derived from singularities in the Green's function;

b) coulomb hole terms denoted by the superscript ch and derived from singularities in the interaction.

In Section 3.1 these two contributions to the self energy are explained and derived. Numerical calculations of these two contributions for the conduction band states $(\Delta E^{sx}_{ck}$ and $\Delta E^{ch}_{ck})$ are presented in Section 3.2. Whilst in section 3.3 the numerical results for the valence band $(\Delta E^{sx}_{vk}$ and $\Delta E^{ch}_{vk})$ are presented. The main results of this chapter, the band gap

reduction due to electron-electron interactions, are given in section 3.4 (Fig 3.6). These are about 4 meV lower that the results published by Berggren and Sernelius (1981). This agreement between these two sets of results shows that the plasmon pole approximation provides a valid means of approximating the Lindhard Dielectric function in silicon at zero temperature.

3.1 DERIVATION OF THE COULOMB HOLE AND SCREENED DYNAMIC EXCHANGE TERMS.

Most of the ground work for the calculation of the exchange energy has been covered in the previous chapter. To a first approximation the change in the band edges due to electron-electron interactions giving rise to the band gap reduction is given by an iterative solution of the real part of Eq. 240.06

$$\epsilon_{nk} = \hbar\omega_{nk} \approx \hbar\omega_{nk}^0 + \hbar Re(\Sigma^{ee}(n;k,\omega_{nk}^0))$$

$$= \hbar\omega_{nk}^0 + \hbar Re(\Sigma_n^{ee}(k)) \qquad (310.01)$$

where a condensed form of the self energy expression $\Sigma^{ee}_n(k)$ has been used. The expression for the electron-electron self energy (Eq. 240.07)

$$\hbar\Sigma^{ee}(n;k,\omega) = \frac{i}{(2\pi)^4} \sum_m \int \int G^0(m;k-q,\omega-\nu) \; e^{i\eta(\omega-\nu)}$$
$$\Lambda_{nm} W_{eff}(q,\nu) \; d^3qd\nu \qquad (310.02)$$

may now be solved to give numerical values for this contribution to the band gap reduction. The frequency integral over ν in the self energy may be evaluated analytically and yields two sets of energy contributions to

which names are assigned (after the work of Hedin (1965)):

a)   'Screened Exchange' terms derived from poles in the Green's

function (Eq. 240.01) at (see Fig 3.1),

$$\nu = \omega_{nk}^{0} - \omega_{m(k-q)}^{0} + i\delta sgn(\omega_{m(k-q)}^{0} - \omega_{f})) \quad (310.03a)$$

b)   'Coulomb Hole' terms derived from poles in the screened

interaction (Eq. 240.07b and 240.07c) at (see Fig 3.1),

$$\nu = \omega_{1}(q) - i\delta \quad \text{and} \quad \nu = -\omega_{1}(q) + i\delta \quad (310.03b)$$

These two contributions collectively are referred to as the exchange energy

of electrons in the heavily doped silicon.

The frequency integral in Eq 310.02 is performed over the

contour marked in Fig 3.1 which is traversed in a clockwise direction so

the integral is given by

$$I = -2\pi i \; Res(enclosed \; poles) \quad (310.04)$$

Jordan's lemma (Arfken 1970) dictates that the integral be performed in the

lower half plane so that the integration over Γ_{1} vanishes.   Only the poles

at

$$\nu = \omega_{nk}^{0} - \omega_{m(k-q)}^{0} - i\delta \quad ; \quad \omega_{m(k-q)}^{0} < \omega_{f} \quad (310.05a)$$

where ω_{f} is the Fermi angular frequency and

$$\nu = \omega_{1}(q) - i\delta \quad (310.05b)$$

remain within the contour.   Thus those poles with angular frequency greater

than ω_{f} (the unoccupied states) do not contribute to the screened dynamic

exchange energy.   After elementary evaluation of the residues at these two

sets of poles the self energy (Eq. 310.02) become
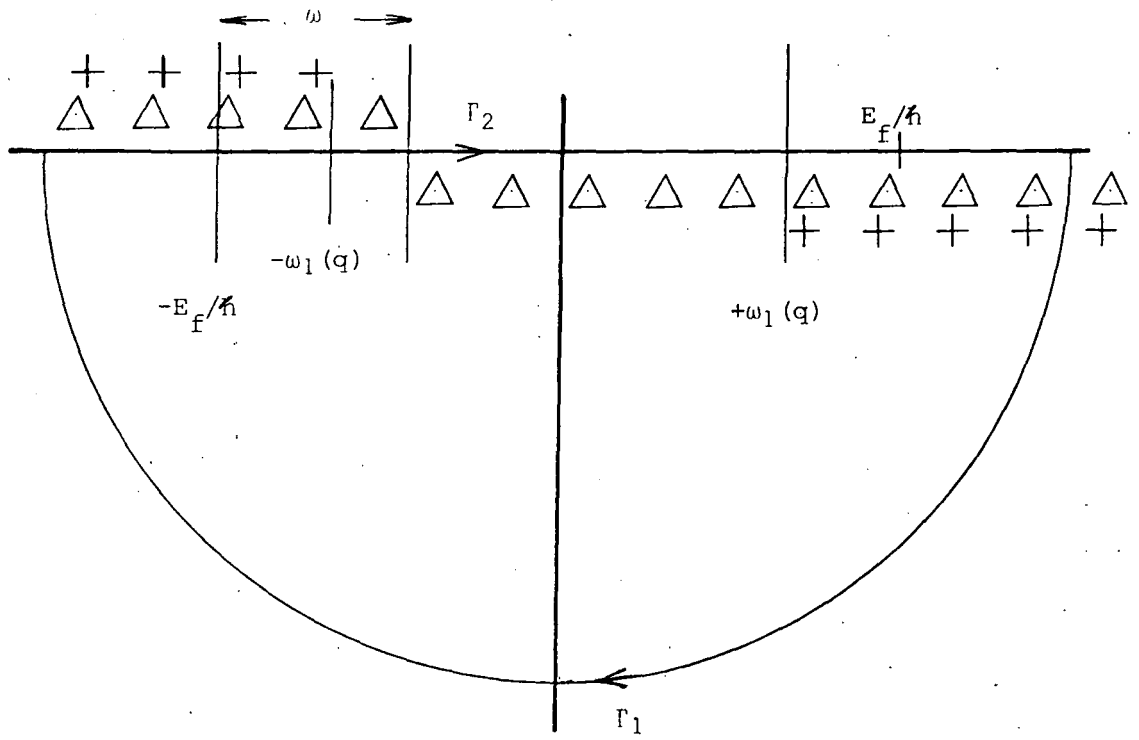
complex ν-plane.

△   poles in the Green's function.

＋   poles in the interaction.

Fig 3.1   Poles in the Green's function (Eq. 310.03a)

and the interaction (Eq. 310.03b) in the

complex ν-plane.

$$\hbar\Sigma_n^{sx}(k) = -\frac{1}{(2\pi)^3}\sum_{\substack{m \\ \text{occupied} \\ \text{states}}}\int W_{eff}(q,\omega_{nk}^0-\omega_{m(k-q)}^0)\Lambda_{nm}d^3q \quad (310.06a)$$

$$\hbar\Sigma_n^{ch}(k) = +\frac{e^2}{(2\pi)^3\epsilon\epsilon_r}\sum_m\int\frac{1}{q^2}\frac{\omega_p^2}{2\omega_1(q)}$$

$$\frac{\Lambda_{nm}\, d^3q}{(\omega_{nk}^0-\omega_{m(k-q)}^0-\omega_1(q)+i\delta sgn(\omega_{m(k-q)}^0-\omega_f^0))} \quad (310.06b)$$

where the additional superscript ee has been omitted for clarity. In Eq. 310.06a the q integration is taken over only the occupied states as dictated by Eq. 310.05a. Whilst in the second expression (Eq. 310.06b) the q integral is to be performed over all positive q.

As mentioned in the introduction to this chapter Inkson (1976) showed that it is the difference between this extrinsic self energy and the intrinsic self energy that is of interest. In this paragraph it is shown that the exchange between conduction and valence band is identical for both the intrinsic and extrinsic silicon. Thus when the change in the band energy (Eq. 300.02 and Eq. 300.03) is calculated these terms cancel leaving the exchange between electrons of the same band as the only contribution. The inter-band exchange is defined by taking the part of Eq. 310.06 with n=c and m=v (or vice versa). In section 2.2.3 the overlap integral (Λ_{nm}) was taken arbitrarily to be zero with n=c and m=v (or vice versa) this is true for small wavevector where the Bloch functions are orthogonal. At large wavevectors the electron dielectric function tends towards unity (see Fig 2.7 or 2.8) so that the effective potential is just the intrinsic value. Thus the extrinsic and intrinsic screened dynamic exchange terms (Eq. 310.06a) with n=c and m=v cancel. For n=v m=c the extrinsic integral is negligible because of the small volume of q

space occupied by the new electrons at large q. The deno-
-minator of the coulomb hole terms (Eq. 310.06) is large
when $m \neq n$ so these give a relatively small contribution.

The intrinsic exchange Σ^{int}_{cc} between electrons in the
conduction band with themselves is zero since the conduction band is
calculated in a one electron model (no states filled in Eq. 310.06a, no
poles in the electron dielectric function to derive Eq. 310.06b). Thus the
change in the energy of conduction band electrons (ΔE^{ee}_{c}) is given by the
Cauchy principle part of Eq. 310.06)

$$\Delta E^{ee}_{c}(k) = \Delta E^{sx}_{c}(k) + \Delta E^{ch}_{c}(k)$$

(310.07a)

$$= Re(\hbar\Sigma^{sx}_{cc}(k)) + Re(\hbar\Sigma^{ch}_{cc}(k))$$

There are however many electrons in the intrinsic valence band so that the
change in energy of this band is given by

$$\Delta E^{ee}_{v}(k) = \Delta E^{sx}_{v}(k) + \Delta E^{ch}_{v}(k)$$

(310.07b)

$$= Re(\hbar\Sigma^{sx}_{vv}(k) - \hbar\Sigma^{int}_{vv}(k)) + Re(\hbar\Sigma^{ch}_{vv}(k))$$

where Σ^{int}_{vv} is the Hartree Fock exchange energy calculated in detail in
section 3.3.

3.2 CHANGE IN EXCHANGE ENERGY OF CONDUCTION BAND ELECTRONS.

In this section the two numerical calculations performed to
evaluate the change in conduction band energy due to the electron-electron
exchange energy are introduced. In section 3.2.1 the details of the ΔE^{sx}
component is presented, whilst section 3.2.2 the ΔE^{ch} component is
considered. The magnitudes of these two electron-electron contributions to
the energy of the conduction band states (Fig 3.2) are found to be additive

In contrast to the equivalent valence band components and reduce the energy of those states (see section 3.2.3 and Fig 3.2), reducing the band gap.

The shift in conduction band states due to electron – electron interactions is given by (Eq. 310.07)

$$\Delta E_C^{ee}(k) = \Delta E_C^{sx}(k) + \Delta E_C^{ch}(k)$$

(320.01a)

$$= Re(\hbar\Sigma_{cc}^{sx}(k)) + Re(\hbar\Sigma_{cc}^{ch}(k))$$

From the self energy expressions (Eq. 310.06), substituting for the inverse dielectric function from Eq. 240.07c, these contributions to the change in the band edge due to the extra electrons in the conduction band become

$$\Delta E_C^{sx}(k) = - \frac{e^2}{(2\pi)^3\varepsilon\varepsilon_r} \int^{\text{occupied states}} \frac{1}{q^2} (1$$

$$- \frac{\omega_p^2}{\omega_1(q)^2 - (\omega_{ck}^0 - \omega_{c(k-q)}^0)^2}) \Lambda_{cc} \, d^3q$$

(320.01b)

and

$$\Delta E_C^{ch}(k) = + \frac{e^2}{(2\pi)^3\varepsilon\varepsilon_r} \int \frac{1}{q^2} \frac{\omega_p^2}{2\omega_1(q)}$$

$$\frac{1}{(\omega_{ck}^0 - \omega_{c(k-q)}^0 - \omega_1(q))} \Lambda_{cc} \, d^3q$$

(320.01c)

The summation over the band index m in 310.06 has been performed and the intrinsic self energy has been subtracted as prescribed by Eq. 300.02. The wavevector integral is evaluated within the spherical band approximation justified in section 2.3.1 for the dielectric function. The angular part of the wavevector integral is then given by

$$\int_0^{2\pi} \int_0^{\pi} \sin\theta \, d\theta \, d\phi = 4\pi$$

(320.02)

so that the change in the screened dynamic exchange and coulomb hole terms

become

$$\Delta E_c^{sx}(k) = - \frac{e^2}{2\pi^2 \epsilon \epsilon_r} \int_0^{k_f} (1 - \frac{\omega_p^2}{\omega_1(q)^2 - (\omega_{ck}^0 - \omega_{c(k-q)}^0)^2}) \, dq$$

(320.03)

$$\Delta E_c^{ch}(k) = + \frac{e^2}{2\pi^2 \epsilon \epsilon_r} \int_0^\infty \frac{\omega_p^2}{2\omega_1(q)} \frac{1}{(\omega_{ck}^0 - \omega_{c(k-q)}^0 - \omega_1(q))} \, dq$$

For these expressions to be evaluated the difference between the two eigenvalues ϵ_{ck}^0 and $\epsilon_{c(k-q)}^0$ has to be defined. In this thesis the main concern is with the change in position of the extremities of the bands. For the conduction band where only one of the six equivalent conduction band valleys need be considered the origin in k space is moved to the centre of one ellipsoidal for simplicity (see the discussion in section 2.1.0) so that the energy difference at the conduction band bottom ($k=k_i$) becomes (using Eq. 210.01 and 231.06c)

$$\epsilon_{ck_i}^0 - \epsilon_{c(k_i-q)}^0 = - \frac{\hbar^2 q^2}{2m_{de}} = - (\frac{3m_{op}\omega_p^2 q^4}{4m_{de}k_f^2 \kappa^2})^{1/2} = - \hbar\omega_{cc}^0(q)$$

(320.04)

This is a negative quantity since the band energy at wavevector q is greater than the band bottom. However the equivalent valence band energy difference is positive since in that band the energy at q is lower than the band edge. The sign of the energy difference is only important in the coulomb hole term.

As mentioned in the previous paragraph the main concern is with the bottom of the conduction band and the top of the valence band in this thesis. However Eq. 320.03, with the appropriate choice of energy difference, will give the electron-electron contribution to the self energy of electrons at any wavevector (k). In particular to calculate the shift in the Fermi energy we require $k=k_i$. The calculations of Berggren and Sernelius (1981) and Abram et al (1978) show this k dependence to be small.

so the calculation of the shift at the Fermi energy is assumed to be identical to the shift at the band edge.

In the following two sections the two contributions to the change in the self energy of the conduction band are calculated separately, ΔE^{sx}_c in section 3.2.1 and ΔE^{ch}_c in section 3.2.2.

3.2.1 Calculation of the conduction band screened dynamic exchange term.

The calculation of this contribution to the exchange energy may be derived analytically, provided the plasmon pole approximation has been made. Numerical results for different concentrations may then be obtained from a simple calculation varying the Thomas Fermi screening length (κ) and Fermi wavevector (k_f, see Eq. 240.07f, Eq. 240.07g and Fig 2.4). So from Eq. 320.03

$$\Delta E^{sx}_c(k) = - \frac{e^2}{2\pi^2 \epsilon \epsilon_r} \int_0^{k_f} (1 - \frac{\omega_p^2}{\omega_1(q)^2 - (\omega^0_{ck} - \omega^0_{c(k-q)})^2}) \, dq$$

(321.01)

Substituting for the difference in eigenvalues (Eq. 320.04) at the bottom of the conduction band (with the origin of k space at the centre of one of the six ellipsoidal valleys) this becomes

$$\Delta E^{sx}_c(k_i) = - \frac{e^2}{2\pi^2 \epsilon \epsilon_r} \int_0^{k_f} (1 - \frac{\omega_p^2}{\omega_1(q)^2 - (\hbar q^2 / 2m_{de})^2}) \, dq$$

(321.02)

Substituting for the dispersion relationship $\omega_1(q)$ from Eq. 240.7d

$$\Delta E_C^{sx}(k_i) = - \frac{e^2 \kappa^2}{2\pi^2 \epsilon \epsilon_r k_f} \int_0^1 \left(\frac{1}{(\kappa/k_f)^2} \right.$$

$$\left. - \frac{1}{(q/k_f)^2 + (\kappa/k_f)^2} \right) d(q/k_f)$$

$$\Delta E_C^{sx}(k_i) = - \frac{e^2 k_f}{2\pi^2 \epsilon \epsilon_r} \left(1 - \frac{\kappa}{k_f} \tan^{-1}\left(\frac{k_f}{\kappa} \right) \right) \qquad (321.03)$$

where the first part of the right hand side represents the Hartree Fock exchange energy of the conduction band electrons. Substituting for the various parameters and the electron (donor) concentrations (N_d) expressed in cm^{-3}

$$\Delta E_C^{sx}(k_i) = - 1.323.10^{-8} N_d^{1/3} \left(1 \right.$$

$$\left. - \frac{4.849.10^3}{N_d^{1/6}} \tan^{-1}\left(\frac{N_d^{1/6}}{4.849.10^3} \right) \right) \quad (eV) \quad (321.04)$$

a contribution that lowers the energy of the conduction band states and reduces the band gap. Values for this term are plotted in Fig 3.2 for a range of concentrations. This contribution to the exchange energy was found to be the same as that obtained in the static or Thomas Fermi limit of the dielectric function (Berggren and Sernelius 1981). When coupled with the results of the next section we find that these are in close agreement with electron-electron exchange calculations made by Berggren and Sernelius using the full Lindhard function also plotted in this figure.
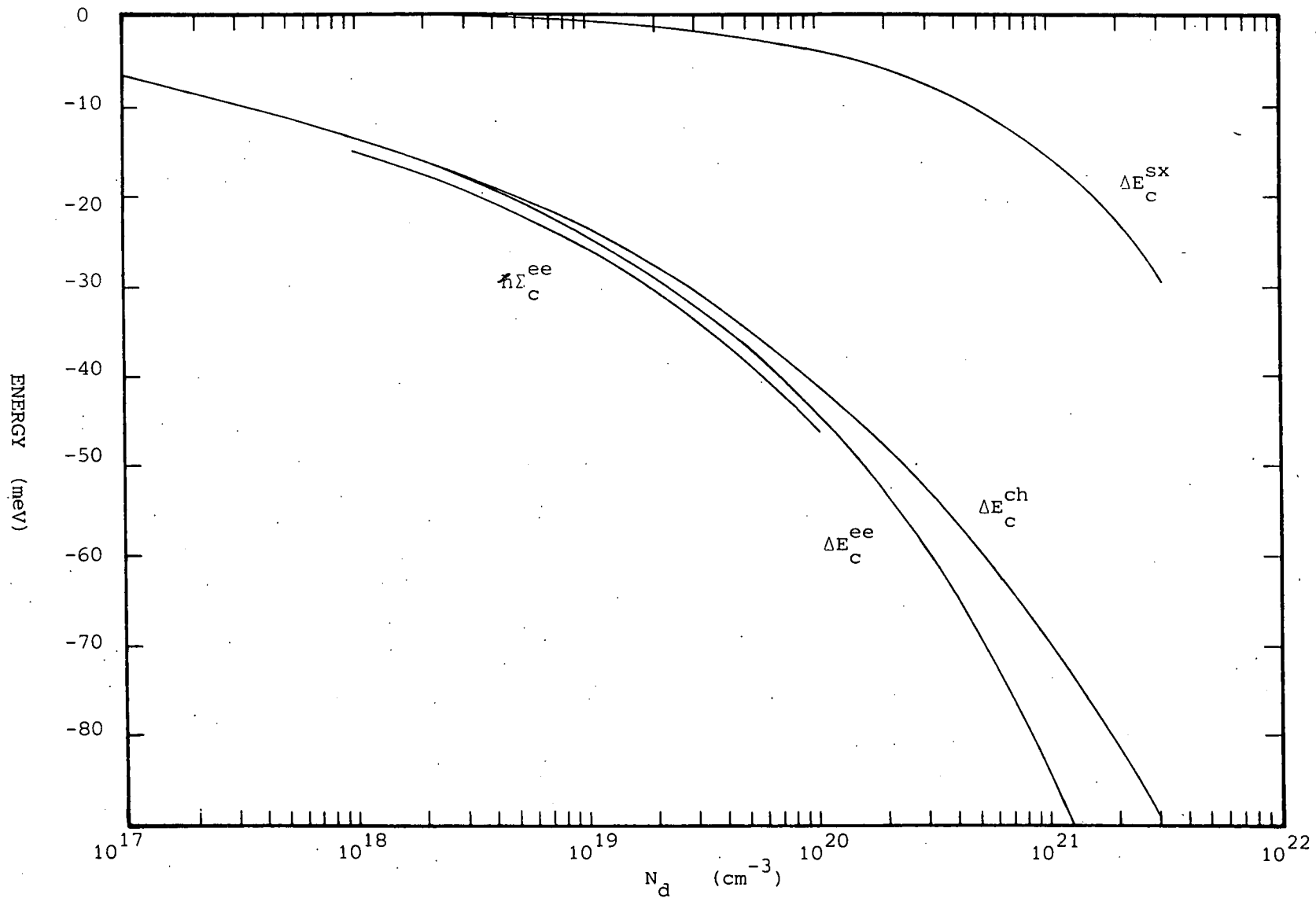
Fig 3.2   Change in energy of the conduction band bottom ΔE_c^{ee}. $\hbar\Sigma_c^{ee}$ from Berggren et al (1981).

3.2.2 Calculation of the conduction band coulomb hole term.

In contrast to the elementary calculation of the screened exchange term above the evaluation of the coulomb hole term (Eq. 320.03) may not be carried out analytically with the plasmon pole approximation to the inverse electron dielectric function. Instead a numerical integration routine was used from the NAG library of Fortran subroutines. The principle of the calculation however was the same as above: Varying the concentration by choosing suitable values for κ, then computing the change in energy of the edge of the band. From Eq. 320.03

$$\Delta E_C^{ch}(k) = + \frac{e^2}{2\pi^2 \epsilon \epsilon_r} \int_0^\infty \frac{\omega_p^2}{2\omega_1(q)} \frac{1}{(\omega_{ck}^0 - \omega_{c(k-q)}^0 - \omega_1(q))} dq$$

(322.01)

Substituting for the energy difference from Eq. 320.04

$$\Delta E_C^{ch}(k_i) = - \frac{e^2}{2\pi^2 \epsilon \epsilon_r} \int_0^\infty \frac{\omega_p^2}{2\omega_1(q)} \frac{1}{(\omega_1(q) + \hbar q^2/2m_{de})} dq$$

(322.02)

As in the valence band calculation (last paragraph of section 3.3.2) the ΔE^{ch}_c contribution lowers the energy of the conduction band states. With the substitutions

$$\beta = \frac{3m_{op}}{4m_{de}} = 0.5951 \quad ; \quad K = \frac{\kappa}{k_f} = 4.849.10^3 \, N_d^{-1/6}$$

$$\left(\frac{q}{k_f}\right)^2 = \frac{1-t}{t}$$

Eq 322.02 becomes

$$\Delta E_C^{ch}(k_i) = - \frac{e^2 \kappa^2}{8\pi^2 \epsilon \epsilon_r k_f} \int_0^1 \left(\frac{t}{1-t}\right)^{1/2}$$

(322.03)

$$\frac{dt}{(K^2+\beta-1)t^2 + (1-2\beta)t + \beta + \sqrt{(((K^2+\beta-1)t^2 + (1-2\beta)t + \beta)\beta(t^2-2t+1))}}$$

On substitution of the various parameters

$$\frac{e^2 \kappa^2}{8\pi^2 \epsilon \epsilon_r k_f} = 77.73 \quad (meV)$$

This integration was performed by the NAG routine D01APF for a series of values of κ and k_f depending on the electron (donor) concentration N_d (see Fig 2.4). The results of this calculation are presented in Fig 3.2. They may be compared with those calculated by Mahan (1980) as part of his valence band shift ($J(s_0)$). Mahan considers an energy difference with the wrong sign (compare his un-labeled expression pp 2642 with Eq. 322.02) for his coulomb hole term thus the comparison is possible only between his valence band term and the conduction band expression calculated here. He finds results of the form

$$\Sigma_{h,c} = -\frac{33}{r_s^{3/4}} \left(\frac{m_h}{m_d}\right)^{1/2} = -13.1 \left(\frac{N_d}{10^{18}}\right)^{1/4} \quad (meV) \quad (322.04)$$

At 10^{20} cm^{-3} this gives $\Sigma_{h,c}$ = 32 meV whilst the equivalent results presented in Fig 3.2 show a reduction of 40 meV. Mahan's values are then 25% too small.

3.2.3   Total conduction band electron-electron exchange.

Finally adding the results from sections 3.2.1 and 3.2.2 the total change in the electron-electron contribution to the self energy of the conduction band (Eq. 320.01a) is calculated (Fig 3.2). These are compared with those derived from the full Lindhard function presented by Berggren and Sernelius (1981) and it can be seen (Fig 3.2) that these two calculations agree within a few meV over the concentration range considered. The plasmon pole approximation thus compares well with the Lindhard function, at least for zero temperature. The plasmon pole approximation then provides a means of extending the calculations to finite

temperature (chapter 7).

3.3   CHANGE IN EXCHANGE ENERGY OF VALENCE BAND ELECTRONS.

In this section the numerical calculations performed to evaluate the change in valence band energy due to the electron–electron exchange energy are introduced. These calculations are however more difficult than the preceding conduction band calculations, because of the inaccuracies of the plasmon pole approximation discussed in section 2.3.3. These problems are overcome by summing the ΔE^{sx} and ΔE^{ch} terms directly. In section 3.3.1 this ΔE^{ch+sx} component is calculated, whilst in section 3.3.2 the calculation of the ΔE^{sx} component is performed. The coulomb hole term may then be derived by simple subtraction of these two contributions (see section 3.3.2). Although the total electron–electron contribution to the energy of valence band states tends to raise that energy, reducing the band gap (see Fig 3.3), the individual contributions work against each other in contrast to the equivalent conduction band contributions (see Fig 3.4 and 3.5). The coulomb hole contributions to both conduction and valence bands then tend to lower each band by a similar energy (within 20 meV, see Fig 3.5).

As mentioned in section 3.1 electrons in the valence band have a self energy contribution in the intrinsic semiconductor. This is due to the interaction of the valence band electrons present in the intrinsic material. It may be obtained merely by evaluating the self energy for the intrinsic semiconductors valence band without the influence of any electron screening from the conduction band. The intrinsic self energy for the heavy hole band will be shown to be the same as for the light hole band at the band top (k=0). This self energy is given by solving Eq. 310.02 for

the self energy with the effective interaction given by its intrinsic value

$$W_{eff}(q,\omega) = W_{int}(q) = e^2/\epsilon\epsilon_r q^2 \qquad (330.01a)$$

$$\hbar\Sigma^{int}(H;k,\omega) = \frac{i}{(2\pi)^4} \sum_m \int\int G^0(m;k-q,\omega-\nu) \, e^{i\eta(\omega-\nu)}$$
$$\Lambda_{Hm} \, W_{int}(q,\nu) \, d^3q d\nu \qquad (330.01b)$$

This self energy must be subtracted from the total valence band self energy to give the change in self energy due to the additional conduction band electrons as prescribed by Eq. 300.03. The change in self energy of the heavy hole valence band is then given by

$$\hbar\Delta\Sigma^{ee}(H;k,\omega) = \hbar\Sigma^{ee}(H;k,\omega) - \hbar\Sigma^{int}(H;k,\omega) \qquad (330.02a)$$

$$\hbar\Delta\Sigma^{ee}(H;k,\omega) = \frac{i}{(2\pi)^4} \sum_m \int\int G^0(m;k-q,\omega-\nu) \, e^{i\eta(\omega-\nu)}$$
$$\Lambda_{Hm} \, W_{val}(q,\nu) \, d^3q d\nu$$

This subtraction amounts to choosing a new effective potential given by subtracting Eq. 330.01a from Eq. 240.07b

$$W_{val}(q,\omega) = W_{eff}(q,\omega) - W_{int}(q) \qquad (330.02b)$$

$$W_{val}(q,\omega) = \frac{e^2}{\epsilon\epsilon_r q^2}[\frac{\omega_p^2}{2\omega_1(q)}(\frac{1}{\omega-\omega_1(q)+i\delta} - \frac{1}{\omega+\omega_1(q)-i\delta})]$$

where Eq. 240.07c for the inverse plasmon pole dielectric function has been used. The change in the valence band self energy due to electron-electron interactions (Eq. 310.07) is given by the Cauchy principle part of Eq. 330.02a.

$$\Delta E_H^{ee}(k) = \Delta E_H^{sx}(k) + \Delta E_H^{ch}(k) = \hbar Re(\Delta\Sigma^{ee}(H;k,\omega_{nk}^0)) \qquad (330.03a)$$

In the intrinsic valence band the effective interaction (Eq. 330.01a) does not provide any poles. The intrinsic coulomb hole term, that derives from poles in the interaction, is then zero. However the intrinsic screened dynamic exchange term is finite and is just the Hartree Fock energy for the

intrinsic valence band thus only the form of the screened dynamic exchange term is different from the conduction band expression (Eq. 320.01). Substituting for the effective potential from (Eq. 330.02b) the change in the self energy calculated from Eq. 310.06 becomes

$$\Delta E_H^{sx}(k) = + \frac{e^2}{(2\pi)^3 \epsilon \epsilon_r} \sum_m \int \frac{1}{q^2} \left(\frac{\omega_p^2}{\omega_1(q)^2 - (\omega_{Hk}^0 - \omega_{m(k-q)}^0)^2} \right) \Lambda_{Hm} \, d^3q$$

and   (330.03b)

$$\Delta E_H^{ch}(k) = + \frac{e^2}{(2\pi)^3 \epsilon \epsilon_r} \sum_m \int \frac{1}{q^2} \frac{\omega_p^2}{2\omega_1(q)} \frac{1}{(\omega_{Hk}^0 - \omega_{m(k-q)}^0 - \omega_1(q))} \Lambda_{Hm} \, d^3q$$

The only difference in form between these and the conduction band expressions is in the screened dynamic exchange term (cf. Eq. 320.01b) because of the subtraction of the Hartree Fock energy from the valence band expression. The summation over the band index m, which may take on the values L, H for the light and heavy valence bands is more complex than in the conduction band calculation since the valence band wavefunctions of the two degenerate hole bands are not orthogonal. Algebraically this interaction manifests itself in values for Λ_{HH} and Λ_{HL} that depend upon the angle θ between wavevectors k and q (Eq. 240.07h discussed in detail in section 2.2.3)

$$\Lambda_{HL} = \Lambda_{LH} = 3/4 \sin^2\theta$$

and

$$\Lambda_{LL} = \Lambda_{HH} = 1/4 (1+3\cos^2\theta)$$

Since we are dealing with the top of the valence band where k=0 the meaning

of the angle between k and q becomes ambiguous. A k of infinitesimal size but well defined direction is taken. The angular part of the wavevector integrals in the four components of Eq. 330.03 give identical results

$$\int_0^{2\pi} \int_0^{\pi} 1/4 \ (1+3\cos^2\theta)\sin\theta \ d\theta \ d\phi = 2\pi$$

and

$$\int_0^{2\pi} \int_0^{\pi} 3/4 \ (\sin^2\theta)\sin\theta \ d\theta \ d\phi = 2\pi$$

so that the changes in the valence band self energy become

$$\Delta E_H^{sx}(k) = + \frac{e^2}{4\pi^2 \epsilon \epsilon_r} \sum_m \int_0^\infty \left(\frac{\omega_p^2}{\omega_1(q)^2 - (\omega_{Hk}^0 - \omega_{m(k-q)}^0)^2} \right) dq$$

(330.04)

$$\Delta E_H^{ch}(k) = + \frac{e^2}{4\pi^2 \epsilon \epsilon_r} \sum_m \int_0^\infty \frac{\omega_p^2}{2\omega_1(q)} \frac{1}{(\omega_{Hk}^0 - \omega_{m(k-q)}^0 - \omega_1(q))} dq$$

To evaluate these scalar wavevector integrals it is convenient to label the two terms in the summation, thus

$$\Delta E_H^{sx}(k) = \Delta E_{HL}^{sx}(k) + \Delta E_{HH}^{sx}(k)$$

and

(330.05a)

$$\Delta E_H^{ch}(k) = \Delta E_{HL}^{ch}(k) + \Delta E_{HH}^{ch}(k)$$

For these expressions to be evaluated the difference between the two eigenvalues ϵ_{Hk}^0 and $\epsilon_{H(k-q)}^0$ (or $\epsilon_{L(k-q)}^0$) has to be defined. In this thesis the main concern is with the change in position of the extremities of the bands. For example for the top of the heavy hole valence band (k=0) this energy difference becomes

$$\epsilon_{HO}^0 - \epsilon_{n(0-q)}^0 = + \frac{\hbar^2 q^2}{2m_n} = \frac{m_{de}}{m_n} \left(\frac{3m_{op}\omega_p^2 q^4}{4m_{de}k_f^2 \kappa^2} \right)^{1/2} = \hbar\omega_{Hn}^0(q)$$

(330.05b)

Where m_n is either the heavy hole mass or the light hole mass depending on

the band index n (L or H).

Now substituting in Eq. 330.04 for the difference between the two eigenvalues ϵ^0_{Hk} and $\epsilon^0_{n(k-q)}$. At the top of the valence band where k=0, the change in energy of the top of the valence band becomes

$$\Delta E^{sx}_{Hn}(0) = + \frac{e^2}{4\pi^2 \epsilon \epsilon_r} \int_0^\infty \left(\frac{\omega_p^2}{\omega_1(q)^2 - (\hbar q^2/2m_n)^2} \right) \, dq$$

(330.05c)

$$\Delta E^{ch}_{Hn}(0) = + \frac{e^2}{4\pi^2 \epsilon \epsilon_r} \int_0^\infty \frac{\omega_p^2}{2\omega_1(q)} \frac{1}{(\hbar q^2/2m_n - \omega_1(q))} \, dq$$

Identical expressions may be derived when considering the light hole band (ΔE_L with $\omega^0_{Ln}(q)$). Thus provided the point k=0 is considered the equivalent expression for the light hole band is identical and the top of the light and heavy bands have the same change in energy. If a point other than the top of the band is considered the change in energy of the heavy and light bands need not be the same (see Eq. 330.05b). As mentioned in the previous paragraph the main concern is with the bottom of the conduction band and the top of the valence band in this thesis. However Eq. 330.04, with the appropriate choice of energy difference, will give the electron-electron contribution to the change in the self energy of electrons at any wavevector. The calculations of Berggren and Sernelius (1981) and Abram et al (1978) show this k dependence to be small, so the effective masses are assumed to have their intrinsic values.

It remains to evaluate numerically the scalar wavevector integral. This proved to be slightly more complicated than might be anticipated for the integrals with the light hole mass since as shown in Fig 2.6, Fig 2.7 and the discussion in section 2.3.3 the plasmon pole curve is bisected resulting in a poorly represented singularity occurring in the

integrand at

$$\omega_1(q) = \frac{\hbar q^2}{2m_L}$$

The numerical problem was avoided by summing the coulomb hole and dynamic screened exchange contributions to the band gap reduction.

$$\Delta E_{HL}^{ch+sx}(0) = \Delta E_{HL}^{ch}(0) + \Delta E_{HL}^{sx}(0)$$

(330.06a)

$$\Delta E_{HL}^{ch+sx}(0) = + \frac{e^2}{4\pi^2 \epsilon \epsilon_r} \int_0^\infty \frac{\omega_p^2}{2\omega_1(q)} \frac{1}{(\hbar q^2/2m_L + \omega_1(q))} \, dq$$

which can be seen to give a more manageable integral since the singularity no longer occurs in the integrand. The individual contributions may then be determined by subtracting the more easily computed $\Delta E^{sx}_{HL}(k)$ term. For the sake of completeness we also write the exchange contribution with the heavy mass band in the same way

$$\Delta E_{HH}^{ch+sx}(0) = + \frac{e^2}{4\pi^2 \epsilon \epsilon_r} \int_0^\infty \frac{\omega_p^2}{2\omega_1(q)} \frac{1}{(\hbar q^2/2m_H + \omega_1(q))} \, dq$$

(330.06b)

Numerical values for these integrals (Eq. 330.06 and Eq. 330.05c) for the change in the electron-electron self energy of the top of the valence band may be found in the next sections. Section 3.3.1 deals with the former, whilst section 3.3.2. by computation of the ΔE^{sx} term and subtraction, deals with the two component parts.

3.3.1   Calculation of the $\Delta E^{sx+ch}_v(k)$ term.

Evaluation of the contribution to the electron-electron exchange resulting from exchange between the valence bands (Eq. 330.06) require the numerical solution of integrals. The appropriate integration routine is the same as was used in the calculation of the coulomb hole term

for the conduction band (c.f. Eq. 322.02). Making the substitutions

$$\beta = \frac{3m_{op}}{4m_{de}} = 0.5951 \quad ; \quad K = \frac{\kappa}{k_f} = 4.849.10^3 \, N_d^{-1/6}$$

$$(331.01)$$

$$\left(\frac{q}{k_f}\right)^2 = \frac{1-t}{t} \quad ; \quad \gamma_L = \beta\left(\frac{m_{de}}{m_L}\right)^2 = 2.488 \quad ; \quad \gamma_H = \beta\left(\frac{m_{de}}{m_H}\right)^2 = .2548$$

Eq. 330.06 become

$$\Delta E_{HL}^{ch+sx}(0) = + \frac{e^2\kappa^2}{16\pi^2\epsilon\epsilon_r k_f} \int_0^1 \left(\frac{t}{1-t}\right)^{1/2} \qquad (331.02a)$$

$$\frac{dt}{(K^2+\beta-1)t^2+(1-2\beta)t+\beta+\sqrt{(((K^2+\beta-1)t^2+(1-2\beta)t+\beta)\gamma_L(t^2-2t+1))}}$$

and

$$\Delta E_{HH}^{ch+sx}(0) = + \frac{e^2\kappa^2}{16\pi^2\epsilon\epsilon_r k_f} \int_0^1 \left(\frac{t}{1-t}\right)^{1/2} \qquad (331.02b)$$

$$\frac{dt}{(K^2+\beta-1)t^2+(1-2\beta)t+\beta+\sqrt{(((K^2+\beta-1)t^2+(1-2\beta)t+\beta)\gamma_H(t^2-2t+1))}}$$

These integrals were performed using the NAG routine D01APF for a series of values of κ depending on the conduction band electron (donor) concentration N_d (see Fig 2.4). The numerical results of these calculations based on the plasmon pole approximation are presented in Fig 3.3 along with the results of Berggren and Sernelius's calculations based on the Lindhard dielectric function. The agreement as can be seen from this graph is within a few meV over the concentration range $10^{18} - 10^{20}$ cm^{-3}. Also plotted in this figure are the results for ΔE_v^{ch+sx} calculated assuming a simple un-coupled valence band with average density of states effective mass

$$m_v = (m_H^{3/2} + m_L^{3/2})^{2/3}$$

These show that results assuming an uncoupled valence band (ie ignoring the Lamda function Eq. 240.07h) overestimate the band gap reduction by 6 meV.
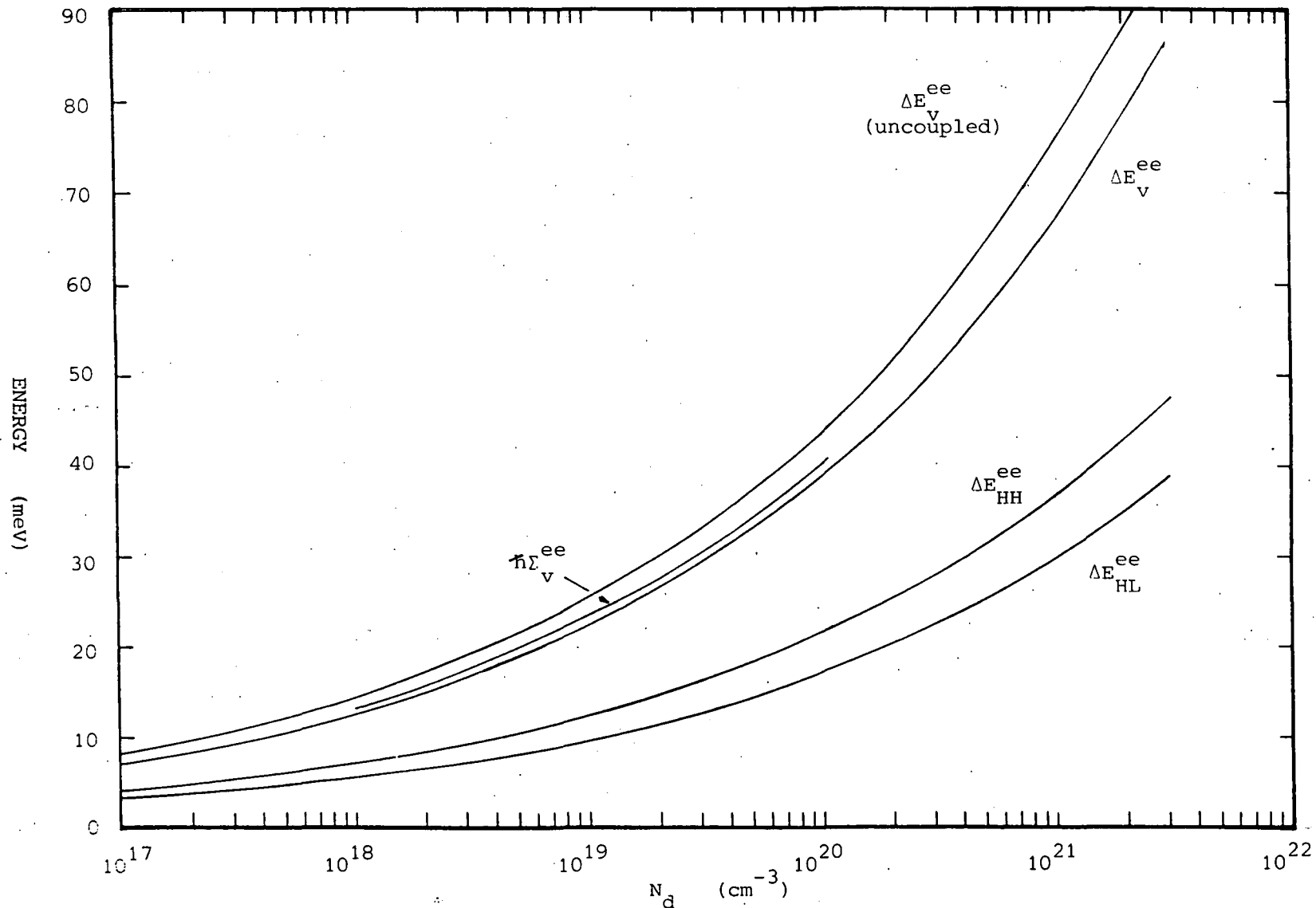
Fig 3.3   Change in the valence band top ΔE_v^{ee}. $\hbar\Sigma_v^{ee}$ from Berggren et al (1981).   Zero Kelvin.

3.3.2 Calculation of the $\Delta E^{sx}_v(k)$ and $\Delta E^{ch}_v(k)$ terms.

In contrast to the difficult calculation required for the coulomb hole exchange term the screened exchange terms ΔE^{sx}_{vL} and ΔE^{sx}_{vH} may be obtained analytically. Numerical results for different concentrations may then be obtained from a simple calculation varying the Thomas Fermi screening length (κ) and Fermi wavevector $(k_f,$ see Eq. 240.07f, Eq. 240.07g and Fig 2.4). So from Eq. 330.05c

$$\Delta E^{sx}_{Hn}(k) = + \frac{e^2}{4\pi^2 \epsilon \epsilon_r} \int_0^\infty \left(\frac{\omega_p^2}{\omega_1(q)^2 - (\hbar q^2/2m_n)^2} \right) dq \quad (332.01)$$

Making the substitutions

$$\alpha_L = \frac{3m_{op}}{4m_{de}} \left(\left(\frac{m_{de}}{m_L}\right)^2 - 1 \right) = 1.893 \quad (332.02)$$

$$\alpha_H = \frac{3m_{op}}{4m_{de}} \left(1 - \left(\frac{m_{de}}{m_H}\right)^2 \right) = 0.3403 \quad (332.03)$$

and substituting for the plasmon dispersion relationship $\omega_1(q)$ the two components of Eq. 332.01 may be written

$$\Delta E^{sx}_{HL}(0) = + \frac{e^2 \kappa^2}{4\pi^2 \epsilon \epsilon_r k_f} \int_0^\infty \quad (332.04)$$

$$\left(\frac{1}{- \alpha_L (q/k_f)^4 + (q/k_f)^2 + (\kappa/k_f)^2} \right) d(q/k_f)$$

and

$$\Delta E^{sx}_{HH}(0) = + \frac{e^2 \kappa^2}{4\pi^2 \epsilon \epsilon_r k_f} \int_0^\infty \quad (332.05)$$

$$\left(\frac{1}{\alpha_H (q/k_f)^4 + (q/k_f)^2 + (\kappa/k_f)^2} \right) d(q/k_f)$$

The analytical solutions for those two integrals are different due to the difference in α_n. We treat these two separately so that Eq. 332.04 has

solution (Gradshteyn and Ryzhik 1963 Eq. 3.223/2)

$$\Delta E_{HL}^{sx}(0) = + \frac{e^2 \kappa^2}{8\pi\epsilon\epsilon_r} \left(\frac{2\alpha_L k_f}{(k_f^2 + 4\alpha_L \kappa^2)((k_f^2 + 4\alpha_L \kappa^2)^{1/2} - k_f)} \right)^{1/2}$$

(332.06)

or on substituting for the various parameters

$$\Delta E_{HL}^{sx}(0) = + 5.036 \cdot 10^{-5} N_d^{1/6}$$

(332.07)

$$\left(\frac{8.900 \cdot 10^7 \ N_d^{-1/3}}{(1 + 1.7801 \cdot 10^8 \ N_d^{-1/3})((1 + 1.7801 \cdot 10^8 \ N_d^{-1/3})^{1/2} - 1)} \right)^{1/2} \text{(eV)}$$

where N_d is expressed in cm^{-3}. Whilst Eq. 332.05 has solution (Gradshteyn and Ryzhik 1963 Eq. 3.252/12)

$$\Delta E_{HH}^{sx}(0) = + \frac{e^2 \kappa}{8\pi\epsilon\epsilon_r} \left(\frac{k_f}{2\kappa\sqrt{\alpha_H} + k_f} \right)^{1/2}$$

(332.08)

which on substitution for the various parameters yields

$$\Delta E_{HH}^{sx}(0) = + 5.036 \cdot 10^{-5} N_d^{1/6} \left(\frac{N_d^{1/6}}{5.657 \cdot 10^3 + N_d^{1/6}} \right)^{1/2} \text{(eV)} \quad (332.09)$$

where N_d is again expressed in cm^{-3}. These two solutions (Eq. 332.06 and Eq. 332.08) may be found to tend towards the same limit as α tends towards unity. As a second check on these results and those of chapter 7 the integrals (Eq. 332.04 and Eq. 332.05) were performed numerically using NAG quadrature routines D01ALF and D01APF respectively. Although the latter integration was successful in that it gave the same results as those of Eq. 332.09, the former more complex integral gave the wrong result. The numerical problems with the solution of Eq. 332.04 are associated with the presence of the extra pole in the integrand due to the intersection of the plasmon dispersion curve shown in Fig 2.6 - 2.7. These problems have a small effect upon the finite temperature calculations of I_{1HL} in section 7.3.2.

Values of the screened dynamic exchange terms from Eq. 332.07

and 332.09 are presented in Fig 3.4 and show that the exchange with electrons in the heavy hole band ΔE_{HH} (or when considering ΔE_L the ΔE_{LH} term) give the greater contribution to the band gap narrowing. Also plotted in this figure is the magnitude of the change in the conduction band exchange term ΔE^{SX}_c which is much smaller than the valence band shift due to the presence of the Hartree Fock contribution in the conduction band (Eq. 321.03) and explicitly extracted from the valence band shift (Eq. 330.03b).

By simple subtraction (Eq. 330.03a) of the change in the valence band screened dynamic exchange term in Fig 3.4 from the total electron-electron exchange term in Fig 3.3 the contribution that the coulomb hole term makes may be obtained. These are presented in Fig 3.5 with those of the magnitude of the coulomb hole term in the conduction band calculation. It can be seen that both the conduction and valence band coulomb hole contributions reduce the energies of those bands and therefore only contribute a small increase (+10 meV at 10^{20} cm^{-3}) to the change in the band gap as pointed out by Inkson (1976) in connection with his "correlation energy".
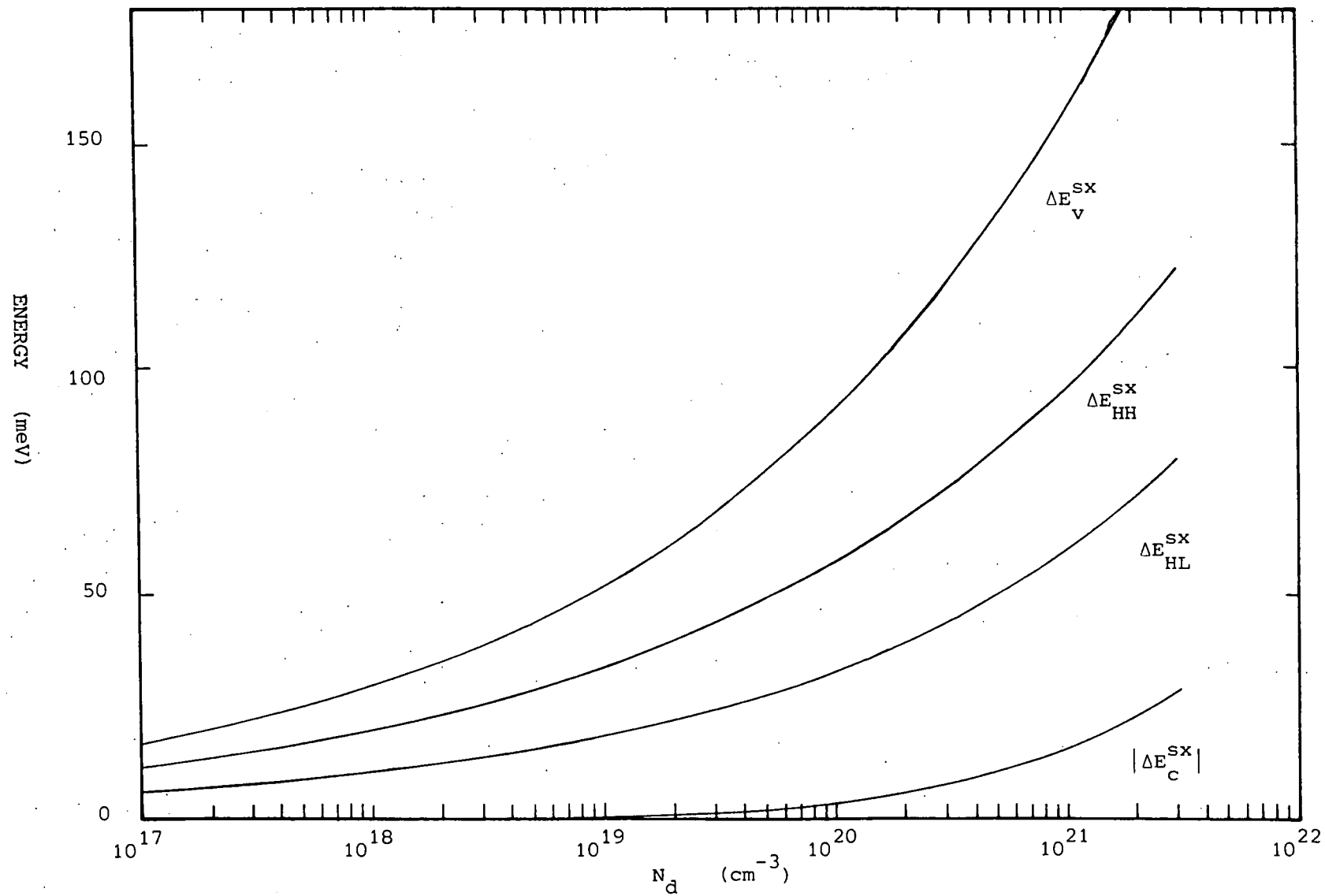
Fig 3.4   Change in the valence band top due to screened dynamic exchange terms at zero Kelvin.
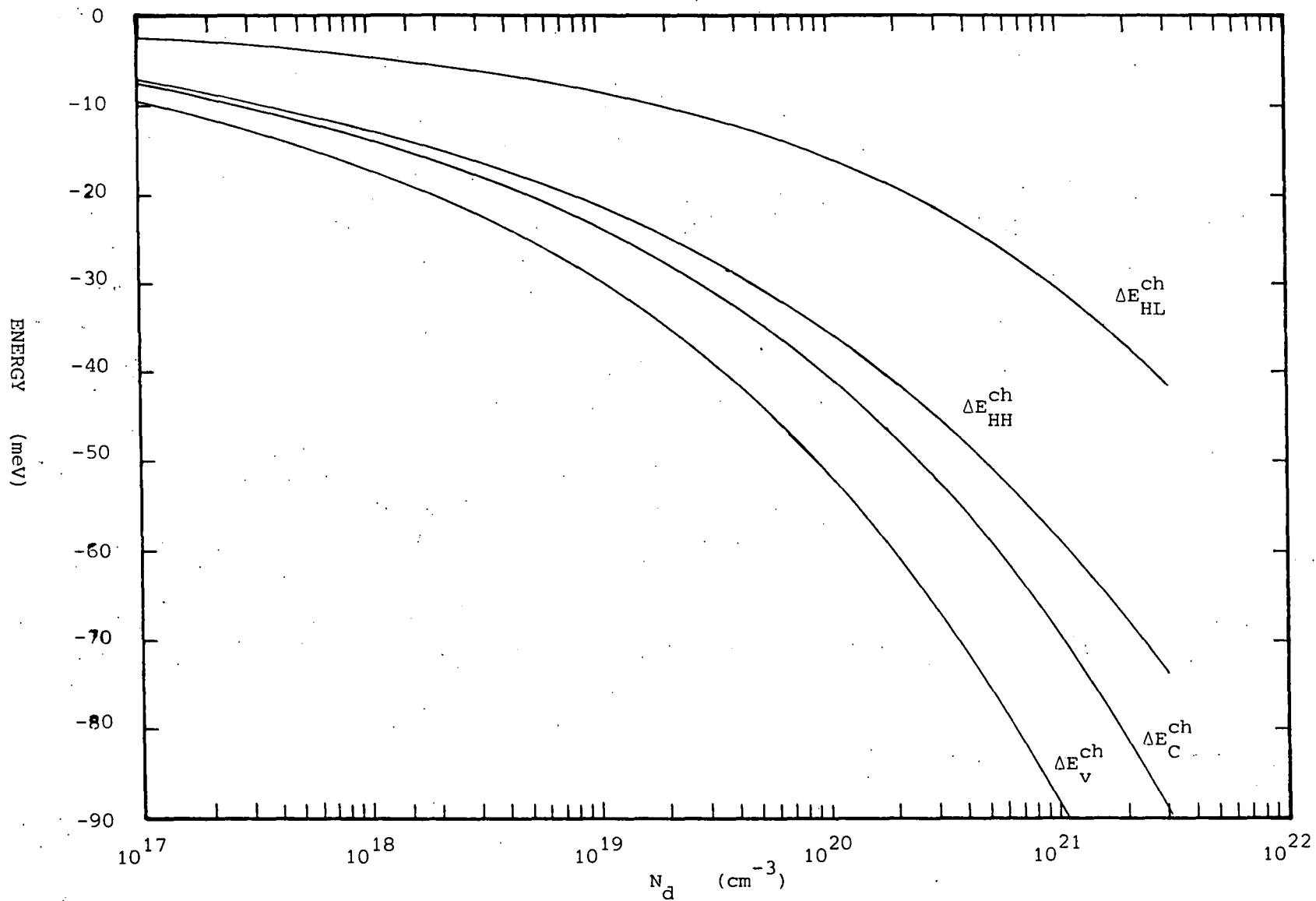
Fig 3.5   Change in the valence band top due to coulomb hole terms at a temperature of zero Kelvin.

3.4   SUMMARY AND CONCLUSIONS.

In this chapter the shifts in the conduction and valence bands due to the change in screened electron-electron exchange energies (Eq. 300.02 and 300.03) have been calculated. It has been found that in the plasmon pole approximation these can be split up into coulomb hole and screened dynamic exchange contributions (named by Hedin 1965 in connection with electrons gases in metals see section 3.1)

$$\Delta E_c^{ee}(k) = \Delta E_c^{sx}(k) + \Delta E_c^{ch}(k)$$

$$\Delta E_v^{ee}(k) = \Delta E_v^{sx}(k) + \Delta E_v^{ch}(k)$$

The coulomb hole contributions (see Eq. 320.03 and 330.04)

$$\Delta E_c^{ch}(k) = + \frac{e^2}{2\pi^2 \epsilon \epsilon_r} \int_0^\infty \frac{\omega_p^2}{2\omega_1(q)} \frac{1}{(\omega_{ck}^0 - \omega_{c(k-q)}^0 - \omega_1(q))} dq$$

$$\Delta E_v^{ch}(k) = + \frac{e^2}{4\pi^2 \epsilon \epsilon_r} \sum_m \int_0^\infty \frac{\omega_p^2}{2\omega_1(q)} \frac{1}{(\omega_{vk}^0 - \omega_{m(k-q)}^0 - \omega_1(q))} dq$$

reduce the energies of both conduction and valence bands contributing a small increase (+10 meV at 10^{20} cm^{-3}) to the change in the band gap as predicted by Inkson 1976 (see Fig 3.5). The screened dynamic exchange contributions of each band (Eq. 320.03 and 330.04) however act in opposite directions, both to reduce the gap (Fig 3.4)

$$\Delta E_c^{sx}(k) = - \frac{e^2}{2\pi^2 \epsilon \epsilon_r} \int_0^{k_f} (1 - \frac{\omega_p^2}{\omega_1(q)^2 - (\omega_{ck}^0 - \omega_{c(k-q)}^0)^2}) dq$$

$$\Delta E_v^{sx}(k) = + \frac{e^2}{4\pi^2 \epsilon \epsilon_r} \sum_m \int_0^\infty (\frac{\omega_p^2}{\omega_1(q)^2 - (\omega_{vk}^0 - \omega_{m(k-q)}^0)^2}) dq$$

With appropriate choice of the energy difference in these expressions the

change in the band energy at any value of k may be determined

$$\omega^0_{ck} - \omega^0_{c(k-q)} = -\omega^0_{cc}(k,q)$$
$$\omega^0_{vk} - \omega^0_{v(k-q)} = \omega^0_{vv}(k,q)$$

In conclusion the sum of contributions from the valence band (Fig 3.3) and the conduction band (Fig 3.2) to obtain the electron-electron contribution to the band gap narrowing is shown in Fig 3.6. It can be seen that these results differ by only a few meV from the results of Berggren and Sernelius calculated with the Lindhard dielectric function (Fig 3.2 and 3.3). It would seem then that the use of the plasmon pole approximation in estimating the electron-electron exchange energy is justified at least at zero temperature. In chapter 7 this method is extended to finite temperature to estimate the finite temperature band gap narrowing.
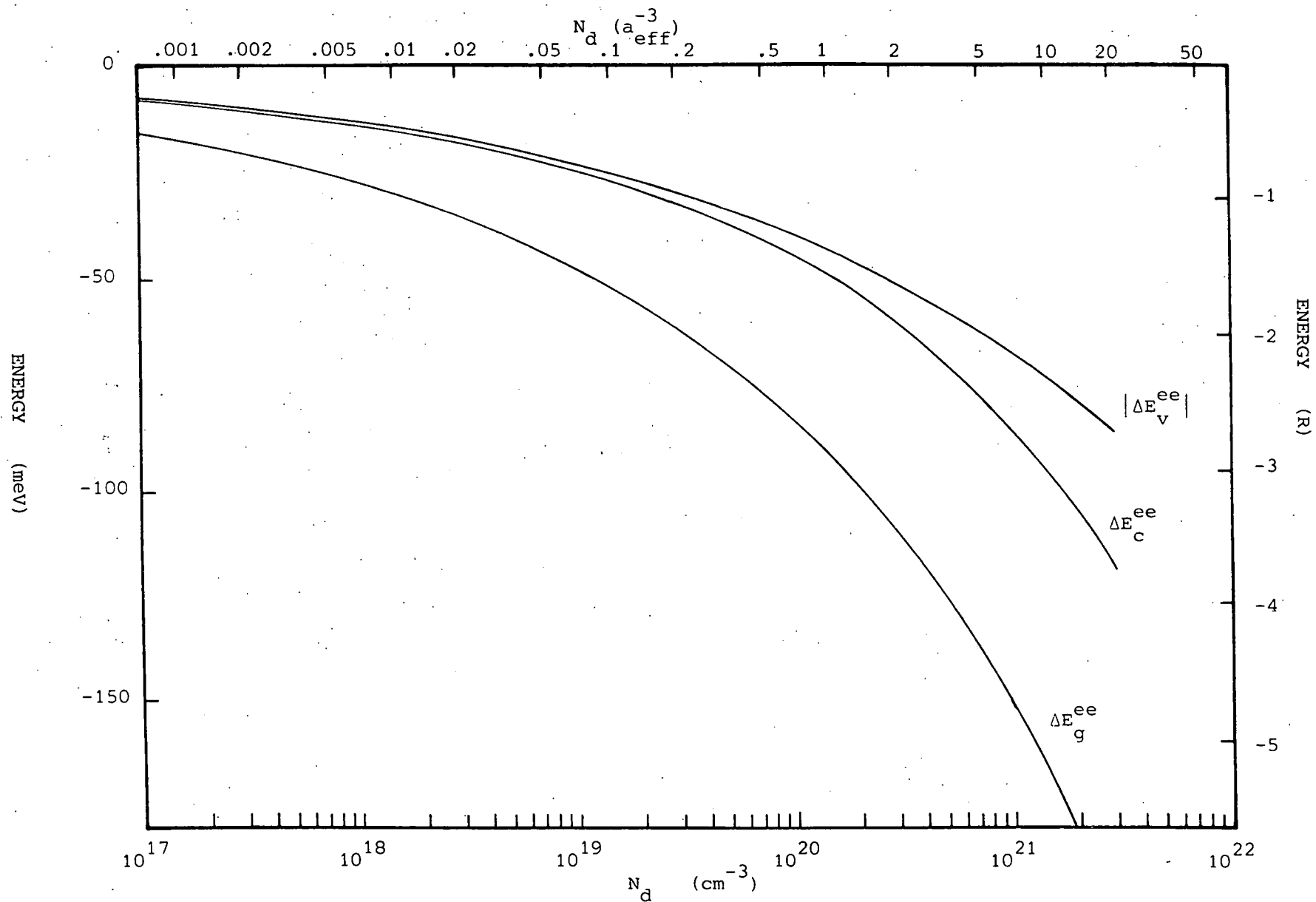
Fig 3.6   Change in the energy gap of silicon due to electron - electron
           Exchange at zero Kelvin.

CHAPTER 4

CHANGES IN THE BAND GAP DUE TO ELECTRON-IMPURITY SELF ENERGIES.

4.0   INTRODUCTION.

Electrons in an impure semiconductor not only interact with other electrons from the semiconductor bands as was shown in the last chapter, but also interact with ionised donor or acceptor impurity centres, lattice imperfections, clusters of impurities and phonons.   This chapter is confined to those scattering events that may be likened to the simple electron scattering off a positively charged impurity with coulombic potential.   The use of the word impurity then includes for example scattering from a simple positively charged lattice imperfection.   Here as in the last chapters the problem is treated by perturbation theory.   The electrons in the model are not allowed to bind themselves to any impurity but are thought of as interacting with all the impurities.   In the real semiconductor of course some electrons may be bound to individual impurities, or indeed to collections of impurities that form an abnormally deep potential well.   Two electron-impurity interactions are identified:

a)   those due to the binding of electrons by collections of impurities forming localized states in the band gap that are the subject of the calculations in the next chapter,

b)   those effects due to the electrons scattering from the many impurity sites that are dealt with in this chapter.

The extent to which this separation is justified is discussed in chapter 5, when it is considered whether or not the electron-impurity self energy has been included implicitly in, for example, calculations by Halperin and Lax (1966, 1967).

Returning to the self energy calculations these are subject to two limits of concentration beyond which they break down. The lowest being the Mott metal insulator transition below which the electrons would have to be considered bound to the impurity centres. And at high concentrations the point when there are sufficient impurities to violate the perturbation approximations. Within these limits the change in energy of the holes or electrons as a function of the impurity concentration may be approximated by two methods. Firstly by a Green's function formulation of the electron-impurity interaction an example of which is presented in section 4.4.1. Secondly by straight forward perturbation theory that is presented in section 4.4.2.

The former approach is performed in a similar way to the electron-electron interactions of chapter 2 and forms the more important part of this chapter. The major results of the derivation are similar to those of the electron-electron chapter. A series expansion of the Green's function in terms of the unperturbed Green's functions (section 4.1) that Edwards (1958, 1961, 1962) and Klauder (1961) developed in the form of a Dyson's equation (section 4.2). And a 'self energy' series that may be approximated and numerically evaluated to give a shift in the band edges. The major difference between this and the electron-electron interaction is that the impurities are assumed to be located at random but well defined sites throughout the host semiconductor lattice. The impurity potential may not then be taken as uniform throughout the structure. This interesting situation is dealt with by taking the spatial average over all possible impurity sites suggested by Kohn and Luttinger (1957) thereby deriving an average self energy (section 4.2). Section 4.3 deals with the important cancellation of the first order terms in the self energy expansions of this chapter and the last. The change in the resulting

average self energy may not represent the local change in the band energy due to the impurities very well, but is taken as a good representation of the average change in band position. These expressions are derived in section 4.4.1.

The perturbation derivation of the self energy in section 4.4.2 that is taken to second order is a more traditional approach and gives the same result as that derived in 4.4.1. To improve these approximations the more powerful Green's function derivation is more useful (Ghazali and Serre 1982, 1983). Indeed the quantitative discussion of the accuracy of the approximations given in sections 4.5 and 4.6 uses terms derived from the Green's function. In this thesis the simplest formulae derived are used (section 4.5) to obtain numerical results (Fig 4.1) and their range of validity for this electron impurity contribution to the band gap reduction in silicon.

4.1 FEYNMAN DIAGRAM REPRESENTATION OF THE PROBLEM.

It is convenient to outline the problem that confronts us in the electron-impurity calculations with the aid of Feynman diagrams. The use of Feynman diagrams for the impurity problem is not new. Edwards (1958), Langer and Vosko (1960) and Klauder (1961) were the first to publish diagrammatic representations of the problem. Mattuck (1976) gives a simple description of the problem and Mahan (1981) goes into some detail in his book. In the present work the coulombic interaction of the nth impurity with an electron is represented by the diagram

$$
\begin{array}{l}
yt' \\
x_1 t_1 \\
xt
\end{array} \Big| \cdots \cdots I_n \tag{410.01}
$$

where

$$
\begin{array}{l}
yt' \\
xt
\end{array} \Big|
$$
represent the unperturbed retarded Green's functions $G_+^0(xt, yt')$

I_n represents the nth ion

$| \cdots \cdots |$ represents the coulombic interaction $V(r) = V(r - R_j)$

The electron-impurity interaction is considered to be a static one where no energy is transferred to or by the impurity in the absence of phonons. This of course makes the electron-impurity problem simpler to cope with than its electron-electron counterpart due to the lack of summations over intermediate frequencies. In what follows the time and spacial co-ordinates are omitted for simplicity so that the Green's function expansion

for N impurities becomes

$$
\text{[diagram]} = \text{[diagram]} + \text{[diagram]} \cdots I_1 + \text{[diagram]} \cdots I_2 + \cdots + \text{[diagram]} \cdots I_N + \text{[diagram]} \begin{matrix} \cdots I_1 \\ \cdots I_1 \end{matrix} + \cdots
$$

$$
+ \text{[diagram]} \begin{matrix} \cdots I_N \\ \cdots I_N \end{matrix} + \cdots + \text{[diagram]} \begin{matrix} \cdots I_{j \neq i} \\ \cdots I_i \end{matrix} + \text{[diagram]} \begin{matrix} \cdots I_i \\ \cdots I_j \\ \cdots I_k \end{matrix} + \cdots \qquad (410.02)
$$

Since the electron gas surrounding the impurities may relax about the impurities, forming a screening cloud, each of the above coulombic interactions may be replaced by a screened interaction of the form calculated in chapter 2. Thus the coulombic interaction of the nth impurity with an electron in the Random Phase Approximation becomes

$$
\text{[diagram]} \begin{matrix} \text{RPA} \\ \vdots \vdots I \end{matrix} = \text{[diagram]} \cdots I + \text{[diagram]} \cdots I + \text{[diagram]} \cdots I + \qquad (410.03)
$$

Where diagrams that do not conserve momentum are included. Wolff (1962) has pointed out that subsequent averaging of the Green's function results in momentum being conserved at the averaged impurity scattering event. The proof of this will be left to the section 4.2.

As is evident from the large number of diagrams in the Green's function expansion it is a significant problem to approximate the series accurately. Not least since the impurities may be located in clusters or in pseudo-random locations in the host lattice. Edwards (1961, 1962) has considered ensemble ranging from complete spacial order to complete disorder. Intermediate states of order, for example clusters, are however more complex. In this chapter only the simpler calculation of an array of randomly located impurities is considered. With these provisors we proceed to calculate the Dyson's equations for electron-impurity interactions.

4.2 KOHN AND LUTTINGER AVERAGING LEADING TO DYSON'S EQUATION.

To develop Dyson's equation the wavevector expansion of the Green's function is first developed (as was done in chapter 2). For this the Fourier transform of the impurity potential

$$V(r) = \sum_{j}^{N} v(r - R_j)$$

(420.01a)

$$v(x) = \frac{e^2}{4\pi\epsilon\epsilon_r x}$$

where R_j are the N impurity locations, is required. For this the impurity density ρ_q is defined

$$\rho_q = \frac{1}{\Omega} \sum_{j}^{N} e^{iq \cdot R_j}$$

(420.01b)

where Ω is the crystal volume. The Fourier transform is then given by

$$V(r) = \int \rho_q^* W(q) e^{iq \cdot r} d^3q$$

(420.01c)

The wavevector expansion of the total Green's function involves interaction matrix elements of the form

$$W(nl, mk) = \int \phi_{nl}^*(r) V(r) \phi_{mk}(r) d^3r$$

$$= \int \int \phi_{nl}^*(r) e^{iq \cdot r} \phi_{mk}(r) d^3r \, W(q) \rho_q^* \, d^3q \quad (420.02)$$

where the $\phi_{nl}(r)$ are Bloch functions belong to the nth band. The overlap integral has been calculated in section 2.2.3 so the Green's function expansion (Eq. 410.02) in functional form becomes

$$G(nk, mq) = G^0(nk) \delta_{kq} \delta_{nm} + G^0(nk) W(nk, mq) G^0(mq) +$$

$$+ \frac{1}{\hbar} \sum_{n'l} G^0(nk) W(nk, n'l) G^0(n'l) W(n'l, mq) G^0(mq)$$

(420.03a)

$$+ \ldots \ldots$$

A self energy may be identified in this expression

$$G(nk,mq) = G^0(nk)\delta_{kq}\delta_{nm} + G^0(nk)\Sigma^1(nk,mq)G^0(mq) +$$

$$+ \frac{1}{\hbar} G^0(nk)\Sigma^2(nk,mq)G^0(mq) \qquad (420.03b)$$

where Σ^1 is the first order self energy and Σ^2 contains second order interactions. This (Eq. 420.03) is simply the wavevector equivalent expression to the Feynman diagrams in Eq. 410.02. Since momentum is not conserved the Green's function is expressed as a Kernel with the wavevector and band before scattering nk and those after mq. The ensemble averaged Green's function is then formed

$$\langle G(nk,mq) \rangle = \int\!\!\int\!\!\int .. \; G(nk,mq) \prod_i^N \frac{d^3R_i}{\Omega} \qquad (420.04)$$

where there are N independent integrals. This form of ensemble average, used initially by (Kohn and Luttinger 1957) has been shown to be the best approximation to all but a negligible number of arrangements of a completely random array of impurities (Landau & Lifshitz 1977). If the Green's function from Eq. 420.03 is substituted in Eq. 420.04, using Eq. 420.02 for the potential the ensemble averaged Green's function may be derived. For example the third term in Eq. 420.03, that corresponds to two electron scatterings from the impurities becomes

$$\langle \sum_l G^0(nk)W(nk,n'l)G^0(n'l)W(n'l,mq)G^0(mq) \rangle = \qquad (420.05)$$

$$\sum_l G^0(nk)\langle W(nk,n'l)W(n'l,mq) \rangle G^0(n'l)G^0(mq)$$

where the averaging has been taken inside the wavevector summations and the unperturbed Green's functions are invariant under the averaging procedure.

The averaged potential is now developed using Eq. 420.02

$$\langle W(nk,n'l)W(n'l,mq)\rangle = \iint I(k,l;k_1)^* I(l,q;k_2)\ W(k_1)W(k_2)$$

$$\langle \rho_{k_1}^* \rho_{k_2}^* \rangle\ d^3k_1\ d^3k_2 \qquad (420.06)$$

The overlap integrals of chapter 2 are used (Eq. 223.18)

$$I(nl,mk;q) = \int \phi_{nl}^*(r)\,e^{iq\cdot r}\phi_{mk}(r)\ d^3r$$

$$I^*I = \delta(q-k+1)\ \Lambda_{nm} \qquad (420.07)$$

It remains to derive the ensemble averaged impurity density in Eq. 420.06. Taking the impurity density defined in Eq. 420.01b and the averaging technique from Eq. 420.04 we find for example

$$\langle \rho_k \rangle = \frac{N}{\Omega}\ \delta(k)$$

$$\qquad (420.08)$$

$$\langle \rho_k \rho_q \rho_l \rho_j \rangle = \frac{N}{\Omega^4}\ \delta(k+q+l+j) + \frac{N(N-1)}{\Omega^4}\Big[\sum_{comb} \delta(k)\delta(q+l+j)$$

$$+ \sum_{comb} \delta(k+q)\delta(l+j)\Big] + \frac{N(N-1)(N-2)}{\Omega^4}\sum_{comb} \delta(k+q)\delta(l)\delta(j)$$

$$+ \frac{N(N-1)(N-2)(N-3)}{\Omega^4}(\delta(k)\delta(q)\delta(l)\delta(j))$$

where the summation is over all combinations (comb) of the wavevectors. The generalization of this series was first developed by Kohn and Luttinger (1957) and later extended by Edwards (1961, 1962) to situations that possess some order. But for large N in a random ensemble

$$\langle \rho_1 \rho_2 \ldots \rangle = \frac{N}{\Omega^N}\ \delta(\sum k_i) + \frac{N^2}{\Omega^N}\ (\sum_1^N \delta(\sum_i k_i)\delta(\sum_{j=l+1}^N k_j)) + \ldots$$

$$(420.09)$$

Using this expression for the ensemble averaged impurity density there are

two parts to the solution of Eq. 420.06. The first derives from

$$\frac{N}{\Omega^2}\delta(k+q)$$ (420.10a)

which corresponds to two electron scatterings form the same impurity or the second set of diagrams in Eq. 410.02. Whilst the second derives from

$$\frac{N(N-1)}{\Omega^2}\delta(k)\delta(q)$$ (420.10b)

which corresponds to two scatterings from different impurities. This second expression can be reproduced by a simple product of one electron scattering events of the form represented by the second term in Eq. 420.03 and does not then contribute to the irreducible self energy. However if the first of these is investigated the integrals over k_1 and k_2 give:

$$\langle W(nk,n'l)W(n'l,mq) \rangle = \frac{\Lambda_{n'n}(k,l)\delta_{nm}\delta(k-q)W(k-l)W(l-k)N}{\Omega^2}$$ (420.11)

Now replacing the summation over l by an integral

$$\frac{N}{\Omega^2}\sum_{l} \longrightarrow \frac{N_d}{(2\pi)^3}\int d^3l$$

$$\langle\frac{1}{\hbar}\sum_{n'l} G^0(nk)\ W(nk,n'l)G^0(n'l)W(n'l,mq)\ G^0(mq)\rangle =$$ (420.12)

$$\frac{N_d}{(2\pi)^3}\sum_{n'}\int \Lambda_{n'n}(k,l)\ \delta_{nm}\ \delta(k-q)\ W(k-l)\ W(l-k)$$
$$G^0(nk)\ G^0(n'l)\ G^0(mq)\ d^3l$$

where N_d is the impurity density. Interpreting this diagrammatically the impurity ions are replaced by crosses. Only 1/Nth of the diagrams (Eq. 410.02) have to be drawn since the different impurities are no longer distinguished. Representing the potentials in Eq. 420.12 by the screened

coulombic interactions shown in Eq. 410.03. Eq. 420.12 may be drawn
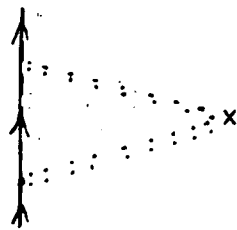
$$\text{(diagram)} \qquad (420.13)$$

Notice that the averaging procedure has resulted in the joining of the loose ends of the coulomb interactions in the un-averaged series and scaling each cross by the donor concentration N_d. This averaged impurity scattering conserves momentum (as in the equivalent electron-electron interaction). The electrons are not now seen as scattering off individual impurities, but rather from the whole ensemble of impurities. All the remaining terms in the average Green's function may be treated in a similar way. It is considerably easier to derive this series by joining the like ends of coulomb interactions of the un-averaged series (Eq. 410.02) directly and then interpreting the resulting diagrams. All the possible terms in the averaging of the impurity density are obtained for example the term representing Eq. 420.10b is the third diagram on the right hand side of the following expansion of Eq. 420.04
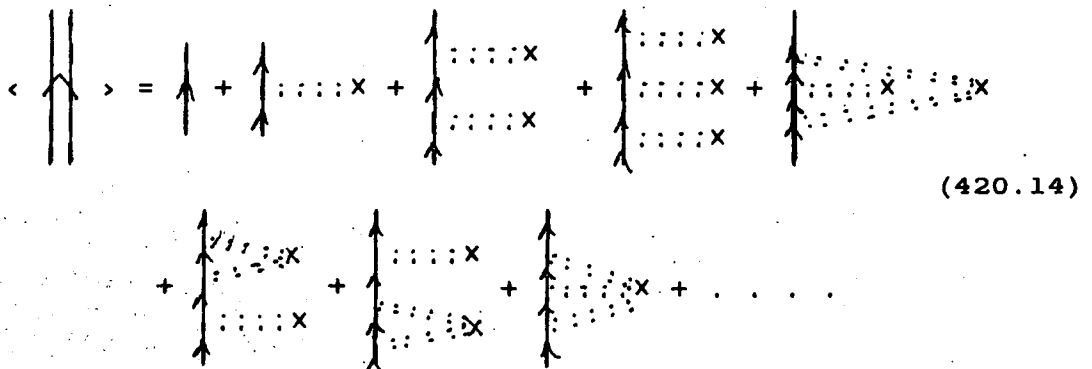
$$\text{(diagrams)} \qquad (420.14)$$

This set of diagrams is already much condensed from the diagrams shown in the last section however this may be condensed further into the abbreviated

form

$$\langle \text{ } \rangle = \text{ } + \left(\Sigma \right) \tag{420.15}$$

which is equivalent to Dyson's equation. The irreducible self energy diagram is defined by the series

$$\left(\Sigma \right) = | \ldots \times + \ldots \times + \ldots \times + \ldots \times$$

$$+ \ldots \times + \ldots \ldots \tag{420.16}$$

It is clear from the above diagrams that there are several important differences between the electron-electron and electron-impurity self energy expressions. The electron may for example interact with the same impurity many times without apparent change to the physical situation (see 3rd and 5th diagrams in Eq. 420.16). In the electron-electron example an electron would interact with the another electron only once, forming an electron hole pair or exciting a plasmon that at some later time could recombine (decay). Secondly an explicit averaging of the electron impurity interaction has been performed. In chapter 5 the fluctuations about this mean interaction are considered. The calculations in this chapter thus incorporate a rather crude but effective approximation to the real situation.

4.3 CANCELLATION OF THE FIRST ORDER TERMS.

At this point the implications of the first order term in Eq. 420.16 are considered

$$| : : : : \times \tag{430.01}$$

This is just the average of the electron-impurity interaction. It must have the same magnitude as the average electron-electron interaction Eq. 222.06

$$| : : : : \bigcirc\!\!\!\!\nearrow \tag{430.02}$$

but because of the opposite sign on the charge of the ionised donor impurities the interaction energy has the opposite sign. The two first order terms above then cancel, a result that was used previously in chapter 2 and chapter 3. This cancellation only occurs for the first order terms since, as Wolff (1962) points out only in this term are both the electron-electron and electron-impurity interactions static. The following simplified expression for the self energy remains.

$$\left(\Sigma\right) \quad = \quad | | \begin{array}{c}\!\! \end{array} \times \ + \ | | : : : \times \ + \ . \ . \ . \ . \tag{430.03}$$

This cancellation is of course only prevalent in the macroscopic system. When looking at the microscopic system there would be some regions where the impurity concentration was above the average. In these areas for an n-type semiconductor there would be a net positive, electron attracting field. There would also be areas where the impurities were few, with the associated effective negative charge. These fluctations in the average impurity potential are dealt with in detail in chapter 5.

4.4   APPROXIMATIONS TO THE SELF ENERGY.

In this section two self energy expressions are derived. The first, derived from the Green's function of the last sections, is detailed in section 4.4.1.   The second from the more conventional perturbation series is presented in section 4.4.2.   This latter derivation is included to outline the essential differences between the two approaches, although both produce the same result to the order of approximation chosen.   The Green's function formulation is by far the most amenable to improving the accuracy of the calculation.

4.4.1   Green's function formulation.

As in the electron-electron calculations to sum the whole series of diagrams would, even if such a sum were possible, be a waste of time considering the approximations already made in deriving the model.   It is quite adequate to sum only the most important diagrams.   Wolff (1962) considers the second order term

$$ \qquad\qquad\qquad\qquad\qquad\qquad\qquad\qquad\qquad (441.01) $$

and suggests the use of the partial sum

$$ \qquad\qquad\qquad\qquad\qquad\qquad\qquad\qquad\qquad (441.02) $$

Mahan (1981) in his book considers at length the series

$$\Sigma = \cdots\cdots\mathrm{x} + \cdots\cdots\mathrm{x} + \cdots\cdots\mathrm{x} + \cdots\cdots\mathrm{x} + \ldots \qquad (441.03)$$

corresponding to multiple scattering from the same impurity. Which he uses in the limit of low impurity concentration. More recently Ghazali and Serre (1982, 1983) use an iterative calculation to obtain the self energy based on Klauders's (1961) theory using the series

$$\Sigma = \cdots + \cdots + \cdots + \cdots + \ldots$$

vertex corrections

$$= \cdots \qquad (441.04)$$

They also include a simple form for the electron-electron self energy in their calculation. However they only use the simplest Thomas Fermi approximation (232.09) to the electron screening. In this thesis the simplest approximation to the self energy is used

$$\qquad (441.05.)$$

whilst indicating in section 4.6 the likely range of accuracy of this approximation. The diagram may be translated as

$$\hbar\Sigma(n;k,\omega) = \frac{N_d}{\hbar(2\pi)^3} \sum_m \int G^0(n;l,\omega) \ |W(l-k,\omega)|^2 \ \Lambda_{nm}(k,l) d^3l$$

$$\qquad (441.06)$$

This expression, as will be shown in the next section, may be derived from second order perturbation theory and has been used by several authors (Sernelius and Berggren 1981, Berggren and Sernelius 1981, Wolff 1962).

To conclude this section one of the more important higher order terms in the self energy expansion is derived for later use. The fourth order term that Wolff believes to give the most important correction to the above approximation is chosen

$$(441.07)$$

This diagram comes from the fourth term in the ensemble averaged self energy Eq. 420.16 and corresponds as shown above to two impurity scattering events. Translated for the simpler case ignoring the inter-band coupling, by dropping the summation over m, gives a contribution to the self energy of

$$\hbar\Delta\Sigma(k',\omega) = \frac{N_d}{\hbar^3 (2\pi)^6} \iint G^0(q,\omega) G^0(k'-q-k,\omega) G^0(k,\omega)$$

$$W(k'-q,\omega)^2 W(k'-k,\omega)^2 d^3q\ d^3k \qquad (441.08)$$

Where it should be noted that even in this simple model omitting the band indices the integral

$$\frac{N_d^2}{(2\pi)^6} \left(\frac{e^2}{\epsilon\epsilon_r}\right)^4 \left(\frac{2m}{\hbar^2}\right)^3 \iiiint \left(\frac{1}{q^2+\kappa^2}\right)^2 \left(\frac{1}{k^2+\kappa^2}\right)^2 \qquad (441.09)$$

$$\frac{\sin\gamma\ \sin\alpha}{q^2+k^2-2qk(\cos\alpha\cos\gamma + \sin\alpha\sin\gamma\cos(\delta-\beta))}\ d\delta d\beta d\alpha d\gamma dkdq$$

where the spherical polar angles defining k and q are (α,β) and (γ,δ) is not straight forward. Wolff uses a simple method of approximating such complex diagrams so that for each of the four coulomb interactions a factor of $e^2/\epsilon\epsilon_r\kappa^2$ is introduced, each of the three energy denominators introduce a factor of κ^2/m, whilst the cut off in the coulomb matrix element give a factor of κ^3 from the integrations. Thus the above term is proportional to

$$N_d^2 \left(\frac{e^2}{\epsilon\epsilon_r\kappa^2}\right)^4 \left(\frac{m}{\kappa^2}\right)^3 \left(\kappa^3\right) = m^3 \left(\frac{e^2}{\epsilon\epsilon_r}\right)^4 \frac{N_d^2}{\kappa^8}$$

This indicates that the perturbation expansion breaks down for a high

concentration at which this term becomes the same size as the second order term (Eq. 441.05)

$$\frac{\Sigma^4}{(\Sigma^2)^2} = m^2 \left(\frac{e^2}{\epsilon \epsilon_r}\right)^2 \frac{N_d}{\kappa^5}$$

since the Thomas Fermi wavevector κ is proportional to $N_d^{1/6}$. A more serious limitation will be encountered at finite temperature (chapter 7) when the concentration dependence of the Thomas Fermi wavevector changes to $N_d^{-1/2}$ for non-degenerate silicon. When this happens the perturbation series fails at low concentrations.

4.4.2   The conventional second order perturbation series.

The principle objective of this section is to point out the essential differences between the conventional perturbation expansion and the Green's function formulation that was considered in the last section. The latter gives a far more precise definition of the electron-impurity self energy, however the former, being grounded in elementary quantum mechanics, gives perhaps a better introduction to the physical processes. In essence one impurity in the ensemble is considered in isolation from the others that are supposed to form a uniform background positive charge. Using its potential as a perturbation on the hamiltonian of the host lattice its effect upon the energy of the surrounding electrons and holes is estimated.   Having obtained the magnitude of this effect it is multiplied by the number of impurities in the solid to obtain the effect of all the impurities.   Inherent in the derivation is the assumption that the impurities are randomly located in the solid since were they placed on a lattice the wavefunctions would be re-enforced coherently by neighbouring scattering centres so that one impurity could not be treated in isolation.

Provided that the impurity potential V(r) is a small perturbation on the host semiconductors hamiltonian H^0 the total hamiltonian is written

$$H = H^0 + V(r) \qquad\qquad (442.01)$$

The unperturbed wavefunctions are taken as plane waves throughout this section in order to reduce the complexity of the expressions though Bloch functions could equally well be used. The perturbed wavefunctions $\psi_k(r)$ and eigenvalues E_k are given by solving

$$H \, \psi_k(r) = (H^0 + V(r))\psi_k(r) = E_k \, \psi_k \qquad\qquad (442.02)$$

From conventional perturbation theory (see for example Landau and Lifshitz 1977 or Schiff 1968) the perturbed energy may be expressed as a series

$$E_k = E_k^0 + E_k^1 + E_k^2 + E_k^3 + \ldots \ldots \qquad\qquad (442.03)$$

Where the superscript denotes the order of smallness of the terms. The first order term, that is just the average potential, must cancel with the average electron-electron energy (see section 4.3). The change in the eigenvalues, and hence the band edges, is then given by the sum of second and higher order terms. The second order term is given by

$$E_k^2 = \sum_q{}' \frac{|M_{k,q}|^2}{(E_k^0 - E_q^0)} \qquad\qquad (442.04)$$

The matrix elements $M_{k,q}$ will be defined later and the eigenvalues E_k are for the moment supposed to form a discrete set. The prime on the summation means that the term when k equals q is omitted. For the third order term

$$E_k^3 = \sum_q{}' \sum_1 {}' \frac{M_{k,q} M_{q,1} M_{1,j}}{\epsilon_{qk}^0 \epsilon_{1k}^0} - M_{k,k} \sum_q{}' \frac{|M_{k,q}|^2}{\epsilon_{qk}^0{}^2} \qquad\qquad (442.05)$$

$$\epsilon_{qk} = \frac{\hbar q^2}{2m} - \frac{\hbar k^2}{2m}$$

The matrix elements are of the form

$$M_{k,q} = \langle k|V|q \rangle = \int \psi_k^*(r) V(r) \psi_q(r) \ d^3r \qquad (442.06)$$

where $\psi_k(r)$ are taken as plane waves. Were they Bloch waves the overlap integral would be dealt with as in chapter 2. Writing the potential as a fourier expansion in W(q)

$$V(r) = \int W(q) \ e^{iq \cdot r} \ d^3q$$

so that

$$M_{k,q} = \frac{1}{\Omega^2} \int e^{-ik \cdot r} \int W(l) \ e^{il \cdot r} \ d^3l \ e^{iq \cdot r} \ d^3r$$

$$= \frac{1}{\Omega^2} \int W(l) \int e^{i(l+q-k) \cdot r} \ d^3r \ d^3l$$

$$= \frac{1}{\Omega} \int W(l) \ \delta_{l,k-q} \ d^3l = \frac{1}{\Omega} W(k-q) \qquad (442.07)$$

where Ω is the volume. Replacing the summation by an integral in the second order term (Eq. 442.04) we get

$$E_k^2 = \frac{1}{\Omega(2\pi)^3} \int \frac{|W(k-q)|^2}{\epsilon^0(k) - \epsilon^0(k-q)} \ d^3q \qquad (442.08)$$

where W(q) must be small for q equal to zero since the k equal q term is effectively included in the integral whilst omitted explicitly from the summation in Eq. 442.04. This must be multiplied by the number of impurities to obtain the effect of all the impurities on the eigenstates.

$$E_k^2 = \frac{N_d}{(2\pi)^3} \int \frac{|W(k-q)|^2}{\epsilon^0(k) - \epsilon^0(k-q)} \ d^3q \qquad (442.09)$$

Where N_d is the impurity concentration. This has the same form as the second order term of the Green's function expansion derived in the last section Eq. 441.06.

At this point it becomes clear that to represent the situation correctly the screening effect that the many electrons in the conduction

band have upon the impurity potential has to be included. In the Thomas

Fermi approximation the unscreened coulombic potential

$$V(r) = \frac{e^2}{4\pi\epsilon\,\epsilon_r r} \qquad\qquad (442.10)$$

Is replaced by the Thomas Fermi screened potential that is often use in the

electron-impurity problem (see for example Chapter 5, Ghazali and Serre

(1982, 1983), Mahan (1981)). The screened potential is

$$V(r) = \frac{e^2}{4\pi\epsilon\,\epsilon_r r}\, e^{-\kappa r} \qquad\qquad (442.11)$$

Where the damping factor κ is the inverse Thomas Fermi screening length

$$\kappa^2 = 4\left(\frac{3}{\pi}\right)^{1/3}\left(\frac{N_d^{1/3}}{a_{eff}}\right)\, M_c^{3/2} \qquad\qquad (442.12)$$

where the symbols have their usual meaning (see Appendix A). The Fourier

Transform of this potential

$$W(q) = \frac{e^2}{\epsilon\,\epsilon_r}\, \frac{1}{(q^2 + \kappa^2)} \qquad\qquad (442.13)$$

Is the static, small q version of the screened potential derived in chapter

2 in the plasmon pole approximation. Substitution of this in Eq. 442.09

results in an integral that may be solved analytically to give

$$\Delta E_c^{ei}(k_i) = -\frac{e^2\, N_d}{a_{eff}\,\epsilon\,\epsilon_r\,\kappa^3} \qquad\qquad (442.14a)$$

This is the second order perturbation shift in the energy of conduction

band states at the bottom of one of the six valleys due to the electron-

impurity interaction in the Thomas Fermi approximation. A similar shift,

but of opposite sign, exists for valence band states so that the total

change in the band gap due to electron-impurity interactions in the Thomas

4.5   CALCULATION OF THE ELECTRON-IMPURITY SELF ENERGIES IN SILICON.

As with the calculations of the preceding chapter the shift in the band edges is given by the real part of the electron-impurity self energy (c.f. Eq. 240.06)

$$\Delta E_n^{ei}(k) = \hbar Re(\Sigma^{ei}(n;k,\omega_{nk}^0)) \qquad (450.01a)$$

where Σ^{ei} is the ensemble averaged self energy, as outlined above. In the above ω_{nk}^0 is the unperturbed energy or in the spherical band approximation

$$\omega_{nk}^0 = \frac{\hbar q^2}{2m_n} \qquad (450.01b)$$

with m_n the effective mass for the band n. The change in the band gap due to the electron-impurity self energy is given by

$$\Delta E_{eg}^{ei} = \Delta E_C^{ei}(k_i) - \Delta E_v^{ei}(0) \qquad (450.02)$$

where the self energy is defined by (see Eq. 441.06)

$$\hbar \Sigma^{ei}(n;k,\omega) = \frac{N_d}{\hbar(2\pi)^3} \sum_m \int G^0(n;l,\omega)|W(l-k,\omega)|^2 \Lambda_{nm}(k,l)d^3l \qquad (450.03a)$$

with unperturbed Green's function

$$G^0(n;k,\omega) = \frac{1}{(\omega - \omega_{nk}^0 + i\delta sgn(\omega_{nk}^0 - \omega_f))} \qquad (450.03b)$$

the approximation to the screened interaction $W(q,\omega)$ is given by

$$W(q,\omega) = e^2/\epsilon\epsilon_r q^2 \epsilon(q,\omega) \qquad (450.03c)$$

with $\epsilon(q,\omega)$ given by the plasmon pole approximation to the electron dielectric function (Eq. 240.07c)

$$\epsilon^{-1}(q,\omega) = 1 \left(\frac{\omega_1^2}{(\omega_1(q) - i0)^2 - \omega^2} \right) \qquad (450.03d)$$

where the plasmon dispersion relationship $\omega_1(q)$, the plasma frequency ω_p

and the Lamda function Λ_{nm} are also defined in Eq. 240.07.

There is a considerable saving in the computation of the electron-impurity band edges over the electron-electron calculations in previous chapters. In the first place the intrinsic electron-impurity interaction is non-existent by definition. Thus no subtraction of intrinsic self energies is required. In the second placed there is no frequency integral, the ensemble averaged electron-impurity interaction being static. Finally the denominator of both conduction and valence expressions are the only band dependent variables. Thus from Eq. 450.01, 450.03 and the energy differences (Eq. 320.04 and Eq. 330.05b)

$$\Delta E_v(k) = - \frac{m_H + m_L}{2m_{de}} \Delta E_C^{ei}(k) \qquad (450.04)$$

as was shown by Berggren and Sernelius 1981, we can reduce Eq 450.02 to one integration.

$$\Delta E_{eg}^{ei} = (1 + \frac{m_H + m_L}{2m_{de}}) \frac{N_d}{\hbar(2\pi)^3} \int \frac{|W(q,\omega_{cO}^0)|^2}{(\omega_{cO}^0 - \omega_{cq}^0)} 4\pi q^2 \, dq \qquad (450.05)$$

Substituting for the screened potential and for the energies in the denominator this becomes

$$\Delta E_{eg}^{ei} = - (1 + \frac{m_H + m_L}{2m_{de}}) \frac{4N_d e^2}{a_{eff}\epsilon\epsilon_r} \frac{1}{k_f^3}$$

$$\int_0^\infty (\frac{1 + \alpha(q/k_f)^2}{(\kappa/k_f)^2 + (q/k_f)^2 + \alpha(q/k_f)^4})^2 \, d(q/k_f)$$

$$\alpha = \frac{3}{4} \frac{m_{op}}{m_{de}} = 0.5951 \qquad (450.06)$$

The integration was carried out on the IBM 370 computer using the NAG library routine D01AJF. Graphs of the results are presented in Fig 4.1.
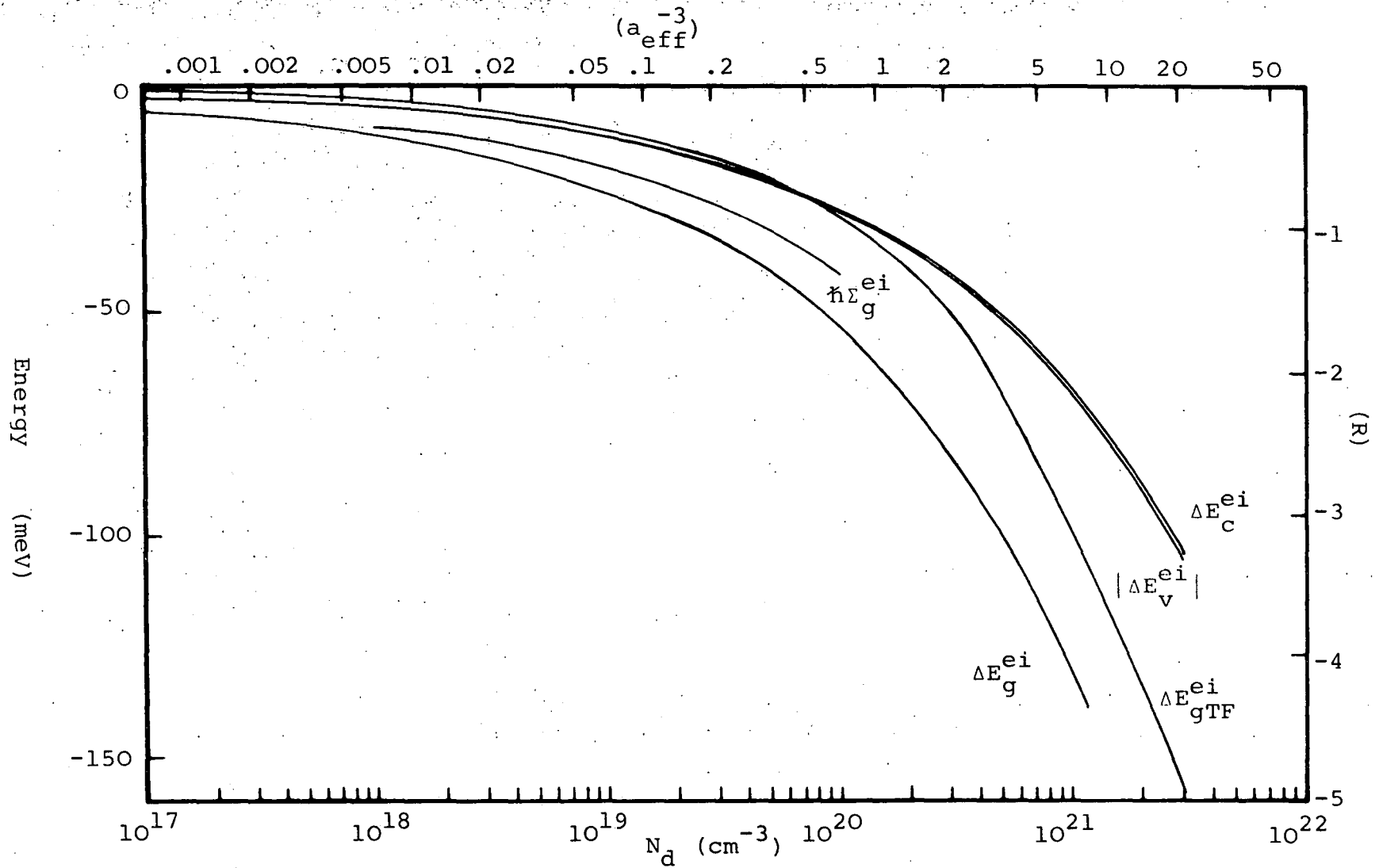
Fig 4.1   Zero temperature change in the electron-impurity self energy of the conduction band (ΔE_c^{ei}), valence band $(|\Delta E_v^{ei}|)$ and band gap in the plasmon pole approximation and the Thomas Fermi approximation. $(\hbar\Sigma_g^{ei})$ from Berggren et al 1981.

4.6   SUMMARY AND DISCUSSION OF RESULTS.

In this chapter the ensemble averaged electron-impurity self energy has been calculated using the ensemble averaged Green's function (Eq. 420.04)

$$\langle \Sigma(nk,mq) \rangle = \int\int\int .. \Sigma(nk,mq) \prod_i^N \frac{d^3R_i}{\Omega}$$

where n and m indicate the band and k and q are wavevectors. This has been found to provide a convenient means of averaging the effect of N randomly sited impurities in the semiconductor, volume Ω. This ensemble averaged total Green's function may conveniently be expressed in terms of an ensemble averaged self energy (Σ) in the form of Dyson's equation (Eq. 420.15)

$$(420.15)$$

The ensemble averaged electron-impurity self energy has been found to be described to second order by the expression (Eq. 441.06)

$$\hbar\Sigma(n;k,\omega) = \frac{N_d}{\hbar(2\pi)^3} \sum_m \int G^0(n;l,\omega) \ |W(l-k,\omega)|^2 \ \Lambda_{nm}(k,l) d^3l$$

where G^0 is the unperturbed Green's function. $W(q,\omega)$ represents the screened electron-impurity interaction (in this thesis, the plasmon pole approximation section 2.3.2) and Λ_{nm} represents the coupling between bands n and m. The intrinsic semiconductor has no electron-impurity interaction so that the change in electron-impurity self energy due to the presence of the positively charged ionised impurities is given by the real part of this

self energy (Eq. 450.01a)

$$\Delta E_n^{ei}(k) = \hbar Re(\Sigma^{ei}(n;k,\omega_{nk}^0))$$

This represents the change in the energy of the band n due to the electron-impurity interaction. The change in the band gap due to these interactions is given by the difference between the change in energy of the bottom of one of the six conduction band valleys ($\Delta E_c^{ei}(0)$) and the change in energy of the top of the valence band ($\Delta E_v^{ei}(0)$, Eq. 450.02)

$$\Delta E_{eg}^{ei} = \Delta E_c^{ei}(k_i) - \Delta E_v^{ei}(0)$$

this is given by (Eq. 450.05)

$$\Delta E_{eg}^{ei} = (1 + \frac{m_H + m_L}{2m_{de}})\frac{N_d}{\hbar(2\pi)^3} \int \frac{|W(q,\omega_{co}^0)|^2}{(\omega_{co}^0 - \omega_{cq}^0)}4\pi q^2 \, dq$$

From the results drawn in Fig 4.1 it can be seen that the electron-impurity interactions result in a band gap narrowing which is numerically smaller than the corresponding reduction due to electron-electron interactions (Fig 3.6). These results are compared to the results obtained by Berggren and Sernelius (1981) who use the Lindhard dielectric function and are also plotted in Fig 4.1. It can be seen that the present results based on the plasmon pole approximation agree within a few meV with these results based on the full Lindhard function. The Lindhard formula may then be approximated by the plasmon pole approximation for the electron-impurity interactions as well as the electron-electron interactions of the previous chapter. This justifies the extension of the plasmon pole calculations to finite temperature in the calculations of chapter 7.

Also plotted in Fig 4.1 are the band gap narrowing results based on the Thomas Fermi screened potential (Eq. 442.14) and used in

chapter 5 (ΔE^{el}_{gTF}). Calculated using the self energy expression Eq. 442.09 where the coupling between the valence bands is ignored, using the average valence band effective mass (Eq. 210.04)

$$m_v = (m_L^{3/2} + m_H^{3/2})^{2/3} m_o = 0.55 m_o$$

These results (ΔE^{el}_{gTF}) plotted in Fig 4.1 show the Thomas Fermi approximation to underestimate the band gap reduction, particularly at low concentrations where plane waves do not represent the electron wavefunctions adequately.

To compare these results with the recent calculations of Ghazali and Serre mentioned in section 4.4.1 a contribution due to the electron-electron interaction needs to be added. In their analysis they solve for the total Green's function (equivalent to Eq. 420.15) using a sum of the electron-impurity (Eq. 441.04) and electron-electron (Σ_{xc} in Ghazali and Serre 1983) self energies. Whilst their calculation is simplified by using the simple Thomas Fermi screened interaction and a very simple expression for the electron-electron interaction they improve the estimation of the total Green's function by taking the series to infinite order. Thus comparison between the two calculations are difficult since the Σ_{xc} term can not just be subtracted. However the plasmon pole change in the conduction band electron-impurity self energy from Fig 4.1 at $N_d = 2$ (a_{eff}^{-3}) is about 1.5 (R) which is the energy of the band bottom shown in Fig 1 of Ghazali and Serre (1983). It is clear from the comparison between Thomas Fermi and plasmon pole results that there is a large discrepancy between results from these interaction. An improvement to the calculations of Ghazali and Serre would be to use the plasmon pole approximation to the electron dielectric function whenever appropriate in preference to the Thomas Fermi results that they use.

The plasmon pole self energies plotted in Fig 4.1 are then valid until the perturbation approximation breaks down at concentrations where the impurity separation ($N_d^{-1/3}$) approaches silicon's atomic spacing. This occurs above donor concentrations of 10^{21} cm^{-3} (see Fig 2.4), where $N_d^{-1/3}$ approaches d ($5.4.10^{-8}$ cm^{-3}) the lattice constant. At low concentrations the limiting concentration is the Mott metal insulator transition that occurs at about 6.10^{18} cm^{-3} at zero temperature. In the region of this transition a modification of Ghazali and Serre's (1982, 1983) using the plasmon pole approximation could be used to describe the merging of the impurity band.

CHAPTER 5

BAND TAIL DUE TO RANDOM IMPURITY LOCATION.

The effects so far considered concerning electron-impurity interactions have relied on a complete cancellation of the first order electron-electron self energies with the first order electron-impurity interactions. From elementary considerations this cancellation may be seen to be maintained in the bulk semiconductor where the net number of electrons equals the net number of ionised centres. However in microscopic regions in the semiconductor this cancellation may be imperfect. In regions of very high donor concentration a net positive charge, or attractive potential exists. Whilst in correspondingly low concentration regions the reverse will be true, so that the macroscopic balance is maintained. Fig 5.1 summarizes these two fundamentally different electron-impurity effects. The upper diagram indicates the lowering of the conduction band and the raising of the valence band due to the change in self energy calculated in the previous chapter. In the lower diagrams the semiconductor is divided into a number of different cells. Although the average impurity concentration in all the cells is fixed the sample concentration in each cell may fluctuate about this mean. In cells with high donor concentrations extra electrons are attracted into states with below average energy formed by these potential wells. Conversely cells with low donor concentrations introduce states above the average valence band energy. Close to the average band edge these states will be more numerous since more cells with the appropriate concentration exist, whilst states deeper in the band gap will be less numerous. The net effect is to introduce a tail on the density of states of each band. Furthermore states deep in the band tail will be highly localized since the cells with the appropriate concentration of impurities will be few and far between. The

E_c

ΔE_c^{ei}

E_c'

E_v'

ΔE_v^{ei}

E_v
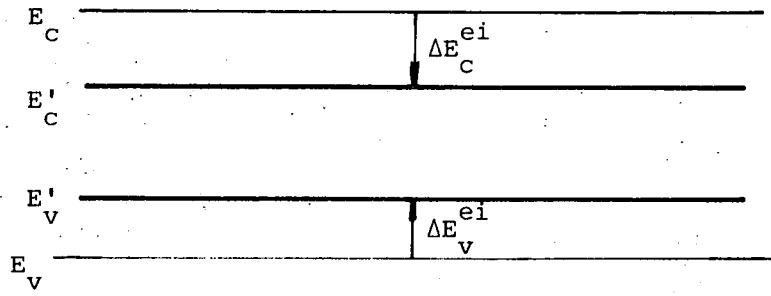
Fig 5.1 a) Change in the band edges due to the average electron
            -impurity interaction.

$N_d(x)$

x

E_c'

$E^{\frac{1}{2}}$

density
of
states.

tail

E_v'

E
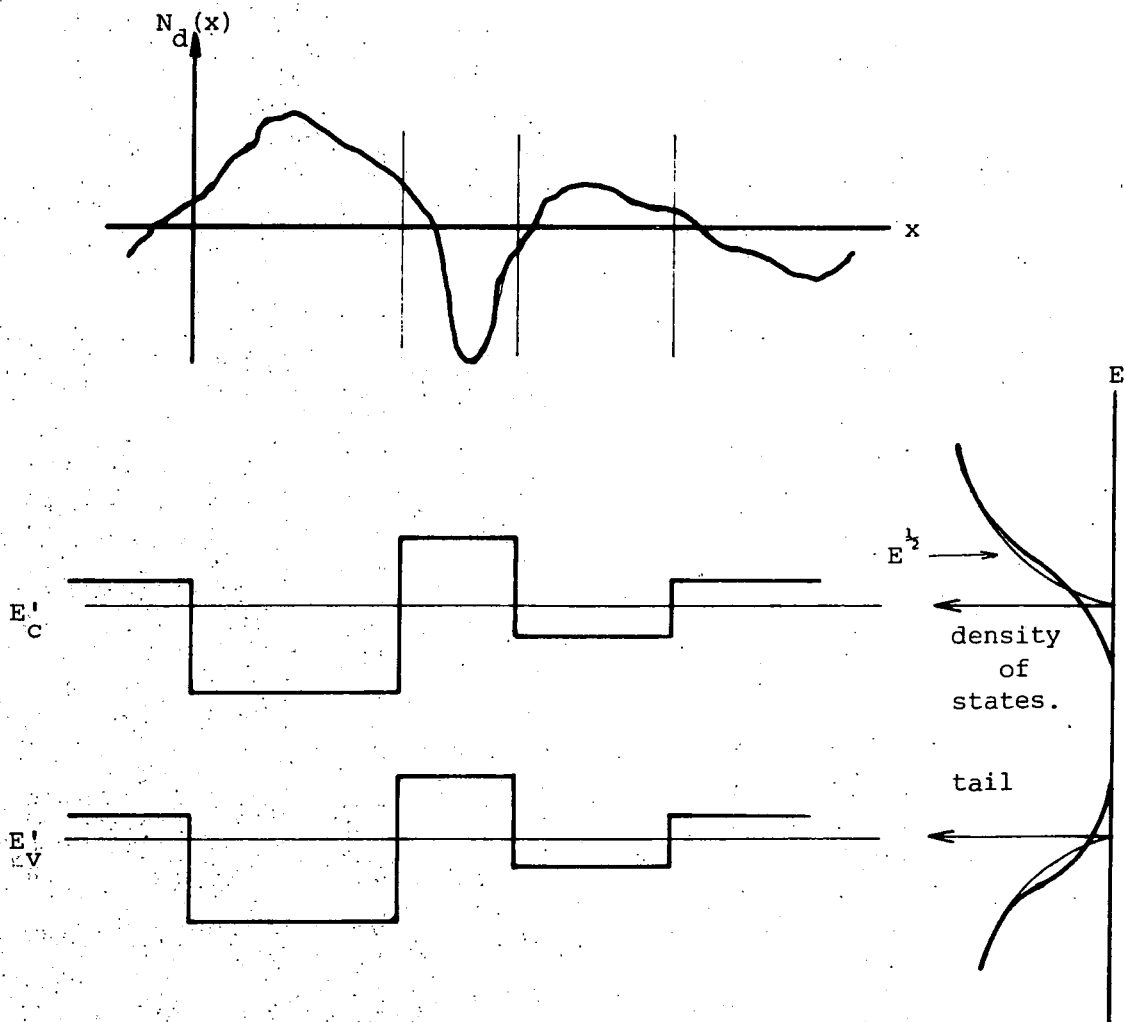
Fig 5.1 b) Local fluctuations in the impurity concentration $(N_d(x))$
            form potential wells in which electron states exist,
            forming a tail on the density of states of both the
            conduction and valence bands.

previous calculations have then to be supplemented in order to further improve the description of heavily doped silicon.

Although electrons in the localized states may contribute to conduction by Hopping, their neighbouring extended states higher in the bands have a higher mobility. A distinction is made between three physical band gaps to do justice in accounting for experimental observations:

a)   First the gap associated with the exitation of electrons from the top of the valence band to the lowest unoccupied state in the conduction band.

b)   Secondly the so called mobility gap or that between the top of the valence band (where the hole states are extended and allow free movement of holes through the crystal) and the lowest extended state in the conduction band.

c)   Finally the minimum energy gap between localized states in valence and those in the conduction band tails.

The studies of this chapter span the localized states deep in the band tail to the extended states in the parabolic band itself. The aim is to find a unified theory from which to calculate the density of states of the band for all energies through localized to extended states. To this end in section 5.1 the localized states deep in the tail are considered using a method frequently used to describe these states in semiconductor lasers (see for example Hwang 1970, Casey and Panish 1979) due to Halperin and Lax (1966, 1967, 1973). The interpretation of Halperin and Lax's results relating to the precise correspondence between band tail and host band is different from the interpretation hither to given. The present interpretation is supported by a study of a quantum mechanical technique due to Lloyd and Best (1975) in section 5.2. that provides similar results.

Numerical results of the calculations for silicon in the spirit of these two techniques are present in sections 5.1.4 and 5.2.6.

5.1 HALPERIN AND LAX APPROACH

Halperin and Lax (1966, 1967, 1973) have produced a formulation where the electron wavefunctions ($\psi_i(x)$) of a given eigenvalue (E_i) deep in the band tail are assumed to have the same shape ($\psi_i(x) \approx f(x-x_o)$) and hence the same kinetic energy (θ). Their argument for the existence of these typical wavefunctions is based on the following simple thought experiment:

Suppose the wavefunction for a state deep in the band tail were spread out over a large volume, it would then have a small kinetic energy of localization. The probability of finding the excess concentration of impurities over the large volume required to support such a large wavefunction would be very small. Conversely supposing the wavefunction to be excessively localized and hence having a very high kinetic energy of localization. The probability of finding the very large excess concentration of impurities, whose potential energy is required to balance this high kinetic energy, will be small.

An optimum shape of wavefunction is then expected that is not too large and not too small, with a corresponding optimum kinetic energy of localization. To find the density of states deep in the tail, Halperin and Lax then compute the probability of finding the necessary magnitude of impurity fluctuation capable of supporting these optimum wavefunctions.

Halperin and Lax modelled the impurity centres of charge $Z_a e$ by a Thomas Fermi screened potential

$$v(x-x_i) = -Z_a \frac{e^2}{4\pi\epsilon_r |x-x_i|} \exp(-\kappa|x-x_i|) \qquad (510.01)$$

where x_i are the impurity locations. It is the position dependent potential fluctuation about the mean value that is required $(V(x))$. If the distribution of impurities within the semiconductor $(n(z))$ is taken to be described by $n(z)$

$$n(z) = \sum_i \delta(z - x_i) \qquad (510.02)$$

Then the position dependent fluctuation of the total impurity potential $(V(x))$ about its mean value for the crystal $(\langle V \rangle)$ is given by

$$V(x) = \sum_i v(x-x_i) - \langle \sum_i v(x-x_i) \rangle = \int v(x-z)(n(z) - N) \, dz$$

$$(510.03)$$

with N the average concentration of impurities. They proceed by estimating the size of the typical wavefunction $(f(x-x_o))$ trapped in a particularly deep potential well at x_o and its energy $(E(x_o))$ by a variational calculation. The energy of this state may be written

$$E(x_o) = \int f(x-x_o) \, H \, f(x-x_o) \, dx = \theta + Vs(x_o)$$

$$= \int f(x-x_o) \, T \, f(x-x_o) \, dx + \int f(x-x_o)^2 V(x) \, dx$$

$$(510.04)$$

this has been split into kinetic (θ) and potential (Vs) parts. Since the eigenfunction $(f(x-x_o))$ is assumed to be short range the potential $Vs(x_o)$ acts as a local average for the potential $V(x)$ that varies with x_o. At various places within the crystal Vs will have an unusually large negative value, corresponding to high accumulations of impurity centres. Halperin and Lax then compute the number of these minima in the potential energy

(Vs) which would support the 'typical' wavefunctions and hence also the density of states ($\rho_f(E)$).

Given the premise that the density of states in the tail falls rapidly as the low energy tail is traversed. Halperin and Lax claim that optimization of f(x) corresponds to maximizing the density of states. They justified this by the following simple argument:

The variational estimate of the energy (Eq 510.04) is bound by definition to over estimate the true ground state energy unless the correct wavefunction were chosen. Thus the density of states ascribed to this estimate of the energy must at worst be an under estimate. The best procedure for the calculation of the actual density is then to maximize the density of states.

In fact Halperin and Lax do not maximize the whole density of states expression, as will be detailed in the next section, but take some care over a thorough evaluation of the errors involved in arriving at their optimum density of states deriving the limits for the validity of their arguments, which are dealt with in section 5.2.4.

5.1.1   Calculation of the density of states.

To calculate the density of states deep within the tail. Halperin and Lax postulate a close one-to-one correspondence between local minima in the potential Vs(y) and the energies of eigenstates, in the vicinity of E. Thus the density of states must depend upon the probability densities that the potential energy Vs(y) takes the value ($E-\theta$), whilst at the same time having zero gradient simultaneously with the double differential being positive (conditions that specify a minima in Vs(y)). Halperin and Lax's minimum counting method (a three dimensional

generalization of that used by Rice (1954 pp 209-213) in random noise problems) reduces the expression for the density of states to

$$\rho_f(E) = \frac{\sigma_1 \sigma_2 \sigma_3 (\theta - E)^3}{(2\pi)^2 \xi^2 \sigma_0^7} \exp\left(- \frac{(\theta - E)^2}{2\xi \sigma_0^2} \right) \qquad (511.01)$$

where the variances of the distribution of the potential (Vs(y)) at a random point y about a mean value of E$-\theta$ is

$$\xi \sigma_0^2 = \langle Vs(y)^2 \rangle - \langle Vs(y) \rangle^2$$
$$= \int f(x-y)^2 f(x'-y)^2 \langle V(x)V(x') \rangle \, dx \, dx' - 0 \qquad (511.02)$$

and the variance that the gradient ($\nabla_x Vs(x)$) of the potential is simultaneously zero is given by

$$\xi \sigma_1^2 = \xi \sigma_2^2 = \xi \sigma_3^2 = \frac{1}{3} \langle [\nabla_y Vs(y)][\nabla_y Vs(y)] \rangle \qquad (511.03)$$

Halperin and Lax maximize this density of states (Eq 511.01) numerically for a function of the form

$$f(x) = (4\pi)^{-1/2} s(|x|)/|x| \qquad (511.04)$$

They only consider states deep in the tail, where the exponent of Eq 511.01 dominates. So the optimization of f(x) is performed by maximizing only the exponent of Eq. 511.01. Having found f(x) they substitute back into the expressions for the variances to obtain the first order approximation of the density of states

$$\rho_1(E) = \frac{E_\kappa^3 \kappa^3}{\xi^2} a(\nu) \exp\left(- \frac{E_\kappa^2}{2\xi} b(\nu) \right) \qquad (511.05)$$

They tabulate values for the dimensionless parameters a(ν) and b(ν) for different values of the energy (ν) that they normalize with respect to the Thomas Fermi screening length (κ). For example in the conduction band tail

they take

$$\nu = (E_C + E_o - E)/E_K \qquad (511.06)$$

where $E_K = \hbar^2 \kappa^2 / 2m$

and with average electron-impurity potential (E_o) given by

$$E_o = \langle V_8 \rangle = - \frac{e^2}{\epsilon \epsilon_r \kappa^2} \sum_a Z_a N_a \qquad (511.07)$$

Recently Samathiyakanit et al (1979, 1982) have published results for an analytical derivation of the functions $a(\nu)$ and $b(\nu)$ that agree well with Halperin and Lax's numerical values (see Table 5.1).

5.1.2   **Asymptotic form for the density of states.**

            Halperin and Lax's density of states may be evaluated for clarity with a particular form of the function $f(x)$ equivalent to the asymptotic form of Halperin and Lax's function (Eq 511.04) namely

$$f(r) = \phi(r) = \left(\frac{\alpha^3}{\pi} \right)^{1/2} e^{-\alpha r} \qquad (512.01)$$

The variance $\xi \sigma_o^2$ (Eq. 511.02) with this function becomes (y=0)

$$\xi \sigma_o^2 = \left(\frac{\alpha^3}{\pi} \right)^2 \int \int e^{-4\alpha(x+x')} \langle V(x)V(x') \rangle \, dx dx' \qquad (512.02a)$$

The autocorrelation function of the Thomas Fermi potential, given by

$$\langle V(x)V(x') \rangle = \xi \, e^{-\kappa|x-x'|} \qquad ; \qquad \xi = \frac{e^4}{(4\pi\epsilon\epsilon_r)^2} \frac{2\pi}{\kappa} \sum_a N_a Z_a^2$$

$$(512.02b)$$

may be approximated for a short range potential by

$$\langle V(x)V(x') \rangle \approx \frac{8\pi\xi}{\kappa^3} \delta(x - x') \qquad (512.02c)$$

giving

$$\xi{\sigma_o}^2 = \frac{\xi\alpha^3}{\kappa^3} \tag{512.03}$$

Whilst the variances ${\xi\sigma_1}^2$, ${\xi\sigma_2}^2$ and ${\xi\sigma_3}^2$ (Eq. 511.03) are given by

$$\xi{\sigma_1}^2 = \xi{\sigma_2}^2 = \xi{\sigma_3}^2 = \frac{4\alpha^5}{3\kappa^3} \tag{512.04}$$

Substituting in Eq 511.01 for the variances

$$\rho_f(E) = \frac{(\kappa E_\kappa)^3}{\xi^2} \frac{2}{3^{3/2}\pi^2}\left(\frac{\kappa}{\alpha}\right)^3 (T+\xi)^3 \exp\left(-\frac{(T+\xi)^2}{(\alpha/\kappa)^3}\frac{{E_\kappa}^2}{2\xi}\right) \tag{512.05}$$

$$T = \left(\frac{\alpha}{\kappa}\right)^2$$

Optimization of the wavefunction by maximizing the argument of the exponential of Eq 512.05 with respect to the range parameter α of the wavefunction results in the expression

$$\rho(E) = \frac{128}{27\pi^2}\frac{(\kappa E_\kappa)^3}{\xi^2} \xi^{3/2} \exp\left(-\frac{16}{3^{3/2}}\frac{{E_\kappa}^2}{2\xi}\xi^{1/2}\right) \tag{512.06}$$

This expression, calculated from the asymptotic form of Halperin and Lax's function, may be compared with the asymptotic form of their density of states. This comparison is presented in Table 5.1 along with a comparison of data from later papers by other workers (Samathiyakanit et al 1979, 1982) taking a density of states expression of the form

$$\rho_1(E) = \frac{{E_\kappa}^3\kappa^3}{\xi^2} a(\nu) \exp\left(-\frac{{E_\kappa}^2}{2\xi}b(\nu)\right) \tag{512.07}$$

Table 5.1

Comparison of $a(\nu)$ and $b(\nu)$ from Eq 512.07,
Halperin and Lax 1966 and Samathiyakanit 1979

	$a(\nu)$	$b(\nu)$
Eq 512.07	$0.48\ \nu^{1.5}$	$3.08\ \nu^{0.5}$
Halperin and Lax 1966	$0.4\ \ \nu^{1.5}$	$3.0\ \ \nu^{0.5}$
Samathiyakanit 1979	$0.23\ \nu^{1.5}$	$3.54\ \nu^{0.5}$

5.1.3 The precise relationship between host band and the tail.

In Halperin and Lax's original paper (1966) and elsewhere (Samathiyakanit 1979), the position of the band tail relative to the host band has been calculated from the normalized energy parameter ν (Eq. 511.06). However from a careful study of the physics behind these expressions this expression (Eq. 511.06) is found to be incorrect.

Following the arguments in Wolff's (1962) paper, outlined in section 4.3, the average first order electron-impurity energy E_0 is cancelled out by the first order electron-electron energy. The position of the band tail relative to the unperturbed band edge will then be given as

$$\nu = (E_c - E)/E_K \qquad (513.01)$$

Also having used the screened impurity potentials (Eq 510.01) in the variational calculation of the energy of the localized wavefunctions of the band tail (Eq 510.04) the effect of these on the conduction band states must be considered as is done in chapter 4. To obtain the correct relative positions of tail states and unperturbed band the corrected conduction band edge (E_c') must be used

$$E_C{'} = E_C + \Delta E_{CTF}^{ei} \qquad\qquad (513.02)$$

Where E_C is the unperturbed band edge, ΔE_{CTF}^{ei} the change in electron-impurity self energy in the Thomas Fermi approximation at the bottom of the conduction band edge (Eq. 442.14a, Fig 4.1).

Finally the effect of electron-electron self energies on both the tail and extended states have to be included. Halperin and Lax explicitly ignore this correction in their paper for simplicity. However in chapters 2 and 3 the effect of electron-electron self energies on the extended states has been calculated. The localized states of the band tail however approach delta functions with a spread of wavevectors in Fourier space. One of the results from the exchange calculations, reported here (chapters 2 and 3) and elsewhere (Berggren and Sernelius 1981, Abram et al 1979) is that ΔE^{ee} be essentially wavevector independent. From this we might logically suppose that the electron-electron shift be the same for both extended and tail states. At worst it might produce a marginal correction to the tail state energies. Combining Eq 513.01 and 513.02 an expression for the energy of the tail states relative to the perturbed band edge is obtained

$$\nu = (E_C + \Delta E_{CTF}^{ei} - E)/E_K \qquad\qquad (513.03)$$

A similar expression exists for the valence band

$$\nu = -(E_V + \Delta E_{VTF}^{ei} - E)/E_K \qquad\qquad (513.04)$$

These expressions can be seen to differ from Eq. 511.06. The net effect of correctly including the electron-impurity self energy in the calculation of the extended states in the band proper, is to decrease the amount by which the band tail extends into the band gap. In Hwang (1970) and Casey and

Panish (1979) the band tail is linked to the host band by an arbitrary
smooth curve however the interpretation above agrees well with the quantum
mechanical method of Lloyd and Best detailed in section 5.2 that is
expected to be more accurate for the states close to and including the
extended states of the host band.

5.1.4   Calculations for silicon's conduction band.

In this section results for the band tail from the Halperin
and Lax model for the conduction (Fig 5.2) band of uncompensated n-type
silicon is presented.   The valence band will have a similar tail (not shown
here).   The effect of compensation on these calculations would be two fold.
In the first case the scaling parameter ξ would be increased since it
depends upon the total impurity concentration (Eq. 512.02b).   Whilst at the
same time the Thomas Fermi screening length would be effected since it
depends upon the difference between impurity types.

Silicon's conduction band has six ellipsoidal energy surfaces
(see section 2.1).   The density of states expression is then modified to
include these by multiplying by the number of valleys (M_c),   whilst   using
the density of states effective mass for one valley in the expressions for
screening length.   The effective mass used for the valence band
calculations is the density of states effective mass.   Finally the
occupancy of the eigenstates is accounted for by multiplying by a factor of
2 to account for the two possible spin states of each occupying electron.
In this fashion the detailed structure of the bands is approximated so that
a simple expression resulted for Halperin and Lax's density of electron

states

$$\rho_1(E) = 2\ M_C\ \frac{E_\kappa^3 \kappa^3}{\xi^2}\ a(\nu)\ \exp\left(-\frac{E_\kappa^2}{2\xi}\ b(\nu)\right) \qquad (514.01)$$

Values of the screening length κ calculated for a donor concentration of 10^{20} cm^{-3} were used to evaluate this expression, using values of $a(\nu)$ and $b(\nu)$ from their paper and Eq. 513.03 and 513.04 for the remaining parameters. The results are plotted in Fig 5.2 for the conduction band. The Thomas Fermi expression used to calculate the electron-impurity self energy is given in Eq. 442.14a. Had this not been included in the normalized energy parameter then (Eq. 513.03 and Eq. 513.04) the host band position shown in the figures would have been attained. The band tail can be seen to be very small in comparison to the host band. It will have little effect on the integrated density of states in device applications. However it may still have an effect on optical transitions.

5.1.5 Validity of Halperin and Lax approach.

In their paper Halperin and Lax (1966, section 7) perform a detailed analysis of the limits to which their density of states expression is valid. In Fig 5.3 these are summarized for silicon. In the first place their condition for linear screening requires that the potential $V(x)$ is small in comparison to the Fermi energy, or (equation 6.9)

$$\xi^{1/2} < E_f \qquad (515.01)$$

this is only true above a concentration of 10^{20} cm^{-3} (Fig 5.3). For the Gaussian statistics used in the derivation of Eq. 511.01 to be valid the average number of scattering centres within the range of the function must be large. The range of the wavefunction is given by the inverse root of the kinetic energy so (equation 7.5)
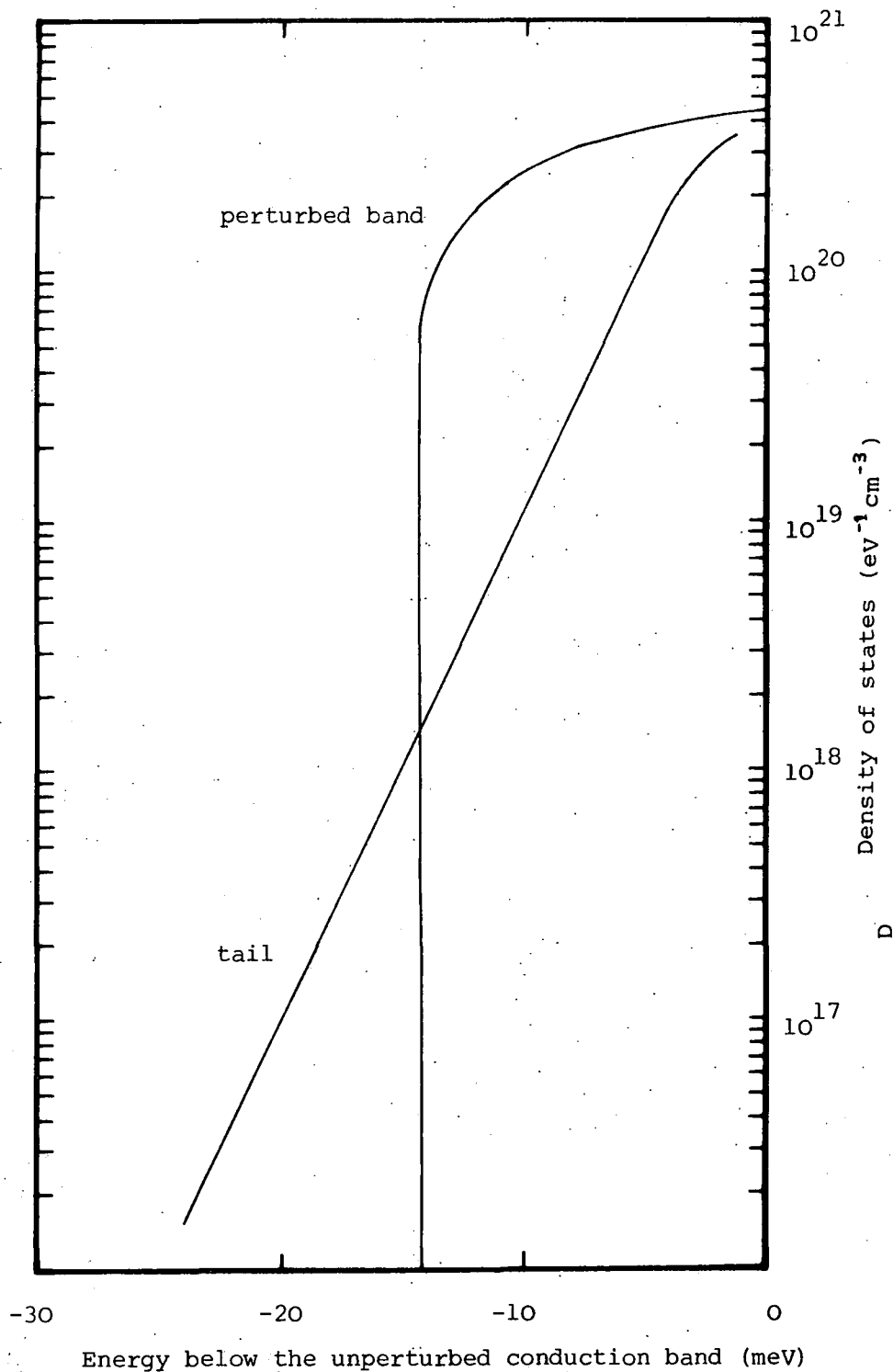
Fig 5.2   Band tail from Halperin and Lax's (1966) calculation,
           also showing the conduction band shifted by the
           electron-impurity self energy in the Thomas Fermi
           approximation (fig 4.1) for a donor concentration of
           10^{20} cm^{-3}.
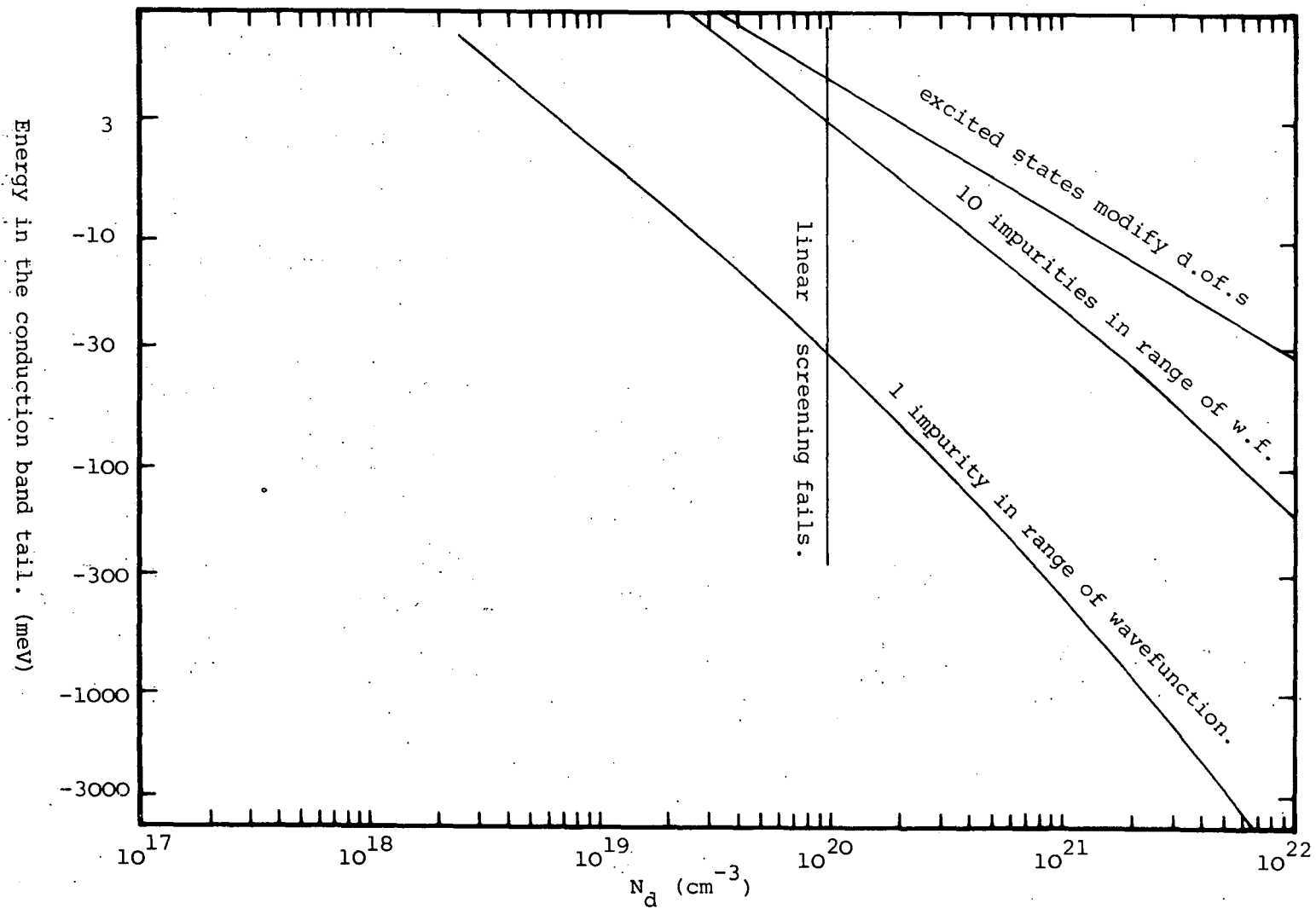
Fig 5.3   Range of validity of Halperin and Lax's calculations defined by Eq. 515.01-515.03.

$$1 << N_d \ (T^{-1/2} \kappa^{-1} + \kappa^{-1})^3 \qquad\qquad (515.02)$$

Finally the method assumes that there are no excited states or (equation 7.6)

$$b(\nu) > 6\xi \qquad\qquad (515.03)$$

These three conditions define a region of validity for the above band tail that spans an order of magnitude in the energy of the tail (see Fig 5.3). At a donor concentration of 10^{20} cm^{-3} this results in the calculated values for the density of states in the tail being valid from 2 meV to 33 meV. However this is very sensitive to the validity of Gaussian statistics (Eq. 515.02). If for example the requirement for 10 centres within the influence of the wavefunction is considered this range at 10^{20} is reduced to 2 meV to about 3 meV (see Fig 5.3). At higher concentrations these conditions become less stringent as the tail extends. It should also be noted that in gallium arsenide for example due to the different effective masses the range of validity will be much greater.

5.2   LLOYD AND BEST APPROACH.

Lloyd and Best (1975) have developed a variational theory and conclude that rather than maximizing the density of states as Halperin and Lax have done, it is the pressure function (P(E)), or the double integral of the density of states (N(E)),

$$P(E) = \int_{-\infty}^{E} \int_{-\infty}^{\epsilon} N(\epsilon) \ d\epsilon \ d\epsilon \qquad\qquad (520.01)$$

that must be maximized to obtain the closest approximation to the true density of states. However deep in the band tail this principle is

equivalent to Halperin and Lax's maximization of the density of states. In their theory Lloyd and Best divide the semiconductor up into a number of equal volume cells. They estimate the average impurity potential within each cell and choose trial wavefunctions assumed to be orthonormal with those in adjacent cells. They then estimate the density of states within each cell optimizing the cell sizes by maximizing the double integral of the density of states, hence obtaining an optimum density of states.

In section 5.2.1 Lloyd and Best's variational principle is outlined. In section 5.2.2 an improvement to their procedure for calculating the optimum density of states is developed. In section 5.2.3 the normalized forms for the density of states, integrated density of states and pressure functions, that allow us to consider a number of different trial wavefunctions are calculated. Section 5.2.4 compares the asymptotic forms of the density of states due to three trial wavefunctions with the asymptotic form of Halperin and Lax. In section 5.2.5 the normalized numerical results for the density of states from the localized tail states to the extended states in the host band are given, discussing some interesting features of Lloyd and Best's approach. Finally in section 5.2.6 results for the best calculations of the tail on the density of states in silicon's conduction and valence bands are presented.

5.2.1   The variational principle.

In this section the variational principle developed by Lloyd and Best (1975) is presented. Lloyd and Best consider a hypothetical many-fermion problem in which the single-particle eigenstates of interest are filled (one fermion to each state ignoring for the moment spin) up to some Fermi energy μ. They like Halperin and Lax ignore electron-electron

exchange energies that have to be included at the end on the calculation. The many electron screening of the impurity centres is included by suitable choices of trial wavefunction and impurity potential. The energy of this many-particle system of volume V is given in terms of the single-particle density-of-states function by

$$E_0(\mu) = V \int_{-\infty}^{\mu} E \ N(E) \ dE \qquad (521.01)$$

But this is the ground state of the many-fermion problem and as such it may be estimated variationally. Letting the trial basis state of the many-fermion wavefunction be represented by $\phi_\alpha(r,\lambda)$, where λ represents the variational parameter(s) and α being convenient quantum number(s). They then write an approximate density-of-states assuming the single-particle states to be orthonormal

$$N(E,\lambda) = \frac{1}{V} \sum_\alpha \delta(E - \langle \alpha | H | \alpha \rangle) \qquad (521.02)$$

where H is the single electron random Hamiltonian of the problem. Substitution of this approximate density of states into Eq 521.01 gives $E_0(\mu,\lambda)$ an approximation to the true ground states energy. The total number of particles $(N(\mu,\lambda)$ may also be expressed in terms of this approximate density of states

$$N(\mu,\lambda) = \int_{-\infty}^{\mu} N(E,\lambda) \ dE \qquad (521.03)$$

These expressions form the basis of the variational approach developed by Lloyd and Best. In what follows three methods of obtaining the variational principle are described.

a)   From the Canonical Ensemble

Given that the total number of particles has to be kept constant, from thermodynamics provided the system is in thermal equilibrium (at T=0) and has fixed volume V the particles will fill up the states in the band so as to minimize the Helmholtz free energy (F). But this is just the ground state energy

$$F = U - TS = U = V \int_{-\infty}^{\mu} E \, N(E, \lambda) \, dE \qquad (521.04)$$

Thus whilst minimizing the ground state energy by varying λ the Fermi energy μ must simultaneously be varied to keep the total number of particles (Eq 521.03) constant.   If the integration of Eq 521.04 is performed by parts

$$E_0(\mu, \lambda) = V \left(\mu \int_{-\infty}^{\mu} N(E, \lambda) \, dE - \int_{-\infty}^{\mu} \int_{-\infty}^{E} N(\epsilon, \lambda) \, d\epsilon \, dE \right) \quad (521.05)$$

Thus the minimization of E_0 corresponds to maximizing the double integral of the density of states provided the first term of Eq 521.05, that is formed by the product of Fermi energy and total number of particles, is kept constant. Notice that by substituting for E_0 the double integral may be re-written

$$P(\mu, \lambda) = \int_{-\infty}^{\mu} \int_{-\infty}^{E} N(\epsilon, \lambda) \, d\epsilon \, dE = \int_{-\infty}^{\mu} (\mu - E) \, N(E, \lambda) \, dE \quad (521.06)$$

This variational principle may be obtained more rigorously by seeking the minimum in the following, equivalent fashion.

For a minimum

$$\frac{\partial U}{\partial \lambda} = 0 = \int_{-\infty}^{\mu(\lambda)} E \, \frac{\partial N(E, \lambda)}{\partial \lambda} \, dE + \frac{\partial \mu}{\partial \lambda} \, \mu \, N(\mu, \lambda)$$

But from the constraint

$$\frac{\partial N}{\partial \lambda} = 0 = \int_{-\infty}^{\mu(\lambda)} \frac{\partial N(E,\lambda)}{\partial \lambda} \, dE + \frac{\partial \mu}{\partial \lambda} \, \mu \, N(\mu,\lambda)$$

Combining these

$$\frac{\partial U}{\partial \lambda} = 0 = \int_{-\infty}^{\mu(\lambda)} (E - \mu) \, \frac{\partial N(E,\lambda)}{\partial \lambda} \, dE$$

Which is equivalent to maximizing the function $P(\mu,\lambda)$ provided μ is taken as a constant

$$P(\mu,\lambda) = \int_{-\infty}^{\mu} \int_{-\infty}^{E} N(\epsilon,\lambda) \, d\epsilon \, dE = \int_{-\infty}^{\mu} (\mu - E) \, N(E,\lambda) \, dE \quad (521.07)$$

b)   From Grand Canonical Ensemble

Above, by varying μ to maintain the total number of particles constant at constant temperature (T=0) and volume, the Helmholtz free energy is minimized. Lloyd and Best claim that an equivalent way to fill up the states in the tail is to keep the fermi energy constant whilst varying the total number of particles. It is then the thermodynamic potential Ω that is a minimum with respect to changes in state at constant chemical potential, temperature (T=0) and volume (see for example Lifshitz and Pitaevskii 1980). The pressure ($\Omega = - PV$) of the many fermion gas must then be maximized. The following outlines the calculation of this pressure function.

To calculate the probability w_{nN} that a system of fixed volume with a variable number (N) of none interacting particles is in the state n with energy E_{nN} the Grand Canonical Ensemble or Gibbs distribution for variable number of particles (Lifshitz and Pitaevskii 1980) is used

$$w_{nN} = \exp((\Omega + \mu N - E_{nN})/kT) \quad\quad (521.08)$$

Where the thermodynamic potential Ω is given by normalizing the

distribution

$$1 = \sum_n \sum_N w_{nN} = \exp(\Omega/kT) \sum_n \sum_N \exp((\mu N - E_{nN})/kT)$$

rearranging

$$\Omega = -kT \log_e (\sum_n \sum_N \exp((\mu N - E_{nN})/kT))$$

In the present calculation particles that may be classified into groups of n_K particles each with energy ϵ_K and different quantum state K are considered. The total number of particles N, the total energy E_{nN} of a particular collection of quantum states K, represented by n, are given by

$$N = \sum_K n_K$$

$$\text{(521.09)}$$

$$E_{nN} = \sum_K n_K \epsilon_K$$

So from standard statistical mechanics the probability of finding the system in this state is given by

$$w_{nN} = \prod_K w_{n_K} = \exp((\Omega + \mu N - E_{nN})/kT) \qquad \text{(521.10a)}$$

Where the probability of the group of n_K particles occupying the quantum state K with energy ϵ_K is given by

$$w_{n_K} = \exp((\Omega_K + n_K(\mu - \epsilon_K))/kT) \qquad \text{(521.10b)}$$

Where Ω_K, the potential of the set of states quantized by K, is given by normalizing

$$1 = \sum_{n_K} w_{n_K} = \exp(\Omega_K/kT) \sum_{n_K} \exp((\mu n_K - \epsilon_K n_K)/kT)$$

rearranging

$$\Omega_K = - kT \log_e (\sum_{n_K} \exp(n_K(\mu - \epsilon_K)/kT)) \qquad (521.10c)$$

By Pauli's principle the occupational number n_K may only be one or zero for fermions. Eq 521.10c may then be simplified

$$\Omega_K = - kT \log_e (1 + \exp((\mu - \epsilon_K)/kT))$$

The total thermodynamic potential Ω is then given by

$$\Omega = - kT \sum_K \log_e (1 + \exp((\mu - \epsilon_K)/kT)) \qquad (521.11)$$

When kT becomes smaller than the difference between chemical potential and eigenvalue then the potential becomes

$$\Omega = - \sum_K (\mu - \epsilon_K) \qquad (521.12)$$

Assuming that the wavevector K is a good quantum number in every cell the summation over K is replaced with an integral

$$\Omega = - V \int (\mu - \epsilon_K) \ N(K) \ d^3K$$

where N(K) is the density of states with wavevector between K and K + dK. Since in the bulk of the semiconductor K is no longer a good quantum number the K integral is replaced by one over the energy to get

$$\Omega = - V \int_{-\infty}^{\mu} (\mu - E) \ N(E) \ dE = - V \ P(\mu) \qquad (521.13)$$

The system will seek to minimize Ω that corresponds to maximizing the pressure function

$$P(\mu) = \int_{-\infty}^{\mu} (\mu - E) \ N(E) \ dE \qquad (521.14)$$

c)   From Matrix theory

Substituting Eq 521.02 for the density of states into the expression for the ground state energy Eq 521.01

$$E_O(E) = \sum_\alpha \langle \alpha|H|\alpha \rangle \qquad (521.15)$$

The ground state energy may then be represented by a sum of ordered eigenvalues.   Also on substitution of the density of states into Eq 520.01 the pressure function becomes

$$P(E) = \sum_\alpha (\mu - \langle \alpha|H|\alpha \rangle) \qquad (521.16)$$

Now Fan (1949) has produced a theorem merely from matrix analysis that states the following inequality

$$\sum_i^N E_i \leqslant \sum_\alpha \langle \alpha|H|\alpha \rangle \qquad (521.17)$$

Where E_i are the true eigenvalues and the $|\alpha\rangle$ form any set of orthonormal vectors.   Thus to obtain the best approximation to the true ground state the pressure function must be maximized.

5.2.2   **Calculations of the best density of states.**

Having outlined the basic variational principle this section deals with the method of obtaining the best density of states.   Because it is a hypothetical many fermion problem that is being considered the Fermi energy used in the above derivation of the variational principle does not necessarily relate to the real Fermi energy.   Choosing an arbitrary energy within the band tail (E) the above principle is used to optimize the variational parameter for that energy $\lambda(E)$.   This was used by Lloyd and

Best to give an estimate for the density of states at that energy

$$N(E) = N(E, \lambda(E))$$ (522.01)

In doing so they ignore the problem of exchange energy between states above the arbitrarily chosen energy that may or may not be filled.

An improvement to Lloyd and Best's method is to choose the optimum values of $\lambda(E)$ as above, but rather than using these values in the original density of states expression, to use the optimized pressure function

$$P(E, \lambda_m(E)) = \frac{maximum}{w.r.t. \lambda} P(E, \lambda)$$ (522.02a)

which is equivalent to solving

$$\frac{\partial P(\mu, \lambda)}{\partial \lambda} = \int_{-\infty}^{\mu} (\mu - E) \frac{\partial N(E, \lambda)}{\partial \lambda} dE = 0$$ (522.02b)

The pressure function as can be seen from Eq. 521.06 (or Lloyd and Best 1979 Eq. 2.3 - 2.4) is just the double integral of the density of states. By double differentiating the optimum pressure function, with respect to energy, the best estimate of the density of states is obtained. This is presented formally as

$$N(E) = \frac{\partial^2 P(E, \lambda_m(E))}{\partial E^2}$$ (522.03)

This rather formidable task, that of numerically double differentiating a maximized function may be simplified. The maximized pressure function is given by (Eq. 522.02a and Eq. 521.06)

$$P(\mu, \lambda_m(\mu)) = \int_{-\infty}^{\mu} (\mu - E) N(E, \lambda_m(\mu)) dE$$

Differentiating once

$$\frac{\partial P(\mu, \lambda_m(\mu))}{\partial \mu} = \int_{-\infty}^{\mu} N(E, \lambda_m(\mu)) \; dE$$

(522.04)

$$+ \frac{\partial \lambda_m(\mu)}{\partial \mu} \int_{-\infty}^{\mu} (\mu - E) \frac{\partial N(E, \lambda_m(\mu))}{\partial \lambda_m(\mu)} \; dE$$

where the second term on the right hand side is just the condition for maximizing $P(\mu, \lambda)$ (Eq. 522.02b), multiplied by a finite constant

$$\frac{\partial \lambda_m(\mu)}{\partial \mu}$$

and is equal to zero unless this gradient becomes infinite. Writing the integral of the density of states as $L(\mu, \lambda)$

$$L(\mu, \lambda) = \int_{-\infty}^{\mu} N(\epsilon, \lambda) \; d\epsilon$$

(522.05)

the optimum density of states is then given by differentiating $L(\mu, \lambda_m(\mu))$ with respect to the energy μ. This single numerical differentiation is easier than the initial double differentiation proposed above. Numerical results for the normalized best density of states are presented in section 5.2.5.

5.2.3   **Expressions for the density of states and Pressure functions.**

Having detailed the calculation of the optimum density of states from the variational principle in the previous sections, in this section the calculation of the trial density of states using Lloyd and Best's trial wavefunction is presented. Normalizing parameters are also presented that make the numerical calculations of later sections independent of semiconductor and trial wavefunction.

To calculate their density of states Lloyd and Best chose the following set of trial functions, normalized with respect to the cell (denoted by c) size λ^3

$$\phi_{c,k}(r,\lambda) = \begin{cases} \lambda^{-3/2} \exp(ik.r) & \text{where cell c contains r} \\ 0 & \text{where r is outside cell c} \end{cases}$$

(523.01)

λ is the variational parameter. The random Hamiltonian of their model is given by

$$H = -\frac{\hbar^2}{2m} \nabla^2 + V(r)$$

(523.02)

Where V(r) is the random fluctuation in the impurity potential given in Eq. 510.03 where the average impurity potential of the crystal as a whole has been subtracted. The density of states (Eq 521.02) is then rewritten in terms of this trial function using the expectation value

$$\langle \alpha|H|\alpha\rangle = \langle c,k|H|c,k\rangle = \frac{\hbar^2 k^2}{2m} + \int \phi_{c,k}^*(r) \; V(r) \; \phi_{c,k}(r) \; d^3r$$

(523.03)

so that the density of states becomes

$$N(E,\lambda) = \frac{1}{N} \sum_C \left[\frac{1}{\lambda^3} \sum_K \delta(E - \frac{\hbar^2 k^2}{2m} - \langle Vc\rangle) \right]$$

(523.04)

Where $\langle Vc\rangle$ is the expectation value of the potential for the cell (c) and N is the total number of cells.

The summations in Eq. 523.04 are now evaluated. First the summation over the cells (c). Just as in the Halperin and Lax calculations it is assumed that there are a large number of impurities within each cell so that the central limit theorem may be implemented, taking the potential to vary with a Gaussian distribution about a mean value, taken to be zero

$$p(\langle Vc\rangle) = \left(\frac{1}{2\pi w}\right)^{1/2} \exp - \frac{\langle Vc\rangle^2}{2w}$$

(523.05a)

The variance (w) is inversely proportional to the cell size (see section 5.2.4), and is expressed in the form

$$w = \langle V^2 \rangle - \langle V \rangle^2 = \sigma^2 / \lambda^3 \qquad (523.05b)$$

Performing the summation over cells thus reduces to an integral over the expectation value of the potential in each cell $\langle Vc \rangle$. From Eq. 523.04

$$N(E,\lambda) = \left(\frac{1}{2\pi w}\right)^{1/2} \frac{1}{\lambda^3} \qquad (523.06)$$

$$\int_{-\infty}^{\infty} \sum_k \delta\left(E - \frac{\hbar^2 k^2}{2m} - \langle Vc \rangle\right) \exp\left(-\frac{\langle Vc \rangle^2}{2w}\right) d\langle Vc \rangle$$

Considering now the summation over k states, the discrete nature of the low k states has to be included, whilst summing over an infinite number of states closely packed further into the host band. The summation over k states is replaced by an integral over k states however to partially to account for the discrete nature of the low energy eigenstates of the cell, Lloyd and Best shift the energy origin by a zero-point energy $((\hbar^2/2m)\chi/\lambda^2)$, calculated from the ground state energy of a square well potential $(\chi = 3\pi^2)$. A better approximation might be found by including more than just the first term in this series (private communications Rees), however this is thought to be too involved for the present calculations.

$$N(E,\lambda) = \left(\frac{1}{2\pi w}\right)^{1/2} \frac{1}{2\pi^2} \qquad (523.07)$$

$$\int_0^{\infty} \int_{-\infty}^{\infty} \delta\left(E - \frac{\hbar^2 k^2}{2m} - \frac{\hbar^2}{2m}\left(\frac{\chi}{\lambda^2}\right) - \langle Vc \rangle\right) k^2 \exp\left(-\frac{\langle Vc \rangle^2}{2w}\right) d\langle Vc \rangle dk$$

The integral over the potential fluctuation is elementary, however the wavevector integral may be most readily expressed in terms of Parabolic Cylinder functions $(U(a,z))$. These are defined by (Abramowitz

and Stegun 1970)

$$U(a,z) = \frac{1}{\Gamma(1/2+a)} e^{-z^2/4} \int_0^\infty s^{a-1/2} e^{-zs-s^2/2} ds \qquad (523.08)$$

so that the density of states expression becomes

$$N(E,\lambda) = \frac{1}{4\pi^2} \left(\frac{m}{\hbar^2}\right)^{3/2} b^{1/2} e^{-z^2/4} U(1,z) \qquad (523.09a)$$

with energy and variational parameter b given

$$b = \frac{\sigma^2}{\lambda^{3/2}} \qquad (523.09b)$$

and

$$z = -\frac{E}{b} + \chi \frac{\hbar^2}{2m} \left(\frac{b}{\sigma^4}\right)^{1/3} \qquad (523.09c)$$

Eq 523.09 gives the total density of eigenstates in the band. However by normalizing the above expressions a more useful expression for the density of states, that is material and trial wavefunction independent may be obtained. Introducing the normalized parameters for energy ϵ,

$$E = \left(\frac{2m}{\hbar^2}\right)^3 \sigma^4 \frac{27\pi^6}{\chi^3} \epsilon \qquad (523.10)$$

and length ρ

$$\lambda = \left(\frac{\hbar^2}{2m}\right)^2 \frac{\chi^2}{9\pi^4 \sigma^2} \rho \qquad (523.11)$$

the density of states N(E) becomes

$$N(E) = \left(\frac{2m}{\hbar^2}\right)^3 \sigma^2 \frac{27\pi^6}{\chi^3} n(\epsilon) \qquad (523.12a)$$

and the normalized density of states $(n(\epsilon))$ is then given by

$$n(\epsilon,\rho) = \left(\frac{\chi}{3\pi^2}\right)^{3/2} \frac{1}{8\sqrt{2\pi}^2} \beta^{3/4} e^{-z^2/4} U(1,z) = \left(\frac{\chi}{3\pi^2}\right)^{3/2} n'(\epsilon,\rho)$$

$$z = -\frac{\epsilon}{\beta^{3/2}} + 3\pi^2 \beta^{1/2} \qquad (523.12b)$$

where $\beta = 1/\rho$

Using these normalized parameters the density of states (N(E)) for a variety of semiconductors with differing effective mass (m) may be calculated. The trial wavefunction may also be adjusted to a limited extent (see section 5.2.4). Varying not only the potential fluctuation parameter σ but also the zero point energy parameter χ. Thus a variety of different results may be obtained from just one set of numerically calculated normalized curves (n'(ϵ)) that are independent of σ, m and χ.

The integral of the density of states L(E,λ) (Eq. 522.05), and its double integral, or the pressure function P(E,λ) (Eq. 521.06) may also be calculated from this normalized density of states. From Eq 523.12b for the normalized density of states and the recurrence relationships for the Parabolic Cylinder functions (Abramowitz and Stegun 1970) the normalized integral of the density of states (I(ϵ,ρ)) becomes

$$l(\epsilon,\rho) = \left(\frac{\chi}{3\pi^2}\right)^{3/2} \frac{1}{8\sqrt{2\pi}^2} \beta^{9/4} e^{-z^2/4} U(2,z) \qquad (523.13)$$

And its double integral, or the normalized pressure function (p(ϵ,ρ))

$$p(\epsilon,\rho) = \left(\frac{\chi}{3\pi^2}\right)^{3/2} \frac{1}{8\sqrt{2\pi}^2} \beta^{15/4} e^{-z^2/4} U(3,z) \qquad (523.14)$$

5.2.4   Comparison of the asymptotic form with Halperin and Lax.

In the previous section useful expressions for the normalized density of states (n(ϵ,ρ)), integrated density of states (I(ϵ,ρ)), and pressure functions (p(ϵ,ρ)) have been derived. These expressions are normalized with respect to the zero point energy parameter χ (Eq. 523.07) and the potential fluctuation parameter σ (Eq. 523.05b). These functions

were derived in the last section with the trial wavefunction (Eq. 523.01) used by Lloyd and Best (1975). In this section the asymptotic form of the density of states, that is only reached deep in the tail ($|\epsilon| > 4.0 . 10^2$), is considered. The maximization of the pressure function and the calculation of the optimum density of states (section 5.2.2) may be performed analytically. By comparison with the Halperin and Lax's asymptotic function (Eq. 512.07) the trial function (Eq. 523.01) used by Lloyd and Best is improved.

From the previous analysis it is clear that the density of states algorithm must consist of two parts. First maximizing the normalized functions and secondly providing suitable values for the variance σ^2 zero point energy χ and effective mass m. In this section the maximization of the normalized function is performed in part a). The principle part of the section (part b)) is devoted to a comparison of the asymptotic forms of Halperin and Lax with Lloyd and Best's functions for three trial wavefunctions (in parts i), ii) and iii)). A table comparing all these functions is presented (Table 5.2).

a)   Maximization in the low energy limit

Maximizing the pressure function (Eq 520.01) in the low energy limit corresponds precisely to maximizing the density of states expression (Eq 523.12) as can be verified by writing the asymptotic forms of these functions. For consistency only the pressure function is maximized here. By differentiating $p(\epsilon, \rho)$ from Eq. 523.14 with respect to β ($\beta = 1/\rho$) apart from the trivial solution ($\beta = 0$ see section 5.2.5) this maximization

corresponds to solving

$$\frac{\partial p}{\partial \beta} = 0 = e^{-z^2/4}(U(1,z) - 4\pi^2 \beta^{1/2} U(2,z))$$

(524.01)

$$z = -\frac{\epsilon}{\beta^{3/2}} + 3\pi^2 \beta^{1/2}$$

Solutions of this equation for different β and ϵ correspond to finding those values of λ that maximize the pressure function. The asymptotic form for the Parabolic Cylinder functions may be reached in one of two ways: By inserting a large negative value of ϵ: Or by inserting a small value for β, whilst ensuring a negative value for ϵ. Both these methods (which correspond to those for obtaining the asymptotic form of Halperin and Lax's density of states function section 5.1) result in a large, positive value for the dimensionless parameter z in Eq 524.01. The appropriate asymptotic form for U(a,z) is (Abramowitz and Stegun 1970)

$$U(a,x) = e^{-x^2/4} x^{-a-.5}(1 - \frac{(a+1/2)(a+3/2)}{2x^2} + ..)$$

(524.02)

So the asymptotic form for this maximization condition becomes

$$\frac{\partial p}{\partial \beta} = 0 = e^{-z^2/2} z^{-3/2}(1 - 4\pi^2 \beta^{1/2} z^{-1})$$

(524.03)

Substituting for z from Eq 524.01 the maximization of p corresponds to setting

$$\beta = \frac{|\epsilon|^{1/2}}{\pi}$$

(524.04)

Having obtained this optimum value of β in the low energy tail it can be substituted into the density of states expression Eq 523.12 (both of the methods for obtaining the density of states mentioned in section 5.2.2 may be shown to be equivalent deep in the tail) and take the asymptotic form for the Parabolic Cylinder function. This gives normalized expression for the optimized density of states

$$n(\epsilon) = \left(\frac{\chi}{3\pi^2}\right)^{3/2} \frac{1}{64\sqrt{2}\pi^5} e^{-8\pi^3|\epsilon|^{1/2}} \qquad (524.05)$$

This is only reached deep in the band tail $(|\epsilon| > 4.0.10^2)$ due to the comparatively large second factor in the parentheses of the parabolic cylinder function asymptotic form Eq. 524.02.

b)   Calculation of the zero point energy and variance

Results for three trial wavefunctions of the asymptotic form to the optimized density of states are presented in parts i), ii) and iii). Table 5.2 summarizes the results for all three.

i)   With the orthonormal set of trial wavefunctions used by Lloyd and Best (Eq 523.01) the ground state energy is simply that corresponding to the minimum wavevectors supported by a box

$$E_o = 3\frac{\hbar^2}{2m}\left(\frac{\pi}{\lambda}\right)^2 \quad ; \qquad \chi = 3\pi^2 \qquad (524.06)$$

Whilst the variance may be calculated as in Eq 523.01 from the autocorrelation function. This is approximated for the short range potential by Eq. 512.03. The variance is then given by

$$w = \frac{1}{\lambda^6}\frac{8\pi}{\kappa^3}\xi\,\lambda^3 \quad ; \quad \sigma^2 = \left(\frac{e^2}{\epsilon\epsilon_r\kappa^2}\right)^2 N_d = \frac{8\pi}{\kappa^3}\xi \qquad (524.07)$$

The variance and zero point energy allow us to calculate the normalizing parameters of Eq 523.10-523.12 for this first trial wavefunction at a donor concentration of 10^{20} cm^{-3}

$$E = 0.35\ \epsilon\ (eV) \quad ; \qquad \lambda = 5.8.10^{-8}\ \rho\ (cm) \qquad (524.08)$$

The density of states may also be written in the form of the Halperin and Lax

asymptotic function (Eq 512.07). Using Eq. 524.05 and 523.12

$$N(E) = \frac{M_C}{8\sqrt{2}\pi^4} \left(\frac{\xi^3}{E_\kappa^6}\right) \frac{\kappa E_\kappa^3}{\xi^2} \exp\left(-2\pi^2 \frac{E_\kappa^2}{2\xi} \nu^{1/2}\right) \qquad (524.09)$$

Comparison of this with Eq 512.07 shows that an extra factor (ξ^3/E_κ^6) has been introduced into the prefactor of the above expression due to the lack of any energy dependence. This factor may easily be shown to be equal to

$$\frac{\xi^3}{E_\kappa^6} = \frac{\pi^5}{576} \left(\frac{\pi}{3}\right)^{1/2} \frac{a_{eff}^{3/2} N_T^3}{N_d^{5/2} M_C^5} \qquad (524.10)$$

where a_{eff} is the effective Bohr radius N_T is the total impurity concentration and N_d is the excess donor concentration. In an uncompensated semiconductor this expression reduces further since the latter two impurity concentrations are the same. At a concentration of 10^{18} cm^{-3} this factor is calculated as $5.83.10^{-6}$, whilst at 10^{21} cm^{-3} it is found to be $1.84.10^{-4}$, varying as the square root of the uncompensated impurity concentration.

A more important difference between the Halperin and Lax and Lloyd and Best asymptotic forms is the difference in argument of the exponential. Two further trial wavefunctions were used in an attempt to improve the agreement between the two asymptotic forms deep in the band tail.

ii) Orthonormal sinusoidal wavefunctions for a box volume λ^3 centred at the origin

$$\phi_k^{(2)}(r) = \left(\frac{2}{\lambda}\right)^{3/2} \cos\frac{n_x \pi x}{\lambda} \cos\frac{n_y \pi y}{\lambda} \cos\frac{n_z \pi z}{\lambda} \qquad (524.11)$$

where x,y and z are the components of r in those directions and the n_ν are integers defining the discrete wavevectors. This wavefunction gives a

variance of

$$\sigma^2 = \frac{27\pi}{\kappa^3} \xi \qquad (524.12)$$

and a density of states

$$N(E) = M_C \frac{27}{64\sqrt{2}\pi^4} \left(\frac{\xi^3}{E_\kappa^6}\right) \frac{\kappa E_\kappa^3}{\xi^2} \exp\left(-\frac{16}{27}\pi^2 \frac{E_\kappa^2}{2\xi}\nu^{1/2}\right) \quad (524.13)$$

iii)   Finally the spherical, almost orthonormal wavefunction

$$\phi^{(3)}(r) = \left(\frac{\alpha^3}{\pi}\right)^{1/2} e^{i k \cdot r} e^{-\alpha r} \qquad (524.14)$$

The ground state (k=0) energy of this wavefunction is given by

$$\langle H \rangle = \frac{\hbar^2 \alpha^2}{2m} + \langle V \rangle = \frac{\hbar^2 \alpha^2}{2m} \qquad (524.15)$$

so that $\chi = 1$ and $\lambda = 1/\alpha$

The variance of this third wavefunction is given by (c.f Eq 512.04)

$$\sigma^2 = \frac{\xi}{\kappa^3} \qquad (524.16)$$

from which the normalized parameters for a concentration of 10^{20} cm^{-3} may be calculated from Eq. 523.10-523.12.

$$E = 14.2 \ \epsilon \ (eV) \qquad ; \qquad \lambda = 1.67.10^{-9} \ \rho \ (cm) \qquad (524.17)$$

and the density of eigenstates becomes

$$N(E) = M_C \frac{27\pi}{64\sqrt{2}} \left(\frac{\xi^3}{E_\kappa^6}\right) \frac{\kappa E_\kappa^3}{\xi^2} \exp\left(-\frac{16}{27}\pi^2 \frac{E_\kappa^2}{2\xi}\nu^{1/2}\right) \quad (524.18)$$

A comparison of the asymptotic forms for the density of states for these three wavefunctions is made in Table 5.2 with the previous results (Table 5.1) from section 5.1.   Taking a density of states

expression of the form

$$N(E) = M_c \frac{E_\kappa^3 \kappa^3}{\xi^2} a(\nu) \exp\left(-\frac{E_\kappa^2}{2\xi} b(\nu)\right) \qquad (524.19)$$

Table 5.2

Comparison of a(ν) and b(ν) from Eq 512.07,

Halperin and Lax 1966, Samathiyakanit 1979,

and Lloyd and Best ($N_d = N_T = 10^{20} cm^3$)

	a(ν)	b(ν)
Eq 512.07	$0.48\ \nu^{1.5}$	$3.08\ \nu^{0.5}$
Halperin and Lax 1966	$0.4\ \nu^{1.5}$	$3.0\ \nu^{0.5}$
Samathiyakanit 1979	$0.23\ \nu^{1.5}$	$3.54\ \nu^{0.5}$
Lloyd and Best 1979 $\phi(1)$	$5.29.10^{-8}$	$19.7\ \nu^{0.5}$
$\phi(2)$	$1.79.10^{-7}$	$5.85\ \nu^{0.5}$
$\phi(3)$	$5.46.10^{-5}$	$3.08\ \nu^{0.5}$

It can be seen from this table that the trial function that best fits the asymptotic form of Halperin and Lax's function is $\phi(3)$. However as the energy normalization in Eq. 524.17 shows, this asymptotic form is only reached at an energy of ($|\epsilon| > 4.0.10^2$) $5.6.10^3$ eV below the host band. It is clear that although the two asymptotic functions do have the same exponential form, this alone is not a sufficient indication of their compatability.

5.2.5   Numerical calculations.

For energies other than deep in the tail or within the host band, where the usual $\epsilon^{1/2}$ limit to the density of states is observed, the best density of states must be optimized numerically.   The numerical algorithm used is straight forward, it is only briefly mentioned here.   The numerical results for the normalized density of states derived as detailed in section 5.2.5 are presented in Fig 5.5.   For energies close to the host band, in the region where the optimum box size becomes infinite corresponding to extended states, the detail of the pressure maximization produces a discontinuity in the box size as shown in Fig 5.4.   An analogy may be drawn between this and the mobility edge, although no conductivity calculations are presented that prove this relationship.   The main results of this section, those of the normalized density of states may be used for any semiconductor, or trial wavefunction depending of the choice of normalization parameters given in Eq. 523.10–523.12.

The algorihm used to determine the optimum density of states has effectively been outlined in section 5.2.5.   Fig 5.4 shows a series of curves for the pressure function $p(\epsilon, \rho)$ for different reciprocal cell size β ($\beta = 1/\rho$) and energy ϵ close to the host band.   For energies below the intrinsic band edge ($\epsilon = 0$) the maximization is simple, and corresponds to solving Eq. 524.01 for $\beta = \beta_{max}$.   These points of maximum pressure are also plotted in Fig 5.4.   However as this figure shows as the energy ϵ approaches positive values a sudden change in β_{max} occurs at an energy of $\epsilon = 7.91.10^{-5}$ beyond which the value of p at the origin (ie $\beta_{max} = 0$)   becomes greater. The change in β_{max} from 3.25 10^{-3} to zero corresponds to a sudden change from a finite cell size, to an infinite cell size.   This change suggests the presence of a sudden change from localized states in the band
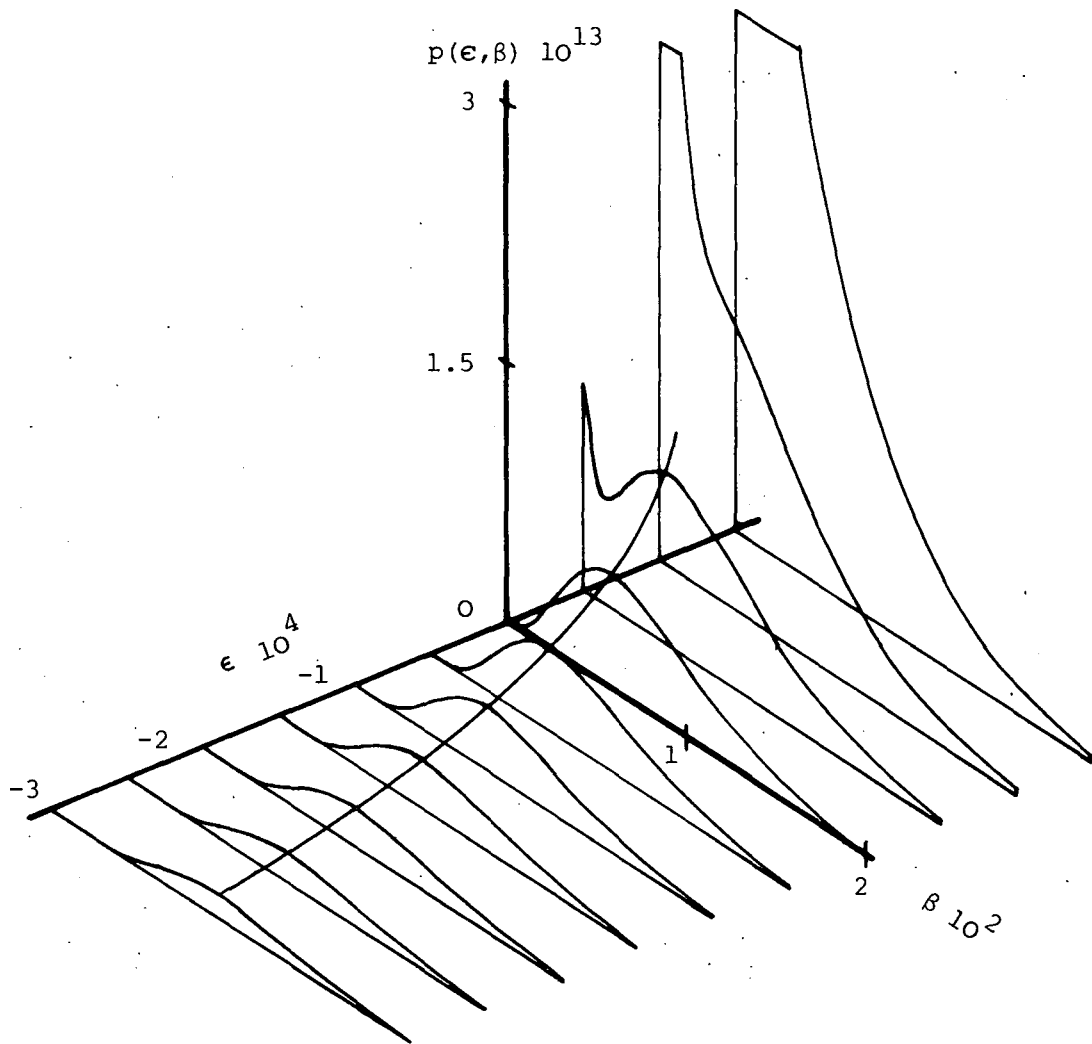
Fig 5.4   Maximizing the pressure function p(ε,β) with respect

to inverse cell size β for energies close to the host

band (ε = + ve).

tail to extended states in the host band that might represent a mobility edge. Above this edge the extended states would contribute to the conductivity in the normal way, whilst the localized states below the edge would contribute by hopping. The present observations do not however present any definitive description of this edge that could only come from conductivity calculations.

Having calculated the optimum pressure (or double integral of the density of states) from β_{max} these can be double differentiated to obtain the optimum density of states. This is achieved by differentiating the integral of the density of states $I(\epsilon, \beta_{max})$ as prescribed by the method of section 5.2.2. Clearly at the point at which β_{max} suddenly moves to $\beta_{max} = 0$ the differentiation routine will produce a singularity that occurs close to the parent band and is not shown in Fig 5.5. Beyond this change with $\beta_{max}=0$ the parent band is generated with density of eigen states given by

$$n(\epsilon) = \frac{1}{4\pi^2} \epsilon^{1/2} \qquad\qquad (525.01)$$

Finally the curve obtained by allowing β_{max} to tending towards its saturation value (β_{sat}) is also given in Fig 5.5. The asymptotic form of this density of states for large positive ϵ is given by

$$n(\epsilon) = \frac{1}{4\pi^2} (\epsilon - \frac{3\pi^2}{\beta_{max}})^{1/2} \qquad\qquad (525.02)$$

that also tends towards the host band shape given in Eq. 525.01 as ϵ increases.

The problems of obtaining the optimum density of states for those energies close to the host band does not alter the principle result of these calculations which is that the density of states within the tail is low in comparison with that in the band, as can be seen from Fig 5.5.

= 5.34 =
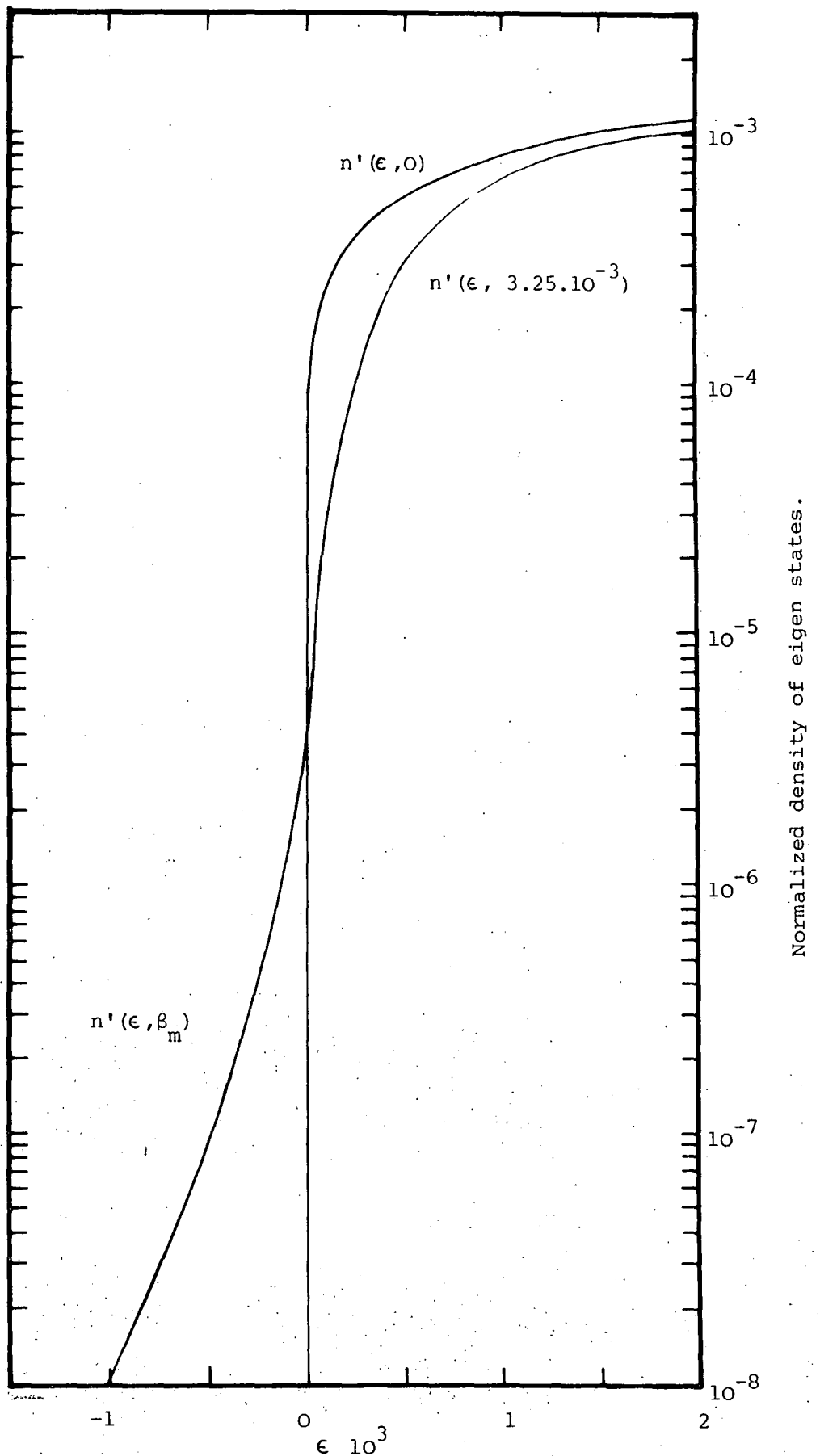
Fig 5.5   Normalized density of states $n'(\epsilon,\beta)$ from calculations based on Lloyd and Best's (1975) model for various β.

<u>**Numerical results for the conduction band.**</u>

Using the normalized curves in Fig 5.5 and the trial function $\phi(1)$ and $\phi(3)$ detailed in section 5.2.4 the density of states for the conduction band of silicon may be generated. This is shown in Fig 5.6 with the results from Halperin and Lax's calculations. In these calculations the detailed nature of silicon's conduction bands is accounted for by calculating the density of states in one of the six ellipsoidal valleys (section 2.1) and multiply the result by the number of valleys (M_c = 6 for silicon).

$$N(E,\lambda) = \frac{M_c}{4\pi^2} \left(\frac{m}{\hbar^2}\right)^{3/2} b^{1/2} e^{-z^2/4} U(1,z) \qquad (526.01)$$

The density of states effective mass (m_{de} = 0.32m_o) is used in all the normalizing expressions (Eq. 523.10–523.12).

5.3   <u>CONCLUDING REMARKS.</u>

Halperin and Lax produced a formulation for the density of states deep in the band tail where they perform four operations:

a)   Choose the form of a typical wavefunction deep in the tail.

b)   Using this wavefunction and modelling the impurities as a superposition of Thomas Fermi screened potentials calculate the ground state by a variational calculation.

c)   Calculate the density of states by counting the number of potential wells, formed by small regions in space accumulating more ionised impurities than the average concentration throughout the semiconductor.
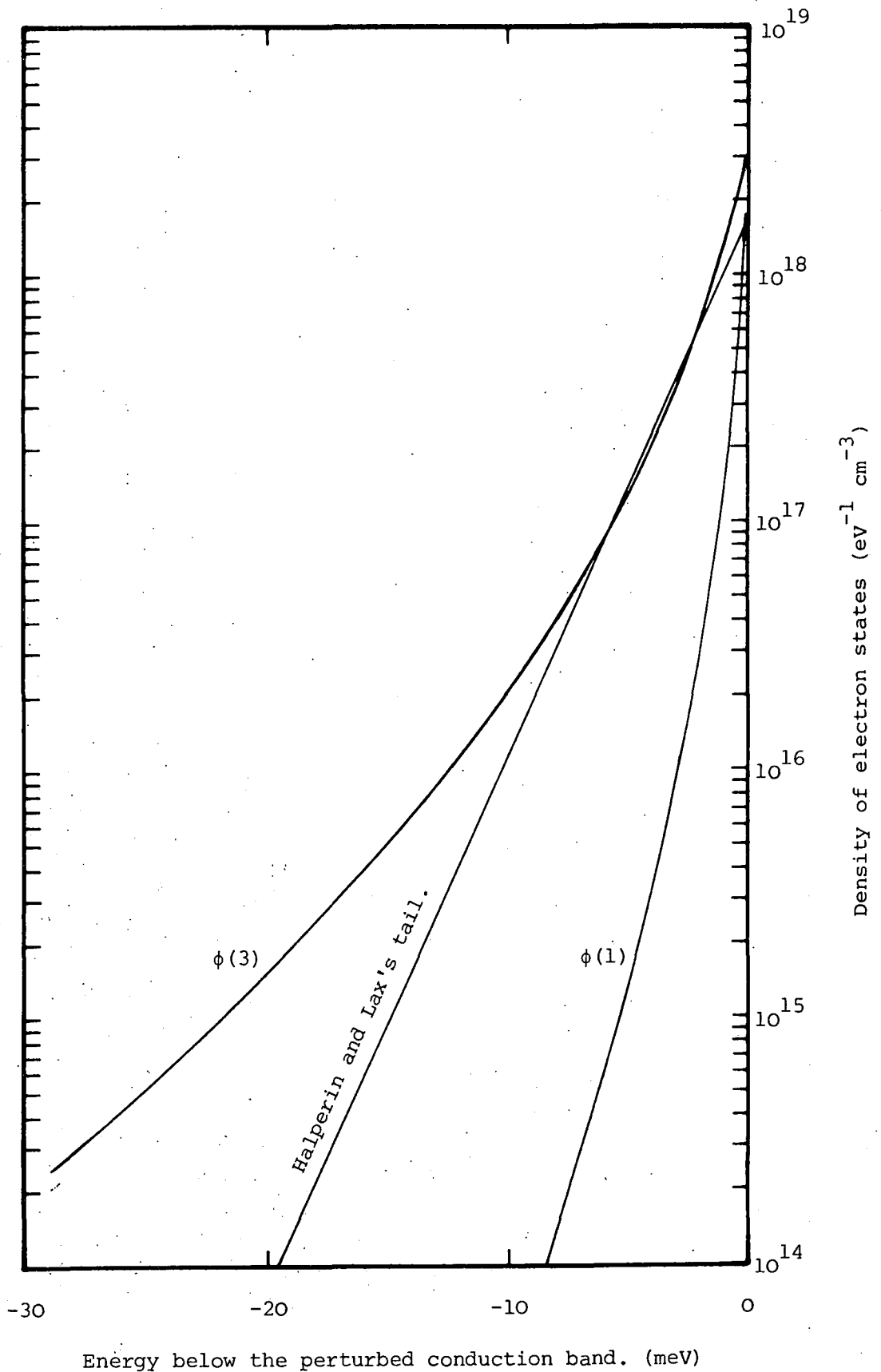
Fig 5.6   Tail on the conduction band density of states calculated using trial wavefunctions $\phi(1)$ and $\phi(3)$ in Lloyd and Best model from Fig 5.5.   Also showing Halperin and Lax's tail from Fig 5.2 for a donor concentration of 10^{20} cm^{-3}.

d)   Optimizing the chosen wavefunction by maximizing this density of states.

This minimum counting method breaks down for energies close to the host band because at these energies the one-to-one relationship between potential wells and their associated eigenstates no longer holds. The localized wavefunctions then begin to extend over more than one minima interfering with neighbouring wavefunctions.

Lloyd and Best in their work (1975) approach the calculation of tail states from the other end, starting with these extended states and moving deeper into the tail. Their method has the following steps:

a)   Divide the whole of space up disjoint cells of the same volume λ^2.

b)   Fit trial wavefunctions ($\phi(1)$) into these boxes.

c)   Calculate the density of states assuming each box contains a sample of impurities, the number of that varies from box to box about a mean value. It is assumed that the impurities are distributed uniformly within each box.

d)   Optimize the cell size by maximizing the double integral of this density of states

Because the cells fill all space, when they optimize the cell size in the band tail they under estimate the density of states because they do not pick out the very short range states counted in Halperin and Lax's method. However closer to the host band where the wavefunctions become extended and begin to fill all space the disjoint cell approximation improves.   For energies within the host band the cell size becomes infinite and the host density of states is reproduced exactly.

Thus the calculation based on Lloyd and Best's variational calculation of the density of states within the band tail must give a

reasonable approximation to the density of states close to the band edge. However although their variational principle may be valid over all energies in the tail it is difficult $\overset{\text{to}}{\underset{\lambda}{}}$ use. At best a trial function, like $\phi(3)$ might be fitted to Halperin and Lax's tail to provide a link between the deep tail and the host band. Deep in the tail Halperin and Lax's calculation is expected to give a better estimate to the density of states. Although the precise means of linking these two calculations remains a problem it is clear from the Lloyd and Best calculations (see Fig 5.5) that the band tail is much smaller than has previously been supposed. Convincing arguments have also been given in section 5.1.3 for relative positions of the host band and the tail calculated from Halperin and Lax's results (Fig 5.2). Recent calculations on high-stress optical birefringence (Sernelius 1983) are also in agreement with the hypothesis presented here that there is not a substantial band tail.

CHAPTER 6

AN ALTERNATIVE APPROACH TO THE ELECTRON-IMPURITY PROBLEM.

6.0   INTRODUCTION.

In   previous   chapters   the   electron-electron   and   electron-
impurity interactions have been considered separately hoping in the final
analysis to sum these contributions to the band gap narrowing.   These
interactions have been studied in a perturbation expansion to second order
of smallness.   In this chapter a self consistent approach to the electron-
impurity interactions is introduced to which the electron-electron self
energy must be added later.   Although it is obviously more useful to
consider a random lattice of donors, as Ghazali and Serre (1982, 1983) do,
a regular lattice of impurity centres is investigated here to study the
salient features of similar calculations by Mahan (1980) that Berggren and
Sernelius (1981) and Selloni et al (1982) have discussed.   This method
might be extended at a later stage for a random system of donors.   However
at first the regular lattice of donors is considered.

As a starting point to the calculation of the electron-impurity
interaction energies the band edges have been calculated in a simple Wigner
- Seitz type calculation.   The calculation is based on those made by
Baltensperger (1953) and is λ similar to those recently made by Engstrom (1983).
This method has been extended using the currently available numerical
routines (from the Numerical Algorithms Group) to improve and extend the
calculations for silicon.   In section 6.1 the details of the Wigner-Seitz
method used are given.

At low concentrations the impurities are far apart in the host
silicon lattice.   To a first approximation the donor impurity centres are

hydrogen like so that the electrons fall into states that have an energy equal to the effective Rydberg constant (R_{eff} = 31.9 meV in silicon) below the continuum or conduction band energy. As the donor concentration increases the donor potentials begin to interact causing a splitting of the impurity level. The broadening of the impurity level into a band with increasing concentrations finally results in its merging with the host band. At this point in the concentration range the bottom of the impurity band is considered to be the same as the parent band edge. The energy of the wavefunction occupying the lowest state in the periodic impurity potential gives a measure of the energy of the band bottom relative to its unperturbed position. In the low density limit this energy might be expected to approach the effective Rydberg value. However the presence of the large number of impurity electrons in the conduction band results in a screening of all the various coulombic interactions in the crystal characterized by κ the Thomas Fermi screening length (see section 4.4.2). Since the screening length ($1/\kappa$) is less than the average impurity separation over all of the concentration range of interest in silicon (see Fig 2.4) the impurity potential is short range. In the Wigner–Seitz method the wavefunction and energy of the states are calculated. It then becomes possible to make a self consistent calculation of the screened potential in this approximation. The choice of screened potential is made in section 6.2. Having thus determined the energy of the conduction band, the wavefunction for the lowest state in this band and the screened impurity potential it is then possible to calculate the energy and wavefunction of a hole from the valence band in the same potential. The shift in energy of the valence band is thus also obtained in section 6.3. Section 6.4 contains a discussion of these results for a regular impurity lattice and a comparison with the results from previous sections.

6.1   WIGNER SEITZ METHOD.

A periodic array of positively charged impurity ions superimposed on the host semiconductor lattice is taken. Each ion may be surrounded by an s- or Voronoi (see Brostow et al 1978) polyhedra that fill all space. The Wigner Seitz assumption that these polyhedra may be replaced by spheres of equal volume is made. These spheres are assumed to be of such a size that they contain many of the host semiconductor lattice sites. Thus to include the screening effect of the host semiconductor the macroscopic value of the relative dielectric constant ϵ_r (11.8 for silicon) is used with the effective mass for the electrons and holes. Clearly close to the centre of the polyhedra where the coulombic potential due to the positive charge varies rapidly the effective mass approximation will fail along with linear screening approximations. Close to the impurity centre an improved model for the impurity potential is required to account for the different impurity types such as is included in Selloni and Pantelides (1982). No attempt has been made to calculate these central cell corrections that will modify the energies in the present regular impurity lattice approximation but may not effect the more realistic random lattice approximation (Berggren and Sernelius (1983)). Implicit in the use of the intrinsic effective masses for the bands is the assumption that the band shapes do not change for high concentrations. If one considers that the total number of states must remain constant, at least for substitutional impurities, then it is clear that the states for the impurity band must come from the parent band which in turn must alter its shape. It is expected that this correction to the effective mass is small (Abram et al 1978).

In common with other Wigner – Seitz calculations the spherical approximation to the polyhedra is made choosing cells of the same volume as the original polyhedra with radius r_s $(= (3/4\pi N_d)^{1/3}$ where N_d is the impurity concentration). This can be justified (Mott & Jones 1958) by noticing that the potential is weak and the electron wavefunction flat far from the impurity centre (see Fig 6.2) thus the actual shape of the boundary is not too critical. This might be of use were the present calculations to be extended to cope with a random arrangement of donors, where different impurity centres have differing surroundings and a distributions of sphere radii might be considered. The potential energy of the impurity lattice may now be divided up into two parts: That which is due to the interaction between the charges in one cell and that part which is due to the interaction of polyhedra with each other. The second of which will be small since the cells are electrically neutral and close to spherical and is neglected. The radial part of the Schrodinger equation is now solved in the spherically symmetric cell for the electrons in the lowest eigenstate (k=0).

$$\nabla^2 \psi_o(r) + \frac{2m_{de}}{\hbar^2}(E_o - V(r))\psi_o(r) = 0 \qquad (610.01)$$

Where m_{de} is the density of states effective mass and $V(r)$ is the screened impurity potential and E_k the eigenvalue to be calculated. To fulfil the requirement for the periodic wavefunction to extend smoothly throughout space the gradient must be zero at the Wigner-Seitz boundary

$$\frac{d\psi}{dr}\bigg|_{r=r_s} = 0 \qquad ; \qquad \psi(0) = \text{finite} \qquad (610.02)$$

(Cohen 1972, Anderson 1963). A condition that might still hold in a high density, random impurity calculation. Also that the wavefunction be finite at the cell centre (r=0). This boundary condition is equivalent to

choosing a hydrogen like wavefunction at the origin.

The problem can be re-expressed in terms of the dimensionless variable $\rho = r/a_{eff}$ where a_{eff} is the effective Bohr radius and with the effective Rydberg constant (R_∞) as the unit of energy:

$$R_\infty = \frac{m_{de}e^4}{32\pi^2(\epsilon\epsilon_r)^2} = 31.97 \text{ meV}$$

(610.03)

$$\frac{1}{\rho^2}\frac{\partial}{\partial\rho}\left(\rho^2\frac{\partial\psi(p)}{\partial\rho}\right) + (\epsilon - \chi(\rho))\,\psi(p) = 0$$

Where $\chi(\rho) = (2m_{de}/\hbar^2)\,a_{eff}^2\,V(r)$

A NAG Library routine DO2KEF was used to solve the above equation. It finds a specific eigenvalue λ of a regular singular second order Sturm − Liouville system

$$(p(x)y')' + Q(x;\lambda)y = 0$$

(610.04)

on a finite or infinite range, using a Pruefer Transformation and a shooting method. It reports values of the eigenfunction and its derivatives subject to boundary conditions of the form

$$C(x,\lambda)p(x)y' + D(x,\lambda)y = 0$$

(610.05)

provided that $p(x)$ is not zero and of one sign and that $\partial Q/\partial\lambda$ is not zero as x varies for any λ and is of one sign throughout the interval.

Clearly in this problem $p(x) = \rho^2$ so the first condition is violated at the origin. However this is just where the wavefunction is expected to be close to the hydrogen like form $(e^{-\rho})$ therefore make the boundary close but not equal to $\rho = 0$. It is only the ratio of the functions $C(x,\lambda)$ and $D(x,\lambda)$ that matter so the actual boundary conditions

are expressed as:

$$\rho = \rho_s \qquad C = 1 \; ; \; D = 0$$
$$\rho = 0 \qquad C = 1 \; ; \; D = \rho^2 \tag{610.06}$$

All that remains is to specify the form of the screened potential to be used in the calculation.

6.2 CHOICE OF IMPURITY POTENTIAL.

A simple Coulombic potential was used in the numerical routine the results of which were checked against the analytical solution expressed in terms of Confluent Hypergeometric Functions $M(a,c;x)$ (Baltensperger 1953). The wavefunction in this approximation is given by

$$\Psi_{l\lambda}(p) = e^{-\rho/2} \rho^l \; M(l+1-\lambda, 2l+2; \rho) \tag{620.01}$$

and the eigenvalues given by

$$E_\lambda = - \; e^2/8\pi\epsilon\epsilon_r a_{eff}\lambda^2 \tag{620.02}$$

The eigenvalues calculated by the numerical routine were found to agree with those calculated from above to an accuracy of 1 part in 10^5.

This first potential corresponds to the condition that must exist at low impurity densities in the semiconductor. Only one electron is allowed to enter each sphere where the central positively charged impurity potential binds the electron in a hydrogen like orbital. The lowest eigenvalue in the impurity band saturates at the effective Rydberg energy of 33 meV in silicon. Indeed if the calculation of the highest state in the band were performed as Baltensperger does, this would also saturates at this energy. For above an impurity concentration of about $5 \; 10^{18} \; cm^{-3}$ the

model predicts a rapid lowering of the bottom of the impurity band and a raising of the top of the band (see Baltensperger Fig 1) that eventually merges with the conduction band. This model then predicts the broadening of the impurity level into an impurity band with the onset of heavy doping.

An improvement to this potential which begins to take into account the screening of the impurity charge by the electron gas in the conduction band is to include a uniform distribution of charge in the cell due to all the other electrons in the crystal (Mott & Jones 1958). In this model the screening electrons are assumed to have plane wave form and the wavefunctions are flat, that is expected to be true in the high density limit. There are then N-1 electrons contributing to the screening where N is the total number of impurities. This amounts to a concentration of one electron distributed uniformly over the cell. The screened potential may then be calculated from Gauss Law to be:

$$V(r) = -\frac{e^2}{4\pi\epsilon\epsilon_r r} - \frac{e^2 r^2}{8\pi\epsilon\epsilon_r r_s^3} + \frac{3e^2}{8\pi\epsilon\epsilon_r r_s} \qquad (620.03)$$

which in terms of the reduced variables becomes

$$\chi(\rho) = -\frac{2}{\rho} - \frac{\rho^2}{\rho_s^3} + \frac{3}{\rho_s} \qquad (620.04)$$

Where the first term is the unperturbed potential, the second is that due to an ever increasing sphere of uniform charge density, and the final term ensures that the potential is zero at the Wigner Seitz boundary.

A first classical calculation may be made for the electron in its ground state using the screened potential above. The eigenvalue may be calculated in a first order perturbation calculation assuming plane

wavefunctions to give:

$$\delta\mu = \langle V \rangle = \frac{3}{4\pi r_s^3} \int V(r) \, 4\pi r^2 \, dr$$

$$= -0.3 \, (e^2/4\pi\epsilon\epsilon_r r_s) = -0.484 \, (e^2/4\pi\epsilon\epsilon_r) \, N_d^{1/3}$$

$$= -5.901 \, (N_d/10^{18})^{1/3} \quad \text{meV} \tag{620.05}$$

where the values have been calculated for silicon. This compares favourably with the values obtained by Sholl (1967) for body-centred cubic, face-centred cubic and hexagonal close-packed lattices. Mahan (1980) quotes these values as

$$E_{total} = -1.444 \, (e^2/4\pi\epsilon\epsilon_r) \, N_d^{1/3}$$
$$\delta\mu = N_d \, \partial E/\partial N_d = -0.481 \, (e^2/4\pi\epsilon\epsilon_r) \, N_d^{1/3} \tag{620.06}$$

This approximation to the energy of the conduction band is presented in Fig 6.1. It can be seen to reduce to zero as the concentration is decreased.

However these calculations suffer from the disadvantage that a plane wave is taken in the calculation to represent the true wavefunction, that is in fact more complex. A second more sophisticated calculation is to put this screened potential into the numerical routine outlined above. In this calculation the actual wavefunction and eigenvalue that would result from an electron occupying a potential well of this form is calculated. The results of this numerical calculation are also presented in Fig 6.1. At low concentrations this energy saturates at the effective Rydberg value (33meV in silicon) since the screening electrons are so thinly spread as to to be ineffectual. Whilst at high concentrations, where the wavefunctions do indeed become flatter, the numerical method and the classical expression (Eq. 620.05) approach each other.
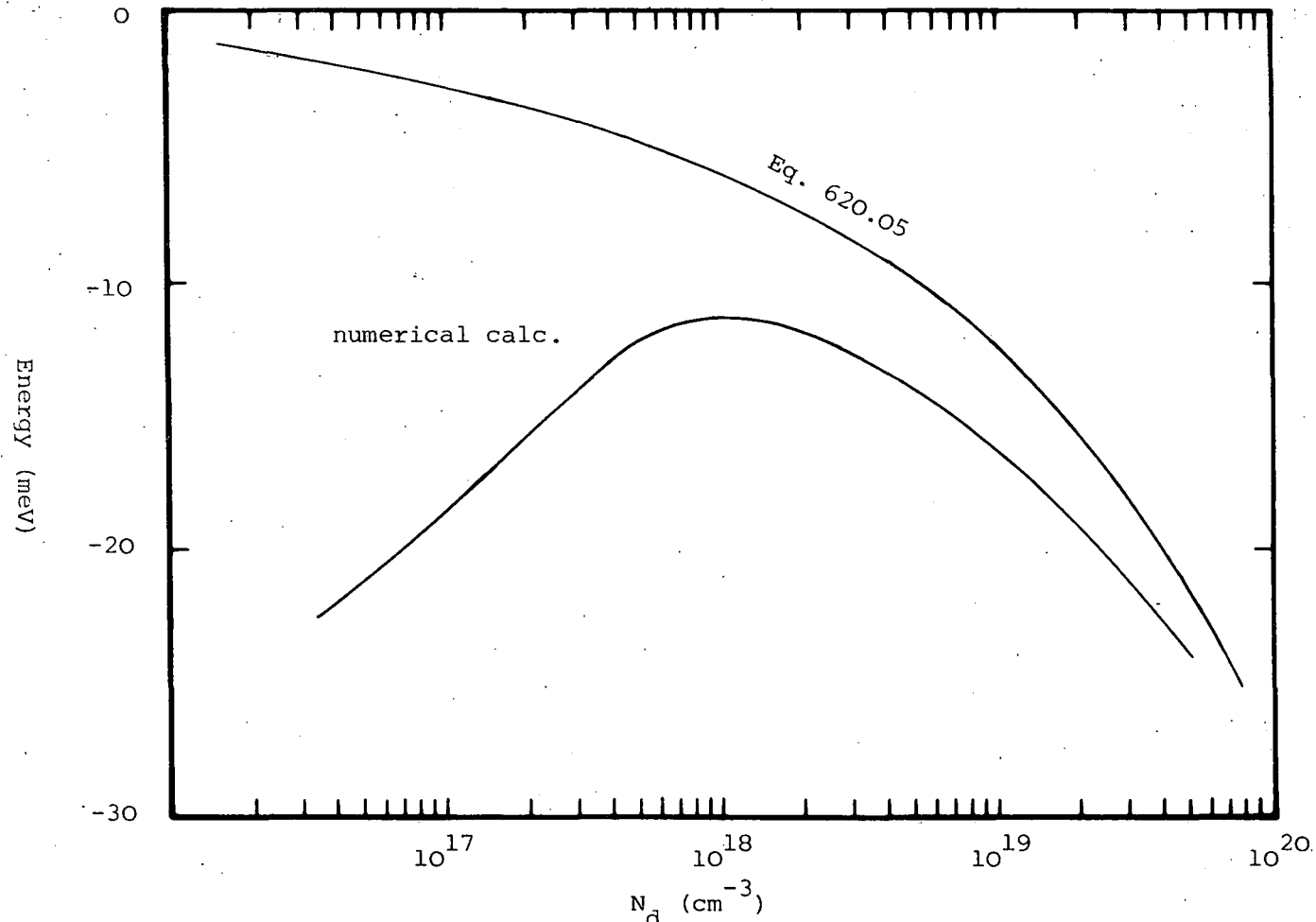
Fig.6.1   First order perturbation calculation (Eq. 620.05) with uniformly screened potential (Eq. 620.03) and numerical solution of the Schrodinger equation (Eq. 610.01) with this potential.

An important failing of this numerical solution is that on one hand a plane wave is assumed for the screening cloud whilst on the other hand a periodic non-uniform charge distribution results from the true ground state wavefunction calculated. A more physically acceptable model is one where the screening cloud is bunched up about the positively charged donor. To make this a more realistic approximation to the screening cloud the screened potential needs to be improved.

The actual form of the wavefunction as well as the lowest eigenvalue are calculated in the numerical calculation as defined by Eq. 610.01– 610.02. A self consistent screening charge may then be calculated from this wavefunction. This self consistent approach screens the impurity potential by exactly the right amount solving the present model exactly. To do this a parabolic band is assumed above the conduction band edge (see for example Mott and Jones 1958)

$$\psi_k(r) = e^{ik \cdot r} \psi(r) \qquad (620.07)$$

Given wavefunctions of this form the charge within a sphere radius r and hence from Gauss's Law the potential seen by the electron may be calculated

$$V(r) = - \frac{e^2}{4\pi\epsilon_r}\left(\frac{1}{r} + \frac{\int^r (1/r')^2 \int^{r'} r''^2 |\psi_k(r'')|^2 dr'' dr'}{r_s \int_0^{r^2} r^2 |\psi|^2 dr}\right)$$

$$- V_{bound} \qquad (620.08)$$

V_{bound} is chosen so that $V(r_s) = 0$ as in Eq. 620.03. The calculation is initiated by choosing a form for the potential V(r) then this potential is used to calculate an approximate wavefunction and eigenvalue. This wavefunction is then used to calculate the wavefunctions of the higher k states (Eq. 620.07) and hence the screening of the coulombic potential. This iterative process is carried on until the eigenvalue saturates at

which point both this and the wavefunction are self-consistent.

6.3 SELF CONSISTENT CALCULATION OF ELECTRON AND HOLE ENERGY.

Following the procedure in the previous sections the impurity potential is found self consistently by solving Eq. 610.01 with the self consistent potential Eq. 620.08 by an iterative calculation. The resulting self consistent impurity potential is plotted in Fig 6.2a. Also plotted in this figure is the Thomas Fermi potential often used in similar problems. This is different from the self consistent potential because it is calculated on the assumption of an infinite cell size it has a non zero value at the cell boundary, whilst the self consistent potential is calculated on the assumption that the potential is zero at the boundary. However as the concentration decreases the two potentials would be expected to give better agreement. The probability densities of the electron wavefunction is also plotted in Fig 6.2 for two values of r_s. It shows the expected rise close to the centre of the cell (see Mahan (1980) Fig 5). As r_s decrease, at higher impurity concentrations, the wavefunction can be seen to get flatter, so that in the high density limit the plane waves used in the classical calculation (Eq. 620.05) become more realistic. Finally Fig 6.3 shows the change in the electron eigenvalue with concentration.

In previous sections in this chapter the change in electron energies due to the presence of various impurity potentials has been considered. A positively charged hole in the valence band however would also be affected by the presence of these impurities. Postulating the presence of a test hole in the valence band the influence that this hole has upon the screening cloud about the impurity centre may be neglected since there is only one hole supposed to be at the top of the valence band.
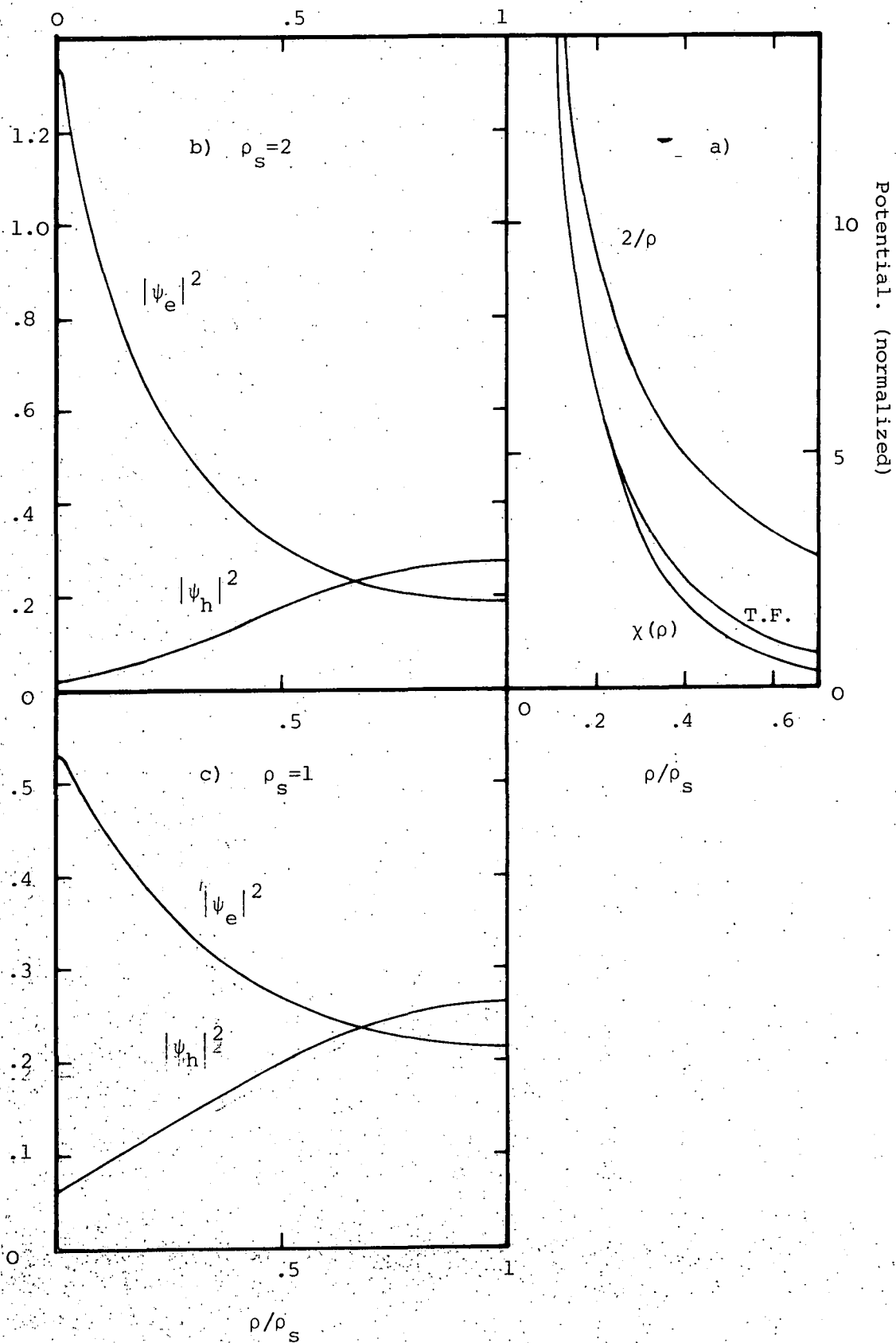
Fig 6.2   Electron (hole) charge density $|\psi_e|^2$ ($|\psi_h|^2$) and self consistent
potential ($\chi(\rho)$) in the Wigner Seitz sphere.
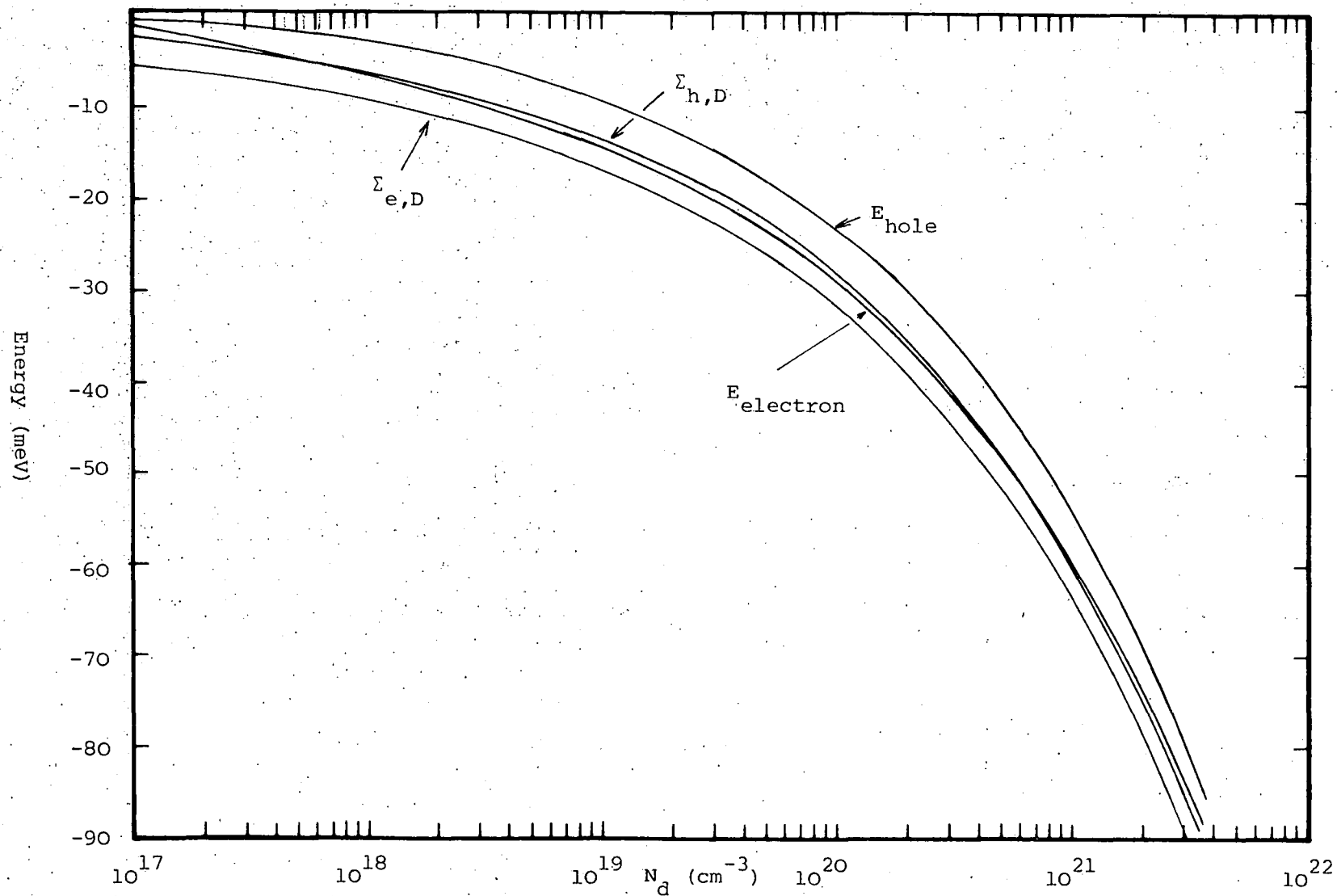
Fig 6.3   Self consistent electron (hole) impurity energies calculated from Eq. 610.01 and
           by Mahan 1980 ($\Sigma_{h,D}$, $\Sigma_{e,D}$).

The appropriate Schrodinger equation to be solved is

$$\nabla^2 \psi_k(r) + \frac{2m_{de}}{\hbar^2}(E_k + V(r))\psi_k(r) = 0 \qquad (630.01)$$

where the sign of the potential term (compare with Eq. 610.01) is consistent with the opposite charge that the hole. $V(r)$ the screened potential has already been discussed in the self consistent electron energy calculation. The boundary conditions for the problem are different from the electron calculation. In this case the hole must be repelled from the positively charged ionised impurity at the centre of the sphere. The wavefunction is chosen to have zero gradient at both the centre and the edge of the sphere in order to satisfy the required smoothness of the wavefunction throughout space. These conditions are expressed in terms of the boundary conditions Eq. 610.04-610.05 as

$$
\begin{aligned}
\rho &= \rho_s & C &= 1 : D = 0 \\
\rho &= 0 & C &= 1 : D = 0
\end{aligned}
\qquad (630.02)
$$

With these modified boundary conditions and the self consistent potential shown in Fig 6.2a the hole energy plotted in Fig 6.3 is calculated. This shows the expected rise in probability density of the hole towards the boundaries of the sphere where the wavefunctions flatten off, with zero gradient at the boundary. This calculation results in a positive value of the eigenvalue E_k for the hole shown in Fig 6.3.

6.4   <u>DISCUSSION OF RESULTS.</u>

The increase in the holes energy results in a downward shift of the valence band edge and hence an additive contribution to the band gap (see Fig 6.3) in contrast to the previous electron-impurity calculations on a random impurity lattice (chapter 4). It should be stressed at this point that the downward shift in the valence band for this model with periodic impurity lattice has been found by Mahan (1980) as well as Berggren and Sernelius (1981) though the magnitudes of the shift vary. In order to understand the downward shifts of conduction and valence bands more fully the average or first order terms must be considered as in previous calculations (chapter 4).

Because the solution of Eq. 610.01 (Eq. 630.01) gives the total change in the energy of electrons (holes) at the bottom (top) of the conduction (valence) band it includes the first order term excluded from our previous calculations (see section 4.3). However the impurity potential has arbitrarily been chosen to be equal to zero at the cell boundary. It might equally well be chosen so that the integral of the potential over the cell is zero as would be expected by the cancellation of the electron-electron and electron impurity interactions (section 4.3). To compare with calculations in previous chapters the volume average of the screened potential has to be removed from the two bands solving instead of

Eq. 610.01 the equation

$$\nabla^2 \psi_o(r) + \frac{2m_{de}}{\hbar^2}(E'_o - V'(r))\psi_o(r) = 0 \qquad (640.01)$$

where

$$V'(r) = V(r) + V_{av} \qquad (640.02)$$

and

$$V_{av} = -\frac{1}{v} \int V(r) \, d^3r \qquad (640.03)$$

where v is the volume of the sphere. Clearly since V_{av} is a constant

$$E'_o = E_o + V_{av} \qquad (640.04)$$

So that the shift in the conduction band edge shown in Fig 6.3 is reduced by V_{av}. At the same time, as can be verified from Eq. 630.01, the valence band shift is also reduced by V_{av} as would be expected since the average term effects both bands equally. These reduced shifts could then be compared with the previously calculated electron-impurity self energies. However they do not effect the much smaller electron-impurity band gap narrowing results (only 5 meV over the entire concentration range), calculated in the present model with a regular impurity lattice. Berggren and Sernelius have explained this large discrepancy in the electron-impurity band gap narrowing in terms of the coherent reinforcing of the impurity potential in the regular lattice as compared to the random lattice. They calculated the second order perturbation energy of a regular lattice and find conclusively that the resulting band gap narrowing is small as has been found above.

CHAPTER 7

CALCULATION OF THE SELF ENERGY INTEGRALS AT FINITE TEMPERATURE.

7.0 INTRODUCTION.

In this chapter the calculations of previous chapters using the plasmon pole approximation are extended to finite temperature. As comparisons between results calculated using the Lindhard dielectric function (Berggren and Sernelius 1981) and those of the previous chapters has shown, the plasmon pole approximation provides a relatively simple means of modelling the electron screening of donors in heavily doped silicon. This then justifies the extension of the present approach to finite temperature. The finite temperature plasmon pole approximation has been used before in other problems (Zimmermann and Rosler (1976), Young, van Driel (1982) for and electron-hole liquid), however this is the first time that the present method including the q^4 term has been used for heavily doped silicon.

For a summary of the contributions to the band gap narrowing dealt with in chapters 2 to 4 see Fig 7.1. The finite temperature contributions to the band gap narrowing are defined by substituting the appropriate finite temperature quantities into the self energy expressions from Eq. 240.07 and 441.06. Sections 7.1 and 7.2 deal with the derivation of the finite temperature variables for substitution into the two self energy expressions Eq. 240.07 and 441.06. Fig 7.2 summarizes the concentration dependent finite temperature quantities calculated in section 7.2 (κ, ϵ_F), comparing them with those calculated at zero temperature (see Fig 2.4). As has been seen from the calculations at finite temperature the Mott metal non-metal transition (N_c) determines the lower bound in

$\Delta E_g = \Delta E_c - \Delta E_v$
$= -136$ meV

ΔE_C
-70.44

ΔE_V
$+65.56$

ΔE_C^{ee}
-44.06

ΔE_C^{ei}
-26.38

ΔE_V^{ee}
$+38.95$

ΔE_V^{ei}
$+26.61$

ΔE_C^{ch}
-40.44

ΔE_C^{sx}
-3.62

ΔE_V^{ch}
-51.02

ΔE_V^{sx}
$+89.97$

ΔE_{HH}^{ch}
-35.35

ΔE_{HL}^{ch}
-15.67

ΔE_{HH}^{sx}
$+56.98$

ΔE_{HL}^{sx}
$+32.99$
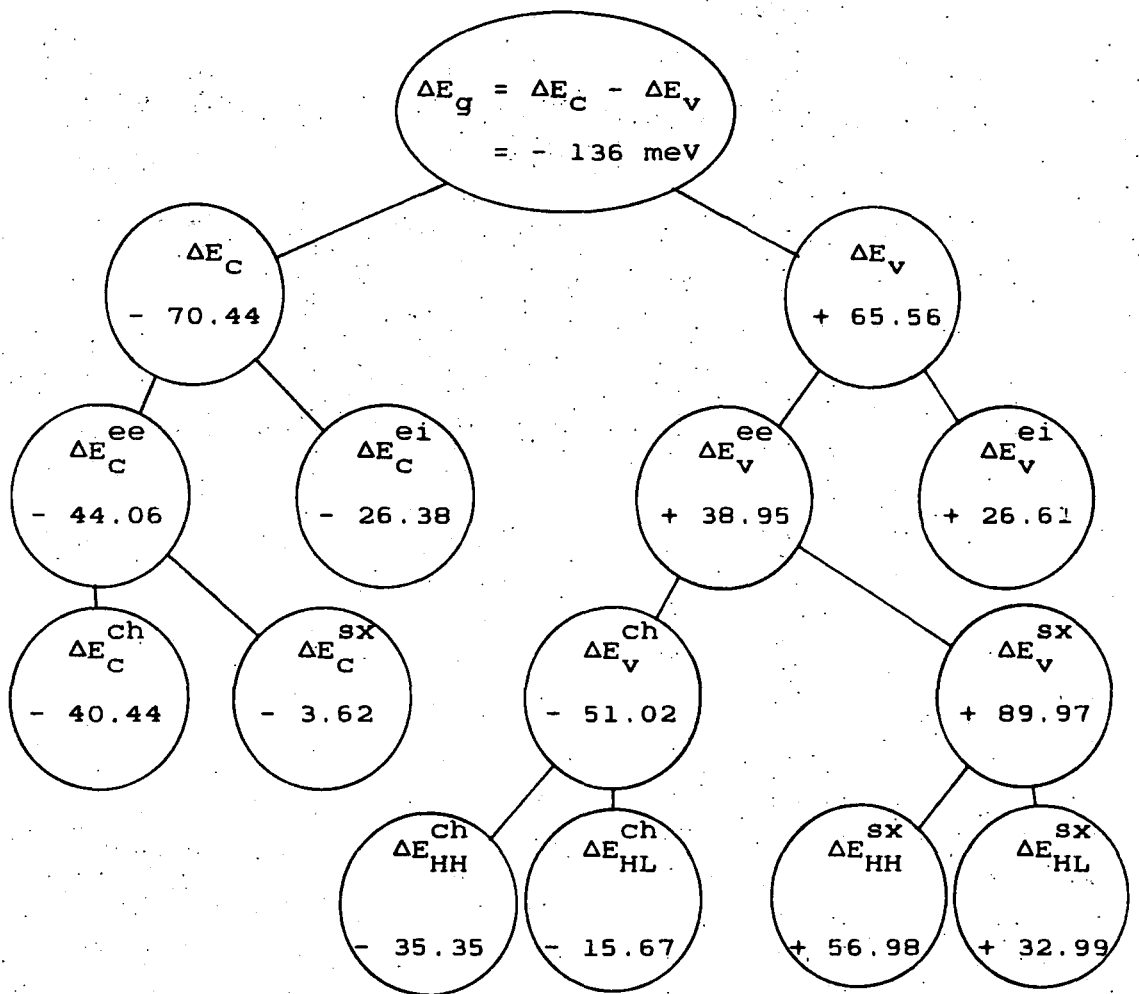
Fig 7.1. In heavily doped silicon (T=0, donor concentration of 10^{20} cm^{-3}) the band gap narrowing (meV) calculated in the plasmon pole approximation (2.3.2) may be divided into shifts in the conduction (ΔE_c) and valence (ΔE_v) band edges. These are divided into electron-electron (ee, chapter 3) and electron-impurity (ei, chapter 4) contributions. The electron-electron contributions are subdivided (3.1.0) into coulomb hole (ch) and dynamic screened exchange (sx) terms. In the valence band the ee exchange energy is again subdivided (3.3.0) into exchange between for example electrons in the heavy hole band (HH) and exchange between heavy and light hole bands (HL). To supplement the electron-impurity self energy calculations the band tailing effect of fluctuations in the average potential are considered in chapter 5.
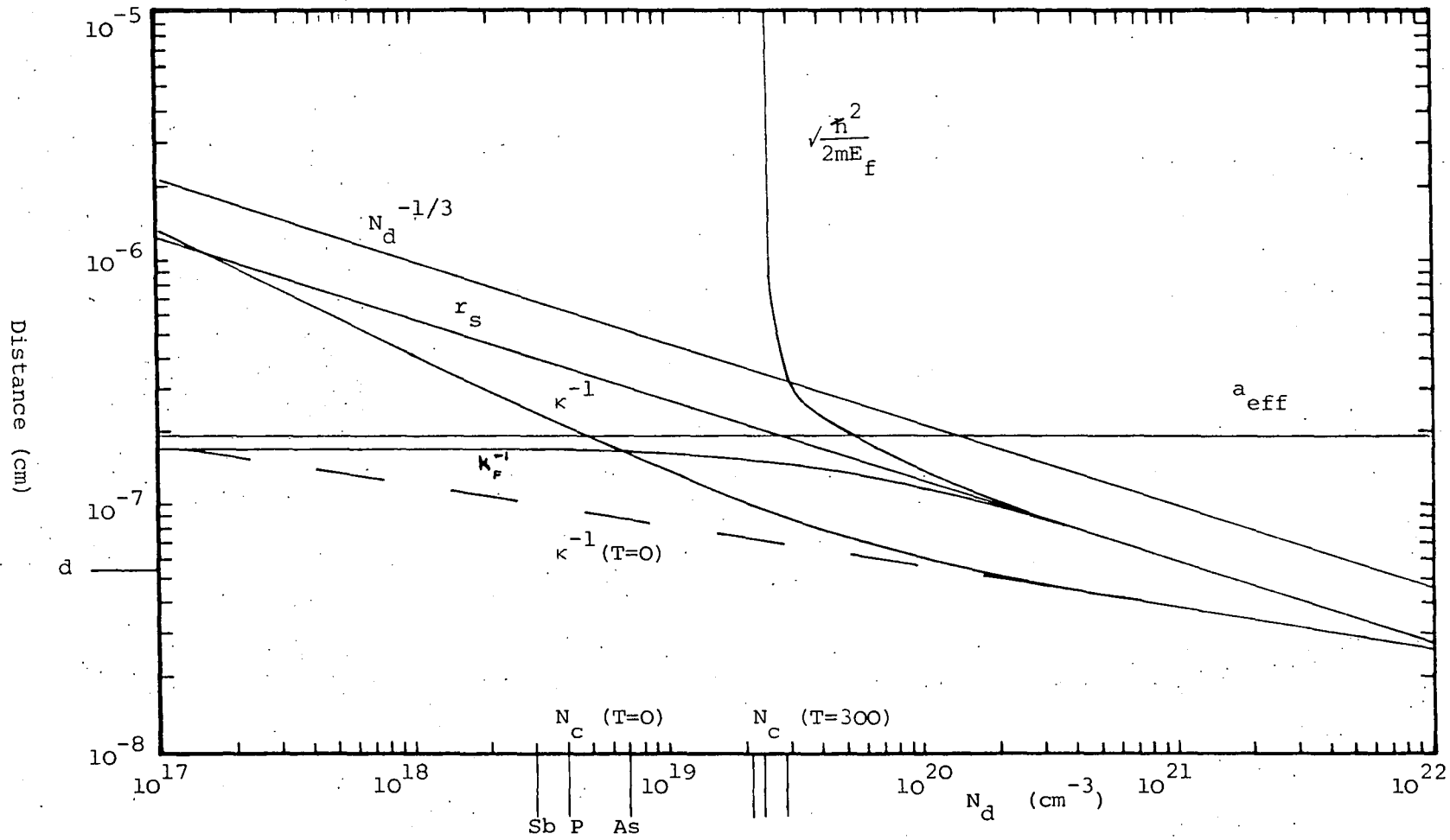
Fig 7.2   Thomas Fermi screening length (κ^{-1}), k_F^{-1}, $N_d^{-1/3}$, r_s, a_{eff}, N_c and other parameters at 300K.

concentration to which the calculations are valid. Before describing the finite temperature calculations the change in this concentration at high temperature is considered.

Below the Mott critical density (N_c) the impurity electrons are well localized about the impurity centres and form a separate impurity band. The low concentration semiconductor has then for example a Curie-Weiss type susceptibility typical for interaction localized magnetic moments. For higher densities however the electron screening length ($1/\kappa$) is reduced (see Fig 7.2) so that eventually the screening due to free electrons in the conduction band reduces the binding energy of the donors to such an extent that the impurity electrons are no longer bound to the impurities and the impurity band is considered to have merged with the host band. The susceptibility is then Pauli-like, consistent with the assumption that a free-electron gas occupies the host band. Similar transitions occur in the extrinsic specific heat capacity (Mott 1974, 1978). The Mott critical density is then dependent upon the ratio between the screening radius ($\lambda = 1/\kappa$) and the effective Bohr radius (a_{eff}) for the bound impurity electrons (Kittel 1976, pp 300). When λ is greater than a_{eff} the impurity electrons are essentially uneffected by the screening and are bound to the impurities. When a_{eff} is greater than λ the impurity electrons are effectively screened from the impurities and behave as in a metal. At finite temperatures and low concentrations the screening length is increased from the zero temperature values as can be seen from Fig 7.2. The finite temperature Mott transition might then be expected to occur at higher concentrations. By maintaining the ratio of a_{eff}/λ the 300 K Mott transition may be estimated from the more rigorous zero temperature calculations. In this way the Mott transitions of between 2 and 3.10^{19} cm^{-3} at 300 K are estimated from zero temperature data due to Sernelius and

Berggren (1981) plotted in Fig 7.2.

The electron-electron calculations of section 7.3 correspond to those in chapter 3, whilst in 7.4 the electron-impurity calculations corresponding to those in chapter 4 are presented. The band tailing calculations of chapter 5 have not been extended to finite temperature, because of the relatively small modification that these make in uncompensated heavily doped n-type silicon at zero temperature. Likewise the calculations of chapter 6 are not extended to finite temperature because they do not constitute a particularly useful approach to the calculation of the band gap narrowing, although they do serve in providing a slightly different approach. The main results of this chapter may be found in Fig 7.12 for the finite temperature band gap narrowing.

7.1   DERIVATION OF THE SELF ENERGY EXPRESSIONS AT FINITE TEMPERATURE.

In this section the finite temperature Green's function (section 7.1.1) and the finite temperature plasmon pole inverse dielectric function (section 7.1.2) are derived.

7.1.1   Finite temperature Green's function.

An equivalent way of writing the zero temperature unperturbed Green's function for the band n (Eq 221.03) is in terms of the step functions $\theta(r)$.

$$G^0(n;k,\omega) = \frac{\theta(\epsilon_f - \epsilon_{nk}^0)}{(\omega - \omega_{nk}^0 - i\delta)} + \frac{\theta(\epsilon_{nk}^0 - \epsilon_f)}{(\omega - \omega_{nk}^0 + i\delta)} \qquad (711.01a)$$

where $\omega_{nk}^0 = \epsilon_{nk}^0/\hbar$

The first term describes the propagator for an excitation beneath the Fermi

surface, whilst the second describes the propagation above that surface. Where at low temperatures the Fermi surface may be described by the above step functions, at higher temperatures the Fermi-Dirac distribution must be used. The correct finite temperature Green's function is then given by (Mahan 1981, Hedin and Lundqvist 1969)

$$G^0(n;k,\omega) = \frac{f_{nk}}{(\omega - \omega_{nk}^0 - i\delta)} + \frac{1 - f_{nk}}{(\omega - \omega_{nk}^0 + i\delta)} \qquad (711.01b)$$

where f_{nk} is the Fermi-Dirac distribution function

$$f_{nk} = \frac{1}{\exp((\epsilon_{nk}^0 - \epsilon_F)/kT) + 1} \qquad (711.01c)$$

To distinguish it from the zero temperature Fermi level ϵ_f, the finite temperature Fermi energy is denoted by ϵ_F. This expression (Eq. 711.01b) reduces to the former (Eq. 711.01a) on letting T the temperature tend towards zero. In calculations in n-type semiconductors for the valence band the Fermi energy will again be many kT from the appropriate energy ϵ_{nk}^0 so that the Fermi distribution reduces to a step function in this band at any temperature.

7.1.2. <u>Finite temperature inverse dielectric function.</u>

In section 2.3 the plasmon pole approximation (including the q^4 term in the plasmon dispersion) was shown to be a good approximation to the zero temperature electron dielectric function. The plasmon pole approximation as discussed above and elsewhere (Du Bois 1959, Pines 1961, Lundqvist 1967) amounts to describing the response of the electron gas to external electric fields by excitation of longitudinal oscillations in the electron gas known as plasmons (Kittel 1976). This description is found only to be strictly valid up to a critical frequency ω_c (see Fig 2.6). For

higher wavevectors the imaginary part of the Lindhard dielectric function becomes non-zero and the pole in the inverse dielectric function complex. Physically this corresponds to damping of the plasmon oscillations. However by comparison with the results of Berggren and Sernelius it has been shown (see chapters 2, 3, 4) that the plasmon pole approximation is good at zero temperature. It therefore seems appropriate to extend the plasmon pole approximation to finite temperature directly rather than going through a detailed derivation of the more involved finite temperature Lindhard dielectric function. This is performed by making the rather arbitrary division of the plasmon term in the inverse dielectric function into Bose propagator and coupling constant (Du Bois 1959, Pines 1961, Lundqvist 1967).

If one looks at the zero temperature Feynman representation of an electron-phonon interaction diagrams like

$$(712.01)$$

occur where

$$(712.02a)$$

represents the phonon and may be interpreted as

$$D(q,\omega) = 2\omega_1(q) \; \frac{1}{\omega^2 - (\omega_1(q) - i\delta)^2} \qquad (712.02b)$$

Each of the vertices introduce the coupling constant

$$\frac{M_q}{\sqrt{v}} \qquad (712.02c)$$

where M_q is the matrix element for the electron-phonon interaction and v is the volume. This is of the same form as the plasmon pole contribution to the zero temperature inverse dielectric function (for example Eq. 240.07c). Use of the plasmon propagator in the effective potential amounts to

replacing the screened interactions shown in previous Feynman diagram expansions of the self energy (like Eq 222.04 or 420.16) by these (Eq 712.01) Bose propagators (see for example Bergersen et al 1973). The expression

$$\frac{1}{\epsilon(q,\omega)} = 1 + \frac{\omega_p^2}{2\omega_1(q)} \text{(Bose propagator)} \qquad (712.03)$$

is then used to define the finite temperature plasmon pole approximation to the inverse dielectric function.

At finite temperature the Bose propagator takes the form (Mahan (1981), Fetter and Walecka (1971), Hedin and Lundqvist (1969))

$$D(q,\omega) = 2\omega_1(q) \left(\frac{1 + N_q}{\omega^2 - (\omega_1(q) - i\delta)^2} - \frac{N_q}{\omega^2 - (\omega_1(q) + i\delta)^2} \right)$$

$$(712.04a)$$

where N_q is the Bose Einstein distribution for the plasmons with energy $\hbar\omega_1(q)$ defined by

$$N_q = \frac{1}{\exp(\hbar\omega_1(q)/kT) - 1} \qquad (712.04b)$$

so that the inverse dielectric function becomes (using Eq. 712.03)

$$\frac{1}{\epsilon(q,\omega)} = 1 + \omega_p^2 \left(\frac{1 + N_q}{\omega^2 - (\omega_1(q) - i\delta)^2} - \frac{N_q}{\omega^2 - (\omega_1(q) + i\delta)^2} \right)$$

$$(712.05a)$$

The same dispersion relationship as in the finite temperature calculations (Eq. 232.10)

$$(\hbar\omega_1(q))^2 = (\hbar\omega_p)^2 + \frac{4m_{de}}{3m_{op}}\epsilon_q\epsilon_F + \epsilon_q^2 \qquad (712.05b)$$

the only difference being the use of the finite temperature Fermi energy ϵ_F that is calculated in the next section.

7.2 EVALUATION OF THE FERMI ENERGY AND THOMAS FERMI SCREENING LENGTH.

The calculation of the Fermi energy is central to the evaluation of the plasmon dispersion relationship (Eq. 712.06) so this is studied in detail below (section 7.2.1). No detailed derivation of the finite temperature Thomas Fermi screening length is presented here since this is a well known quantity (Dingle 1955, Fistul 1969, Panish et al 1967, Abram et al 1978). However its calculation includes the same approximations needed for the calculation of the Fermi energy, it is then quoted in section 7.2.2. Finally in section 7.2.3 a useful expression for the plasmon dispersion relationship at finite temperature that has the same form as its zero temperature counterpart (Eq. 240.07d) is derived.

7.2.1 Calculation of the Fermi energy.

First let us dispel the notion that it is Fermi energy modified by the exchange energies that should be included in the expressions. Looking first at the contribution of the self energy to the band energy (for example Eq. 240.04 and 240.05), the band energy is given by an iterative solution of Eq. 240.04. This has been taken to first order (Eq. 240.05). The quantities used to evaluate this first order expression are then the unperturbed values. To improve this approximation both better approximations to the self energy and further iteration of Eq. 240.04 would be required.

For the present calculations each of the impurities is assumed to allow one electron into the conduction band Fermi sea. The impurity band is assumed to have merged with the host band and the hole structure to have the same shape as the intrinsic conduction band (density of states

proportional to (energy)$^{1/2}$). Indeed this approximation is made implicitly at zero temperature when using equations like Eq. 221.04 for the Fermi wavevector. The number of electrons in one conduction band valley (n_e) is then (see Blakemore 1962)

$$n_e = 4\pi \left(\frac{2m_{de}kT}{\hbar^2}\right)^{3/2} \int_0^\infty \frac{\epsilon^{1/2}}{1 + \exp(\epsilon - \eta)} d\epsilon$$

$$= 4\pi \left(\frac{2m_{de}kT}{\hbar^2}\right)^{3/2} \frac{1}{2} \pi^{1/2} F_{1/2}(\eta) \qquad (721.01a)$$

where m_{de} is the density of states effective mass of the conduction band valley and η is the normalized Fermi energy given by

$$\eta = \frac{E_F - E_C}{kT} \qquad (721.02b)$$

and $F_{1/2}(\eta)$ is a Fermi Dirac integral. The effective mass m_{de} does not vary very significantly with the increase in doping (Abram et al 1978), nor is the k dependence of the self energy significant (Berggren and Sernelius 1981), so this parabolic approximation may well be justified. The impurity concentration is given by multiplying the above electron concentration per valley by the number of valleys (M_c = 6 for silicon see section 2.1)

$$N_d = M_c n_e = M_c 4\pi \left(\frac{2m_{de}kT}{\hbar^2}\right)^{3/2} \frac{1}{2} \pi^{1/2} F_{1/2}(\eta) \qquad (721.02)$$

To solve the above equation the electron (impurity) concentration (Eq. 721.02) is calculated for a series of trial Fermi energies, measured with respect to the conduction band edge. The Fermi Dirac integral was calculated using the NAG quadrature routine D01AJF. In Fig 7.3 the results of this calculation both for zero (Eq. 221.04) and 300 K are presented. This shows that the Fermi energy drops below the conduction band edge at a concentration of about $2.5.10^{19}$ cm^{-3} with this simple model for the band. At higher concentrations in strongly degenerate conditions the Fermi energy tends towards the zero temperature value. In
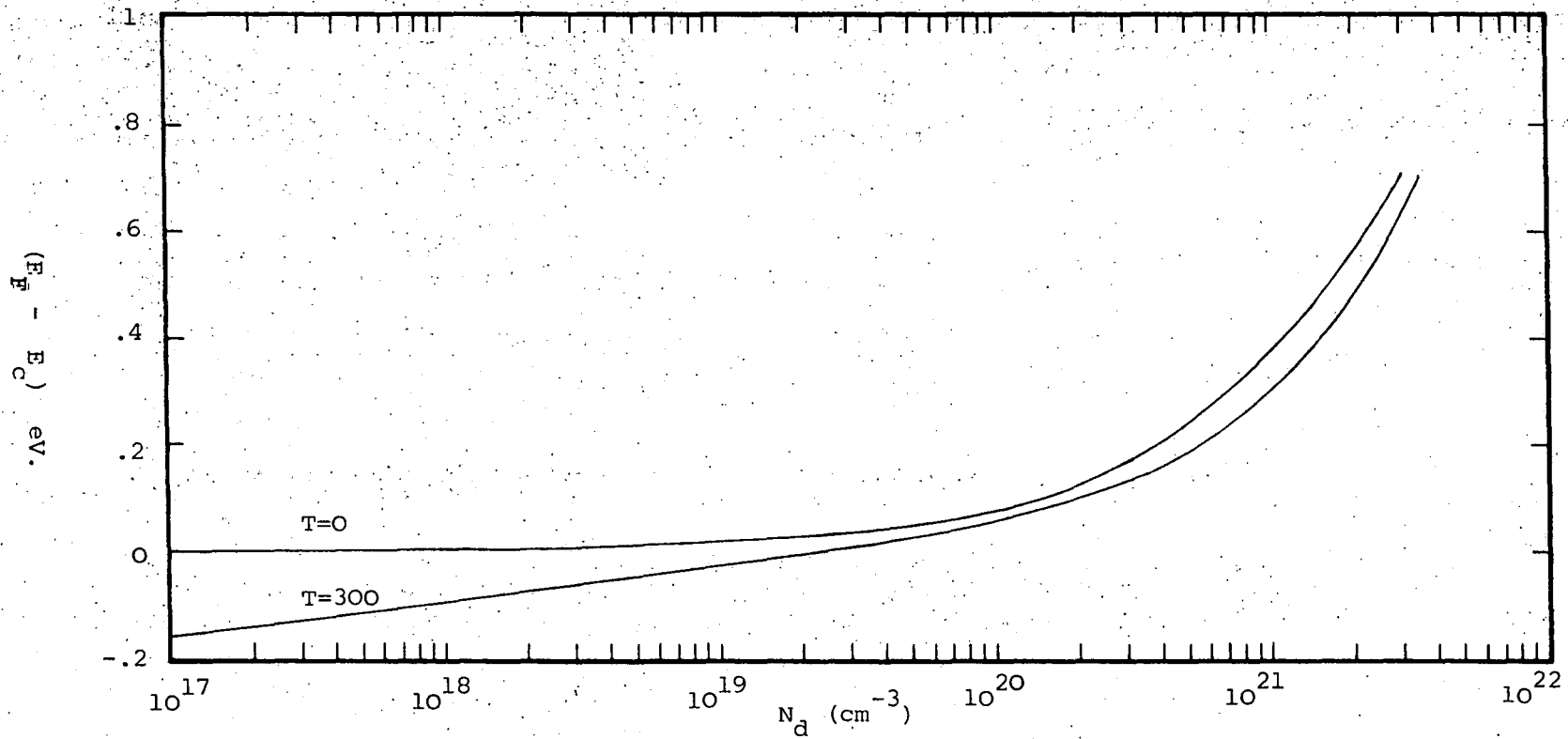
Fig 7.3   Fermi energy at zero and 300 K relative to conduction band.

Fig 7.2 a comparison is made between

$$\left(\frac{2m_{de}E_F}{\hbar^2}\right)^{1/2}$$

and the normalizing parameter k_F used in later sections of this chapter (see Eq. 723.02). Although both tend towards the zero temperature expression (Eq. 221.04b) in the strongly degenerate semiconductor k_F is only an expression used to make easy the comparison between finite and zero temperature expressions.

7.2.2 Calculation of the Thomas Fermi screening length.

In the calculation of the Thomas Fermi screening length the parabolic approximation for the conduction band is again made, arriving at the expression (Fistul 1969, Panish et al 1967, Abram et al 1978, Appendix A)

$$\kappa^2 = M_c \; 2 \; \left(\frac{m_{de}}{2\pi\hbar^2}\right)^{3/2} \frac{e^2}{\epsilon\epsilon_r} \; (kT)^{1/2} \; F_{-1/2}(\eta) \qquad (722.01)$$

which reduces to the zero temperature expression (Eq. 231.12) on letting T tend towards zero.

7.2.3 The finite temperature plasmon dispersion relationship.

The finite temperature plasmon dispersion relationship may be expressed in a way to ease comparisons between the finite temperature expressions and their zero temperature counterparts. Thus Eq. 712.05b may be simplified by normalizing the wavevectors and Thomas Fermi inverse screening length with respect to the quantity

$$\frac{1}{k_F^2} = \left(\frac{M_c}{3\pi^2 N_d}\right) \left(\frac{2m_{de}}{\hbar^2}\right)^{1/2} \frac{(kT\eta)^{1/2}}{2} \; F_{-1/2}(\eta) \qquad (723.01)$$

which reduces to the expression for the inverse square of the Fermi

wavevector at zero temperature (Eq. 221.04). Eq. 712.05b then becomes

$$\omega_1(q)^2 = \frac{\omega_p^2}{K^2} \left(K^2 + q^2 + \frac{4m_{de}}{3m_{op}} q^4 \right) \tag{723.02}$$

with the normalized inverse Thomas Fermi screening length given by

$$K^2 = \frac{\kappa^2}{k_F^2} = \frac{M_c^2}{3\pi^2 N_d} \left(\frac{2m_{de}}{\hbar^2}\right) \frac{kT}{a_{eff}} \left(F_{-1/2}(\eta)\right)^2 \tag{723.03}$$

which on letting T tend towards zero reduces to the normalized parameter used previously (for example in 322.03). Using this normalized parameter highlights the similarity between the zero temperature and finite temperature expressions below.

7.3 CALCULATION OF THE ELECTRON-ELECTRON EXCHANGE ENERGIES.

In chapter 2 and 3 the zero temperature self energy was defined (Eq. 240.07)

$$\hbar\Sigma^{ee}(n;k,\omega) = \frac{i}{(2\pi)^4} \sum_m \iint G^0(m;k-q,\omega-\nu)\ e^{i\eta(\omega-\nu)}\ \Lambda_{nm}$$
$$W_{eff}(q,\nu)\ d^3q d\nu \tag{730.01a}$$

where the screened interaction $W_{eff}(q,\omega)$ used is defined by

$$W_{eff}(q,\omega) = e^2/\epsilon\epsilon_r q^2 \epsilon(q,\omega) \tag{730.01b}$$

with

$$\Lambda_{nm} = \Lambda_{mn}$$
$$\Lambda_{cm} = \delta_{cm} \tag{730.01c}$$
$$\Lambda_{vc} = 0 \qquad \Lambda_{LH} = 3/4\ \sin^2\theta \qquad \Lambda_{HH} = 1/4\ (1+3\cos^2\theta)$$

In the present calculations the finite temperature Green's function (from Eq. 711.02) and the inverse dielectric function (from Eq. 712.05) are substituted into these expressions. On performing the frequency integral in the self energy (Eq. 730.01a) poles in the Green's function (leading to the screened dynamic exchange terms) and poles in the interaction (leading

to the coulomb hole terms) are found (Eq. 310.03). The same contour (Fig 3.1) is used as dictated by the exponential convergence factor introduced into Eq. 730.01a. The resulting expressions for the coulomb hole and screened exchange terms are as follows

$$\hbar\Sigma_n^{sx}(k) = -\frac{1}{(2\pi)^3} \sum_m \int f_{m,k-q} W_{eff}(q, \omega_{nk}^0 - \omega_{m(k-q)}^0) \Lambda_{nm} d^3q$$

(730.02a)

Notice that where previously this wavevector integral was from zero to the Fermi wavevector, now the integral will be over all q and the explicit inclusion of the Fermi Dirac function $f_{m,k-q}$ will provide the cut-off.

$$\hbar\Sigma_n^{ch}(k) = +\frac{e^2}{(2\pi)^3 \epsilon\epsilon_r} \sum_m \int \frac{1}{q^2} \frac{\omega_p^2}{2\omega_1(q)} ((N_q + 1)$$

(730.02b)

$$G^0(m;k-q, \omega_{nk}^0 - \omega_1(q)) + N_q G_0(m;k-q, \omega_{nk}^0 + \omega_1(q))) \Lambda_{nm} d^3q$$

which can be seen to reduce to the zero temperature expressions (Eq. 310.06) on letting the temperature tend towards zero.

It is the change in the self energy due to the inclusion of the many electrons in the conduction band that is of interest. As in chapter 3 the intrinsic self energy must be subtracted from the perturbed self energy so that the change in energy of the conduction band is given by (Eq. 310.07a)

$$\Delta E_c^{ee}(k) = \Delta E_c^{sx}(k) + \Delta E_c^{ch}(k) = Re(\hbar\Sigma_{cc}^{sx}(k)) + Re(\hbar\Sigma_{cc}^{ch}(k))$$

(730.03a)

where only the exchange between electrons in the conduction band with each other need be considered. Whilst for the valence band the intrinsic silicon already has an unscreened exchange energy (Σ^{int}) which must be

subtracted (Eq. 310.07b)

$$\Delta E_v^{ee}(k) = \Delta E_v^{sx}(k) + \Delta E_v^{ch}(k)$$

$$(730.03b)$$

$$= (Re(\hbar\Sigma_{vv}^{sx}(k)) - Re(\hbar\Sigma_{vv}^{int}(k))) + Re(\hbar\Sigma_{vv}^{ch}(k))$$

The sum of the two parts to the exchange energy may also be derived as was done in section 3.3.3. Taking the Cauchy principle parts

$$\Delta E_n^{ch+sx}(k) = \frac{1}{(2\pi)^3} \sum_m \int \frac{e^2}{\epsilon\epsilon_r q^2} \left(- f_{m,k-q} + \frac{\omega_p^2}{2\omega_1(q)} \right($$

$$\frac{N_q + 1 - f_{m,k-q}}{\omega_{n,k}^0 - \omega_{m,k-q}^0 - \omega_1(q)} + \frac{N_q + f_{m,k-q}}{\omega_{n,k}^0 - \omega_{m,k-q}^0 + \omega_1(q)} \Big)\Big)\Lambda_{nm} \, d^3q$$

$$(730.04)$$

which may be compared with the related example of the electron-phonon self energy calculated by Hedin and Lundqvist (1969). As mentioned in section 3.2 and 3.3, the main concern is with the bottom of the conduction band and the top of the valence band in this thesis. However Eq. 730.02 and Eq. 730.04 with the appropriate choice of energy difference will give the electron-electron contribution to the self energy of electrons at any wavevector at finite temperature. In the following two sections (7.3.1 for conduction band calculations and 7.3.2 for valence band calculations) we confine ourselves to the calculation of the change in energy of the band gap using Eq. 730.02 and Eq. 730.04.

7.3.1 Numerical results for the conduction band terms at finite temperature.

When the Cauchy principle part of the self energy integrals (Eq. 730.03) is taken the resulting expressions for the conduction band may be evaluated numerically. Full use of the NAG library of Fortran subroutines was made to furnish the necessary quadrature routines. The procedure followed having first chosen a temperature is to select a Fermi energy, calculate the appropriate concentration as described in section 7.2.1 and finally calculate the various contributions to the change in self energy at the band edge (see Fig 7.6).

From Eq. 730.02 and the energy difference (Eq. 320.04) the electron-electron contributions to the conduction band self energy at the bottom of one of the six conduction band valleys is

$$\Delta E_C^{sx} = - \frac{e^2}{2\pi^2 \epsilon \epsilon_r} \int_0^\infty f_{c,q} \left(1 - \frac{\omega_p^2}{\omega_1(q)^2 - \omega_{cc}^0(q)^2} \right) dq$$

$$(731.01a)$$

this reduces to the zero temperature expression (Eq. 322.02). The coulomb hole contribution is

$$\Delta E_C^{ch} = \frac{e^2}{2\pi^2 \epsilon \epsilon_r} \int_0^\infty \left(N_q \frac{\omega_{cc}^0(q)}{\omega_1(q)} \frac{\omega_p^2}{\omega_1(q)^2 - \omega_{cc}^0(q)^2} \right.$$

$$\left. - \frac{\omega_p^2}{2\omega_1(q)} \frac{1}{(\omega_{cc}^0(q) + \omega_1(q))} \right) dq \quad (731.01b)$$

which also reduces to the zero temperature expression (Eq. 322.02). These integrals are calculated separately.

a)   for the ΔE^{sx}_c terms

This screened exchange term reduces to the difference between two integrals derived from the two terms in the inverse dielectric function: The Hartree Fock contribution (I_1):   and   the   screening contribution (I_2).

$$\Delta E^{sx}_c(k_i) = - I_1 + I_2$$

$$\Delta E^{sx}_c(k_i) = - \frac{e^2}{2\pi^2 \epsilon \epsilon_r} \int_0^\infty f_{c,q} \left(1 - \frac{\omega_p^2}{\omega_1(q)^2 - \omega^0_{cc}(q)^2} \right) \, dq$$

$$(731.02)$$

where I_1, the finite temperature Hartree Fock contribution, is given by

$$I_1 = \frac{e^2}{2\pi^2 \epsilon \epsilon_r} \left(\frac{m_{de} kT\pi}{2\hbar^2} \right)^{1/2} F_{-1/2}(\eta)$$

$$(731.03)$$

the Fermi Dirac integral is calculated as described in section 7.2.1. The numerically calculated values for this integral may be compared with those of the zero temperature Hartree Fock contribution, or the first parts of Eq. 321.03

$$\Delta E^{HF}_c = - 1.323 . 10^{-8} N_d^{1/3} \qquad (eV)$$

$$(731.04)$$

Both the numerical results of Eq. 731.03 and Eq. 731.04 are plotted in Fig 7.4. As can be seen from this plot the finite temperature Hartree Fock term is 20 meV smaller than the 0K counterpart, merging with the former only above a donor concentration of 10^{20} cm^{-3} when n-type silicon becomes strongly degenerate. The second integral I_2, or the screening contribution to the exchange energy, is given on normalizing the wavevectors with
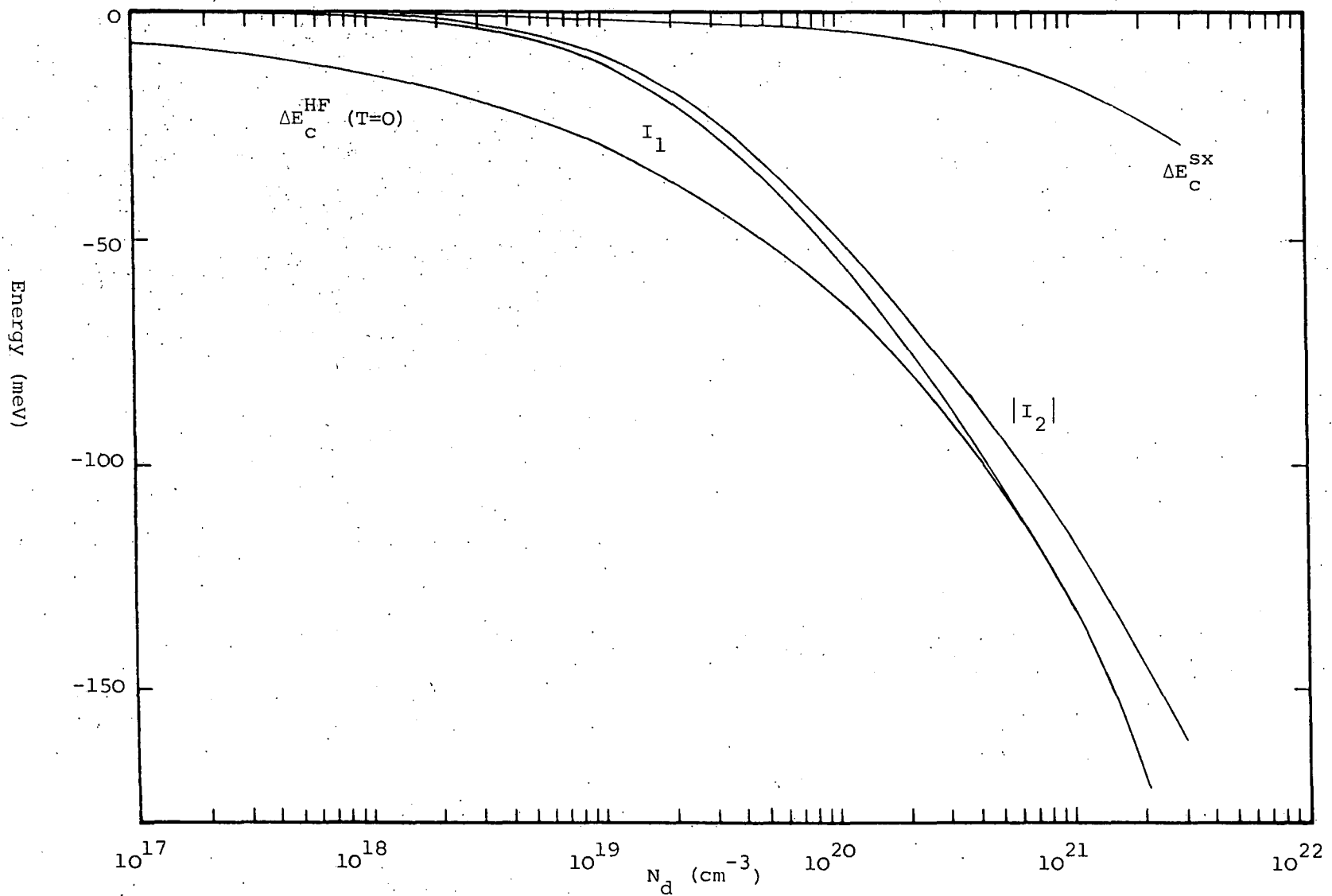
Fig 7.4   Change in energy of the conduction band due to screened dynamic exchange at 300K and constituent parts.

respect to the parameter k_F (see Eq. 723.01 and Fig 7.2)

$$x^2 = \frac{q^2}{k_F^2} = (\frac{q^2 M_c}{3\pi^2 N_d}) \; (\frac{2m_{de}}{\hbar^2})^{1/2} \; \frac{(kT\pi)^{1/2}}{2} \; F_{-1/2}(\eta) \qquad (731.05a)$$

by

$$I_2 = \frac{e^2 k_F K^2}{2\pi^2 \epsilon \epsilon_r} \int_0^\infty \frac{dx}{(\exp(\hbar^2 k_F^2 x^2 / 2m_{de} kT - \eta) + 1)(K^2 + x^2)}$$

$$(731.05b)$$

This integral apart from the Fermi Dirac distribution function is similar to the second part of Eq. 321.03. The numerical integration was performed using the NAG routine D01AJF. The results of this numerical calculation are plotted in Fig 7.4.

The results of these two integrals and there difference are plotted in Fig 7.4 over a range of concentrations, for a temperature of 300K. The contribution ΔE^{SX}_c at zero temperature differ from the finite temperature contribution only by a fraction of a meV over the entire energy range. The calculation of ΔE^{SX}_c involves the difference between two large contributions (I_1 and I_2). The large difference between the zero and finite temperature Hartree Fock contributions (I_1) is matched by a similar large change in screening contribution, so that the net change in ΔE^{SX}_c is small (less than 2 meV at most). For high concentrations ($> 10^{20}$), at 300K the Fermi Dirac distribution function is little different from the step function used in the zero temperature calculations so the two contributions I_1 and I_2 reduce to the zero temperature result for these high concentrations.

b)　　for the ΔE^{ch} terms

The coulomb hole contribution to the conduction band exchange energy at the bottom of one of the six valleys may also be performed in two parts and is formed by the difference between these contributions

$$\Delta E_C^{ch}(k_i) = I_1 - I_2 \qquad (731.06)$$

$$\Delta E_C^{ch} = \frac{e^2}{2\pi^2 \epsilon \epsilon_r} \int_0^\infty \left(N_q \frac{\omega_{cc}^0(q)}{\omega_1(q)} \frac{\omega_p^2}{\omega_1(q)^2 - \omega_{cc}^0(q)^2} \right.$$

$$\left. - \frac{\omega_p^2}{2\omega_1(q)} \frac{1}{(\omega_{cc}^0(q) + \omega_1(q))} \right) dq$$

where I_1 is given by

$$I_1 = \frac{e^2}{2\pi^2 \epsilon \epsilon_r} k_F K^2 \int_0^\infty \frac{1}{\exp(\hbar\omega_p (K^2 + q^2 + \alpha q^4)^{1/2}/(KkT)) - 1}$$

$$\left(\frac{\alpha q^4}{K^2 + q^2 + \alpha q^4} \right)^{1/2} \frac{1}{K^2 + q^2} dq \qquad (731.07)$$

where the wavevectors have been normalized with respect to the parameter k_F as recommended in section 7.2.3. This integral was evaluated numerically using the NAG routine D01AJF, the results are plotted in Fig 7.5. This is an entirely new contribution to the shift of the conduction band, not found in the zero temperature expressions it is however less than 2 meV for all concentrations. I_2 on the other hand is equivalent to the zero temperature
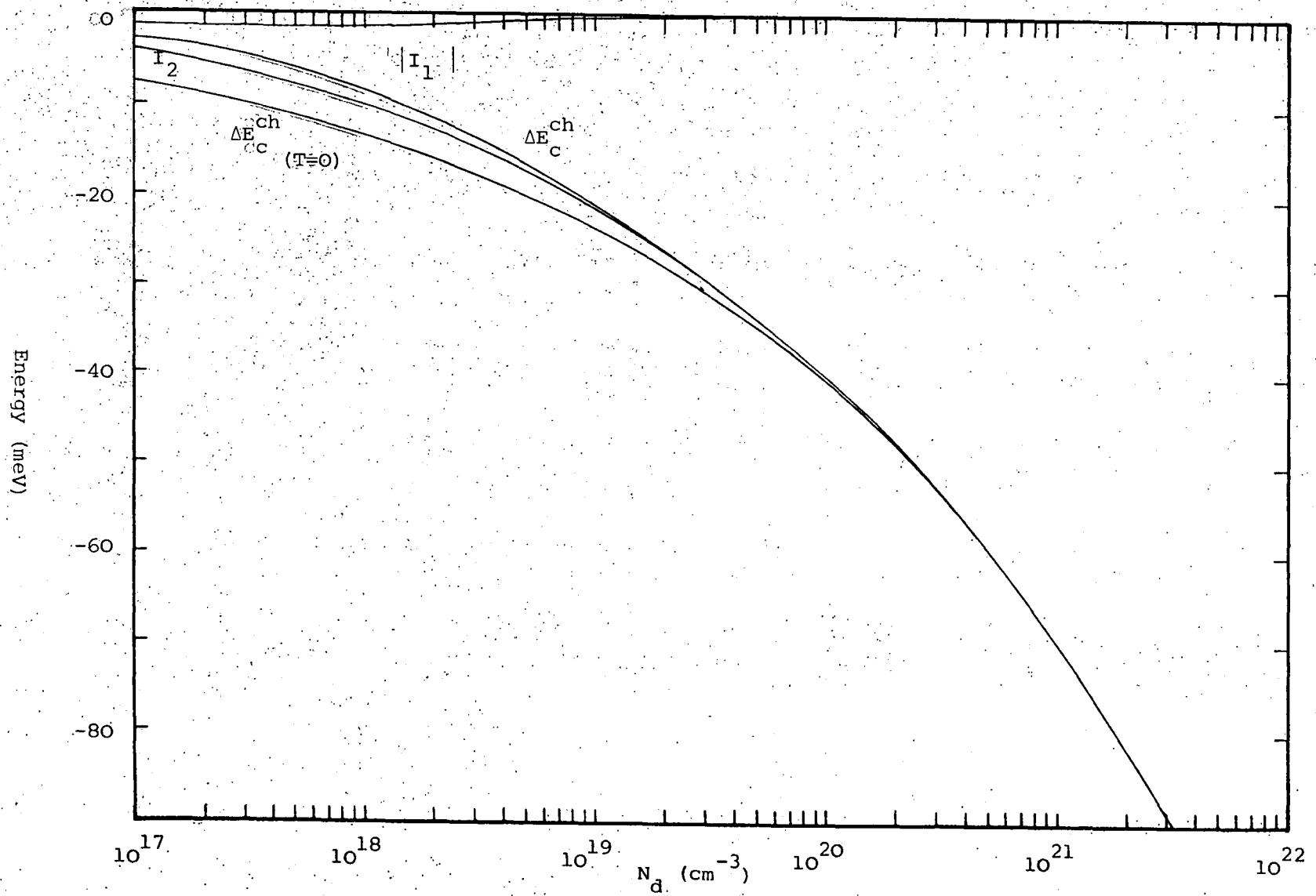
Fig 7.5   Change in energy of the conduction band due to coulomb hole terms at 300K and component parts.
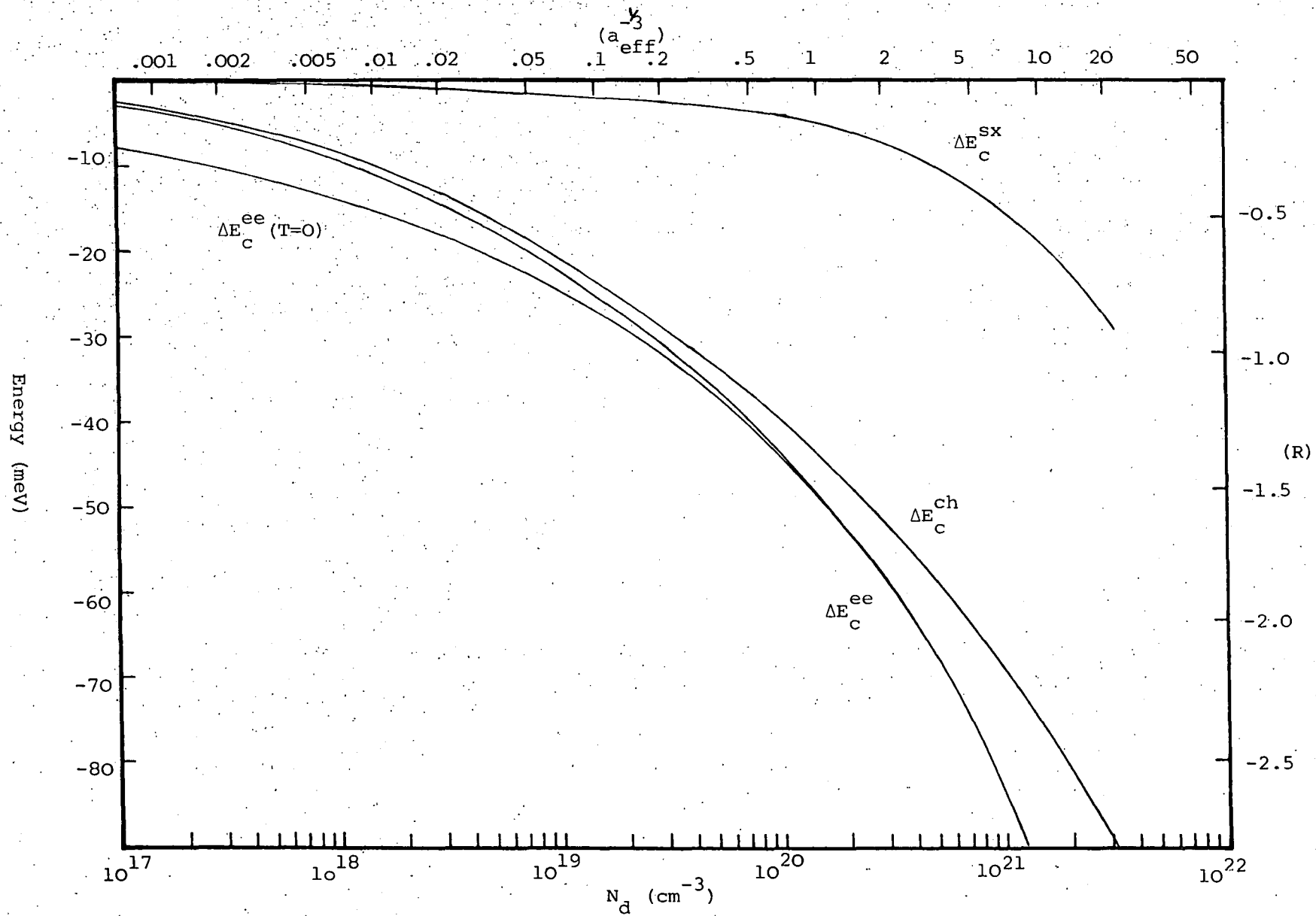
Fig 7.6   Change in the total electron-electron exchange energies for the conduction band at 300K.

coulomb hole term (Eq. 322.01). It is given after making the substitutions

$$\beta = \frac{3m_{op}}{4m_{de}} = 0.5951 \quad ; \quad K = \frac{\kappa}{k_F} \quad ; \quad \left(\frac{q}{k_F}\right)^2 = \frac{1-t}{t}$$

by

$$I_2 = \frac{e^2}{8\pi^2 \epsilon \epsilon_r} k_F \kappa^2 \int_0^1 \left(\frac{t}{1-t}\right)^{1/2} \qquad\qquad (731.08)$$

$$\frac{dt}{(K^2+\beta-1)t^2+(1-2\beta)t+\beta+\sqrt{(((K^2+\beta-1)t^2+(1-2\beta)t+\beta)\beta(t^2-2t+1))}}$$

The integral I_2 was performed by the NAG routine D01APF. The calculated values of I_2 are compared with the zero temperature values in Fig 7.5. The difference between them, large at low concentrations and small at high concentrations, is due to smaller electron screening at finite temperature. This increases the negative charge surrounding a test charge, hence decreasing the energy of the coulomb hole. Numerical results for both these contributions to the conduction band self energy and there difference are plotted in Fig 7.5.

7.3.2 Numerical results for the valence band terms at finite temperature.

When considering the valence band, in sympathy with the calculations at zero temperature, it is convenient to deal with the total electron-electron exchange contribution (Eq. 730.04) and the screened exchange contribution (Eq. 730.02a) separately. The coulomb hole term is again more difficult to evaluate due to the pole at the intersection of the plasmon dispersion curve with the electron energy. The summed contribution however avoids this problem. When the Cauchy principle part of the valence band self energy integrals (Eq. 730.03) are taken they result in expressions that may be evaluated numerically. Full use of the NAG library

of Fortran subroutines was made to furnish the necessary quadrature routines, some of which are the same as have been used previously. The procedure followed having first chosen a temperature was to select a Fermi energy, calculate the appropriate concentration as described in section 7.2.1 and finally calculate the various contributions to the self energy at the band edge (see Fig 7.7).

From Eq. 730.04 and the energy difference (Eq. 330.05b) the electron-electron contributions to the valence band self energy may be derived. However only the change in self energy of the valence band electrons due to the additional conduction band electrons is of interest. The Hartree Fock term must then be subtracted from the total valence band self energy as it was in the zero temperature calculations (see section 3.3). This amounts to adding one to the bracketed part of the integrand of Eq. 730.04. The change in self energy of for example the heavy hole valence band electrons are then given by

$$
\Delta E_H^{ch+sx}(k) = \frac{1}{(2\pi)^3} \sum_m \int \frac{e^2}{\epsilon \epsilon_r q^2} \left(1 - f_{m,k-q} + \frac{\omega_p^2}{2\omega_1(q)} \left(\frac{N_q + 1 - f_{m,k-q}}{\omega_{H,k}^0 - \omega_{m,k-q}^0 - \omega_1(q)} + \frac{N_q + f_{m,k-q}}{\omega_{H,k}^0 - \omega_{m,k-q}^0 + \omega_1(q)} \right) \right) \Lambda_{nm} d^3q
$$

$$(732.01)$$

Performing the angular part of the wavevector integral for $k=0$, using Eq. 330.05b for the energy difference in the valence band the following simplification (with $f_{m,k-q}=1$) may be made

$$
\Delta E_H^{ch+sx}(k) = \frac{1}{4\pi^2} \sum_m \int_0^\infty \frac{e^2}{\epsilon \epsilon_r} \left(N_q \frac{\omega_{Hm}^0(q)}{\omega_1(q)} \frac{\omega_p^2}{\omega_{Hm}^0(q)^2 - \omega_1(q)^2} \right.
$$

$$
\left. + \frac{\omega_p^2}{2\omega_1(q)} \frac{1}{(\omega_{Hm}^0(q) + \omega_1(q))} \right) dq \qquad (732.02)
$$

the first part of which may be compared with the zero temperature expression. Eq. 332.01. Whilst the second part can be compared to Eq. 330.06. The screened dynamic exchange part is given by

$$\Delta E_H^{sx} = - \frac{e^2}{4\pi^2 \epsilon \epsilon_r} \sum_m \int_0^\infty \left(\frac{\omega_p^2}{\omega_{Hm}^0(q)^2 - \omega_1(q)^2} \right) dq \qquad (732.03)$$

where the Hartree Fock contribution has again been subtracted as in Eq. 330.03. The coulomb hole contribution has to be evaluated by subtraction.

a)   for the ΔE_v^{sx+ch} terms.

Treating the two parts of the valence band summation separately. Contributions due to exchange between for example electrons in the heavy hole band with those from the same band (HH) and those between heavy and light hole bands (HL) are identified. The shift in the heavy hole band is obtained by summing these contributions. This sum is found to be the same for the light hole band since the energy differences (Eq. 330.05b) are the same for both bands at k=0. The four contributions to the electron-electron shift of the valence band are

$$\Delta E_H^{sx+ch} = - I_{1HH} + I_{2HH} - I_{1HL} + I_{2HL} = \Delta E_L^{sx+ch}$$

$$\Delta E_H^{sx+ch}(k) = \frac{1}{4\pi^2} \sum_m \int_0^\infty \frac{e^2}{\epsilon \epsilon_r} \left(N_q \frac{\omega_{Hm}^0(q)}{\omega_1(q)} \frac{\omega_p^2}{\omega_{Hm}^0(q)^2 - \omega_1(q)^2} \right.$$

$$(732.04)$$

$$\left. + \frac{\omega_p^2}{2\omega_1(q)} \frac{1}{(\omega_{Hm}^0(q) + \omega_1(q))} \right) dq$$

where

$$I_{1Hm} = \frac{e^2}{4\pi^2 \epsilon \epsilon_r} \int_0^\infty N_q \frac{\omega_{Hm}^0(q)}{\omega_1(q)} \frac{\omega_p^2}{\omega_1(q)^2 - \omega_{Hm}^0(q)^2} dq \qquad (732.05)$$

a completely new integral similar to that in the zero temperature screened

exchange integral Eq. 330.05c. and an integral equivalent to the zero temperature integral Eq. 330.06

$$I_{2Hm} = \frac{e^2}{4\pi^2 \epsilon \epsilon_r} \int_0^\infty \frac{\omega_p^2}{2\omega_1(q)} \frac{1}{(\omega_1(q) + \omega_{Hm}^0(q))} dq \qquad (732.06)$$

I_{1HH} is given by the expression

$$I_{1HH} = \frac{e^2}{4\pi^2 \epsilon \epsilon_r} k_F \kappa^2 \int_0^\infty \frac{1}{\exp(\hbar\omega_p \sqrt{(K^2+x^2+\beta x^4)}/kTK) - 1}$$

$$\left(\frac{\gamma_H x^4}{K^2+x^2+\beta x^4}\right)^{1/2} \frac{1}{\alpha x^4+x^2+K^2} dx$$

$$(732.07)$$

$$\beta = \frac{3m_{op}}{4m_{de}} = 0.5951 \quad ; \quad \gamma_H = \beta \left(\frac{m_{de}}{m_H}\right)^2 = 0.2548$$

$$\alpha = \beta - \gamma = 0.340 \quad ; \quad K = \frac{\kappa}{k_F}$$

which was evaluated using the NAG routine D01AJF. Results for this integral are shown in Fig 7.7 and show that it contributes less than 1 meV to the total valence band exchange over the entire density range. However the comparable integral for the exchange between the heavy and light hole electrons

$$I_{1HL} = \frac{e^2}{4\pi^2 \epsilon \epsilon_r} k_F \kappa^2 \int_0^\infty \frac{1}{\exp(\hbar\omega_p \sqrt{(K^2+x^2+\beta x^4)}/kTK) - 1}$$

$$\left(\frac{\gamma_L x^4}{K^2+x^2+\beta x^4}\right)^{1/2} \frac{1}{\alpha x^4+x^2+K^2} dx \qquad (732.08)$$

$$\beta = \frac{3m_{op}}{4m_{de}} = 0.5951 \quad ; \quad \gamma_L = \beta \left(\frac{m_{de}}{m_L}\right)^2 = 2.488$$

$$\alpha = \beta - \gamma = -1.893 \quad ; \quad K = \frac{\kappa}{k_F}$$

is more difficult to evaluate numerically due to the poor modelling of the
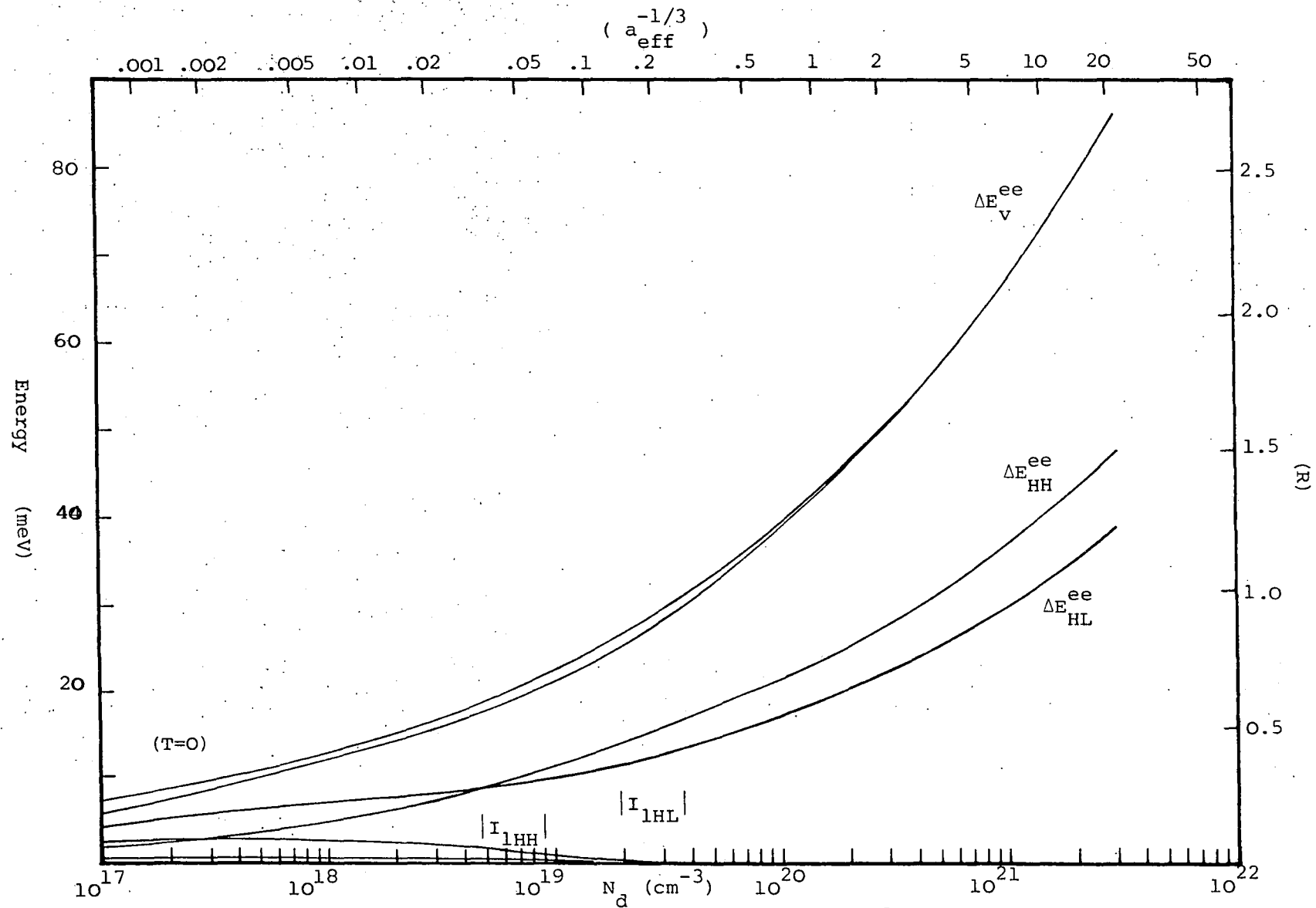
Fig 7.7   Change in the total valence band self energy at 300K (ΔE_v^{ee}) and constituent parts.

plasmon peak by the present inverse dielectric function. The same problems were encountered when attempting to evaluate the zero temperature screened exchange contribution in section 3.3.2. and has been commented on in section 2.3.3. The problem arises because the plasmon peak is not damped as it should be (see Fig 2.7 for zero temperature). The plasmon peak occurs when the plasmon dispersion curve intersects the light electron energy $(\omega_1(q) = \epsilon^0_{Lq})$. This point changes in energy since the dispersion relationship depends upon the Thomas Fermi screening length. In Table 7.1 a list of the energy values of this intersection are presented for different concentrations.

Table 7.1

Plasmon energy, and the exchange contribution
between heavy and light hole bands I_1 and I_2.

N_d (cm^{-3})	$\hbar\omega_p$ (meV)	energy of peak (meV)	ϵ/kT T=300K	I_{1HL} (meV)	I_{2HL} (meV)
1.10^{17}	6.71	43.3	1.68	- 2.32	1.79
1.10^{18}	21.22	53.5	2.07	- 2.97	4.36
1.10^{19}	67.09	104.0	4.02	- 0.76	9.19
1.10^{20}	212.15	292	11.31	- 0.003	17.15
1.10^{21}	670.89	974	37.68		29.84

Also shown in Table 7.1 is the value of this intersection energy normalized with respect to the thermal energy (ϵ/kT). This shows that the multiplying factor N_q acts as a strong damping factor above a concentration of about 10^{18} where $\epsilon/kT > 3$. The values of I_1 calculated from Eq. 732.07 using the NAG routine D01AQF reduce to zero beyond this concentration. Thus the problems of numerically calculating this integral are unimportant for the concentration region of interest to us above the Mott transition. The values of I_{1HL}, which are negative because of the large negative contribution from the integrand of Eq. 732.08 below the intersection point,

are not reliable. The comparable numerical routine to calculate the zero temperature screened exchange terms does not given the correct results either, as indicated after Eq. 332.09. However these values for I_{HL} are included in the following analysis and there magnitude is shown in Fig 7.7.

The contribution I_{2Hn} is just the zero temperature contribution with the finite temperature $\omega_1(q)$ (Eq. 331.02). And gives

$$\beta = \frac{3m_{op}}{4m_{de}} = 0.5951 \quad ; \quad K = \frac{\kappa}{k_F} \quad ; \quad \left(\frac{q}{k_F}\right)^2 = \frac{1-t}{t}$$

$$\gamma_L = \beta \left(\frac{m_{de}}{m_L}\right)^2 = 2.488 \quad ; \quad \gamma_H = \beta \left(\frac{m_{de}}{m_H}\right)^2 = 0.2548$$

$$I_{2HL} = + \frac{e^2 \kappa^2}{16\pi^2 \epsilon \epsilon_r k_F} \int_0^1 \left(\frac{t}{1-t}\right)^{1/2} \qquad (732.09a)$$

$$\frac{dt}{(K^2+\beta-1)t^2+(1-2\beta)t+\beta+\sqrt{(((K^2+\beta-1)t^2+(1-2\beta)t+\beta)\gamma_L(t^2-2t+1))}}$$

and

$$I_{2HH} = + \frac{e^2 \kappa^2}{16\pi^2 \epsilon \epsilon_r k_f} \int_0^1 \left(\frac{t}{1-t}\right)^{1/2} \qquad (732.09b)$$

$$\frac{dt}{(K^2+\beta-1)t^2+(1-2\beta)t+\beta+\sqrt{(((K^2+\beta-1)t^2+(1-2\beta)t+\beta)\gamma_H(t^2-2t+1))}}$$

which were calculated using the NAG routine D01APF. The numerical results for the sum of the I_1 and I_2 contributions are given in Fig 7.7. The I_2 contributions form the greater part of the sum. The zero temperature contribution of the ΔE_v^{sx+ch} terms is also plotted and it shows that this is less than 2 meV greater than the 300K values. Thus the change in the band gap reduction due to temperature below an electron concentration of 10^{20} cm^{-3} comes mainly from the conduction band contribution shown in Fig 7.6.

b)   for the E^{sx}_v terms.

The screened exchange part of the finite temperature electron-electron self energy (Eq. 732.03) reduces to the same form as the zero temperature expressions with the appropriate choice of K and k_F (see section 3.3.2). The resulting expressions at finite temperature are (see Eq. 332.06 and 332.08)

$$\alpha_L = \frac{3m_{op}}{4m_{de}} \left(\left(\frac{m_{de}}{m_L} \right)^2 - 1 \right) = 1.893$$

$$\alpha_H = \frac{3m_{op}}{4m_{de}} \left(1 - \left(\frac{m_{de}}{m_H} \right)^2 \right) = 0.3403$$

$$\Delta E^{sx}_{vL}(0) = + \frac{e^2 \kappa^2}{8\pi\epsilon\epsilon_r} \left(\frac{2\alpha_L k_F}{(k_F^2 + 4\alpha_L\kappa^2)((k_F^2 + 4\alpha_L\kappa^2)^{1/2} - k_F)} \right)^{1/2}$$

(732.10a)

$$\Delta E^{sx}_{vH}(0) = + \frac{e^2 \kappa}{8\pi\epsilon\epsilon_r} \left(\frac{k_F}{2\kappa\sqrt{\alpha_H} + k_F} \right)^{1/2}$$ (732.10b)

These expression are evaluated with the finite temperature parameters replacing K and k_F.

The results for these two expressions are presented in Fig 7.8 and the difference between the total (Fig 7.7) and screened exchange (Fig 7.8), or the coulomb hole terms are presented in Fig 7.9. These graphs show that although the screened exchange contributions do decrease in size with increasing temperature, so do the coulomb hole terms. Since these contributions are subtractive this results in only a small decrease in the valence band energy. The conduction band contributions are however additive, resulting in a large change in energy of the conduction band edge due to temperature (see Fig 7.6).
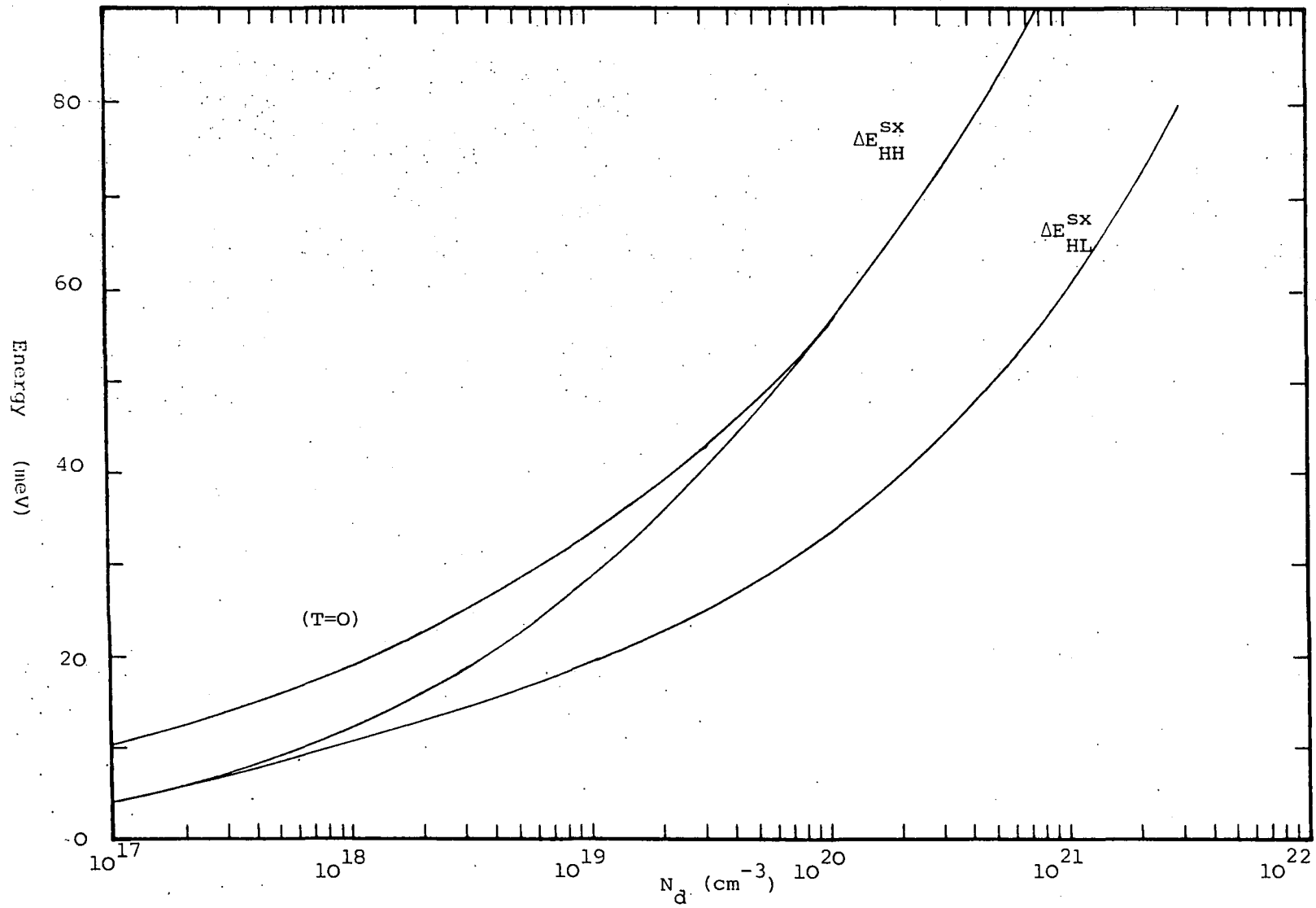
Fig 7.8   Change in the valence band screened dynamic exchange energy at finite temperature (T=300)
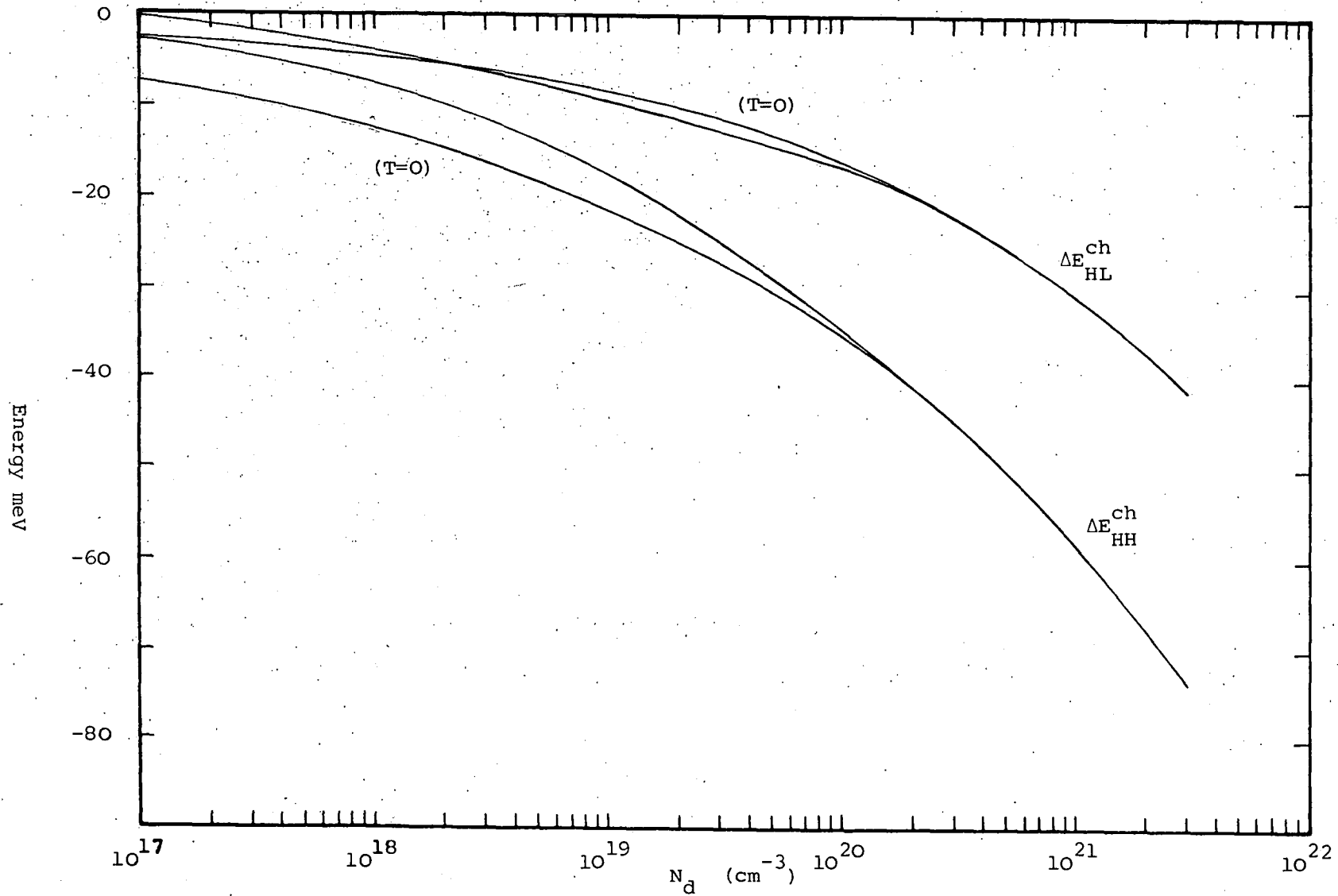
Fig 7.9   Change in the valence band coulomb hole energy at 300 K.

In this section the shifts in the conduction and valence bands due to the change in screened electron-electron exchange energies (Eq. 300.02 and 300.03) have been calculated at finite temperature. It has been found that in the plasmon pole approximation these can be split up into coulomb hole and screened dynamic exchange contributions (named by Hedin 1965 in connection with electrons gases in metals see section 3.1)

$$\Delta E_c^{ee}(k) = \Delta E_c^{sx}(k) + \Delta E_c^{ch}(k)$$

$$\Delta E_v^{ee}(k) = \Delta E_v^{sx}(k) + \Delta E_v^{ch}(k)$$

The coulomb hole contributions (see Eq. 731.01b and 732.02, 732.03)

$$\Delta E_c^{ch}(k) = \frac{e^2}{2\pi^2 \epsilon \epsilon_r} \int_0^{\infty} (\ N_q \ \frac{\omega_{cc}^0(k,q)}{\omega_1(q)} \ \frac{\omega_p^2}{\omega_1(q)^2 - \omega_{cc}^0(k,q)^2}$$

$$- \frac{\omega_p^2}{2\omega_1(q)} \ \frac{1}{(\omega_{cc}^0(k,q) + \omega_1(q))}) \ dq$$

$$\Delta E_v^{ch}(k) = \frac{e^2}{4\pi^2 \epsilon \epsilon_r} \sum_m \int_0^{\infty} (\ N_q \ \frac{\omega_{vm}^0(k,q)}{\omega_1(q)} \ \frac{\omega_p^2}{\omega_{vm}^0(k,q)^2 - \omega_1(q)^2}$$

$$+ \frac{\omega_p^2}{2\omega_1(q)} \ \frac{1}{(\omega_{vm}^0(k,q) - \omega_1(q))}) \ dq$$

reduce the energies of both conduction and valence bands contributing a small increase (+10 meV at 10^{20} cm^{-3}) to the change in the band gap as in the zero temperature results of chapter 3 (see Fig 7.5 and Fig 7.9). The screened dynamic exchange contributions of each band (Eq. 731.01a and

732.03) however act in opposite directions, both to reduce the gap (Fig 7.4 and 7.8)

$$\Delta E_c^{sx}(k) = - \frac{e^2}{2\pi^2 \epsilon \epsilon_r} \int_0^\infty f_{c,q} \left(1 - \frac{\omega_p^2}{\omega_1(q)^2 - \omega_{cc}^0(k,q)^2} \right) dq$$

$$\Delta E_v^{sx}(k) = + \frac{e^2}{4\pi^2 \epsilon \epsilon_r} \sum_m \int_0^\infty \left(\frac{\omega_p^2}{\omega_1(q)^2 - \omega_{vm}^0(k,q)^2} \right) dq$$

With appropriate choice of the energy difference in these expressions the change in the band energy at any value of k may be determined

$$\omega_{ck}^0 - \omega_{c(k-q)}^0 = - \omega_{cc}^0(k,q)$$

$$\omega_{vk}^0 - \omega_{v(k-q)}^0 = \omega_{vn}^0(k,q)$$

The major difference between the zero temperature calculations of chapter 3 and the values for the change in the conduction (valence) band bottom (top) at a temperature of 300K shown in this chapter is a small increase in the finite temperature band gap at low concentrations. This increase is caused mainly by the reduction (7 meV at 10^{17} cm^{-3}) in the conduction band shift (Fig 7.6). The valence band shift (Fig 7.7) remains within a 2 meV of its zero temperature value. The large change in the conduction band shift is due to the decreased screening (small $1/\kappa$) at low concentrations (Fig 7.2). This has a disproportionate effect on the conduction band where the magnitudes of the screened dynamic exchange and coulomb hole terms are additive. The sum of this electron-electron band gap reduction and the electron-impurity band gap reduction calculated in the next section results in a net increase in the band gap reduction due to the large increase in the latter contribution.

7.4 CALCULATION OF THE ELECTRON-IMPURITY SELF ENERGIES.

In this section the extension of the electron-impurity self energies calculated in chapter 4 to finite temperature is considered. The electron-impurity energies are by far the most simple to evaluate since the interaction is essentially static.

7.4.1 Numerical results for silicon.

The ensemble averaged self energy expression used was derived in detail in chapter 4 and is unchanged at finite temperature apart from the use of the appropriate finite temperature parameters. The electron-impurity self energy of the band n is then given by (Eq. 450.03a)

$$\hbar\Sigma^{ei}(n;k,\omega) = \frac{N_d}{\hbar(2\pi)^3} \sum_m \int G^0(n;l,\omega) |W(l-k,\omega)|^2 \Lambda_{nm}(k,l) \; d^3l$$

(740.01)

whilst the appropriate shift in the band edge is given by the real part of this self energy

$$\Delta E_n^{ei}(k) = \hbar Re(\Sigma(n;k,\omega_{nk}^0))$$

(740.02)

The change in the band gap due to the electron-impurity self energy is given by

$$\Delta E_{eg}^{ei} = \Delta E_c^{ei}(k_i) - \Delta E_v^{ei}(0)$$

(740.03)

This is reduced to one integral in Eq. 450.06

$$\Delta E_{eg}^{ei} = - \left(1 + \frac{m_H + m_L}{2m_{de}}\right) \frac{4N_d e^2}{a_{eff} \epsilon \epsilon_r} \frac{1}{k_F^3}$$

$$\int_0^\infty \left(\frac{1 + \alpha(q/k_F)^2}{(\kappa/k_F)^2 + (q/k_F)^2 + \alpha(q/k_F)^4}\right)^2 d(q/k_F)$$

(740.04)

$$\alpha = \frac{3}{4} \frac{m_{op}}{m_{de}} = 0.5951$$

where in place of the zero temperature quantities k_f and κ the finite temperature variables k_F (Eq. 722.02) and the finite temperature Thomas Fermi screening length κ (Eq. 723.01) are substituted.

This integral was solved numerically using the NAG library routine D01AJF for a number of different impurity concentrations. A number of different Fermi energies were selected that were then used to calculate the impurity concentration they represented as indicated in section 7.2.0. These impurity concentrations and Fermi energies were then used to evaluate the Thomas Fermi screening length and hence the band gap reduction detailed in Eq. 740.01. Results for this calculation for a temperature of 300K are presented in Fig 7.10 which also shows the zero temperature results from Fig 4.1. These show that for low concentrations ($< 3 \times 10^{19}$ cm^{-3}) the 300K results diverge. However at high concentrations (above 10^{20} cm^{-3}) in the strongly degenerate semiconductor the results tend towards the zero temperature results.
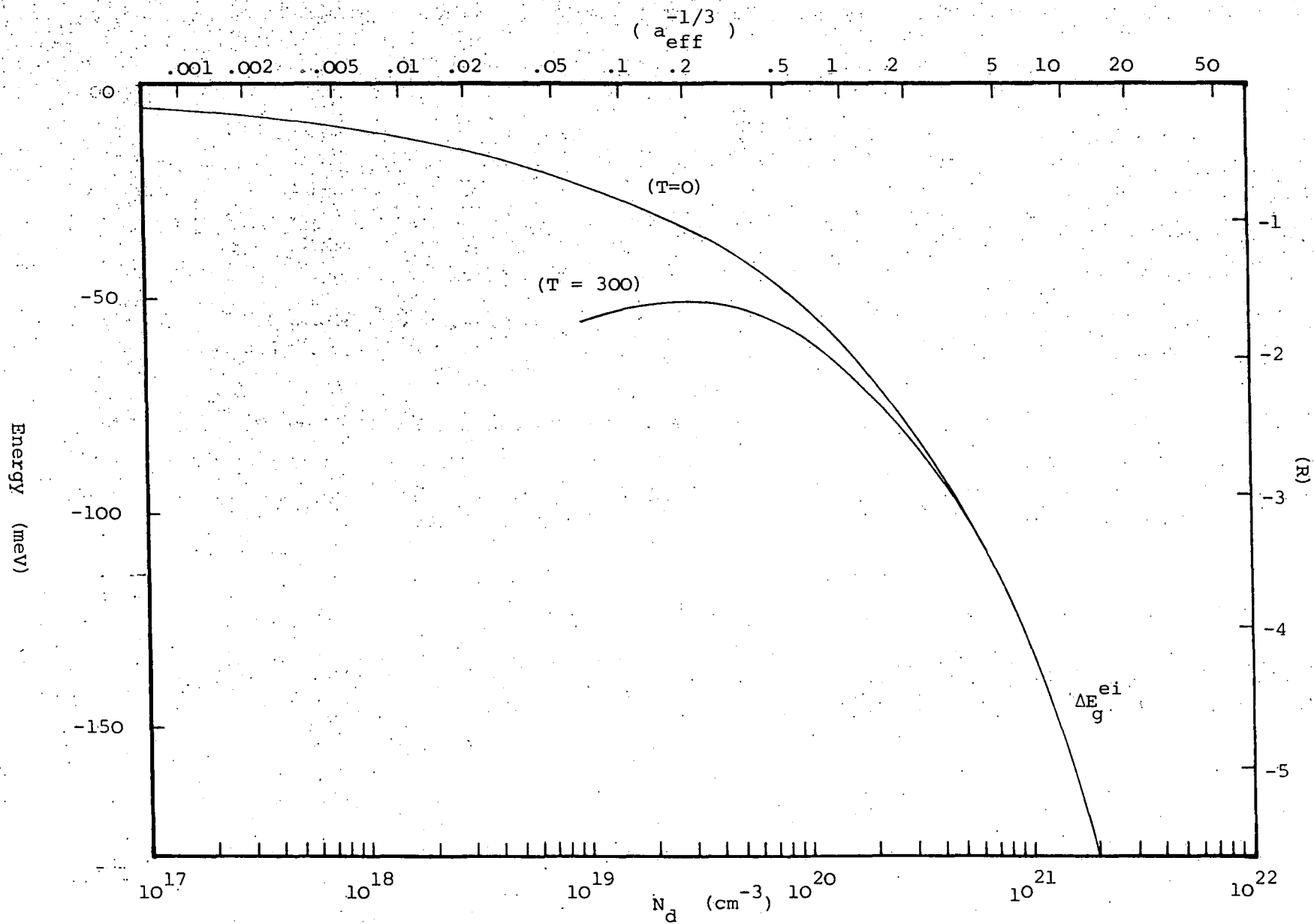
Fig 7.10   Change in the electron-impurity self energy at 300K and OK in the plasmon pole approximation.

7.4.2   Conclusions and validity of results.

To clarify the above results calculated from the plasmon pole approximation Fig 7.11 shows the zero and 300K Thomas Fermi results (ΔE^{TF}_{g}). These are calculated by substituting the appropriate finite temperature values into Eq. 442.14. The average first order interaction given by

$$E_0 = \frac{1}{\Omega} \int_0^\infty V(r) \ d^3r = - \frac{e^2}{\epsilon \epsilon_r \kappa^2} N_d$$

$$= - 1.53 \ 10^{-7} \ \frac{N_d}{\kappa^2} \qquad (eV) \qquad (742.01)$$

is also presented in this figure. As has been discussed (section 4.3 and Wolff 1962) this first order term is cancelled by the first order electron-electron self energy. However as shown in Fig 7.11 at 300 K this first order term becomes smaller than the second order self energy below a concentration of about 2.10^{19} cm^{-3}. Clearly this indicates a break down of the perturbation series at low concentrations. As has been discussed in section 4.6 the perturbation series breaks down even in the degenerate material if terms of high enough order are considered. However as Ghazali and Serre (1982, 1983) have shown if the self energy diagrams are summed to infinite order a meaningful result is still obtained. For the present calculations where the only interest is with concentrations above the Mott transition at about 3.10^{19} cm^{-3} the second order self energy calculated is still useful. The upper concentration limit to the electron-impurity calculations is still the same being defined by the point at which the impurity potential may no longer be considered as a small perturbation to the crystal potential. This point has been estimated in chapter 4 to be above a donor concentration of 10^{21} cm^{-3} silicon where the donor separation is of the order of the lattice parameter d (see Fig 7.2).
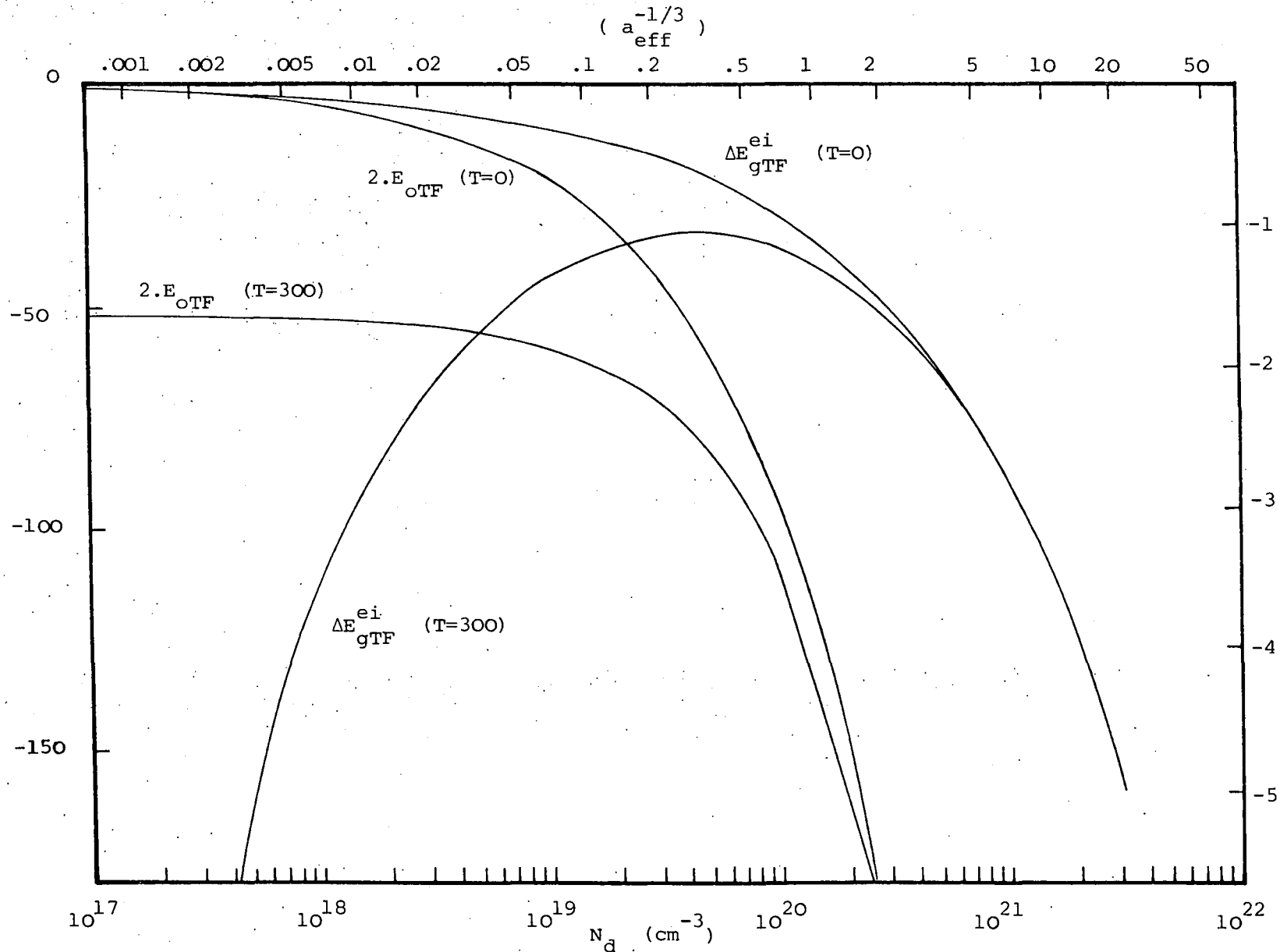
Fig 7.11   First (E_{oTF}) and second (ΔE^{ei}_{gTF}) order electron-impurity self energy at T=300 in the Thomas Fermi
approximation.

7.5   CONCLUSIONS.

In Fig 7.12 the sum of the electron-electron and electron-impurity self energies is presented for both zero and 300 K. As detailed in the introduction these results are only valid above the Mott critical concentration which is higher than zero temperature value due to the increased low concentration electron screening length ($1/\kappa$ see Fig 7.2). Below this concentration, although the electron-electron self energies shown in Fig 7.6 and Fig 7.7 are still valid when there are N_d electrons in the conduction band, the electron-impurity self energy is no longer valid (section 7.4.2 and 4.5). The Mott transition then defines the lower concentration limit to the results. At concentrations below 10^{19} cm^{-3} the experimental band gap narrowing results might well be best described by the statistical approaches of Heasell (1979) and Popovic (1979) where a degenerate semi-populated impurity band separate from the host band is considered. However above the Mott critical density the true many body effects calculated in the previous sections should be used, assuming a merged conduction and impurity band.

Perhaps the most promising recent work in the intermediate concentration range close to the Mott transition has been carried out by Ghazali and Serre (1982, 1983) where the self energy is summed to infinite order and the density of states is derived directly from the imaginary part of the total Green's function. With the use of the plasmon pole approximation and the electron-electron exchange energies from section 7.3 this could also be extended to finite temperature.
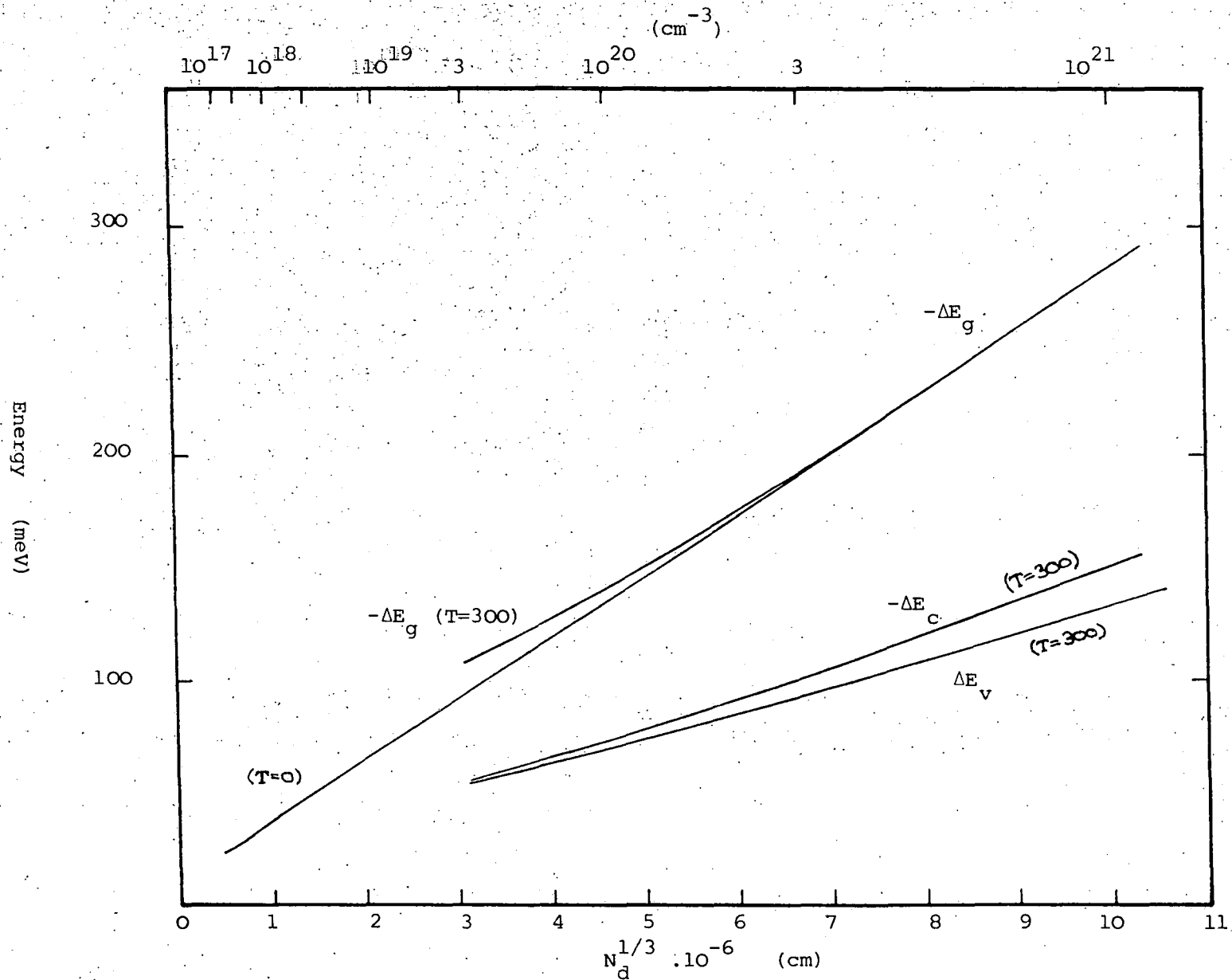
Fig 7.12   Band gap reduction in n-type silicon at zero and 300K, showing the change in conduction and valence band edges.

CHAPTER 8

A METHOD FOR THE EXPERIMENTAL MEASUREMENT OF BAND GAP NARROWING.

8.0   INTRODUCTION.

A recent review of experimental techniques has been made by Mertens et al (1981). In the past the measurement of band gap narrowing in semiconductors has been performed by the measurement of the absorption coefficient for band to band photoexcitation (Volf'son and Subashiev (1967)) and by the measurement of the pn product (Slotboom and de Graff 1976, Mertens et al 1980). The present method to measure band gap narrowing in heavily doped n-type silicon may be classed amongst the latter conductivity type measurements. It involves the novel use of a wide base parasitic transistor formed by the p-type substrate on which Integrated Injection Logic structures are fabricated (all the devices were fabricated with ion implantation of impurities by Plessey (Caswell) Ltd). Based upon the measurement of the substrate saturation current density (J_{pso}) over a range of temperatures (200 to 400 K) the measurements require the knowledge of the transport factor, minority carrier diffusion coefficient (or mobility) in the heavily arsenic doped buried layer, the intrinsic band gap (section 8.2.4) and carrier concentration (section 8.2.5). The temperature dependences of these various parameters including junction areas (section 8.2.6) through which the currents flow are also considered. For the present work values for the mobility at 300K are taken from the literature (section 8.2.3). The transport factor is calculated (section 8.2.1) from a measurement of the hole current injected into the heavily doped buried layer from the Integrated Injection Logic cells $(J_{pv}$ section 8.2.2). The results obtained include not only the band gap narrowing (100 ± 25 meV) in the heavily doped buried layer ($2.4.10^{19}$ cm^{-3}), but also temperature

dependences of the carrier mobilities in the various regions of the device and the minority carrier lifetime in the buried layer (30 ± 10 ns).

The use of Integrated Injection Logic transistors to measure band gap narrowing is not new (Mertens 1980). however the previous method used a heavily doped n-type substrate making minority diffusion length measurements on the back of the slice using optical techniques that rely upon the optical bandgap shrinkage occurring at much higher doping levels than those used in the device.

The experimental method requires the introduction of many different symbols, not used in any other chapter of this thesis. For this reason we summarize in section 8.1 all the important symbols used. Section 8.2 treats the salient features of the theory required to analyse Integrated Injection Logic structures. Section 8.2.1 and 8.2.2 give the main expressions required to measure the band gap narrowing. In section 8.3 the method of analysing the various terminal currents for the range of temperatures is discussed. In section 8.4 the details of the experimental results are presented outlining the general agreement between these results for the temperature dependence of carrier mobility in lightly p-type and heavily n-type doped regions of the Integrated Injection Logic structures with those published in the literature. Finally in section 8.4.5 the band gap narrowing results are presented.

A_b area of buried layer junction A_b.

A_c area of IIL base contact.

A_{col} area of IIL collector junction.

              general junction area.

A^j junction area of the lateral pnp transistor.

A_{o+} (A_{o-}) area of IIL collector oxide covered p+ (p-) base.

A_β area of IIL super β base junction.

D_{av} average minority carrier diffusion coefficient.

D_b minority (hole) carrier diffusion coefficient in buried
              layer.

D_l minority (hole) carrier diffusion coefficient in lateral pnp
              base.

$D_n = D_{no} T^n$ minority carrier diffusion coefficient.

D_p (D_n) minority carrier diffusion coefficients.

D_s minority (hole) carrier diffusion coefficient in substrate.

D_β minority (electron) carrier diffusion coefficient in super β
              base.

E_c (E_v) energies of conduction and valence bands.

E_F Fermi energy.

E_g intrinsic energy gap.
              E_g = 1.1209 eV (T=300K)   see section 8.2.4.

$E_g(N_d)$ concentration dependent energy gap.
              $E_g(N_d) = E_g - \Delta E_g(N_d)$ see section 8.2.4.

$\Delta E_g(N_d)$ concentration dependent band gap narrowing.

F_j Fermi Dirac integral jth order.

G_b Gummel number for the buried layer.

G_l Gummel number for the base of the lateral pnp transistor.

G_β Gummel number for the super β base.

I_b I_{col} I_{inj} IIL terminal currents.

I_d difference current $(I_d = I_b - I_{inj})$.

I_{sub} substrate current.

J_{col} vertical collector current density.

J_{nc} vertical injection of electrons into contact covered base.

J_{ni} vertical injection of electrons into n+ collector.

J_{no+} (J_{no-}) vertical injection of electrons into oxide covered p+ (p-)
              base.

J_{ns} J_{nv} vertical injection of electrons in substrate transistor.

J_{pl} lateral injection of holes into p+ injector.

J_{ps} (J_{pso}) vertical injection of holes to substrate (saturation value).

J_{pv} (J_{pvo}) vertical injection of holes to n+ buried layer from IIL base
              (saturation value of J_{ps}).

k Boltzmann constant = $1.381.10^{-23}$ JK^{-1}.

L_b minority (hole) carrier diffusion length in buried layer.

L_n L_p minority carrier diffusion lengths.

M_c Number of valleys in conduction band (M_c = 6 in silicon).

m_c (m_v) conduction (valence) density of states effective masses.

$N_a(x)$ $N_d(x)$ impurity concentration as a function of distance x.

N_c effective conduction band density of states for one valley.

n_i intrinsic carrier concentration.
              $n_i^2 = n_{io}^2 T^3 \exp(-E_g/kT)$ see section 8.2.5.

n_{ie} effective intrinsic carrier concentration.
              $n_{ie} = n_i \exp(E_g - E_g(N_d))$ see section 8.2.5.

n_s electron concentration in the collector of the substrate

	transistor.
N_v	effective valence band density of states.
p_b	hole concentration in the buried layer.
q	numerically equal to the electronic charge $= 1.6 . 10^{-19}$ C.
T	temperature (K).
V_{be}	base emitter voltage.
V_{cb}	collector base voltage.
V_{cc}	collector supply voltage.
V_{mean}	mean value of V_{be}'s measured for a particular temperature.
V_{sb}	substrate buried layer junction voltage.
W_l	width of lateral pnp base.
W_b	width of buried layer.
W_β	width of super β base.
x	distance.
μ	minority carrier mobility.
τ	minority carrier lifetime.

Some subscripts:

E,B,C,inj,sub	denote emitter base collector injector substrate of the IIL gate.
b	n+ buried layer.
β	super β base.
l	lateral transistor.
s (sub)	substrate.
n,p	denote electron and hole density respectively.
n− n+	denote light and heavy impurity concentrations respectively.
1,2,3,4	used to distinguish cells 1,2,3,4.
ν	general subscript.

8.2   THEORETICAL BACKGROUND.

The complexity of the Integrated Injection Logic devices is such that a detailed transport analysis of the structures is not feasible for a short study.   However the results obtained indicated that the simple expressions used were adequate to describe the terminal currents.   In this section the detailed expressions used to describe the terminal currents are presented.

A typical Integrated Injection Logic cell of the type used in the present experiments is shown in Fig 8.1.   The equivalent circuit and biasing arrangements for the cell are shown in Fig 8.2.   As can be seen from Fig 8.1 the cells are of a composite base structure, with heavily p-type doped implants surrounding the active low doped p-type base to lower the base resistance (Plunkett et al 1978).   The whole structure is surrounded by a heavily n-type doped guard ring that extends into the heavily n-type doped buried layer and to which the emitter contact (not shown in Fig 8.1) is made.   It is this buried layer, detailed in Fig 8.3, that is of primary interest since it forms the base of the pnp parasitic transistor (marked as T3 in Fig 8.2).   The Integrated Injection Logic transistor is used to measure the electron (J_{ni}) and hole currents (J_{pv}) that pass through the upper pn junction, whilst the substrate current (J_{ps}) gives a measure of the hole current that succeeds in traversing this layer. By comparing J_{pv} and J_{ps} the transport parameters for the heavily doped buried layer may be determined.

In section 8.2.1 the details of the transport through the buried layer are presented.   In 8.2.2 the principle behind the measurement of J_{pv} is presented.   In the remaining sections (8.2.3 to 8.2.6) the most important parameters (mobility, intrinsic band gap, intrinsic carrier

p+ injector

collector contact
and n+ implant

p-type super β base

p and p+ implant

second base contact

p+ implant

PLAN VIEW OF CELL 2

9.5 μm

Injector   B   C   C   C   C   B   SiO₂

p+   p+   n+   p⁺   p+   ─O   μm
                                                            ─0.36 μm
                      p   ─0.55 μm
                                                            ─1   μ m

n epi layer   ─~2   μm

n+ buried layer (emitter E)   ─~5   μm

p substrate

Substrate contact
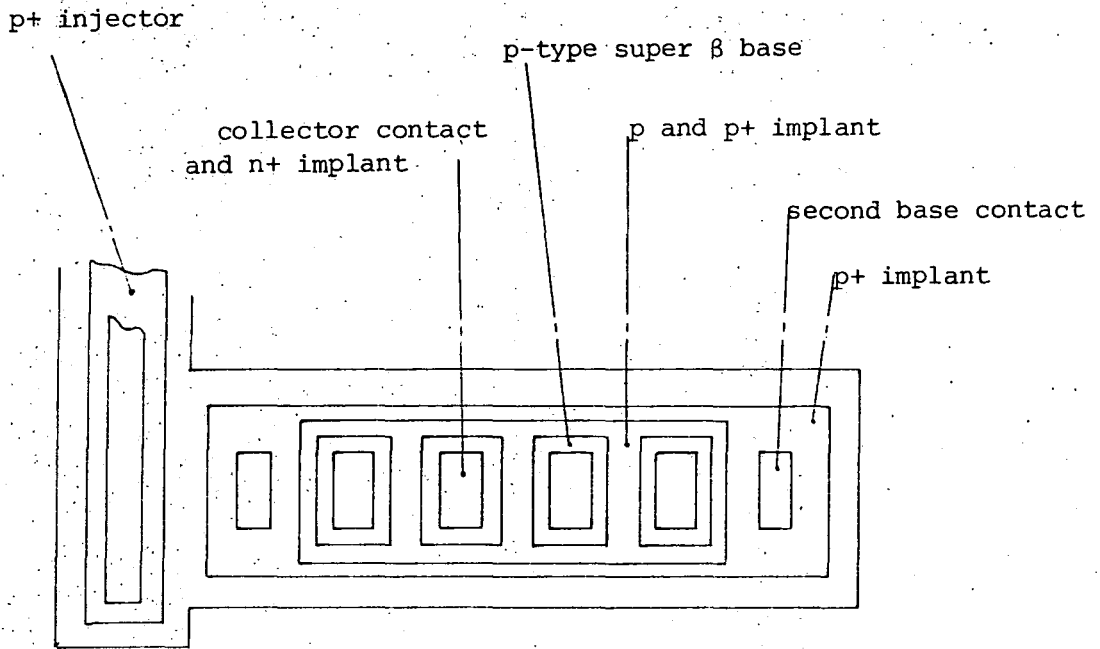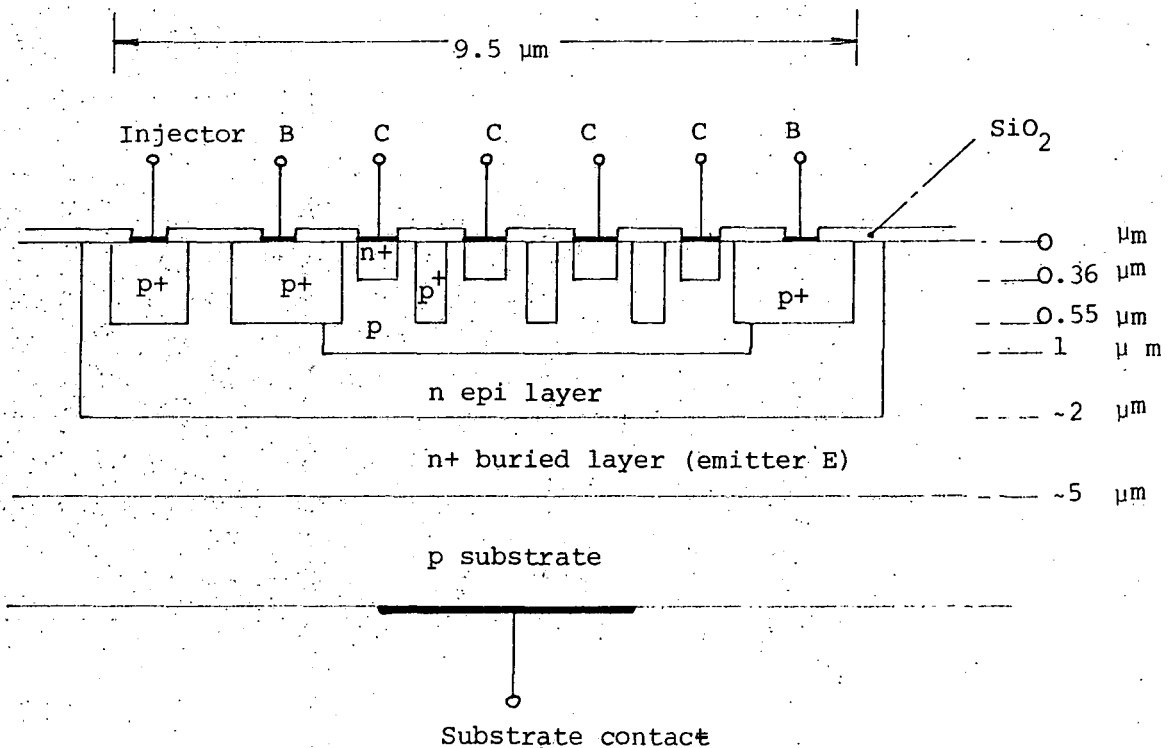
Fig 8.1   Plan and section view of cell 2, a four collector
           IIL transistor.
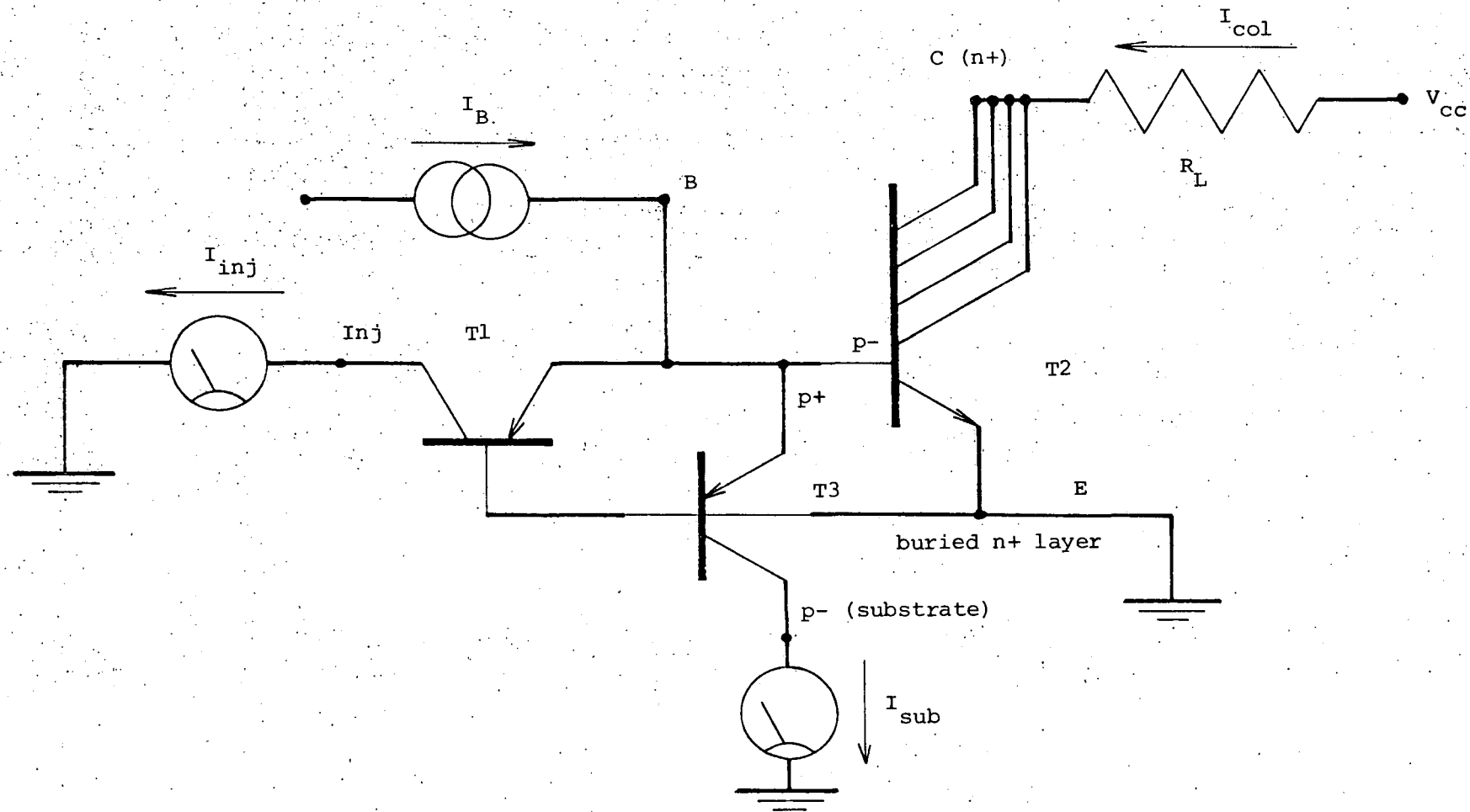
Fig 8.2   Equivalent circuit and biasing arrangements for cell 2, T1 and T2 form the standard
IIL cell, T3 is the parasitic substrate transistor.

concentration, depletion layer widths) required for the above expressions are discussed.

8.2.1 Transport through the buried layer.

Using simple theory, with recombination in the base and zero hole density at T_3's base collector depletion layer edge, the current densities shown in Fig 8.3 for the wide base parasitic pnp transistor may be described by the following expressions (Sze 1981 pp 137)

$$J_{pv} = \frac{qD_b P_b}{L_b} \coth\left(\frac{W_b}{L_b}\right) \left(\exp(qV_{be}/kT) - 1 \right) \qquad (821.01)$$

$$J_{ps} = \frac{qD_b P_b}{L_b} \frac{1}{\sinh(W_b/L_b)} \left(\exp(qV_{be}/kT) - 1 \right) \qquad (821.02)$$

$$J_{ns} = - \frac{qD_s n_s}{L_s} \left(\exp(qV_{sb}/kT) - 1 \right) \qquad (821.03)$$

Where J_{pv} is the hole current entering the buried layer and J_{ps} is the current which succeeds in traversing the layer. J_{ns} the electron current from the substrate is held at zero ($V_{sb} = 0$). J_{ni} is not detailed here since it depends upon the precise nature of the region above the buried layer, in this case an Integrated Injection Logic transistor. Often the influence of the non-uniform heavily doped n+ base region are taken into account by replacing p_b by

$$p_b = \frac{n_{ie}^2 W_b}{G_b} \qquad (821.04)$$

Where G_b is the Gummel number (Gummel 1961, and Eq. 821.11) and n_{ie} is the effective intrinsic carrier concentration (see section 8.2.5) given by

$$n_{ie}^2 = n_i^2 e^{\Delta E_g/kT} = n_{io}^2 T^3 e^{-E_g(N,T)/kT} \qquad (821.05)$$
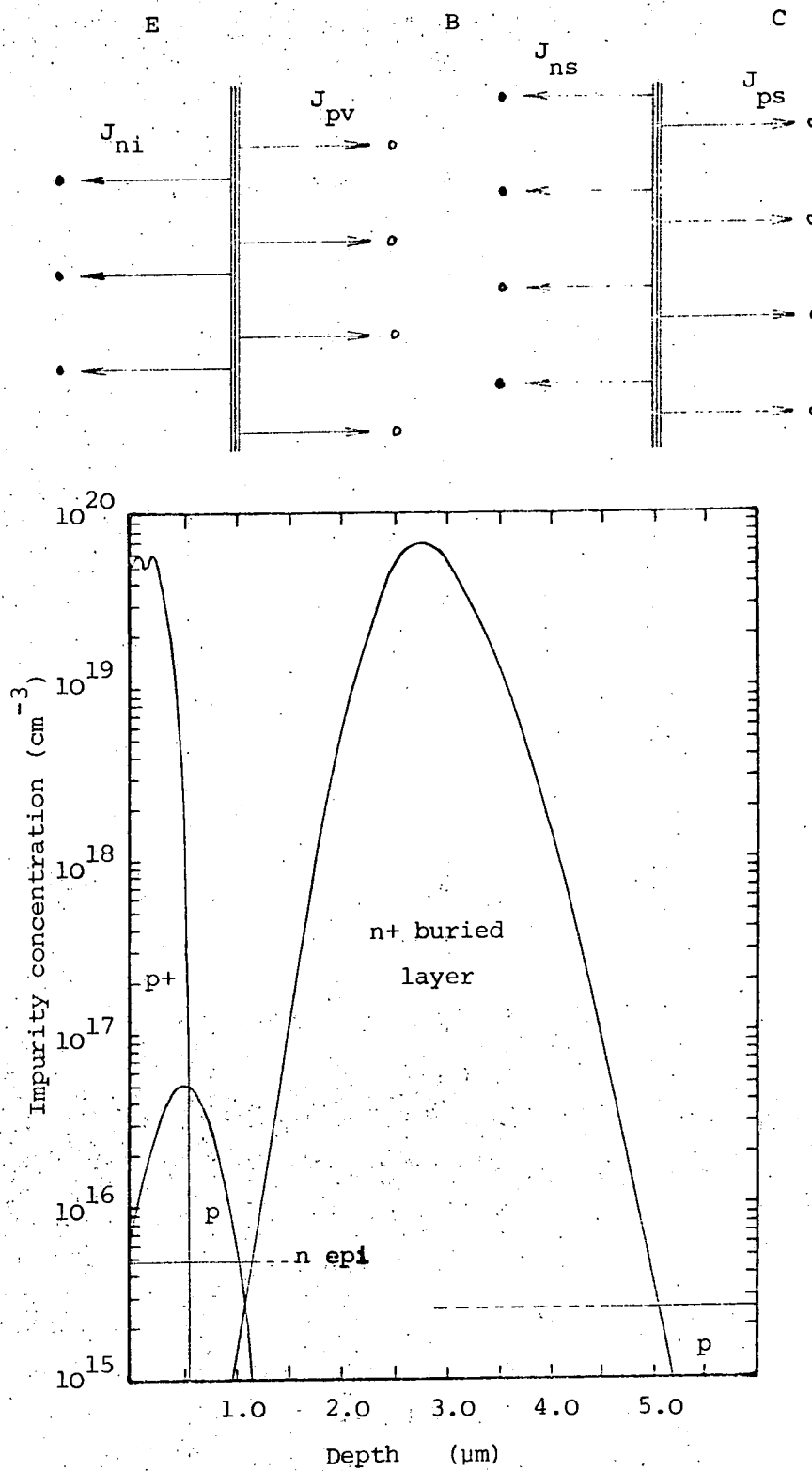
Fig 8.3   Impurity profile of the arsenic buried layer used
           to measure band gap narrowing. Also shown are the
           principle hole and electron current densities involved.

With temperature and concentration dependent band gap (see section 8.2.4) given by the expression

$$E_g(N_d, T) = E_g(T) - \Delta E_g(N_d) \tag{821.06}$$

$\Delta E_g(N_d)$ the effective band gap narrowing is supposed to be temperature independent in what follows. Substituting these expressions into the expressions for J_{pv} and J_{ps} (Eq. 821.01 and 821.02) gives

$$J_{pv} = \frac{qD_b n_{ie}^2}{G_b} \frac{W_b}{L_b} \coth\left(\frac{W_b}{L_b}\right) \exp(qV_{be}/kT) \tag{821.07}$$

$$J_{ps} = \frac{qD_b n_{ie}^2}{G_b} \frac{W_b}{L_b \sinh(W_b/L_b)} \exp(qV_{be}/kT)$$

$$= J_{pso} \exp(qV_{be}/kT) \tag{821.08}$$

The Gummel calculation is usually performed within a narrow base transistor and assumes no recombination in the base region. However the current density expressions above (Eq. 821.01 and Eq. 821.02) are calculated on the specific assumption that recombination does occur in the base. This apparent contradiction of using the Gummel number whilst allowing for recombination is not reconcilable using simple theory. However it has been shown at least for low impurity concentrations that a fair amount of recombination does not significantly change the Gummel number (Gummel 1961, 1970). If one required a more exact analysis of the current densities the continuity and current density equations would have to be solved numerically within the n+ buried layer. A more important approximation made above is that the concentration dependent band gap narrowing is constant throughout the buried layer shown in Fig 8.3. Band gap narrowing results derived in the following sections correspond then to some sort of average narrowing through the buried layer. The variation of intrinsic carrier concentration and mobility in the n+ buried layer could be

accounted for with use of the generalized Gummel number (Hart 1981 pp 110)

$$G_b = \int_0^W \frac{D_{av}}{D_p} \left(\frac{n_i}{n_{ie}} \right)^2 N(x) \, dx \qquad (821.09)$$

D_p and n_{ie} both concentration dependent with average diffusion coefficient

$$D_{av} = \frac{1}{W} \int_0^W D_p(x) \, dx \qquad (821.10)$$

and the inherent knowledge of the concentration dependent band gap narrowing and mobility. In what follows the simpler definition of the Gummel number is used

$$G_b = \int_0^W N(x) \, dx \qquad (821.11)$$

being merely a convenient way of averaging the impurity profile N(x).

As to the method of calculation of the band gap narrowing provided V_{sb} (the substrate to buried layer voltage) is kept equal to zero, the substrate current is unaffected by J_{ns} and gives a measure of J_{ps} directly. The transport factor is given by

$$tr = \frac{J_{ps}}{J_{pv}} = \frac{1}{\cosh\left(\frac{W_b}{L_b} \right)} \qquad (821.12)$$

hence by rearranging

$$W_b/L_b = \log_e\left(\frac{1}{tr} + \left(\frac{1}{tr^2} - 1 \right)^{1/2} \right) \qquad (821.13)$$

(the negative sign gives an un-physical solution) which on substitution into the expression for the substrate current (Eq. 821.08) gives the effective band gap narrowing

$$\Delta E_g = - kT \, Log_e\left(\frac{qD_b n_i^2}{G_b} \right) + kT \, Log_e(J_{pso})$$

$$- kT \, Log_e\left(\frac{W_b}{L_b \sinh\left(\frac{W_b}{L_b} \right)} \, W_b \right) \qquad (821.14)$$

The saturation hole current J_{pvo} might equally be used to provide a less accurate (because of extrapolation errors) value for the band gap narrowing, however the hole current chosen gives a more direct result. Using the relationship

$$L_p = (D_p \tau_p)^{1/2} \qquad\qquad (821.15)$$

and the buried layer width (W_b) the minority carrier diffusion length (L_p) and life time (τ_p) of the carriers may also be calculated. By varying both voltage V_{be} and the temperature it was hoped to test the validity of the above expressions and thus to estimate the band gap narrowing.

8.2.2 **Measurement of J_{pv}**

Measurement of the transport factor (Eq. 821.12) requires the measurement of J_{pv}. Berger et al (1972 also see Berger 1979) introduced the basic method of separating out the various injection currents in the Integrated Injection Logic transistor. The structure used is different from the original Integrated Injection Logic transistors in that it incorporates a composite base region, with p+ implants surrounding the active low doped super β base to reduce base recombination (Plunkett et al 1978). Fig 8.4 shows a cross section of a typical cell. Berger's method has been extended to include other current densities for example recombination in base region and sideways leakage to the n+ guard ring (Yang et al 1978). However choosing cells with large aspect ratio and narrow base (see Fig 8.1) it is expected that the major current densities are those shown in Fig 8.4.

The principle of the method may be summarized with the help of Fig 8.4. In describing the base current (I_b) five components are

= 8.9 =
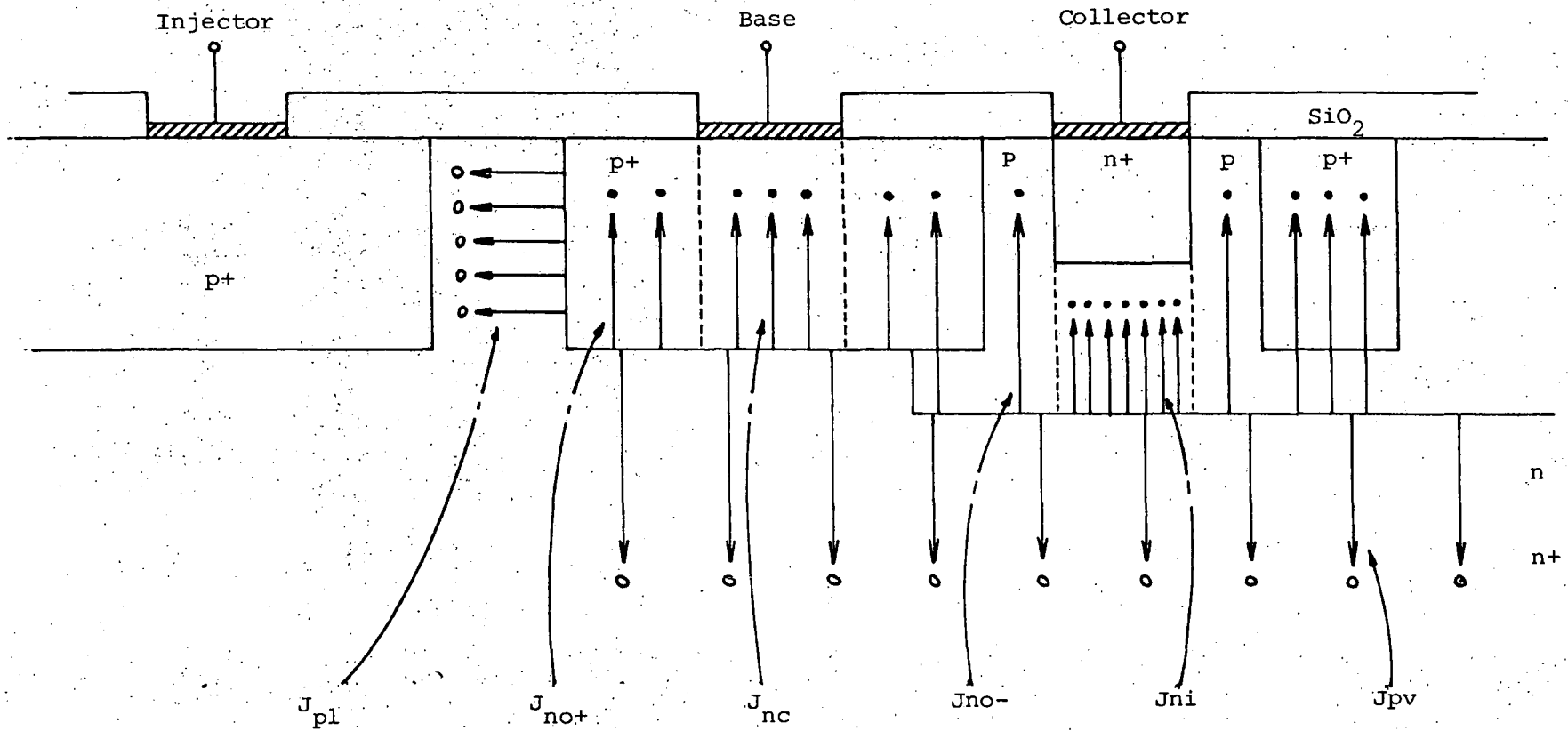
Fig 8.4   Section view of an IIL cell showing the principle injection current densities.

identified characterized by J_{pl}, J_{no+}, J_{no-}, J_{nc}, J_{pv} and the associated junction areas.

$$I_b = A_1 J_{pl} + A_{o-} J_{no-} + A_{o+} J_{no+} + A_c J_{nc} + A_b J_{pv} \qquad (822.01)$$

Since the injector current ($A_1 J_{pl}$) is measured directly and may be subtracted from the base current there are only four unknown current densities (J_{no+}, J_{no-}, J_{nc}, J_{pv}). So that the difference current I_d for four similar Integrated Injection Logic cells (denoted by 1, 2, 3, 4) may be given by the matrix equation

$$\begin{pmatrix} I_d 1 \\ I_d 2 \\ I_d 3 \\ I_d 4 \end{pmatrix} = \begin{pmatrix} A_{o-} 1 & A_{o+} 1 & A_c 1 & A_b 1 \\ A_{o-} 2 & A_{o+} 2 & A_c 2 & A_b 2 \\ A_{o-} 3 & A_{o+} 3 & A_c 3 & A_b 3 \\ A_{o-} 4 & A_{o+} 4 & A_c 4 & A_b 4 \end{pmatrix} \begin{pmatrix} J_{no-} \\ J_{no+} \\ J_{nc} \\ J_{pv} \end{pmatrix} \qquad (822.02)$$

The substrate (collector) currents are given by the substrate (collector) current density J_{sub} (J_{col}) and junction area A_b (A_{col}).

Provided the area matrix in Eq. 822.02 has a non - zero determinant (hence the need for the collector implant to avoid the sum of two columns equaling a third) the matrix equation can be solved for the various current densities. Thus the two merged transistors are not essential to the measurement of J_{pv} since the injector current does not effect the difference current. In the present measurements the injector is however used to provide the fourth cell as can be seen in Fig 8.5 of the four cells. The first has no collector implant ($A_{col} 1 = 0$), the second is a complete Integrated Injection Logic cell, the third has only the heavily doped p-type base implant and the fourth is created by reversing the role of base and injector so that the three previous contacts used to collect I_b 1 to 3 were then earthed to provide the measurement of I_{inj} 4. Fig 8.6

A ——— A

section AA

Cell 1

B ——— B

section BB

Cell 2

C ——— C

section CC

Cell 3

D ——— D

section DD

Cell 4
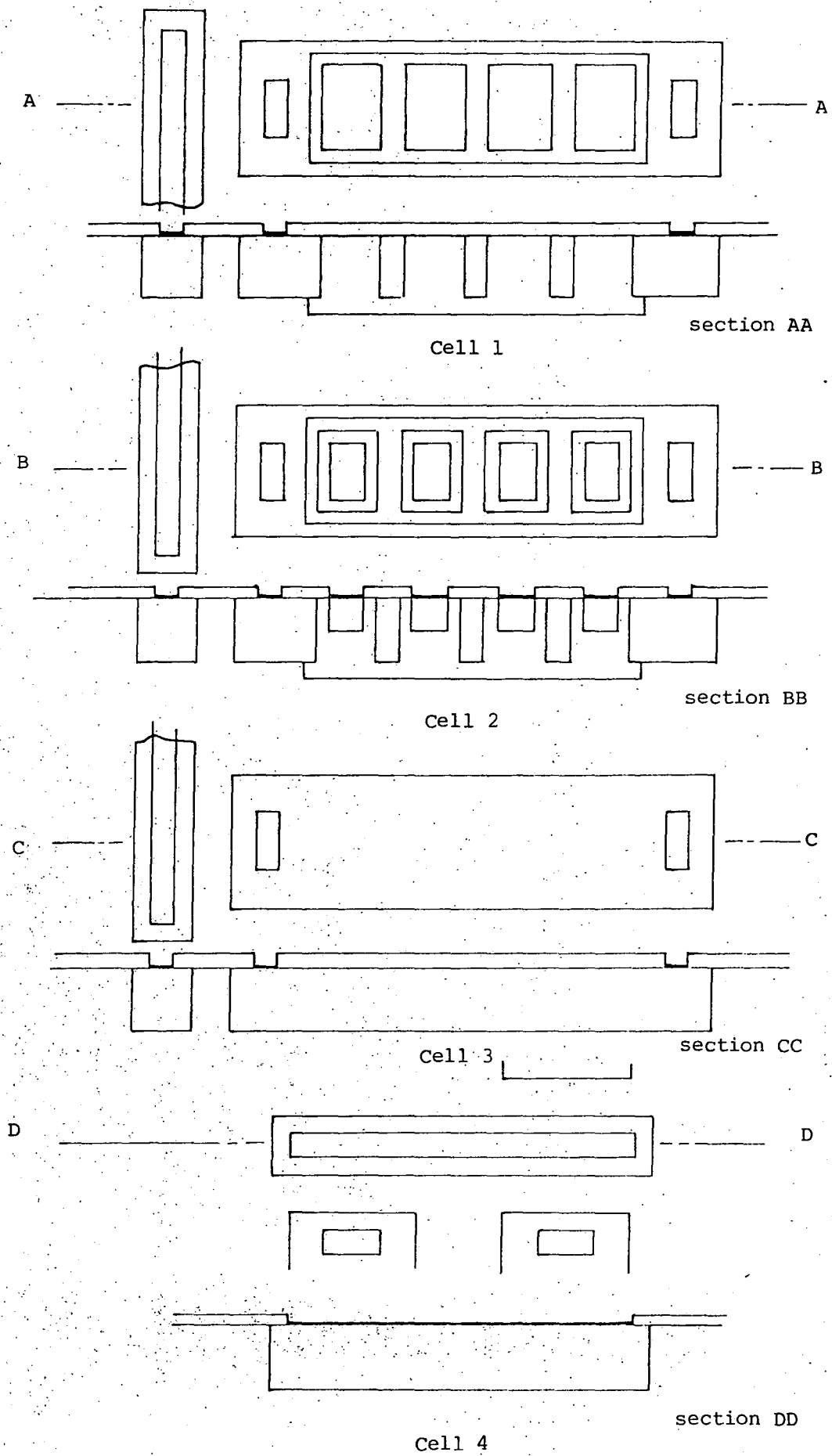
Fig 8.5   Plan and section views of the four IIL cells used in the experiments.
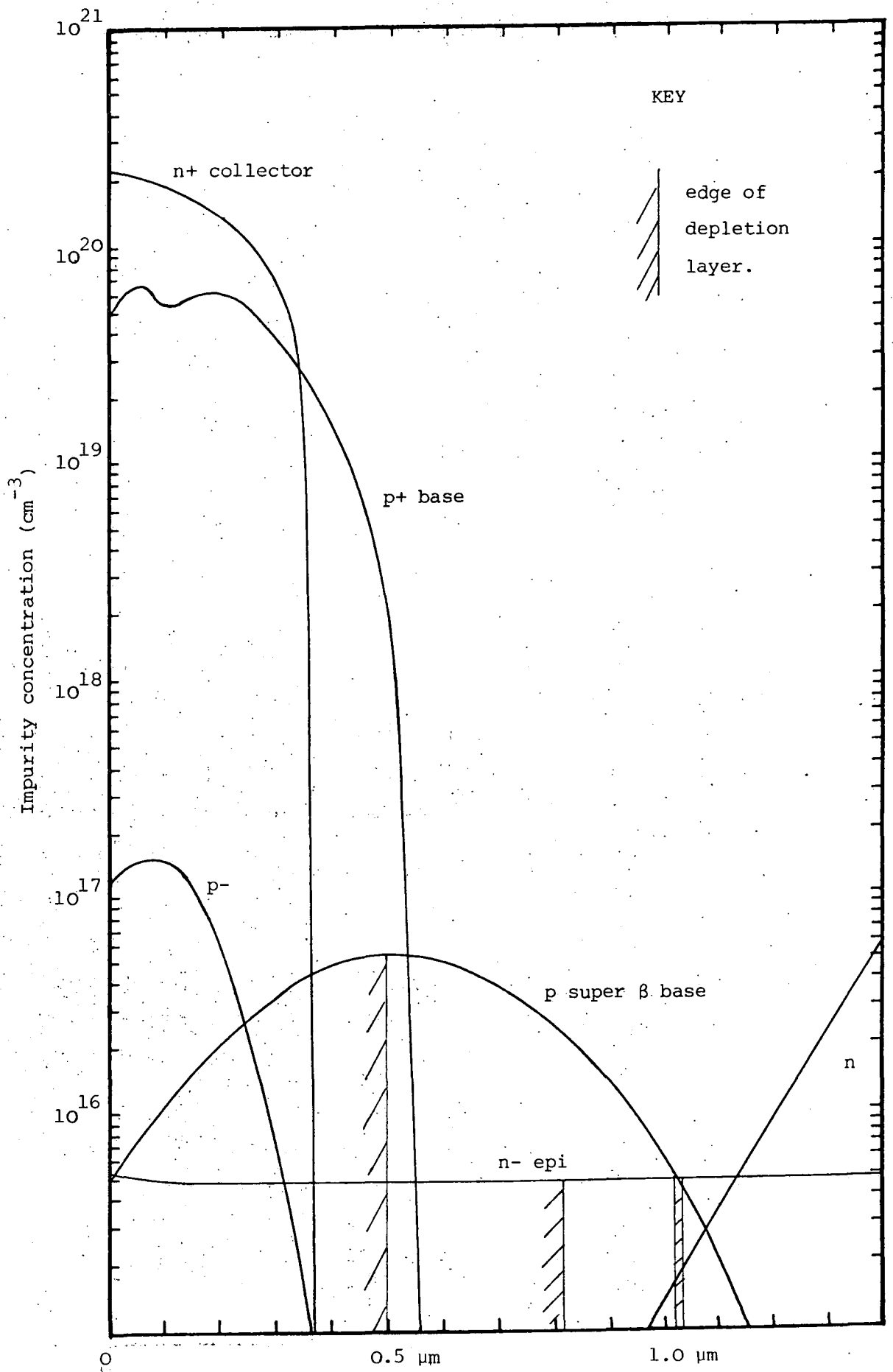
Fig 8.6   Impurity profiles for the IIL cells showing depletion widths
(see section 8.2.7).

shows the impurity profiles for the n-type collector (2.10^{20}), p+ base $(5 \cdot 10^{19})$, super β base (peak concentration 6.10^{16}, n-type epitaxial layer $(5 \cdot 10^{15})$. The p-type surface top up implant that peaks at 0.1 μm from the surface is to ensure a p-type oxide covered p- base region.

The basic method can and has been extended to measure more current densities (Yang et al 1978) merely by choosing the appropriate geometries for a larger number of Integrated Injection Logic like cells. The only apparent criterion to be satisfied is the non-zero determinant of the area matrix equivalent to that in Eq. 822.02. However apart from this care is required in the design of such cells since the resulting current densities are essentially calculated from differences between currents. If these subtractions involve large component parts and derive small results the errors so produced in the calculated current densities may be large. For example given the results of the following sections for the present set of devices (Fig 8.5) and areas (Table 8.8) the error resulting from a 1% increase in each of the junction areas is presented in Table 8.1. Thus a 1% increase in the measured area for the oxide covered p+ implant in cell 2 results in a 22% decrease in the calculated value of J_{pv} but only a 2% increase in J_{no}-. A similar error analysis of the effects of inaccuracies in the measurement of the four difference currents on the values of the current densities calculated from Eq. 822.02 is presented in Table 8.2.

It is clear from these results that surprisingly large errors in J_{pv} may be generated particularly if I_d2 or the oxide covered p+ area on cells 2 and 3 were inaccurately measured. These errors are hard to predict since they depend in detail upon the relative sizes of terminal currents and junction areas. Indeed even the small change in areas due to depletion widths were important.

Table 8.1

% change in current densities produced by increasing junction areas by 1%

V_{be}=528.5 mV, T=297.4 K, I_d1=28.8 nA, I_d2=21.2 nA, I_d3=21.8 nA, I_d4=11.7 nA, J_{no-}=2.39.10^{-3}, J_{no+}=8.82.10^{-4}, J_{nc}=2.12.10^{-3}, J_{pv}=1.84.10^{-4}

	$A_{o-}1$	$A_{o+}1$	A_c1	A_b1	$A_{o-}2$	$A_{o+}2$	A_c2	A_b2
J_{no-}	0.0	-1.6	-0.3	-0.5	0.5	1.7	0.3	0.4
J_{no+}	0.0	-1.4	-0.2	-0.4	1.3	4.6	0.7	1.2
J_{nc}	0.0	-0.6	-0.1	-0.2	0.5	1.9	0.3	0.5
J_{pv}	0.0	6.6	1.0	2.0	-6.1	-21.9	-3.3	-5.8

	$A_{o-}3$	$A_{o+}3$	A_c3	A_b3	$A_{o-}4$	$A_{o+}4$	A_c4	A_b4
J_{no-}	0.0	0.0	0.0	0.0	0.0	0.0	0.0	0.0
J_{no+}	0.0	-3.8	-0.5	-0.9	0.0	0.0	0.0	0.0
J_{nc}	0.0	-0.3	-0.1	-0.1	0.0	-0.9	-1.1	-0.3
J_{pv}	0.0	13.2	1.6	3.1	0.0	0.5	0.6	0.2

Table 8.2

% change in current densities produced by
increasing different currents by 1%

	I_d1	I_d2	I_d3	I_d4
J_{no-}	3.8	-2.8	0.0	0.0
J_{no+}	3.3	-7.6	5.3	0.0
J_{nc}	1.4	-3.2	0.4	2.4
J_{pv}	-15.7	36.4	-18.4	-1.3

In a thorough follow up experiment the current densities calculated below could be used to assist in the design of a second set of device structures to improve the present error prone cells. However reasonable results are obtained from the present cells justifying the method of averaging used below to improve the current measurements.

8.2.3   Carrier mobilities and diffusion coefficients.

In section 8.3 we show how the temperature dependence of the minority carrier mobility may be calculated from the experimental results. Although a direct measurement of the temperature and concentration dependent mobility $\mu(N)$ would be desirable in a more thorough analysis of Eq. 821.07 and Eq. 821.08 the present values are adequate. The values used are derived from the expression (Caughey et al 1967)

$$\mu(N) = \frac{\mu_{max} - \mu_{min}}{1 + (N/Nref)^{\alpha}} + \mu_{min} \tag{823.01}$$

The values of the constants μ_{max} and μ_{min} in Table 8.3 are taken from Hart (1981 pp 101).

Table 8.3

Mobility data

T = 300K	μ_{max} (cm^2/Vs)	μ_{min} (cm^2/Vs)	α	Nref (cm^{-3})
Electrons	1360	92	0.91	$1.3.10^{17}$
Holes	495	47.7	0.76	$1.9.10^{17}$

The minority carriers are not subject to Fermi Dirac statistics so that the thermal equilibrium relationship between diffusion coefficient (D) and mobility (μ) reduces to the Einstein relationship (Sze 1981 pp 29)

$$D = \frac{kT}{q} \mu \tag{823.02}$$

8.2.4 Intrinsic band gap.

The temperature dependent intrinsic band gap is clearly a very important parameter and is obtained from a best fit of the data of Macfarlane et al (1958). Their data obtained from optical absorption measurements were obtained using very high resolution ($\sim$ 0.0015 eV) equipment and falls near the average of other measurements (Barber 1967). In what follows the expression

$$E_g(T) = 1.165 - \frac{4.879\ 10^{-4}\ T^2}{T + 180} + 1.58.10^{-4}\ T \quad (eV) \quad (824.01)$$

was used. The concentration dependent change in the band gap ($\Delta E_g(N_d)$) is assumed to have no temperature dependence. Thus the concentration dependent band gap ($E_g(N_d,T)$) is given by

$$E_g(N_d,T) = E_g(T) - \Delta E_g(N_d) \quad\quad\quad (824.02)$$

8.2.5 Intrinsic carrier concentration.

The square of the temperature dependent intrinsic carrier concentration used in Eq. 821.14 may be written

$$n_i^2 = 4 \left(\frac{2\pi (m_c m_v)^{1/2} kT}{h^2} \right)^3 M_c \exp(-E_g(N_d,T)/kT) \quad (825.01)$$

This slightly under estimates the temperature dependence since the effective masses of the conduction and valence bands are temperature dependent (Barber 1967 Jaeger et al 1980). In what follows the 300K value of $1.45.10^{10}$ cm^{-3} (Sze 1981) for the intrinsic carrier concentration is used extrapolating other values from this.

Using the band gap quoted in Eq. 823.01 the square of the intrinsic carrier concentration becomes

$$n_i^2 = 4.9161.10^{31} \ T^3 \ \exp(-E_g/kT)$$

$$= n_{io}^2 \ T^3 \ \exp(-E_g/kT) \qquad (cm^{-6}) \qquad\qquad (825.02)$$

When extending this expression to deal with the heavily doped degenerate silicon Fermi Dirac statistics should be used (Blakemore 1962) writing

$$n = N_c \ M_c \ F_{1/2}((E_F - E_c)/kT)$$

$$\approx N_c \ M_c \frac{\exp((E_F - E_c)/kT)}{1 + 0.27 \ \exp((E_F - E_c)/kT)} \qquad (825.03)$$

$$p = N_v \ \exp((E_v - E_F)/kT)$$

where an approximation for the Fermi Dirac integral developed by Blakemore has been used. Eq. 825.02 becomes

$$n_{ie}^2 = np = N_v \ N_c \ M_c \frac{\exp((E_v - E_c)/kT)}{1 + 0.27 \ \exp((E_F - E_c)/kT)} \qquad (825.04)$$

using the simple formula

$$n_{ie}^2 = n_i^2 \ \exp(\Delta E_g/kT) \qquad\qquad (825.05)$$

to evaluate the concentration dependent carrier concentration thus under estimates the physical band gap narrowing $(\Delta E_g{}')$ by the amount

$$\Delta E_g{}' = \Delta E_g + kT \ Log_e(1 + 0.27 \ \exp((E_F - E_c)/kT)) \qquad (825.06)$$

This expression is valid whilst $(E_F - E_c)/kT < 1.3$

Numerically this amounts to a small correction of about 6 meV to the band gap depending on the separation between conduction band and Fermi level (Fig 7.3). These expressions also ignore the small concentration dependence of the effective mass due to electron-electron

exchange that has been noted in chapter 2.

8.2.6 Depletion layer calculations.

Sideways depletion widths of the n+ collector and of the p+ base are the only widths to effect the junction areas used in calculating J_{pv}. The vertical collector depletion width is required when comparing calculated and measured Gummel numbers and is also calculated. Since the experimental estimation of J_{pv} and to a lesser extent J_{ps} rely critically upon the junction areas which in turn depend upon the depletion layer calculation it would seem that an improvement would be to measure the depletion widths with perhaps an AC measurement of depletion capacitance. This was thought to be beyond the scope of the present work where we rely upon depletion widths calculated under the depletion approximation. More detailed study of the performance would require both the inclusion of band gap narrowing (and the corresponding use of heterostructure analysis) as well as space charge in the depleted region. The results of the present depletion width calculations are presented in Fig 8.6. superimposed on the various impurity implant profiles.

Ignoring space charge the solution of Poisson's equation (Sze 1981) reduces to

$$V_j = \int_{x1}^{x2} \int_{x1}^{s} \frac{1}{\epsilon \epsilon_r} (N_a(x) - N_d(x)) \, dx \, ds \qquad (eV) \qquad (826.01)$$

where the junction voltage (V_j) is expressed in electron volts. The junction voltage is reduced by any forward biased voltage applied externally to the junction

$$V_j = V_{bi} - V_e \qquad\qquad (826.02)$$

Where V_e is the external voltage applied to the junction and V_{bi} is the built in voltage. In terms of the band diagram shown in Fig 8.7 the junction voltage may be expressed as

$$V_j = E_g - V_n - V_p \qquad (826.03)$$

With separation between Fermi energy and conduction band (V_n) on the n side given by

$$N_d(x) \approx n = 2 \left(\frac{2\pi m_c kT}{h^2} \right)^{3/2} M_c \, F_{1/2}\left(\frac{-V_n}{kT} \right) \qquad (826.04)$$

where kT is expressed in eV. The separation of valence band edge and Fermi energy on the p side of the junction given by

$$N_a(x) \approx p = 2 \left(\frac{2\pi m_v kT}{h^2} \right)^{3/2} F_{1/2}\left(\frac{-V_p}{kT} \right) \qquad (826.05)$$

Where $F_{1/2}(\eta)$ is a Fermi Dirac integral (Blakemore 1962). With the approximation to the Fermi Dirac integral used above (Eq. 825.03) Eq. 826.02 can be rewritten

$$V_n = kT \, Log_e(N_c M_c / N_d(x) - .27)$$
$$V_p = kT \, Log_e(N_v / N_a(x) - .27) \qquad (826.06)$$
$$V_{bi} = E_g - V_n - V_p$$

All of the junctions in the device may be represented by the superposition of some combination of step or Gaussian like distributions of impurities as can be seen from Fig 8.6. The super β base – collector junction is an example of a Gaussian like distribution meeting an effectively square collector profile. Thus to solve for the depletion widths of these junctions the double integral of a Gaussian is required
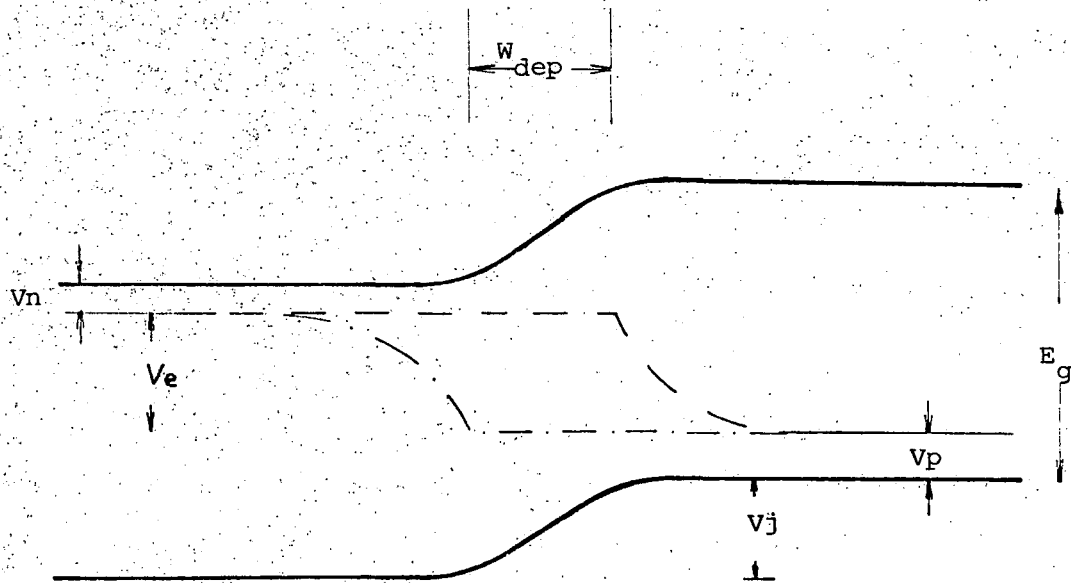
Fig 8.7   Energy band diagram defining the variables used in the depletion
width (W_{dep}) calculations.

(Eq. 826.01) for which the expressions (Abramowitz and Stegun 1970)

$$\int_{a}^{by}\int_{a} \exp\left(-\frac{x^2}{2}\right) \, dxdy = b\,(Q(a)-Q(b)) + (Z(b)-Z(a)) \qquad (826.07a)$$

$$Q(x) = \int_{a}^{b} \exp\left(-\frac{x^2}{2}\right) \, dx \qquad (826.07b)$$

$$Z(x) = \exp\left(-\frac{x^2}{2}\right) \qquad (826.07c)$$

are used. The depletion widths of all the junctions were calculated and are summarized in Fig 8.6. In the p+ epitaxial interface the temperature and voltage dependence of this depletion width are presented with the theoretical Gummel number (Eq. 821.11) for the lateral base in Tables 8.4 and 8.5.

Table 8.4

Voltage variation of lateral base length T=300K

$$N_d = 5.10^{15} \text{ cm}^{-3}, \ N_a = 3.10^{19} \text{ cm}^{-3}$$

V applied (meV)	depletion width (μm)	base length W_l (μm)	Gummel number G_l (cm^{-2})
0	0.484	4.298	$2.149.10^{12}$
200	0.427	4.356	$2.178.10^{12}$
400	0.360	4.422	$2.211.10^{12}$
600	0.279	4.504	$2.252.10^{12}$
800	0.159	4.623	$2.312.10^{12}$

The Gummel number for the lateral base varies by about 3% over a typical 200 mV change in V_{be} the applied voltage. The small change in depletion widths will however not effect the area of this junction significantly. Table 8.5 shows that the various sampling voltages (V_{mean}) chosen for each temperature result in the Gummel number and depletion widths being held constant despite the change in temperature. A depletion with of .32 μm is taken for the area A_l measurements in section 8.4.1.

Table 8.5

Lateral Gummel number and depletion width at V_{mean}

$$N_d = 5.10^{15} \text{ cm}^{-3}, \quad N_a = 3.10^{19} \text{ cm}^{-3}$$

tempe- rature (K)	applied voltage (mV)	depletion width (μm)	Gummel number G_l (cm^{-2})
365.96	364.5	0.3401	$2.234.10^{12}$
355.88	389.0	0.3360	$2.234.10^{12}$
339.85	427.5	0.3398	$2.234.10^{12}$
322.81	468.5	0.3225	$2.234.10^{12}$
313.04	491.0	0.3187	$2.234.10^{12}$
312.75	492.0	0.3185	$2.234.10^{12}$
297.40	528.5	0.3119	$2.235.10^{12}$
283.51	559.0	0.3068	$2.235.10^{12}$
264.59	603.5	0.2984	$2.246.10^{12}$
236.67	734.0	0.2539	$2.253.10^{12}$
207.32	665.0	0.3040	$2.223.10^{12}$

Considering the lateral depletion width of the collector base junction the booster compensating p- implant at the surface (Fig 8.6) results in a grading in the concentration and hence the depletion width will not be uniform. Rather it will vary from as little as 0.11 μm at the surface (Table 8.6 net acceptor concentration $\approx 1.10^{17}$ cm^{-3}) to perhaps as much as .16 μm deeper in the device (net acceptor concentration $\approx 5.10^{16}$).

Table 8.6

Sideways depletion layer (μm) on collector ($N_d = 1.25.10^{20}$) for various temperatures and acceptor concentrations ($N_a = 5.10^{16}, 1.10^{17}$)

T (K)	366.0	355.9	339.9	322.8	313.0	312.8	297.4	283.5	264.6	236.7	207.3
1E17	0.11	0.11	0.11	0.11	0.11	0.11	0.11	0.11	0.11	0.12	0.12
5E16	0.15	0.15	0.16	0.16	0.16	0.16	0.16	0.16	0.16	0.16	0.17

The diffusion length of the electrons in this region ($N_a \approx 5.10^{16}$) is of the order of tens of microns (Wolf 1969), as such much of this non-

uniformity must be transparent to the electrons. A value of .16 μm is taken as the sideways depletion width in the measurement of A_{col} (section 8.4.1).

The vertical depletion width below the collector is calculated assuming the n+ collector to have a step profile whilst fitting the super β base profile (Fig 8.6) to a Gaussian. With the collector held at the base voltage ($V_e = 0$) the junction voltage (Eq. 826.02) is the built in voltage (Eq. 827.06) for the junction. Results for these calculations are shown in Table 8.7.

Table 8.7

Temperature variation of the collector depletion width

and Gummel number G_β. $N_d = 1.25.10^{20}$ cm^{-3}. N_a see Fig 8.6.

tempe-rature (K)	depletion width (μm)	base length W_β (μm)	Gummel number $G_{\beta 2}$ (cm$^{\beta 2}$)
365.96	0.159	0.481	$1.180.10^{12}$
355.88	0.160	0.480	$1.176.10^{12}$
339.85	0.161	0.479	$1.171.10^{12}$
322.81	0.162	0.478	$1.165.10^{12}$
313.04	0.163	0.477	$1.162.10^{12}$
312.75	0.163	0.477	$1.162.10^{12}$
297.40	0.164	0.476	$1.157.10^{12}$
283.51	0.165	0.475	$1.152.10^{12}$
264.59	0.166	0.474	$1.146.10^{12}$
236.67	0.168	0.472	$1.137.10^{12}$
207.32	0.170	0.470	$1.129.10^{12}$

The depletion width of the lower junction of the super β base with the epitaxial layer and heavily doped buried layer however has the full V_{be} applied reducing the built in voltage. Coupled with this the small impurity concentrations (Fig 8.6) result in a very small depletion width at this junction (less than .01 μm). Taking this as zero and the junction at 1 μm below the surface the theoretical Gummel number for the active base is calculated (Eq. 821.11) and is also tabulated in Table 8.7.

The depletion widths are summarized in Fig 8.6, where the edge of the depletion layer is indicated by a vertical line. This clearly shows that the base emitter junction (see Fig 8.1) for the p+ epitaxial junction occurs at about 0.55 μm, whilst the super β epitaxial junction occurs at about 1 μm. This difference results in a small difference in buried layer width as shown in Fig 8.1. This is not important since as shown in Fig 8.3 the bulk of the arsenic impurity concentration lies deeper in the device so that the fluctuation of G_b beneath the cells is small.

8.3   EXPERIMENTAL TECHNIQUE.

In section 8.2.1 the basic method of calculating the band gap narrowing was presented (Eq. 821.14). It requires the measurement of the transport parameter (Eq. 821.12) for the heavily doped buried layer shown in Fig 8.3. This in turn requires the measurement of both the substrate current and buried layer junction area A_b (hence J_{ps}) and the hole current density J_{pv}. This latter current density is measured by Berger et al (1972) injection method outlined in section 8.2.2. Thus the measurement of the band gap narrowing is reduced to the measurement of areas, and currents with the additional data presented in section 8.2 of diffusion coefficients intrinsic band gap and intrinsic carrier concentration. The temperature of the cells is determined iteratively (section 8.4.2) from the collector current using both the intercept current (V_{be} = 0) and the current at a mean value of the voltage (V_{mean}) to reduce errors in the temperature sensitive intercept currents.

In section 8.3.1 the basic experimental technique and equipment used is outlined. The method of averaging the currents and obtaining the temperature dependence of the diffusion coefficients (mobilities) is

outlined in section 8.3.2. The experimental results are left until section 8.4.

8.3.1   Basic experimental technique.

Measurement of the current voltage characteristics of the cells, that were fabricated by Plessey (Caswell) Ltd. was performed by selecting a range of base currents using a Keighley current source whilst biasing the device as shown in Fig 8.2. All external wiring was screened and the devices were mounted in a screened metal box in order to reduce interference when making the low current measurements. The collector current (I_{col}) was provided through a Tektronix 576 curve tracer the supply voltage Vcc being varied in order that the collector base voltage was zero. All other currents and voltages were monitored using Keighley electrometers. The temperature of the devices was controlled by an overhead cooling head placed in contact with the packages using a silicon compound to improve thermal contact between the package and the head.

Typical current voltage measurements on the devices are shown in Fig 8.8 to Fig 8.11. The results that follow are based on measurements made at eleven different temperatures in the range 200K to 400K on one set of cells. The base currents chosen (10 nA to 0.3 μA) restrict the current voltage characteristics to their linear region with ideality factor approximately equal to unity (m ~ 1). As can be seen from the current voltage plots all the currents fall on good straight lines thus only four base currents of 10nA 30nA 100nA and 300nA were used the difference currents (Eq. 822.02) being measured at each base current. Despite the small number of base currents the eleven temperatures and four cells with thirteen currents and four voltages to measure represent over 500 different
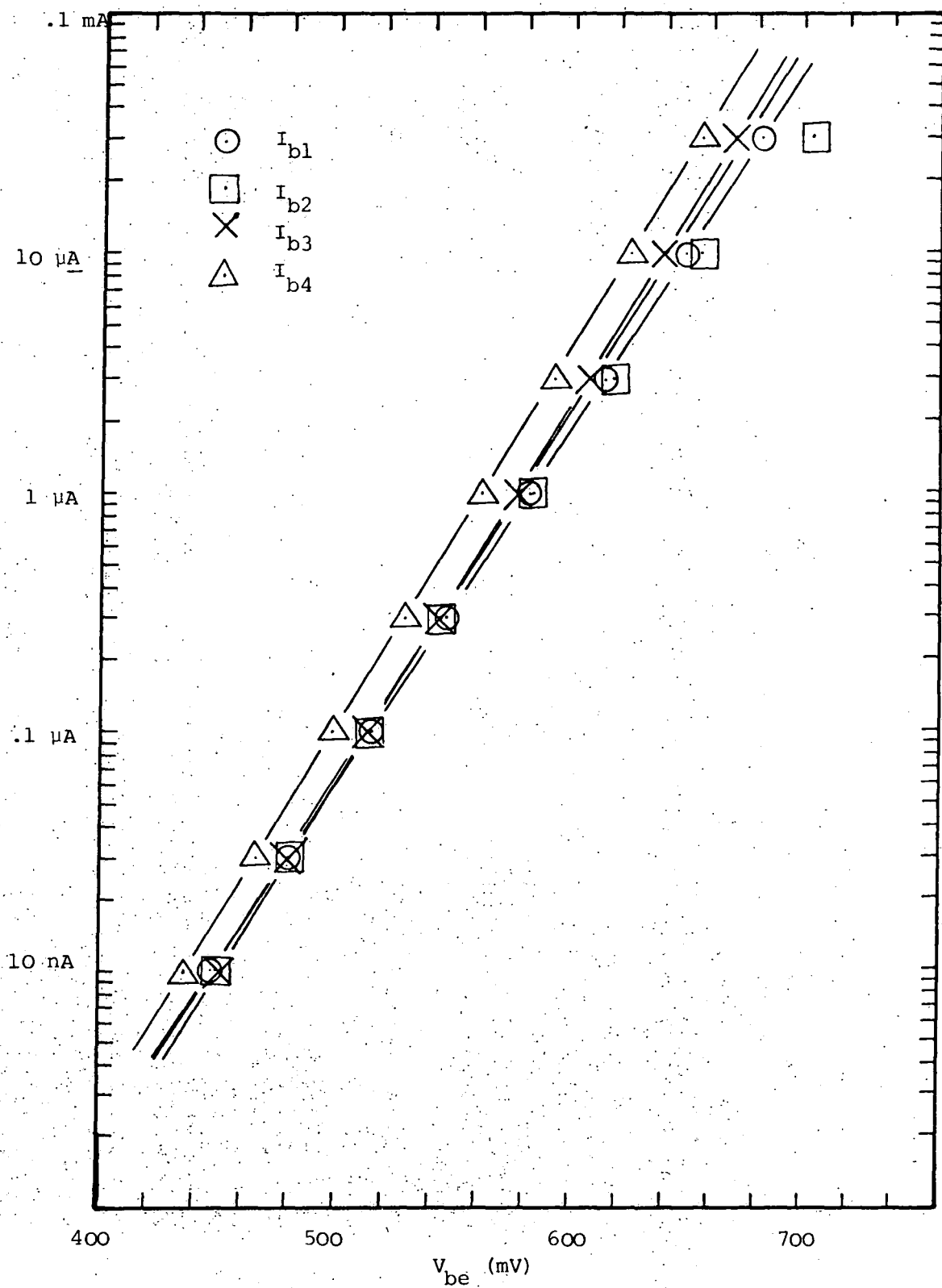
Fig 8.8   Typical plot of base currents against base emitter voltage.
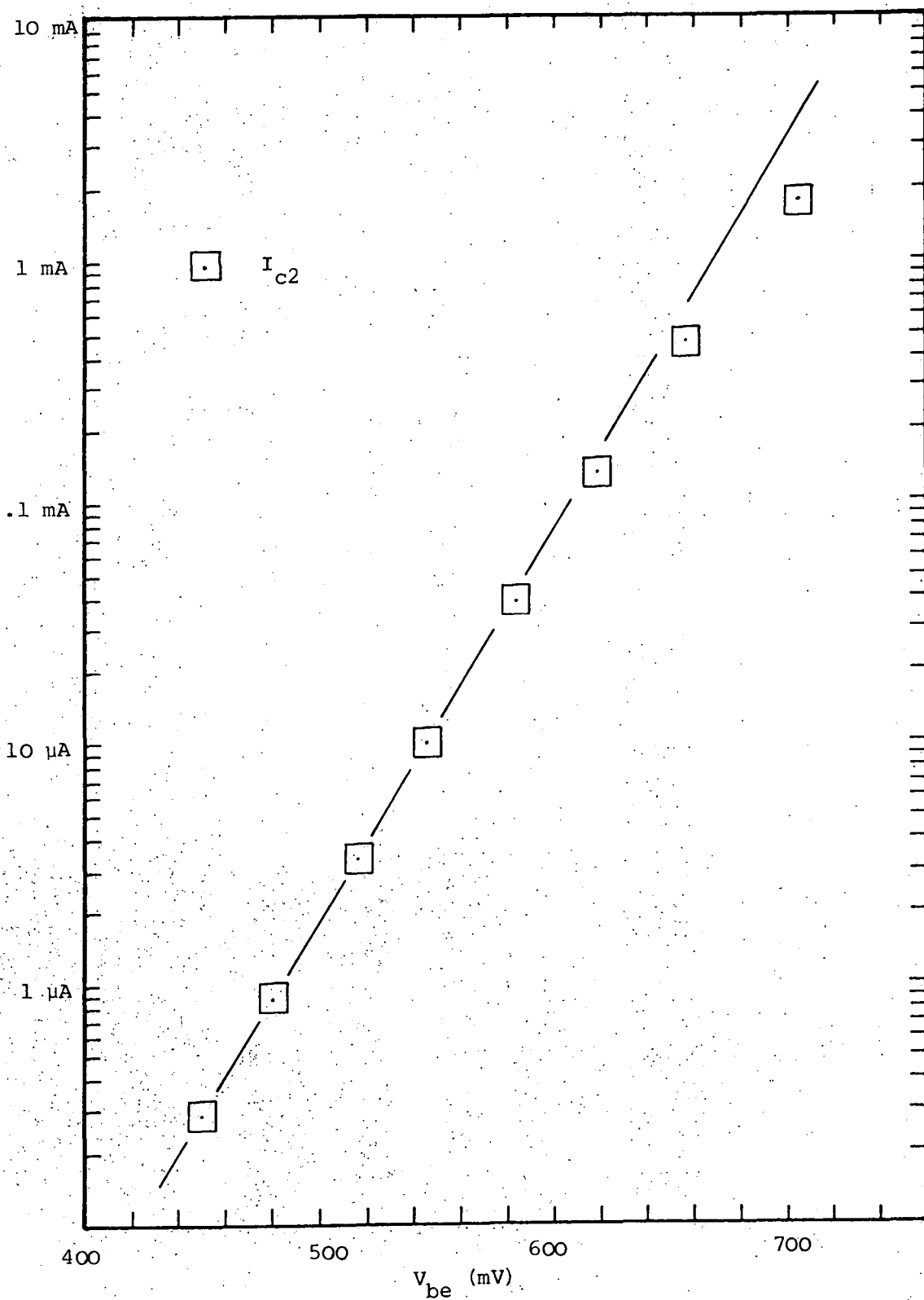
Fig 8.9   Typical plot of the collector current against base emitter voltage.
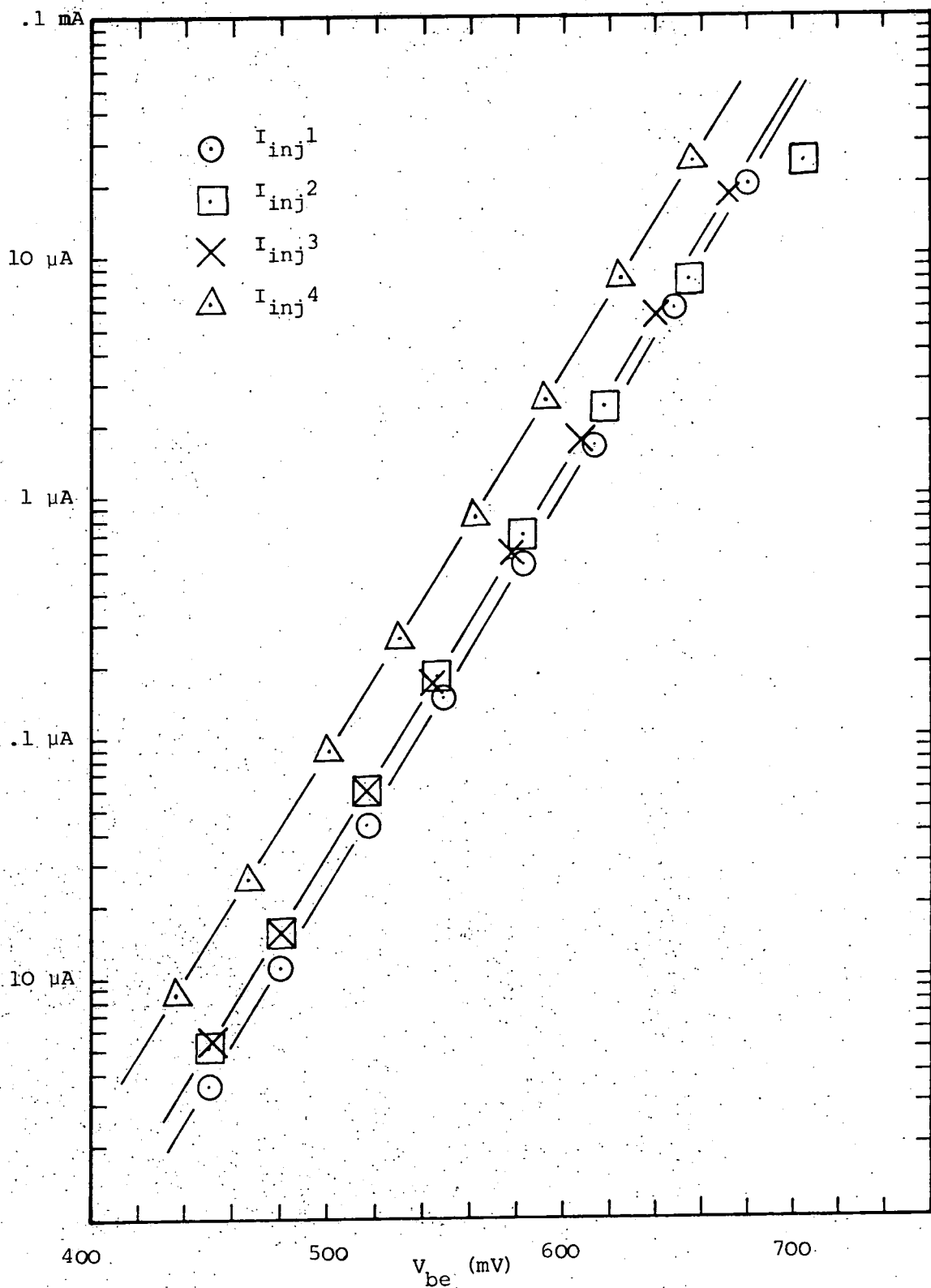
Fig 8.10   Typical plot of the injector currents against base emitter
            voltage.
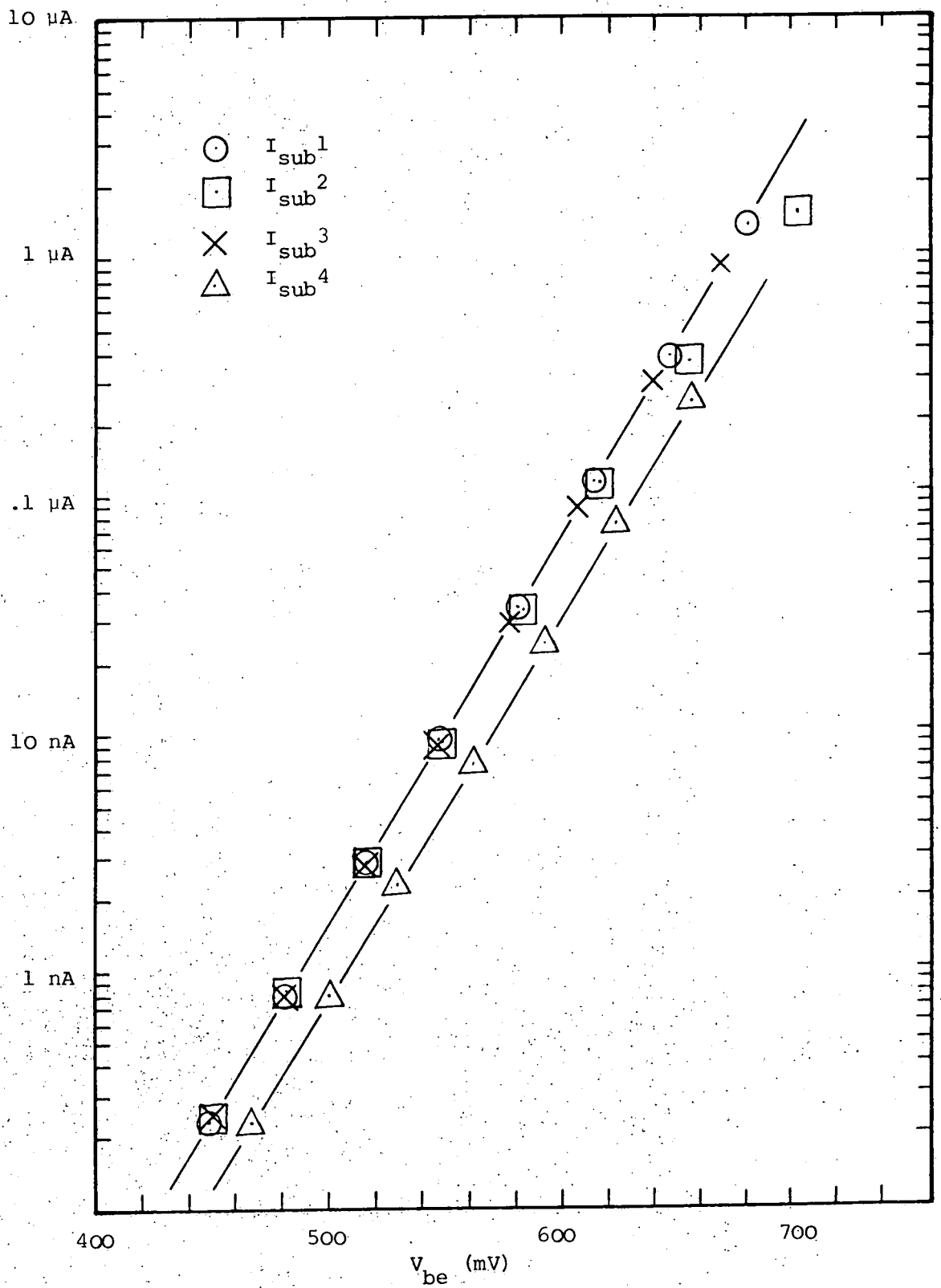
Fig 8.11   Typical plot of the substrate currents against base emitter
           voltage.

current measurements that make up the calculation of the band gap narrowing. For this reason only one set of cells was measured in detail although all the available sets were tested to ensure that the set chosen was representative of the whole. Measurement of a larger sample of devices would be very tedious without automation.

8.3.2   <u>Averaging currents.</u>

From section 8.2.2 it is clear that the measurement of the currents is critical to the estimation of J_{pv} and thus by Eq. 821.14 to the band gap narrowing. In order to improve this measurement, averaging of the various currents is performed for all temperatures used. In this way the change in the band gap is calculated from an average over the eleven different temperatures. This however poses several problems since as defined by for example Eq. 821.08 the current densities depend upon temperature (D_b, n_{ie}, G_b, W_b and L_b) and applied voltage (from voltage dependence of depletion widths G_b, W_b) dependent parameters. Hence in future measurements it would be advisable to make independent measurements of at least the diffusion coefficient (mobility) over the whole range of temperature. In the present work however the temperature measurements are used to obtain a best fit for the currents at a temperature of 300 K. The temperature dependence of the mobility (or diffusion coefficients) is then an indirect result of the measurements and is compared with published values to support the accuracy of the principle measurement, that of the band gap narrowing.

Averaging the currents is performed by considering a simple expressions for the terminal currents (see for example Eq. 821.08) with ideality factor m of the form given in Eq. 832.01.

$$I = \frac{q \, A_j \, D \, n_i^2}{G} \, \exp(qV_{be}/mkT) + I_{sat}$$

$$= I_o \, \exp(qV_{be}/mkT) + I_{sat} \qquad (832.01)$$

Where A_j is the appropriate junction area, D the minority carrier diffusion coefficient and G the Gummel number for the base region and I_{sat} is small (< 0.1 nA for the substrate current). From section 8.2.6 it is clear that G, and to a lesser extent A_j depend upon the applied voltage V_{be} (Table 8.4). A_j, D, n_i and G all have temperature dependences. Thus we might expect Eq. 832.01 to reduce to an expression of the form

$$I = A \, v^\nu \, T^{(3+n)} \, \exp(-E_g/kT) \, \exp(qV/mkT) \qquad (832.02)$$

where A, ν, n and m are constants. In the following sections it is hoped to measure these constants for each of the terminal currents using least squares fits to average the input data. Unfortunately in the absence of any direct measurement of the voltage dependence of G (and A_j) and with only two variables (V and T) this appears to be an insurmountable problem. We consider in what follows a functional form of

$$I = A \, T^{(3+n)} \, \exp(-E_g/kT) \, \exp(qV/mkT) \qquad (832.03)$$

Where the Voltage dependence of G and A_j will modify the value of m slightly (m $\approx$ 1.003 rather than m = 1). Two plots were considered that together obtain the best values for A, n and m. First a plot of

$$\log_{10}(I_o) - 3 \log_{10}(T) + E_g/kT \, \log_{10}(e) \qquad (832.04)$$

against $\log_{10}(T)$ is used to obtain values for A and n. This plot (see for example Fig 8.13, 8.15, 8.16) however suffers from the disadvantage of having only a small range of temperatures from which to extrapolate

($\log_{10}(T)$ varies from 2.32 to 2.57) the constants. The second plot is of

$$\log_{10}(I(V=V_{mean})) - (3+n)\log_{10}(T) + E_g/kT\log_{10}(e) \qquad (832.05a)$$

where V_{mean} is the mean value of V_{be}'s from the measurements for that temperature (used in section 8.2.6) against

$$qV_{mean}/kT \ \log_{10}(e) \qquad (832.05b)$$

This plot (see for example Fig 8.14, 8.17) gives a much more accurate extrapolation of A since the latter varies over a larger range than the previous $\log(T)$ plot (typically 5 to 16). This improved value of A is then used with a convenient average value from the first plot (at $\log(T) = 2.5$) to give an improved value for n.

$$n = \frac{(av \ ordinate \ at \ \log(T) = 2.5)}{2.5} - \frac{A}{2.5} \qquad (832.06)$$

This alters the plot defined by Eq. 832.05 which is then repeated. Thus by iteration best fit values for the constants A, n, and m in Eq. 832.03 are obtained.

By choosing a different value for the potential (V_{mean}) at each temperature the p+ epitaxial depletion width is held constant (Table 8.5 in section 8.2.6) so that the lateral and vertical base areas remain the same throughout the temperature range. Any temperature dependence detected (T^n) will then be a result of the temperature dependence of the diffusion coefficient D and to a lesser extent the effective masses used in the calculation of the intrinsic carrier concentration. This latter temperature dependence which may be as much as $T^{.44}$ (from the data of Jaeger et al 1980) is ignored assigning n to the temperature dependence of the diffusion coefficient

$$D = D_o \, T^n \qquad\qquad\qquad (832.07)$$

Having evaluated the temperature dependence of the diffusion coefficient (and by virtue of the Einstein relationship the mobility) the Gummel number (G) may be evaluated from Eq. 832.01 and Eq. 832.03

$$G \approx \frac{q \, A_j \, D_o \, n_{io}^{\,2}}{A} \qquad\qquad\qquad (832.08)$$

where the intrinsic carrier concentration is given by (section 8.2.5)

$$n_i^{\,2} = n_{io} \, T^3 \, \exp(-E_g/kT) = 4.9161.10^{31} \, T^3 \, \exp(-E_g/kT)$$

8.4   EXPERIMENTAL RESULTS.

The theoretical expressions used to analyse the experimental data have been outlined in section 8.2. In section 8.3 the basic experimental technique has been detailed. In this section the measurements of junction area (8.4.1), and temperature (8.4.2) complete the information required to analyse the 11 sets of current voltage measurements made on the four Integrated Injection Logic cells detailed in Fig 8.5. To test the validity of the depletion layer calculations in section 8.2.6 the Gummel numbers for the super β base ($G_\beta = 1.204.10^{12}$ cm^{-2}, section 8.4.2) and lateral pnp transistor ($G_l = 2.2 \pm 0.4.10^{12}$ cm^{-2}, section 8.4.3) are measured. These compare within a few percent with the theoretical values of $1.16.10^{12}$ (Table 8.7) and $2.23.10^{12}$ (Table 7.5) calculated in section 8.2.6. The temperature dependence of mobility is also measured for the two base regions.

In section 8.4.4 the substrate current is averaged by a method

similar to that detailed in section 8.3 thus, using the junction area A_b, the substrate current density J_{ps} is measured. However due to the recombination in the buried layer the expression used for the substrate current (Eq. 821.08) involves a term in W_b/L_b that introduces an additional temperature dependence. The difference currents (I_d) are analysed to provide values for the current density J_{pv} at each of the temperatures following the procedure set out in section 8.2.2. These current densities are used to evaluate the temperature dependence of the transport factor (Eq. 821.12). Thus the temperature dependence of the factor in W_b/L_b is measured (Fig 8.18) and the minority carrier mobility $(N_d = 2.4.10^{19}, \mu_p = 58 \ T^0 \ cm^2/Vs)$ in the heavily doped buried layer may be extracted from the least squares fit substrate current data. The minority carrier lifetime in the heavily doped region may also be calculated (Eq. 821.15) and is found to be 30 ± 10 ns. Finally in section 8.4.5 the preceeding data is used in the expression for the band gap narrowing (Eq. 821.14) to obtain a value for the band gap reduction in the buried layer of 100 ± 15 meV.

8.4.1   Area measurements.

Measurements of the junction areas were made through a shearing microscope on the fabricated devices. These were supplemented by measurements made from the mask set and from photographs of the devices with and without the metalization removed. The above areas were then adjusted for sideways solid state diffusion by adding on 2/3 of the junction depth (Fig 8.6) to the horizontal dimensions. Corrections for the depletion layer widths calculated in section 8.2.6 were made resulting in the following junction areas:

Table 8.8

Junction areas.

Cell	Area in μm^2					
	A_{o-}	A_{o+}	A_c	A_{β}	A_{col}	A_l
1	464.87	1384.29	89.71	1938.87	0.0	20.47
2	148.05	1384.29	89.71	1938.87	288.9	20.47
3	0.0	1849.16	89.71	1938.87	0.0	20.47
4	0.0	526.88	264.69	791.56	0.0	61.40

8.4.2   Temperature measurement.

The collector current is determined mainly from parameters in the lightly doped super β base. As such it is taken to be independent of heavy doping effects. Using simple theory (Sze 1980, Hart 1981) the collector current may be described by an expression of the form

$$I_{col} = \frac{q \, A_{col} \, D_n \, n_i^2}{G_{\beta}} \exp(qV_{be}/kT) + I_{colsat} \qquad (842.01)$$

With Gummel number $G_{\beta} = \int N_a(x) \, dx$

Using the first averaging plot detailed in Eq. 832.04 an estimate may be made of the temperature dependence of the mobility in the super β base using the temperature calculated from the slope of the current voltage plots (for example Fig 8.9, assuming an ideality factor m=1 in the usual way). This graph is presented in Fig 8.12. When these first estimates to the temperature are used they produce a systematic scatter on the later results. This can be avoided by using the line of regression (x on y) shown (A=0.97, n= − 1.32) to predict the best fit value of the
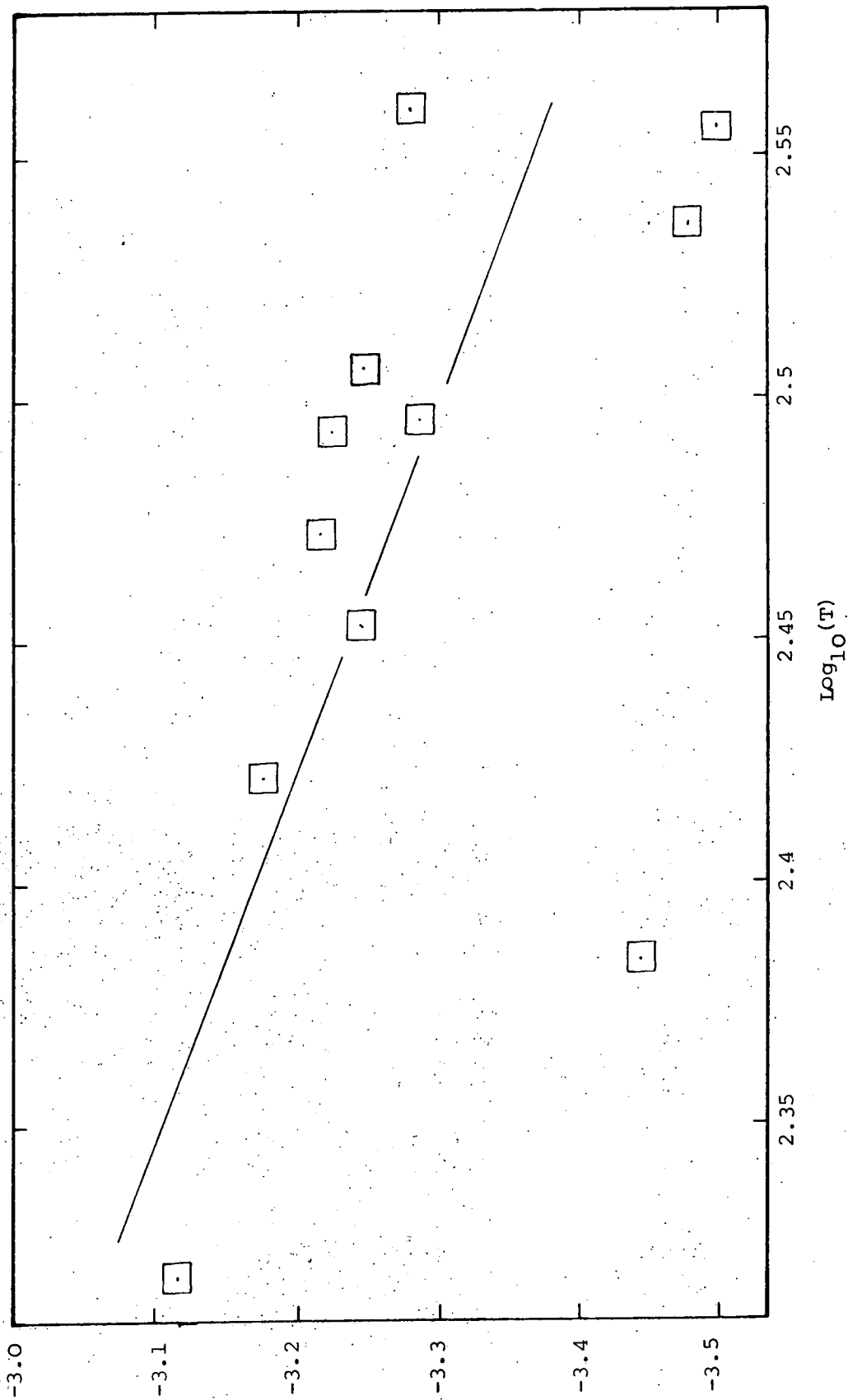
Fig 8.12   Collector saturation current plot (Eq. 832.04).

$$\log_{10}(I_{co}) = 3 \log_{10}(T) + E_g/kT \log_{10}(e)$$

intercept parameter I_{co} for a given temperature

$$I_{co} = A \; T^n \; \exp(-E_g/kT) \qquad\qquad (842.02)$$

Hence using values for the collector current at the voltage V_{mean} the optimum slope of the current voltage plots may be calculated and a more accurate value for the temperature may be determined. These results for the temperature before optimization and after are presented in Table 8.9.

The temperature dependence of the diffusion coefficient is now found from the values of A and n above using Eq. 832.07 and values from section 8.2.4

$$D_n = D_{no} \; T^n = 51565.4 \; T^{-1.3156} = kT/q \; \mu_n \qquad (842.03)$$

This results in a temperature dependence for the mobility of $T^{-2.32}$ that compares favourably with those quoted in Sze (1981) -2.42 and Wolf (1969)

Table 8.9

Temperature from the collector current (K)

from IV curves	Improved temperature	E_g (eV)
363.0	365.96	1.1031
359.5	355.88	1.1059
343.5	339.85	1.1103
321.0	322.81	1.1149
312.8	313.04	1.1175
311.3	312.75	1.1176
296.2	297.40	1.1216
283.6	283.51	1.1252
264.1	264.59	1.1300
242.6	236.67	1.1368
208.2	207.32	1.1436

The collector area (A_{col}) given in Table 8.8 is 288.9 μm^2 which substituted into Eq. 832.08 gives $G_\beta = 1.204.10^{12}$. This is very close to the the value calculated in section 8.2.6 from the integral of the super β

base of $1.16 \pm 0.04.10^{12}$ cm^{-2}. This indicates that the temperature measurements quoted in Table 8.9 have been succesfull.

8.4.3 G_1 and temperature dependence of μ in the lateral transistor.

Another measure of the success of the experimental measurements is found in a comparison of the injector current with its theoretical value. The injector current is also essentially a collector current and from simple theory provided the injector is held at the same potential as the epitaxial layer it may be described by an expression similar to Eq. 842.01

$$I_{inj} = \frac{q\ A_1\ D_n\ n_i^2}{G_1} \exp(qV_{be}/kT) + I_{injsat} \qquad (843.01)$$

With Gummel number $G_1 = \int N_d(x)\ dx$

However where in the case of the previous collector current the base epitaxial depletion width is very small due to the similarity of impurity concentrations in that junction (section 8.2.6), in the injector the p+ epitaxial junctions have much larger depletion widths due to the contrast in impurity concentration. Consequent the voltage dependence of the lateral Gummel number is expected to be more pronounced (see Table 8.4). This is reflected in an apparently non – unity ideality factor in the injector current (see discussion after Eq. 832.03). From the change in Gummel number shown in Table 8.4 the apparent ideality factor would be about 0.3% greater than unity (ie m $\approx$ 1.003). The effect of the temperature and voltage dependence of the depletion widths shown in Table 8.4 are reduced by using the injector current at the voltages V_{mean}. The calculated Gummel number with these voltages varies by only a few percent with increase in temperature (Table 8.5).

The method outlined in section 8.3.2 for averaging the values
for the constants A, n and m in Eq 832.03 applied to 843.01 is adopted.
The first plots defined by Eq. 832.04 is shown in Fig 8.13. As expected
from the increased voltage dependence of the lateral Gummel number, and
hence inaccurate values for the ideality factor, the intercept plot has a
greater scatter than in the Fig 8.12 for the collector current. Indeed the
four lowest temperature intercepts for cell 4 consistently over estimate
the intercept. These values were ignored when taking the average of the
cell 4 data since they appear to represent a systematic error in the
measurements. Intercepts from the remaining cells lie close to one another
and result in three lines of regression (x on y) that almost coincide.

The second plot defined by Eq. 832.05 is presented in Fig 8.14.
It is clear that this second figure gives more accurate values for the
intercept than the first, because of the increased range of the abscissa.
In Table 8.10 the values of A, n and m from the two plots are presented.

Table 8.10

Best fit parameters for the injector current.

| cell | A | | n | | m | G_i (cm^{-2}) |
	Fig 13	Fig 14	Fig 13	Fig 14	Fig 14	Fig 14
1	7.35	0.9697	−2.3762	−2.0242	1.0118	$2.08 \cdot 10^{12}$
2	23.68	0.2468	−2.5425	−1.7497	1.0065	$1.71 \cdot 10^{12}$
3	68.67	0.7157	−2.7241	−1.9313	1.0074	$1.66 \cdot 10^{12}$
4	5.81	2.2202	−2.1162	−1.9490	1.0087	$1.78 \cdot 10^{12}$

From Eq. 832.07 the temperature dependence of the diffusion coefficient may
be measured and hence by the Einstein relationship (Eq. 823.01) the
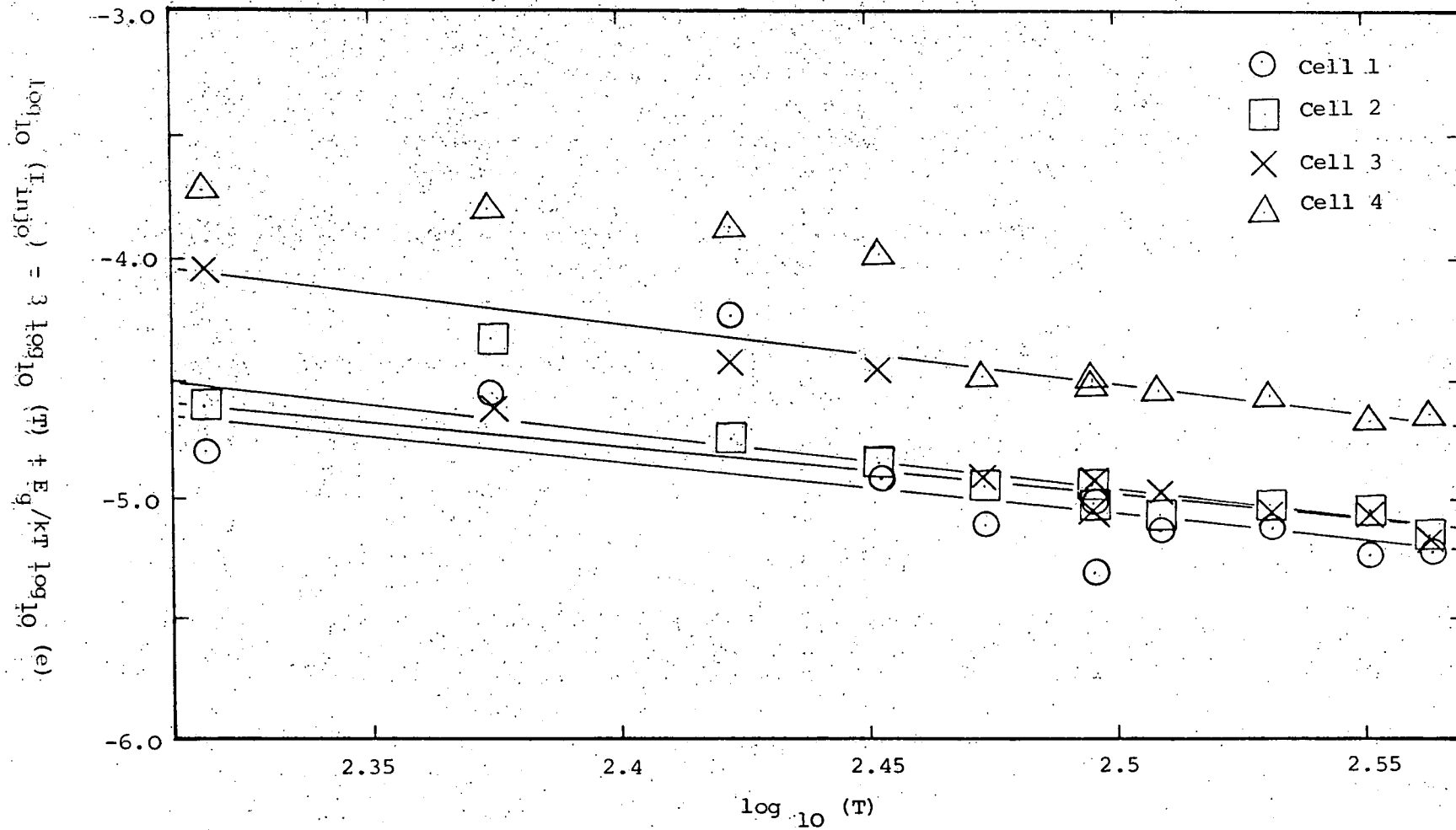
Fig 8.13 · Injector saturation current plot (Eq. 832.04).
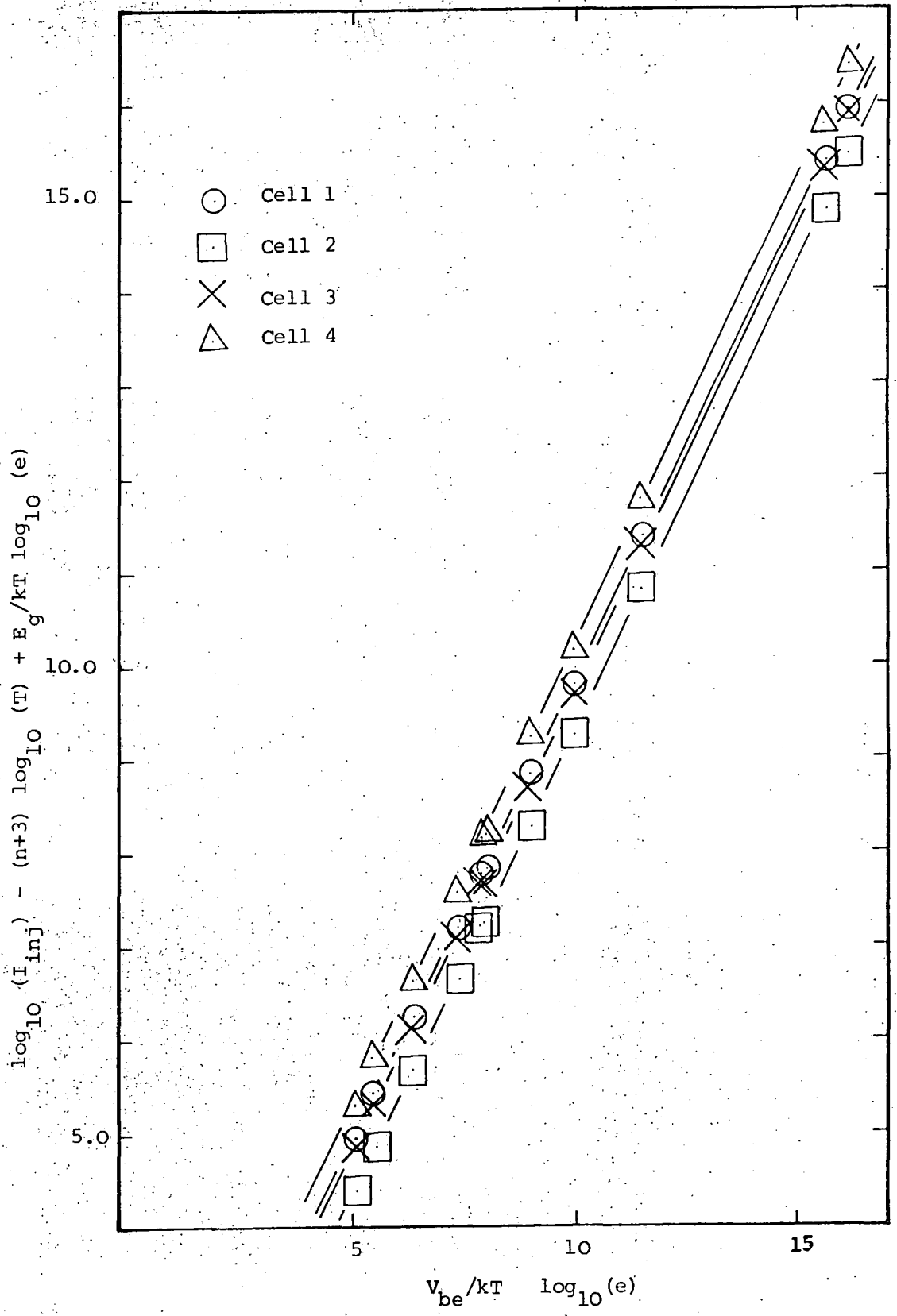
Fig 8.14   Injector current intercept plot (Eq. 832.05)

mobility. Using Eq. 823.02 and Table 8.3 ($N_d = 4.7.10^{16}$ cm^{-3})

$$\mu_n = 1.53.10^{10} \ T^{-2.9} \ cm^2/Vs \qquad\qquad (843.02)$$

This temperature dependence of $T^{-2.9}$ for the mobility is rather steeper than those quoted in the literature (eg Sze $T^{-2.2}$). Whilst the Gummel number calculated from Eq. 832.08 is given in Table 8.10. The theoretical Gummel number from Table 8.5 derived from the integral of the base concentration is $2.2.10^{12}$ cm^{-2} that agrees well with those shown in Table 8.10.

8.4.4 <u>Temperature dependent mobility in the heavily doped buried layer.</u>

In order to calculate the band gap narrowing the substrate and difference data also need averaging. The same technique introduced in section 8.3.2 is used with the exception that the intrinsic carrier concentration n_i is replaced by the effective intrinsic carrier concentration introduced in Eq. 825.05. This requires a first approximation to the band gap narrowing, that will later be improved. For the substrate current the temperature dependence of the W_b/L_b factor in Eq. 821.08 has also to be considered.

Given an estimate for the band gap narrowing (ΔE_g) the substrate current (Eq. 825.05) at the voltages V_{mean} is best fitted to an expression of the form.

$$I_{sub} = A \ T^{(3+n)} \ \exp(-(E_g - \Delta E_g)/kT) \ \exp(V_{be}/kT) \qquad (844.01)$$

The first plot (Eq. 832.04) is adapted by including the estimated band gap narrowing of 100 meV and are given in Fig 8.15 for the four cells. Except at low temperatures, where the substrate current is particularly small and
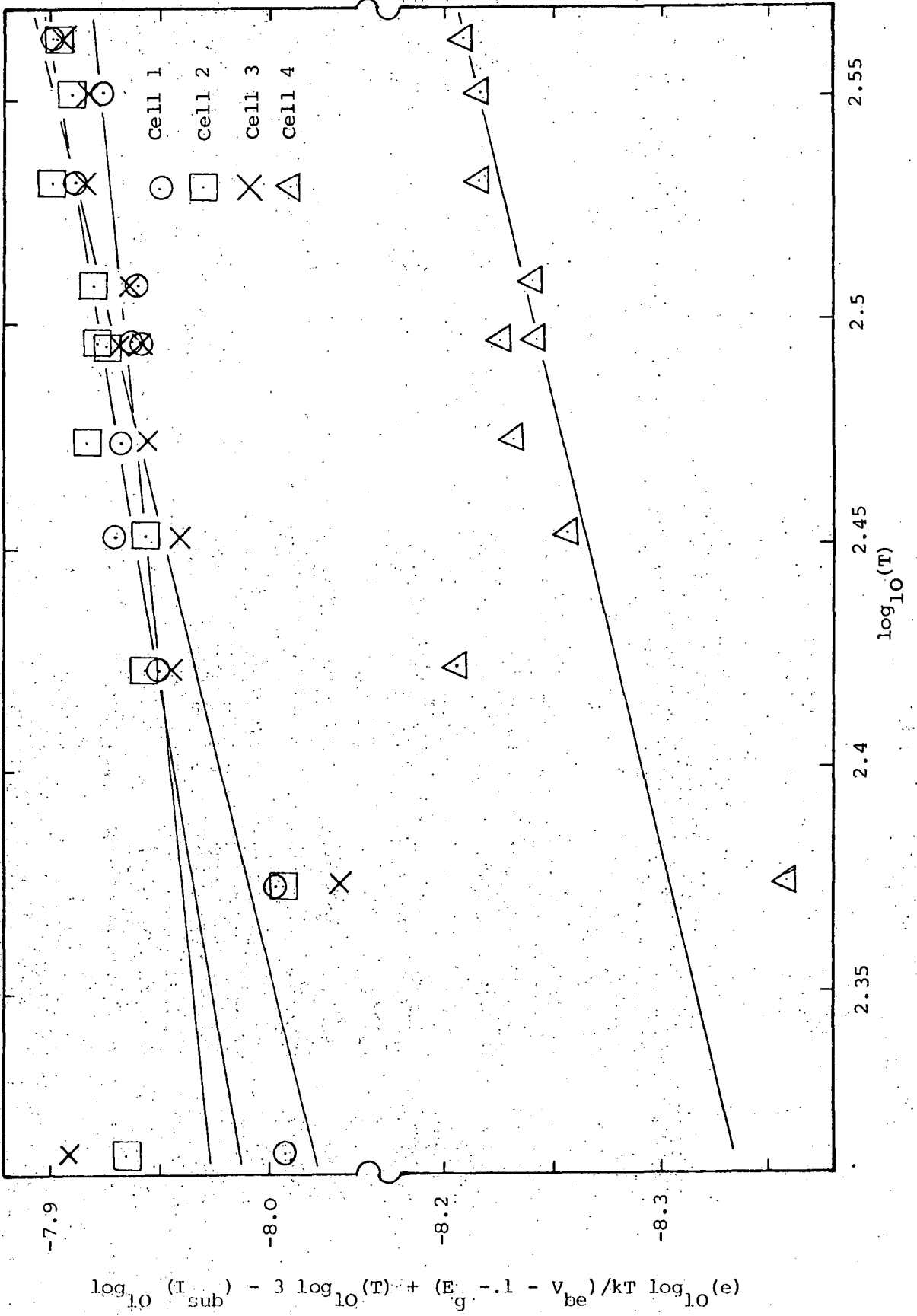
Fig 8.15   Substrate saturation current plot (Eq. 844.01)

$\log_{10}(I_{sub}) - 3 \log_{10}(T) + (E_g - .1 - V_{be})/kT \log_{10}(e)$

difficult to measure, the intercepts lie on good straight lines. The least squares fits for these points reveal the data for A and n (Eq. 844.01) given in Table 8.11 for a value of ΔE_g of 100 meV. However the W_b/L_b parameter in Eq. 821.08 is still needed before these parameters (A, n) may be analysed for this the difference current has to be analysed.

Table 8.11

Substrate current best fit parameters ΔE_g = 100meV

cell	A	n
1	$3.22.10^{-10}$	0.6237
2	$1.58.10^{-9}$	0.3508
3	$3.36.10^{-9}$	0.2160
4	$2.53.10^{-10}$	0.5450

The difference currents I_d were calculated at each value of I_b chosen (the alternative approach is to use the least squares data from the base and injector currents). Thus a graph similar to those in Fig 8.8 – Fig 8.12 could have been drawn up showing each measured difference current. In this way errors introduced by averaging the injector and base current data are avoided. The difference current data is then averaged following the procedure outlined in section 8.3.2. Fitting the data to expressions of the form

$$I_d = A \, T^{(3+n)} \, \exp(-(E_g - \Delta E_g)/kT) \, \exp(V_{be}/mkT) \qquad (844.02)$$

The inclusion (or exclusion) of the ΔE_g in this expression is not strictly valid since I_d is made up the sum of four different current density contributions (see section 8.2.2). Its presence (or absence) merely adjusts the value of n obtained in the temperature range considered. Fig 8.16 shows the saturation plot for this current (Eq. 832.04, with ΔE_g = 100 meV) and the best fit parameters obtained from the second plot (Eq. 832.05) shown in Fig 8.17 are presented in Table 8.12.
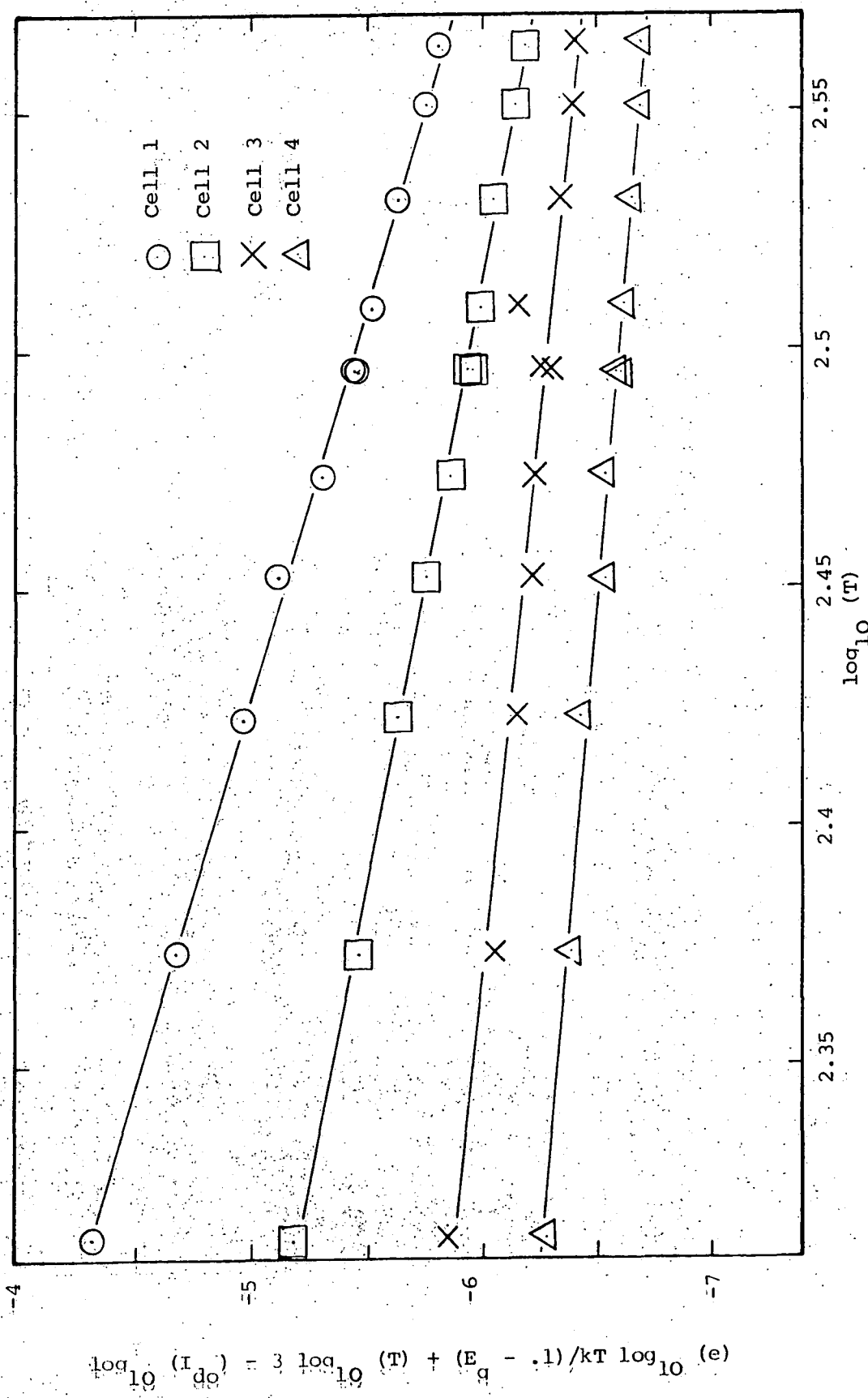
Fig 8.16   Difference current saturation plot (Eq. 832.04).

$$\log_{10} (I_{do}) = 3 \log_{10} (T) + (E_g - .1)/kT \log_{10} (e)$$
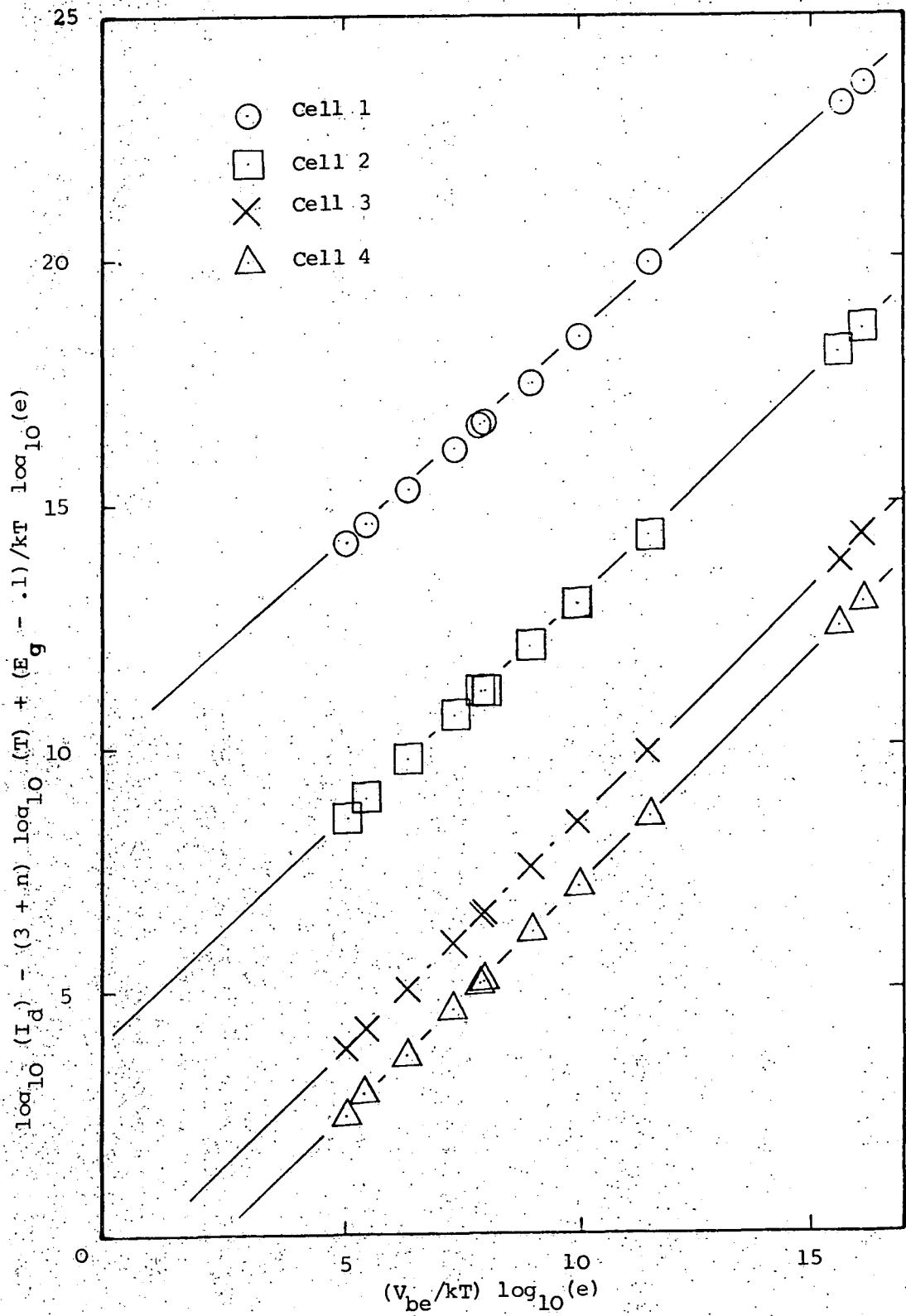
Fig 8.17   Difference current intercept plot (Eq. 832.05)

Table 8.12

Best fit parameters for difference currents I_d

A	n	m
$8.077.10^9$	−6.1380	1.17396
$1.058.10^4$	−3.9885	1.11124
$1.242.10^{-1}$	−2.1535	1.05990
$5.352.10^{-3}$	−1.7292	1.05995

The best fit difference data presented in Table 8.12 are then processed (see section 8.2.2) using the areas given in Table 8.8 to calculate the values of J_{pv} that are presented in Table 8.13 under the heading J_{pv}(a). The unaveraged difference data was also processed to give values presented as J_{pv}(b).

Table 8.13

J_{pv} calculated from best fit (a) and raw (b) difference data

temp (K)	applied voltage (mV)	J_{pv}(a) (Acm^{-2})	J_{pv}(b) (Acm^{-2})
365.96	364.5	$2.644.10^{-4}$	$2.103.10^{-4}$
355.88	389.0	$2.723.10^{-4}$	$3.224.10^{-4}$
339.85	427.5	$2.773.10^{-4}$	$4.844.10^{-4}$
322.81	468.5	$2.922.10^{-4}$	$3.291.10^{-4}$
313.04	491.0	$2.892.10^{-4}$	$4.272.10^{-4}$
312.75	492.0	$2.921.10^{-4}$	$1.777.10^{-4}$
297.40	528.5	$2.969.10^{-4}$	$1.841.10^{-4}$
283.51	559.0	$2.743.10^{-4}$	$-1.338.10^{-4}$
264.59	603.5	$2.651.10^{-4}$	$3.883.10^{-4}$
236.67	734.0	$-8.859.10^{-4}$	$-1.685.10^{-4}$
207.32	665.0	$6.499.10^{-6}$	$1.293.10^{-4}$

Considering the first set of values, the negative value at T=237K corresponds exactly to the one collector current intercept that did not fall close to the average in Fig 8.12 (− 3.44, log(T) = 2.385) and for which a large correction to T is made (242K to 237K). The last three measurements suffer from poor choice of V_{mean} as shown by Table 8.5 where

the calculated Gummel number is significantly different from the previous values. These values may then be ignored due to errors arising from inaccuracy in the temperature and poor averaging. The second set of J_{pv} data illustrates the sensitivity of J_{pv} to the difference data input and gives an order of magnitude illustration of the errors in the measurement that range from a factor of 2 larger than the averaged value at T=340K to 1.6 smaller at T=312.75. This large error in J_{pv} does not however effect the calculation of ΔE_g significantly, because of the relative sizes of the components that make up Eq. 821.11.

Values for the transport factor and hence values for W/L and the lifetime may be calculated (Eq. 821.12 to 821.13) from either of the values of J_{pv} given in Table 8.13, and the values of I_{sub} (Table 8.11 and Eq. 844.01). These are given in Table 8.14 and show consistent values for minority carrier lifetime of (30 ± 10) ns in agreement with those published in Hart (1981 pp 97) for a concentration of $2.4.10^{19}$.

Table 8.14a

W/L and lifetime (τ) data calculated with
data from the four substrate currents

temp (K)	applied voltage (mV)	W/L from best fit data				τ (nsec)			
		1	2	3	4	1	2	3	4
365.96	364.5	2.3	2.3	2.3	2.1	17	17	17	21
355.88	389.0	2.3	2.3	2.3	2.1	18	18	18	22
339.85	427.5	2.3	2.3	2.3	2.1	19	20	19	23
322.81	468.5	2.2	2.2	2.2	2.0	21	22	21	26
313.04	491.0	2.2	2.2	2.2	2.0	23	23	23	28
312.75	492.0	2.2	2.2	2.2	2.0	23	23	23	28
297.40	528.5	2.1	2.1	2.1	1.9	26	27	26	32
283.51	559.0	2.1	2.0	2.0	1.9	29	31	30	36
264.59	603.5	1.9	1.8	1.8	1.7	38	40	40	48
236.67	734.0								
207.32	665.0	1.5	1.4	1.3	1.3	80	94	97	113

Table 8.14b

W/L and lifetime (τ) data calculated with
data from the four substrate currents

temp (K)	applied voltage (mV)	W/L from raw data				τ (nsec)			
		1	2	3	4	1	2	3	4
365.96	364.5	2.0	2.1	2.1	1.8	24	24	23	29
355.88	389.0	2.4	2.5	2.5	2.3	17	17	17	20
339.85	427.5	2.8	2.8	2.9	2.6	13	13	13	15
322.81	468.5	2.3	2.3	2.4	2.1	20	20	20	24
313.04	491.0	2.6	2.6	2.6	2.4	17	17	17	20
312.75	492.0	1.7	1.7	1.7	1.5	40	41	40	53
297.40	528.5	1.6	1.6	1.6	1.4	44	46	45	59
283.51	559.0								
264.59	603.5	2.3	2.2	2.2	2.1	24	26	25	30
236.67	734.0								
207.32	665.0	2.3	2.1	2.1	2.0	30	33	33	37

Finally the logarithm of the parameter in Eq. 821.08 for the
substrate current

$$\frac{W_b}{L_b \, sinh(W_b/L_b)}$$

(844.03)

is plotted against log(T) in Fig 8.18. Least squares fits were performed
on these data, from which the temperature dependences of the parameter for
the four cells ($T^{-0.1}$, $T^{-0.3}$, $T^{-0.4}$ and $T^{-0.2}$) are calculated. Using these
values and the n and A values from Table 8.11 the temperature dependent
diffusion coefficient may be calculated and is presented in Table 8.15.
The raw data also is used to determine a similar plot to that in Fig 8.18
deriving a second set of data (b) also presented in this table.

Clearly the error introduced by the sensitivity of J_{pv} to the
difference currents results in inaccuracies in the temperature dependence
of the mobility. However from the data in Table 8.15 we might reasonably
expect zero temperature dependence for the mobility. Slotboom et al (1976)
in their work on the band gap narrowing also found that the mobility of
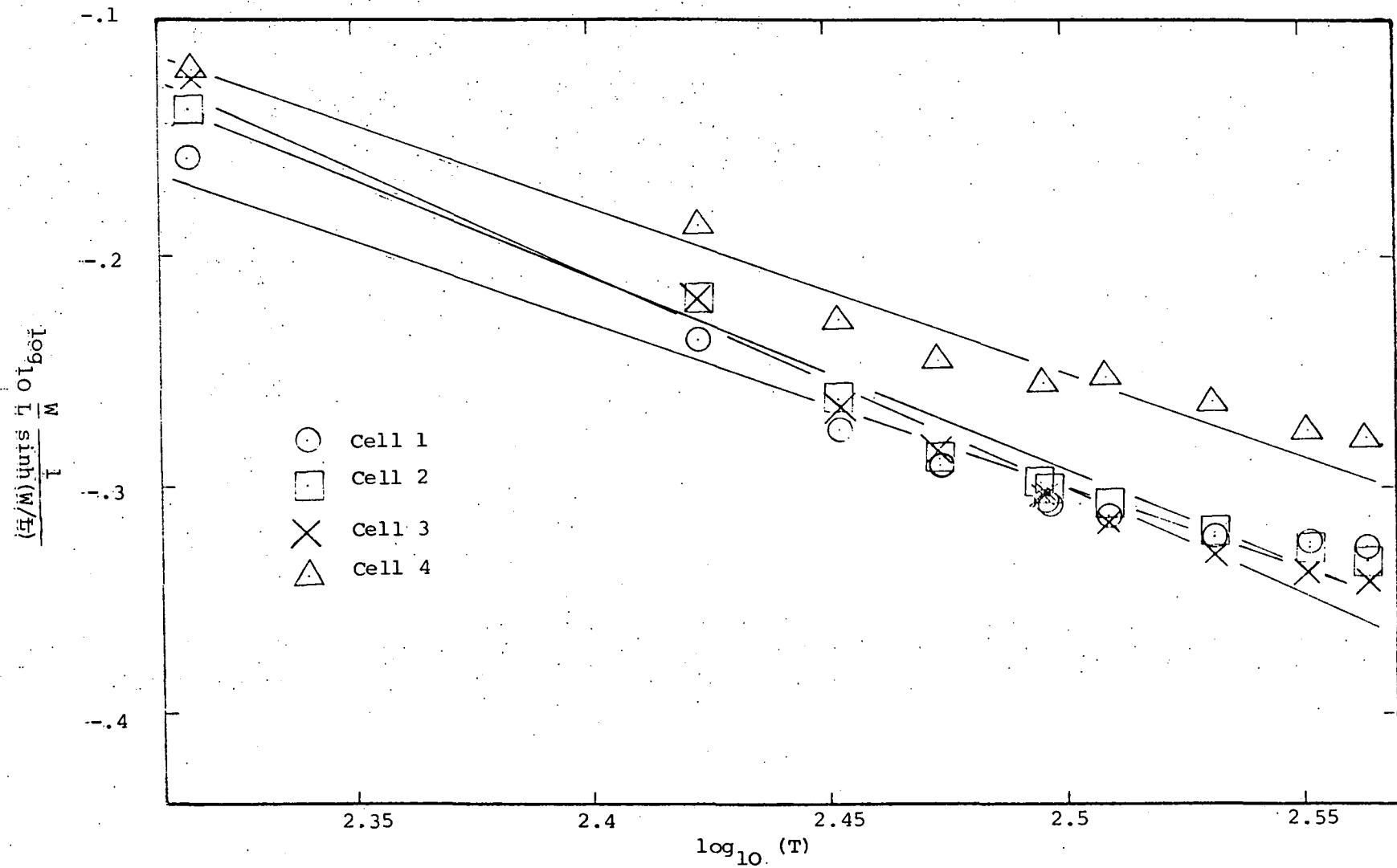
Fig 8.18   Plot of $\log_{10}$ (W/Lsinh(W/L)) against $\log_{10}$ (T).

holes in heavily doped silicon was constant with temperature.

<div align="center">

Table 8.15

Mobility data ($\mu_p = \mu_{p0} T^n$ cm^2/Vs) for the n+

buried layer from best fit (a) and raw (b) data

</div>

cell	μ_{p0}(a)	n	μ_{p0}(b)	n
1	8.6	0.336	202	-0.217
2	19	0.198	388	-0.331
3	27	0.137	530	-0.386
4	14	0.256	254	-0.257

8.4.5   <u>Measurement of band gap narrowing.</u>

Having now determined the values and temperature dependence of all the components making up Eq 821.14 a new value for the band gap narrowing may be calculated. This will of course adjust the temperature dependences calculated in the previous section so to be thorough the calculation must be iterative. However with the data presented in the previous sections the band gap narrowing for 300K may be calculated.

The substrate current density at 300 K may be evaluated from Fig 8.15 so that the natural logarithm of J_{pso} is given by

$$\log_e(J_{pso}) = Y \log_e(10) - \log_e(A_b)$$

$$+ 3 \log_e(T) - \frac{(E_g - 0.1)}{kT} \qquad (845.01)$$

where Y is the ordinate taken Fig 8.15 at X = $\log_{10}(300)$. This varies from − 29.77 for cells 1,2 and 3, to − 29.57 for cell 4. The remaining measured parameter, that of the function in W/L, may be calculated from Fig 8.18

$$\log_e\left(\frac{W_b}{L_b \sinh\left(\frac{W_b}{L_b}\right)} W_b\right) = - 0.58 \pm 0.1 \qquad (T=300K) \qquad (845.02)$$

It is clear that this latter parameter has a small influence upon the

<div align="center">

= 8.37 =

</div>

eventual band gap narrowing result. The Gummel number for the heavily doped buried layer is taken directly from the fabrication details for the buried layer. This ion implantation was an Arsenic implant of 10^{16} atoms cm^{-2} at 25KeV. Supposing all the ions implanted to be electrically active this gives a Gummel number of 10^{16} cm^{-2}. Using the mobility data from Table 8.3 the hole diffusion coefficient for an average concentration for the buried layer ($G_b/W_b = 2.4 \pm 1.0.10^{19}$ cm^{-3}) is 1.53 $cm^2 sec^{-1}$. Finally the electronic charge ($q = 1.6.10^{-19}$ C) and intrinsic carrier concentration ($n_i = (1.45 \pm 0.05) 10^{10}$ cm^{-3}) complete the necessary data. Using these values in Eq. 821.14 the band gap narrowing becomes

$$\Delta E_g = 25.89 \ (32.9-29.67+0.58) = (99.6 \pm 15.) \ meV \quad (845.03)$$

The major error in the above figure for the band gap narrowing for heavily doped ($2.4.10^{19}$ cm^{-3}) n-type silicon arises from the uncertainty in the concentration to which this band gap narrowing should be ascribed. The buried layer (Fig 8.3) is seen to have a peak concentration of 7.10^{19} cm^{-3}. Considering the theoretical calculations of the band gap narrowing (Fig 7.12), the band gap narrowing at this donor concentration is of the order of 50 meV greater than at 2.10^{19} cm^{-3}.

The error due to the use of Maxwell Boltzmann rather than Fermi Dirac statistics throughout the analysis expressed in the form of Eq 825.06 amounts to an error of

$$- kT \ log_e (1 + 0.27 \ exp((E_F - E_c)/kT)) \quad (845.04)$$

which since the Fermi level is almost at the same energy as the conduction band (Fig 7.3) at 300K and 2.10^{19} cm^{-3} is only 6 meV.

8.5 CONCLUSION

To summarize the measurements made in this chapter the theoretical (Tables 8.5, 8.7) and experimentally measured (Table 8.10, section 8.4.2) Gummel numbers for the sensitive lateral base region are within 18%, whilst the more stable super β base measurements are within 3% of the theoretical value. The more accurate result is due to maintaining the collector depletion width by holding the collector base voltage at zero, whilst the inaccuracy of the lateral Gummel number is due to the voltage dependent (Table 8.4) variation of the depletion width on p^+ base implant shown in Fig 8.4.

The temperature dependences of the minority carrier mobility in lateral ($N_d = 4.7.10^{16}$ cm^{-3}, $\mu_p = 6.88.10^9$ T$^{-2.9}$ cm^2/Vs), super β ($N_a = 2.5$ 10^{16} cm^{-3}, $\mu_n = 6.30.10^8$ T$^{-2.32}$ cm^2/Vs) and heavily doped buried layer ($N_d = 2.4.10^{19}$ cm^{-3}, $\mu_p = 58.7$ T^0 cm^2/Vs) compare well with values quoted else where of T$^{-2.5}$, T$^{-2.7}$ (Sze 1980) and T^0 (Mertens 1980) respectively.

Measurement of the transport factor through the buried layer with the devices chosen was difficult because of the large error in calculated values of J_{pv} (Table 8.1, 8.2) caused by poor choice of cell shapes. However these measurements resulted in a minority carrier lifetime in the buried layer ($N_d = 2.4.10^{19}$ cm^{-3}) of (30 ± 10) ns in agreement with published values (Hart 1981 pp 97). The band gap narrowing measured in this buried layer is (100 ± 15) meV. This measurement is mainly affected by the non-uniformity of the buried layer through which the band gap narrowing varies from 0 to perhaps as much as 140 meV at the peak donor concentration of 7.10^{19} cm^{-3}. This error could be overcome in future measurements by using a more detailed Gummel calculation which included band gap narrowing considerations (Eq. 821.09). The error in the

measurement of J_{pv} could also easily be improved by a different choice of geometries for the cells (section 8.2.2) and would then provide further check on the band gap narrowing (Eq. 821.14) that could equally be written in terms of J_{pvo} rather than J_{pso}.

SUMMARY AND CONCLUSIONS

9.0   SUMMARY AND CONCLUSIONS

Both experimental and theoretical results have been presented that support the claim that a physical band gap narrowing exists in the heavy doping region. The concentration at which this band gap narrowing starts depends upon the metal insulator transition characterised by the Mott critical density (N_c). At concentrations below this density the impurity band is well separated from the host band edge. However above this concentration the impurity band has merged with the host band. The concentration at which this blending of host and impurity band occurs varies with temperature $(4.10^{18}$ at 0 K, $2.2.10^{19}$ at 300 K) and type of impurity $(3.10^{18}$ (Sb), 7.10^{18} (As) Sernelius et al 1981). The electron-electron and electron-impurity calculations presented in this thesis assume that the bands have merged so the above concentration acts as a lower bound to the validity of these results.

In summary the change in the self energies $(\Delta\Sigma(k))$ of electron due to electron-electron (ee) and electron-impurity (ei) interactions have been calculated. This change in the self energy due to the presence of the extra carriers and impurities is interpreted as a shift in the dispersion curves for the conduction $(\Delta E_c(k))$ and valence $(\Delta E_v(k))$ bands. The concentration (N_d) dependent change in band edges due to these interactions has been calculated

$$\Delta E_g(N_d) = \Delta E_c(k_i) - \Delta E_v(0) = \Delta\Sigma_c(k_i) - \Delta\Sigma_v(0) \qquad (900.01)$$

$$= \Delta E_c^{ee}(k_i) + \Delta E_c^{ei}(k_i) - \Delta E_v^{ee}(0) - \Delta E_v^{ei}(0)$$

k_i is the wavevector of one of the six conduction band valley bottoms.

whilst the shift at k=0 describes the change in the valence band top.

Expressions for the self energy in silicon are derived in chapter 2. From this chapter the self energy of electron in the band n is given by (Eq. 223.19)

$$\hbar\Sigma^{ee}(n;k,\omega) = \frac{i}{(2\pi)^4} \sum_m \int \int G^0(m;k-q,\omega-\nu) \ e^{i\eta(\omega-\nu)}$$
$$\Lambda_{nm} \ W_{eff}(q,\nu) \ d^3q d\nu \qquad (900.02)$$

with $G^0(n;k,\omega)$ the unperturbed Green's function in the band (Eq. 240.01) and the screened interaction $W_{eff}(q,\omega)$ (Eq. 231.02) with the overlap integrals Λ_{nm} defined in Eq. 223.18. This first approximation to the self energy ignores the vertex corrections and uses the free particle propagator rather than the total Green's function.

The effective potential

$$W_{eff}(q,\omega) = e^2/\epsilon\epsilon_r q^2 \epsilon(q,\omega) \qquad (900.03)$$

is in this thesis modelled by the plasmon pole approximation to the electron dielectric function ($\epsilon(q,\omega)$). This is given by (Eq. 240.07c)

$$\epsilon^{-1}(q,\omega) = 1 - \left(\frac{\omega_p^2}{(\omega_1(q) - i\delta)^2 - \omega^2} \right) \qquad (900.04)$$

with dispersion relationship (Eq. 232.10), where a term in q^4 is included to give better large q agreement with the Lindhard function

$$\omega_1(q)^2 = \omega_p^2 + \omega_p^2 q^2/\kappa^2 + \epsilon_q^2/\hbar^2 \qquad (900.05)$$
$$= \omega_p^2 \left(1 + \frac{q^2}{\kappa^2} + \frac{3m_{op}}{4m_{de}} \frac{q^4}{k_f^2 \kappa^2} \right)$$

The real part of the self energy expression (Eq. 240.07a) describes the exchange energy of an electron in the band n. This is made up of several parts characterised by the summation over band index m. Thus

the self energy contribution to the conduction band is made up of exchange energies between electrons in the same band (Σ^{ee}_{cc}) and exchange between the electrons in the conduction band and the valence band (Σ^{ee}_{cv})

$$\Sigma^{ee}_{c} = \Sigma^{ee}_{cc} + \Sigma^{ee}_{cv} \qquad\qquad (900.06)$$

However as Inkson (1976) points out it is the change in the band energies that is of interest. This is derived from the difference between this self energy and that present in the intrinsic semiconductor (Σ^{int}_{n}). Thus the change in the conduction band energy is defined by (chapter 3)

$$\Delta\Sigma^{ee}_{c} = \Sigma^{ee}_{cc} + \Sigma^{ee}_{cv} - \Sigma^{int}_{cc} - \Sigma^{int}_{cv} = \Sigma^{ee}_{cc} = \Delta E^{ee}_{c} \qquad (900.07)$$

A similar expression may be derived for the valence band

$$\Delta\Sigma^{ee}_{v} = \Sigma^{ee}_{vc} + \Sigma^{ee}_{vv} - \Sigma^{int}_{vc} - \Sigma^{int}_{vv} = \Sigma^{ee}_{vv} - \Sigma^{int}_{vv} = \Delta E^{ee}_{v} \qquad (900.08)$$

However in this case the intrinsic valence band has a self energy since it is full of electrons in contrast to the intrinsic conduction band. This Hartree Fock energy must be subtracted from the valence band contribution.

In chapter 3 the shifts in the conduction and valence bands due to the change in screened electron-electron exchange energies (Eq. 300.02 and 300.03) are calculated. It is found that in the plasmon pole approximation these can be split up into coulomb hole and screened dynamic exchange contributions (named by Hedin 1965 in connection with electrons gases in metals see section 3.1)

$$\Delta E^{ee}_{c}(k) = \Delta E^{sx}_{c}(k) + \Delta E^{ch}_{c}(k)$$

$$\qquad\qquad\qquad\qquad\qquad\qquad (900.09)$$

$$\Delta E^{ee}_{v}(k) = \Delta E^{sx}_{v}(k) + \Delta E^{ch}_{v}(k)$$

The coulomb hole contributions (see Eq. 320.03 and 330.04)

$$\Delta E_c^{ch}(k) = + \frac{e^2}{2\pi^2 \epsilon \epsilon_r} \int_0^\infty \frac{\omega_p^2}{2\omega_1(q)} \frac{1}{(\omega_{ck}^0 - \omega_{c(k-q)}^0 - \omega_1(q))} dq$$

$$(900.10)$$

$$\Delta E_v^{ch}(k) = + \frac{e^2}{4\pi^2 \epsilon \epsilon_r} \sum_m \int_0^\infty \frac{\omega_p^2}{2\omega_1(q)} \frac{1}{(\omega_{vk}^0 - \omega_{m(k-q)}^0 - \omega_1(q))} dq$$

reduce the energies of both conduction and valence bands contributing a small increase (+10 meV at 10^{20} cm^{-3}) to the change in the band gap as predicted by Inkson 1976 (see Fig 3.5). The screened dynamic exchange contributions of each band (Eq. 320.03 and 330.04) however act in opposite directions, both to reduce the gap (Fig 3.4)

$$\Delta E_c^{sx}(k) = - \frac{e^2}{2\pi^2 \epsilon \epsilon_r} \int_0^{k_f} (1 - \frac{\omega_p^2}{\omega_1(q)^2 - (\omega_{ck}^0 - \omega_{c(k-q)}^0)^2}) dq$$

$$(900.11)$$

$$\Delta E_v^{sx}(k) = + \frac{e^2}{4\pi^2 \epsilon \epsilon_r} \sum_m \int_0^\infty (\frac{\omega_p^2}{\omega_1(q)^2 - (\omega_{vk}^0 - \omega_{m(k-q)}^0)^2}) dq$$

With appropriate choice of the energy difference in these expressions the change in the band energy at any value of k may be determined

$$\omega_{ck}^0 - \omega_{c(k-q)}^0 = - \omega_{cc}^0(k,q)$$

$$(900.12)$$

$$\omega_{vk}^0 - \omega_{v(k-q)}^0 = \omega_{vn}^0(k,q)$$

The sum of electron-electron contributions from the valence band (Fig 3.3) and the conduction band (Fig 3.2) is made in Fig 3.6 were the total electron-electron contribution to the band gap narrowing is shown. It can be seen that these results differ by only a few meV from the results of Berggren and Sernelius calculated with the Lindhard dielectric function (Fig 3.2 and 3.3). This agreement justified the use of the plasmon pole approximation in chapter 7 at finite temperature.

Chapter 4 is concerned with the ensemble averaged electron-impurity self energy. This is calculated using the ensemble averaged Green's function (Eq. 420.04)

$$\langle \Sigma(nk,mq) \rangle = \int\int\int \ldots \Sigma(nk,mq) \prod_{i}^{N} \frac{d^3R_i}{\Omega} \qquad (900.13)$$

where n and m indicate the band and k and q are wavevectors. This has been found to provide a convenient means of averaging the effect of N randomly sited impurities in the semiconductor, volume Ω. The ensemble averaged electron-impurity self energy has been found to be described to second order by the expression (Eq. 441.06)

$$\hbar\Sigma(n;k,\omega) = \frac{N_d}{\hbar(2\pi)^3} \sum_m \int G^0(n;l,\omega) \; |W(l-k,\omega)|^2 \; \Lambda_{nm}(k,l) d^3l$$

$$(900.14)$$

where G^0 is the unperturbed Green's function. $W(q,\omega)$ represents the screened electron-impurity interaction (in this thesis, the plasmon pole approximation section 2.3.2) and Λ_{nm} represents the coupling between bands n and m. The intrinsic semiconductor has no electron-impurity interaction so that the change in electron-impurity self energy due to the presence of the positively charged ionised impurities is given by the real part of this self energy (Eq. 450.01a)

$$\Delta E_n^{ei}(k) = \hbar Re(\Sigma^{ei}(n;k,\omega_{nk}^0)) \qquad (900.15)$$

This represents the change in the energy of the band n due to the electron-impurity interaction. The change in the band gap due to these interactions is given by the difference between the change in energy of the bottom of one of the six conduction band valleys ($\Delta E_c^{ei}(k_i)$) and the change in energy of the top of the valence band ($\Delta E_v^{ei}(0)$). Eq. 450.02)

$$\Delta E_{eg}^{ei} = \Delta E_c^{ei}(k_i) - \Delta E_v^{ei}(0) \qquad (900.16)$$

this is given by (Eq. 450.05)

$$\Delta E_{eg}^{ei} = \left(1 + \frac{m_H + m_L}{2m_{de}}\right)\frac{N_d}{\hbar(2\pi)^3} \int \frac{|W(q,\omega_{co}^0)|^2}{(\omega_{co}^0 - \omega_{cq}^0)}4\pi q^2 \, dq$$

From the results drawn in Fig 4.1 it can be seen that the electron-impurity interactions result in a band gap narrowing which is numerically smaller than the corresponding reduction due to electron-electron interactions (Fig 3.6). These results are compared to the results obtained by Berggren and Sernelius (1981) who use the Lindhard dielectric function and are also plotted in Fig 4.1. It can be seen that the present results based on the plasmon pole approximation agree within a few meV with these results based on the full Lindhard function. The Lindhard formula may also be approximated by the plasmon pole approximation for the electron-impurity interactions.

The plasmon pole self energies plotted in Fig 4.1 are valid until the perturbation approximation breaks down at concentrations where the impurity separation ($N_d^{-1/3}$) approaches silicon's atomic spacing. This occurs above donor concentrations of 10^{21} cm^{-3} (see Fig 2.4), where $N_d^{-1/3}$ approaches d ($5.4.10^{-8}$ cm^{-3}) the lattice constant. At low concentrations the limiting concentration is the Mott metal insulator transition that occurs at about 6.10^{18} cm^{-3} at zero temperature.

The effect of the random impurity potential and the associated random average potential is studied in chapter 5 by two methods. Halperin and Lax produced a formulation for the density of states deep in the band tail. This has until now been interpreted as producing a finite band tail that extends some 30 meV into the band gap. In this thesis the average electron-impurity interaction is shown to lower the unperturbed band edge so as to diminish the scale of this tail. This is qualified by the second

set of calculations based on Lloyd and Best's variational calculation of the density of states within the band tail that gives a good approximation to the density of states close to the band edge. whilst deeper in the tail Halperin and Lax's calculation is expected to give a better estimate to the density of states. Although the precise means of linking these two calculations remains a problem it is clear. especially from the Lloyd and Best calculations (see Fig 5.3) that the band tail is much smaller than has previously been supposed. Indeed both the modified Halperin and Lax tail in shown in Fig 5.2 (and Fig 5.6) and the Lloyd Best tail shown in Fig 5.6 both intercepts with the host density of states at $(2 \pm 1).10^{18} \text{ eV}^{-1} \text{ cm}^{-3}$. This is in agreement with the recent work of Sernelius 1983 on the high-stress birefringence and piezoresistance in heavily doped germanium.

In chapter 6 the electron-impurity interaction in an ordered array of impurity centres is calculated. In common with other workers (Berggren and Sernelius (1981, 1983) Mahan (1980)) the electron-impurity interaction in this model is found to be small because the inter-valley scattering included by Selloni and Pantelides (1983) has not been included. However this model is not physicaly acceptable since in the real semiconductor the impurities are more likely to be sited randomly than in ordered arrays.

The most promising calculations of chapter 3 and chapter 4 for the electron-electron and electron-impurity interactions are extended to finite temperature in chapter 7. This is made possible by the simple structure of the plasmon pole dielectric function used in these chapters. The coulomb hole and screened dynamic exchange contributions to the change in the electron-electron self energy (named by Hedin 1965 in connection

with electrons gases in metals see section 3.1)

$$\Delta E_c^{ee}(k) = \Delta E_c^{sx}(k) + \Delta E_c^{ch}(k)$$

(900.17)

$$\Delta E_v^{ee}(k) = \Delta E_v^{sx}(k) + \Delta E_v^{ch}(k)$$

at finite temperature become (see Eq. 731.01b and 732.02, 732.03)

$$\Delta E_c^{ch}(k) = \frac{e^2}{2\pi^2 \epsilon \epsilon_r} \int_0^\infty \left(N_q \frac{\omega_{cc}^0(k,q)}{\omega_1(q)} \frac{\omega_p^2}{\omega_1(q)^2 - \omega_{cc}^0(k,q)^2} \right.$$

$$\left. - \frac{\omega_p^2}{2\omega_1(q)} \frac{1}{(\omega_{cc}^0(k,q) + \omega_1(q))} \right) dq$$

(900.18)

$$\Delta E_v^{ch}(k) = \frac{e^2}{4\pi^2 \epsilon \epsilon_r} \sum_m \int_0^\infty \left(N_q \frac{\omega_{vm}^0(k,q)}{\omega_1(q)} \frac{\omega_p^2}{\omega_{vm}^0(k,q)^2 - \omega_1(q)^2} \right.$$

$$\left. + \frac{\omega_p^2}{2\omega_1(q)} \frac{1}{(\omega_{vm}^0(k,q) - \omega_1(q))} \right) dq$$

reducing the energies of both conduction and valence bands contributing a small increase (+10 meV at 10^{20} cm^{-3}) to the change in the band gap as in the zero temperature results of chapter 3 (see Fig 7.5 and Fig 7.9). The screened dynamic exchange contributions of each band (Eq. 731.01a and 732.03) however act in opposite directions, both to reduce the gap (Fig 7.4 and 7.8)

$$\Delta E_c^{sx}(k) = - \frac{e^2}{2\pi^2 \epsilon \epsilon_r} \int_0^\infty f_{c,q} \left(1 - \frac{\omega_p^2}{\omega_1(q)^2 - \omega_{cc}^0(k,q)^2} \right) dq$$

(900.19)

$$\Delta E_v^{sx}(k) = + \frac{e^2}{4\pi^2 \epsilon \epsilon_r} \sum_m \int_0^\infty \left(\frac{\omega_p^2}{\omega_1(q)^2 - \omega_{vm}^0(k,q)^2} \right) dq$$

With appropriate choice of the energy difference in these expressions the

change in the band energy at any value of k may be determined

$$\omega^0_{ck} - \omega^0_{c(k-q)} = -\omega^0_{cc}(k,q)$$

$$(900.20)$$

$$\omega^0_{vk} - \omega^0_{v(k-q)} = \omega^0_{vv}(k,q)$$

,

The major difference between the zero temperature calculations of chapter 3 and the values for the change in the conduction (valence) band bottom (top) at a temperature of 300K shown in chapter 7 is a small increase in the finite temperature band gap at low concentrations. This increase is caused mainly by the reduction (7 meV at 10^{17} cm^{-3}) in the conduction band shift (Fig 7.6). The valence band shift (Fig 7.7) remains within a 2 meV of its zero temperature value. The large change in the conduction band shift is due to the decreased screening (small $1/\kappa$) at low concentrations (Fig 7.2). This has a disproportionate effect on the conduction band where the magnitudes of the screened dynamic exchange and coulomb hole terms are additive. The sum of this electron-electron band gap reduction and the electron-impurity band gap reduction calculated in the section 7.4 results in a net increase in the band gap reduction due to the large increase in the latter contribution.

In Fig 7.12 the sum of the electron-electron and electron-impurity self energies is presented for both zero and 300 K. As detailed in the introduction to chapter 7 these results are only valid above the Mott critical concentration which is higher than zero temperature value due to the increased low concentration electron screening length ($1/\kappa$ see Fig 7.2). Below this concentration, although the electron-electron self energies shown in Fig 7.6 and Fig 7.7 are still valid when there are N_d electrons in the conduction band, the electron-impurity self energy is no longer valid (section 7.4.2 and 4.5). The Mott transition then defines the lower concentration limit to the results. At low concentrations below 10^{19}

cm^{-3} the experimental band gap narrowing results might well be best described by the statistical approaches of Heaseli (1979) and Popovic (1979) where a degenerate semi-populated impurity band separate from the host band is considered. However above the Mott critical density the true many body effects calculated in the previous sections should be used, assuming a merged conduction and impurity band.

Finally in chapter 8 the experimental measurements of the band gap narrowing and minority carrier lifetime in a heavily n-type doped silicon buried layer are detailed. These measurements are made in and Integrated Injection Logic transistor and many other parameters are measured. Measurement of the transport factor through the buried layer with the devices chosen was difficult because of the large error in calculated values of the minority current entering the buried layer $(J_{pv}$ Table 8.1, 8.2) caused by poor choice of cell shapes. However these measurements resulted in a minority carrier lifetime in the buried layer $(N_d = 2.4.10^{19} cm^{-3})$ of (30 ± 10) ns in agreement with published values (Hart 1981 pp 97). The band gap narrowing measured in this buried layer is (100 ± 15) meV. This measurement is mainly affected by the non-uniformity of the buried layer through which the band gap narrowing varies from 0 to perhaps as much as 140 meV at the peak donor concentration of $7.10^{19} cm^{-3}$.

This error could be overcome in future measurements by using a more detailed Gummel calculation which included band gap narrowing considerations (Eq. 821.09). The error in the measurement of J_{pv} could also easily be improved by a different choice of geometries for the cells (section 8.2.2) and would then provide further check on the band gap narrowing (Eq. 821.14).

To put these experimental results into perspective Fig 9.1

shows the band gap narrowing calculated in chapter 7 at zero and 300 K. Also plotted are results by Balkanskii et al (1969) for 35K and 300K derived from optical measurements. Although these experimental results are much lower than the present theoretical results the trend of increasing band gap narrowing for higher temperatures at low concentrations is clearly indicated. Also plotted is the empirical formula derived from collector current measurements by Slotboom et al (1976)

$$\Delta E_g(N_d) = 9 (R + (R)^2 + 0.5)^{1/2}) \quad (meV)$$

$$R = \log_e(\frac{N_d}{10^{17}})$$

(900.21)

This can be seen to give band gap narrowing results within 10 meV of the zero temperature theoretical values. Finally the present result of (100 ± 15) meV at a concentration of $2.4.10^{19}$ cm^{-3} is plotted. Recently the difference between optical and transport measurements of the band gap narrowing has been reduced by the interpretation of luminescence results by Dumke (1983).

9.1 FUTURE WORK

Improvements to the present theoretical calculations for heavily doped silicon could be made at two levels. In the first place the present calculations can easily be extended to cope with other materials. For this reason in Appendix A values quoted are for silicon and gallium arsenide. In the second place the accuracy of the present calculations could be improved by numerically evaluating the overlap integrals $(\Lambda_{nm}(k,q))$ or by increasing the number of terms in the self energy as outlined below.

A major improvement to the theoretical calculations presented here it is to consider Klauder's (1961) best approximation to the static
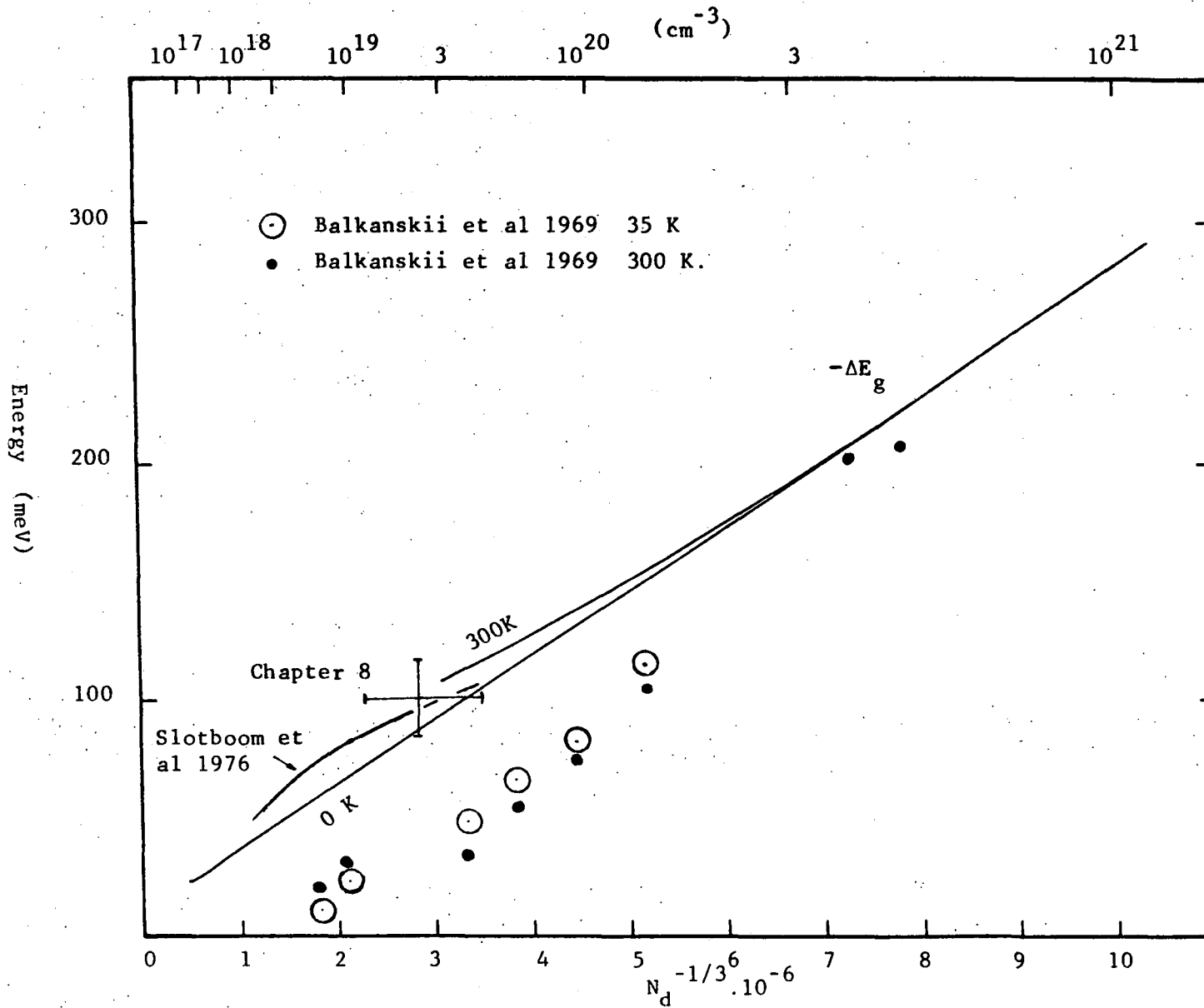
Fig 9.1 Theoretical band gap narrowing in n-type silicon at 0 and 300K. Experimental points from Chapter 8, Slotboom et al 1976, Balkanskii et al 1969.

(energy E or ω independent) electron-impurity Green's function used recently by Ghazali and Serre (1983, and Eq. 441.04). In functional form Eq. 441.04 reduces to (Ghazali and Serre Eq. 2)

$$K(q,p) = \frac{N_d}{(2\pi)^3} \int W(k-q)G(p-k)(W(-k) + K(k,p)) \, d^3k$$

$$\Sigma^{ei}(k) = K(0,k) \tag{910.01}$$

k, q and p are wavevectors. $K(q,p)$ is the vertex function that when solved by iteration gives a series like Eq. 441.04. On setting q=0 in $K(q,p)$ the electron-impurity self energy shown in Eq. 441.04 is derived. $G(k)$ is the total Green's function

$$G(k) = \frac{1}{(G^0(k))^{-1} + \Sigma(k)} \tag{910.02}$$

$G^0(k)$ is the unperturbed Green's function and the total self energy is given by the sum of electron-electron and electron-impurity self energies (Ghazali and Serre (1983) Eq. 2c)

$$\Sigma(k) = \Sigma^{ei}(k) + \Sigma^{ee}(k) \tag{910.03}$$

The spectral density $(A(k,E))$ and hence the density of electron states $(\rho(E))$ is given by the imaginary part of the total Green's function (Ghazali and Serre (1983) Eq. 3 and 4)

$$A(k,E) = \pm (1/\pi) \text{ Im } G(k,E)$$

$$\rho(E) = (1/\Omega) \text{ Tr } A(k,E) \tag{910.04}$$

Ω is the volume and Tr means sum over the k's and spin states.

On solving the equations Eq. 910.01 to 910.04 Ghazali and Serre calculate the density of states due to electron-impurity and electron-electron interactions in a simple semiconductor (non degenerate parabolic bands). However for the electron-impurity interaction they use the Thomas

Fermi potential. In future work the plasmon pole approximation to the electron dielectric function derived in chapter 2 could be used. For the constant contribution from the electron-electron interactions they include only the Hartree Fock exchange energy at the Fermi energy. An improvement would be to use the electron-electron shifts calculated in chapters 3 or 7 shown in Fig 7.6 and Fig 7.7. Still further improvement would come from including the degeneracy of the valence band although this would result in significant extra complexity.

Containing selected variables and constants for silicon doped n-type with N_d (cm^{-3}) donor impurities. Values [13.1] are for n-type GaAs as a comparison.

INTRINSIC BAND GAP (see section 8.2.4)

$$E_g(T) = 1.165 - \frac{4.879.10^{-4} \, T^2}{T + 180} + 1.58.10^{-4} \, T \quad (eV)$$

INTRINSIC EFFECTIVE MASSES AT 4 K.

Conduction band

$m_t = 0.19 \, m_o$

$m_l = 0.97 \, m_o$

Number of equivalent conduction band valleys $M_c = 6$

$$[= 1]$$

$$m_{de} = (m_l m_t^2)^{1/3} = 0.3272 \, m_o$$

$$[= 0.067 \, m_o]$$

$$m_{op} = 3(\frac{2}{m_t} + \frac{1}{m_l})^{-1} = 0.2596 \, m_o$$

$$[= 0.067 \, m_o]$$

Valence band

$m_L = 0.16 \, m_o \; [= 0.082 \, m_o]$

$m_H = 0.5 \, m_o \; [= 0.45 \, m_o]$

$m_v = (m_L^{3/2} + m_H^{3/2})^{2/3} = 0.559 \, m_o \; [= 0.47 \, m_o]$

RELATIVE DIELECTRIC CONSTANT $\varepsilon_r = 11.8 \; [= 13.1]$

LATTICE PARAMETER 5.43 Å. [5.65 Å]

ATOMIC DENSITY $5.0.10^{22}$ cm^{-3} [$4.42.10^{22}$ cm^{-3}]

EFFECTIVE BOHR RADIUS

$$a_{eff} = \frac{4\pi \epsilon \epsilon_r \hbar^2}{m_{de} e^2} = 1.9086 \cdot 10^{-7} \text{ cm } [= 1.035 \cdot 10^{-6} \text{ cm}]$$

EFFECTIVE RYDBERG

$$R_{eff} = \frac{e^2}{8\pi \epsilon \epsilon_r a_{eff}} = 31.965 \text{ meV } [= 5.311 \text{ meV}]$$

THOMAS FERMI SCREENING LENGTH

$$\kappa^2 = \frac{e^2}{\epsilon \epsilon_r} \int \rho(E) \left(- \frac{\delta f(E)}{\delta E}\right) dE$$

Parabolic band

$$\kappa^2 = M_c \, 2 \left(\frac{m_{de}}{2\pi \hbar^2}\right)^{3/2} \frac{e^2}{\epsilon \epsilon_r} (kT)^{1/2} F_{-1/2}(\eta)$$

Boltzmann statistics

$$\kappa^2 = \frac{e^2 N_d}{\epsilon \epsilon_r kT} = 1.775 \cdot 10^{-3} \frac{N_d}{T} \text{ cm}^{-2}$$

Degenerate statistics

$$\kappa = 2 \left(\frac{3}{\pi}\right)^{1/6} \frac{M_c^{1/3}}{\sqrt{a_{eff}}} N_d^{1/6} = 8.2549 \cdot 10^3 \, N_d^{1/6} \text{ cm}^{-1}$$

$$[= 1.951 \cdot 10^3 \, N_d^{1/6} \text{ cm}^{-1}]$$

THOMAS FERMI ENERGY

$$E_\kappa = \frac{\hbar^2 \kappa^2}{2m_{de}} = 7.9352 \cdot 10^{-8} \, N_d^{1/3} \text{ eV } [= 2.165 \cdot 10^{-8} \, N_d^{1/3} \text{ eV}]$$

FERMI WAVEVECTOR (T=0)

$$k_f = \left(\frac{3\pi^2}{M_c}\right)^{1/3} N_d^{1/3} = 1.7025 \, N_d^{1/3} \text{ cm}^{-1} [= 3.094 \, N_d^{1/3} \text{ cm}^{-1}]$$

FERMI ENERGY (T=0)

$$E_f = \hbar\omega_f = \frac{\hbar^2 k_f^2}{2m_{de}} = 3.375 \cdot 10^{-15} \, N_d^{2/3} \text{ ev}$$

$$[= 1.1145 \cdot 10^{-14} \, N_d^{2/3} \text{ eV}]$$

PLASMA ENERGY

$$\hbar\omega_p = \hbar \left(\frac{N_d e^2}{\epsilon \epsilon_r m_{op}}\right)^{1/2} = 2.1215 \cdot 10^{-11} \, N_d^{1/2} \text{ ev}$$

$$[= 3.963 \cdot 10^{-11} \, N_d^{1/2} \text{ eV}]$$

IMPURITY STRENGTH PARAMETER (CHAPTER 5)

$$\xi = \frac{e^4}{(4\pi\epsilon\epsilon_r)^2} \frac{2\pi}{\kappa} N_T = 1.1304 \cdot 10^{-19} \, N_d^{5/6} \text{ (ev}^2)$$

$$[= 3.881 \cdot 10^{-19} \, N_d^{5/6} \text{ eV}^2]$$

$$N_T = N_d + N_a$$

REFERENCES

Abram, R.A. Rees, G.J. Wilson, B.L.H. 1978. "Heavily Doped Semiconductors and Devices". Advances in Physics, Vol 27, pp 799-892.

Abramowitz, M. Stegun, I.A. 1970. "Handbook of Mathematical Functions: with Formulas, Graphs and Mathematical Tables". (Dover Publications Inc., New York). 9th Dover print (1970). SBN 486-61272-4. LCCCN 65-12253.

Anderson, P.W. 1963. "Concepts in Solids". (W.A. Benjamin Inc., New York). LCCCN 63-21516.

Arfken, G. 1970. "Mathematical Methods for Physicists". (Academic Press. New York and London). 3rd print.

Balkanskii, M. Aziza, A. Amzallag, E. 1969. "Infrared Absorption in Heavily Doped n-type Si". physica status solidi. Vol 31, pp 323-330.

Baltensperger, W. 1953. "Conduction in Impurity Bands". Philosophical Magazine, Vol 44, pp 1355-1363.

Barber, H.D. 1967. "Effective Mass and Intrinsic Concentration in Silicon". Solid-State Electronics, Vol 10, pp 1039-1051.

Berger, H.H. 1979. "Modelling IIL/MTL cells". Microelectronics, Vol 9, No. 4 pp 16-23.

Berger, H.H. Helwig, K. 1979. "An Investigation of the Intrinsic Delay (Speed Limit) in MTL/IIL". IEEE ED-26, pp 405-414.

Bergersen, B. Kus, F.W. Blomberg, C. 1973. "Single Particle Green's Function in the Electron Plasmon approximation". Canadian Journal of Physics, Vol 51, pp 102-110.

Berggren, K-F. Sernelius, B.E. 1981. "Band-gap Narrowing in Heavily Doped Many-Valley Semiconductors". Physical Review B, Vol 24, pp 1971-1986.

Berggren, K-F. Sernelius, B.E. 1983. "Intervalley Mixing Versus Disorder in Heavily Doped N-type Silicon". (to be published)

Bir, G.L. Pikus, G.E. 1974. "Symmetry and Strain-Induced Effects in Semiconductors". (Wiley, N. York).

Blakemore, J.S. 1962. "Semiconductor Statistics". (Pegamon Press. Oxford, London).

Brostow, W. Dussault, J.-P. Fox, B.L. 1978. "Construction of Voronoi Polyhedra". Journal of Computational Physics, Vol 29, pp 81-92.

Casey, H.C. Panish, M.B. 1978. "Heterostructure Lasers". (Academic Press, N. York). ISBN 0-12-163101-X.

Caughey, D.M.   Thomas, R.E.   1967.   "Carrier Mobilities in Silicon Empirically Related to Doping and Field".   Proceedings IEEE, Vol 55, pp 2192-2193.

Cohen, M.M.   1972.   "Introduction to the Quantum Theory of Semiconductors". (Gordon and Breach, New York).

Combescot, M.   Nozieres, P.   1972.   "The Dielect in Constant and Plasma Frequency of P-type Ge like S/c".   Solid State Communications, Vol 10, pp 301-305.

Dingle, R.B.   1955.   "Scattering of Electrons and Holes by Charged Donors and Acceptors in Semiconductors".   Philosophical Magazine, Vol 46, pp 831-840.

Dresselhaus, G.E.   Kip, A.F.   Kittel, C.   1955.   "Cyclotron Resonance of Electrons and Holes in Silicon and Germanium Crystals".   Phys. Rev. Vol 98, pp 368-384.

Du Bois, D.F.   1959.   "Electron Interactions: Part 1.   Field Theory of a Degenerate Electron Gas".   Annals of Physics, Vol 7, pp 174-237.

Dumke, W.P.   1983.   "Band-Gap Narrowing from Luminescence in p-type Si".   J. Appl Physics, Vol 54, pp 3200-3203.

Dyson.   1949a.   Phys. Rev. Vol 75, p 486.

Dyson.   1949b.   Phys. Rev. Vol 75, p 1736.

Edwards, S.F.   1958.   "A New Method for the Evaluation of Electric Conductivity in Metals".   Philosophical Magazine, Vol 3, pp 1020-1031.

Edwards, S.F.   1961.   "The Electronic Structure of Disordered Systems".   Philosophical Magazine, Vol 6, pp 617-638.

Edwards, S.F.   1962.   "The Electronic Structure of Liquid Metals".   Proceedings of the Royal Society A, Vol 267, pp 518-540.

Engstrom, L.   1983.   "Band-gap Narrowing in n-Si and n-Ge: Effects of Non-linear Impurity Scattering".   J. Phys. C, Vol 16, pp 1437-1449.

Fan, K.   1949.   "On a Theorem of Weyl Concerning the Eigenvalues of Linear Transformations I".   Proc. Natl. Acad. Sci. U.S., Vol 35, pp 652-655.

Ferrell, R.A.   1957.   "Characteristic Energy Loss of Electrons Passing Through Metal Foil: II   Dispersion Relation and Short Wavelength Cutoff for Plasma Oscillations".   Phys. Rev. Vol 107, pp 450-462.

Fetter, A.L.   Walecka, J.D.   1971.   "Quantum Theory of Many-Particle Systems".   (McGraw Hill Inc., New York).   LCCCN 70-122271.

Fistul, V.I.   1969.   "Heavily Doped Semiconductors".   (Plenum Press, New York).   LCCCN 68-28095.

Ghazali, A.   Serre, J.   1982.   "Multiple-Scattering Approach to the Formation of the Impurity Band in Semiconductors".   Physical Review Letters, Vol 48, pp 886-889.

Ghazali, A. Serre, J. 1983. "Electronic States of Doped Semiconductors: A Multiple-Scattering Approach". Proc. 16th International Conference on the Physics of Semiconductors. (North-Holland, Amsterdam) Ed. M. Averous. Part 1. pp 84-86. Re-print from Physica 117B pp 84-86.

Gradshteyn, I.S. Ryzhik, I.M. 1963. "Table of Integrals Series and Products". (Academic Press, N. York & London).

Gummel, H.K. 1961. "Measurement of the Number of Impurities in the Base Layer of a Transistor". Proceedings I.R.E., Vol 49, p 834.

Gummel, H.K. 1970. "A Charge Control Relation for Bipolar Transistors". Bell. System Technical Journal, Vol 49, pp 115-120.

Halperin, B.I. 1973. "Electronic States in Disordered Systems". Physical Fernica, Vol 8, pp 215-251.

Halperin, B.I. Lax, M. 1966. "Impurity-Band Tails in the High-Density Limit. I. Minimum Counting Methods". Physical Review, Vol 148, pp 722-740.

Halperin, B.I. Lax, M. 1967. "Impurity-Band Tails in the High-Density Limit. II High Order Corrections". Physical Review, Vol 153, No. 3, pp 802-814.

Hart, K. 1981. "Handbook on Semiconductors: Volume 4, Device Physics". (N. Holland, Amsterdam) Volume Ed. C. Hilsum, Series Ed. T.S. Moss. ISBN 0-444-85347-2. pp 87-250

Heasell, E.L. 1979. "The Emitter Efficiency of Silicon Bipolar Transistors - An Unperturbed Band Model". IEEE Trans. ED, Vol ED-26, No 6, pp 919-923.

Hedin, L. 1965. "New Method of Calculating the One-Particle Green's Function with Application to the Electron Gas Problem". Physical Review, Vol 139, pp A796-A823.

Hedin, L. Lundquist, S. 1969. "Effects of Electron-Electron and Electron-Phonon Interactions on the One-Electron States of Solids". Solid State Physics, Vol 23, pp 1-181.

Herman, F. Kortum, R.L. Kuglin, C.D. 1967. "Energy Band Structure of Diamond Cubic Silicon Carbide, Silicon and Germanium". Int. Jour. Quantum Chemistry, Vol 1S, pp 533-566.

Hwang, C.J. 1970. "Properties of Spontaneous and Stimulatd Emission in Ga As Junction Lasers' I Density of States in the Active Regions". Physical Review B, Vol 2, No. 10, pp 4117-4125.

Hwang, C.J. 1970. "Calculation of Fermi Energy and Band-tail Parameters in Heavily doped and Degenerate n-type GaAs". J. App. Phys. Vol 41, No. 6, pp 2668-2674.

Inkson, J.C. 1976. "The Effect of Electron Interaction on the Band Gap of Extrinsic Semiconductors". Journal of Physics C, Vol 9, pp 1177-1183.

Jaeger. R.C.   Gaensslen. F.H... 1980.   "Simulation of Impurity Freezeout Through Numerical Solution of Poisson's Equation with Application to MOS Device Behaviour". IEEE ED 27, pp 914-920.

Kane, E.O. 1956. "Energy Band Structure in P-type Germanium and Silicon". Journal of Physical and Chemical Solids, Vol 1, pp 82-99.

Kane, E.O. 1963. "Thomas-Fermi Approach to Impure S/C Band Structure". Physical Review, Vol 131, pp 79-88.

Kane, E.O. 1982. "Handbook on Semiconductors: Volume 1, Band Theory and Transport Properties". (N. Holland, Amsterdam) Volume Ed. W. Paul. Series Ed. T.S. Moss. ISBN 0-444-85346-4. pp 193-217

Kittel, C. 1976. "Introduction to Solid State Physics". (John Wiley & Sons, Inc., New York). ISBN 0-471-49024-5.

Klauder, J.R. 1961. "The Modification of Electron Energy Levels by Impurity Atoms". Annals of Physics, Vol 14, pp 43-76.

Kohn, W. Luttinger, J.M. 1957. "Quantum Theory of Electrical Transport Phenomena". Physical Review, Vol 108, pp 590-611.

Landau, L.D. Lifshitz, E.M. 1977. "Quantum Mechanics: Non-Relativistic Theory". (Pergamon Press,New York). 3rd edition. ISBN 0-08-020940-8

Langer, J.S. Vosko, S.H. 1959. "The Shielding of a fixed charge in an High-Density Electron Gas". J. Phys. Chem. Solids. Vol 12, pp 196-205.

Lax, B. 1958. "Experimental Investigations of the Electronic Band Structure of Solids". Reviews in Modern Physics, Vol 30, pp 122-154.

Lifshitz, E.M. Pitaevskii, L.P. 1980. "Statistical Physics". (Pergamon Press Ltd., New York) 3rd edition. Part 1 & 2. 0-08-023039-3.

Lloyd, P. Best, P.R. 1975. "A Variational Approach to Disordered Systems". J. Phys. C, Vol 8, pp 3752-3766.

Lundquist, B.I. 1967. "Single-partical Spectrum of the Degenerate Electron Gas". Phys. Kondens. Materie, Vol 6, pp 193-205.

Luttinger, J.M. Kohn, W. 1955. "Motion of Electrons and Holes in Perturbed Periodic Fields". Phys. Rev., Vol 97, pp 869-883.

Macfarlane, G.G. McLean, T.P. Quarrington, J.E. Roberts, V. 1958. Phys. Rev., Vol 111, pp 1245-1254.

Mahan, G.D. 1980. "Energy Gap in Si and Ge: Impurity Dependence". J. Appl. Physics, Vol 51, pp 2634-2646.

Mahan, G.D. 1981. "Many-Partical Physics". (Plenum Press, N. York) ISBN 0-306-40411-7.

Mattuck, R.D. 1976. "A Guide to Feynman Diagrams in the Many-Body Problem". (McGraw-Hill, N. York) 2nd Edition. ISBN 0-07-040954-4.

Mertens, R.P.   van Meerbergen, J.L.   Nijs, J.F.   van Overstraeten, R.J.
    1980.   "Measurement of the Minority-carrier Transport Parameters in
    Heavily Doped Silicon".   IEEE, Ed 27, pp 949-955.

Mertens, R.P.   van Overstraeten, R.J.   de Man, H.J.   1981.   "Heavy Doping
    Effects in Silicon".   Advances in Electronics and Electron Physics,
    Vol 55, pp 77-118.

Mott, N.F.   1974.   "Metal Insulator Transitions".   (Taylor and Francis Ltd,
    London)

Mott, N.F.   1978.   "The Metal Non-Metal Transition in Disordered Systems".
    Proc. 19th Scottish Universities Summer School in Physics.   Ed.
    Friedman, L.R. Tunstall, D.P. ISBN 0-905945-02-6

Mott, N.F.   Jones, H.   1965.   "The Theory of the Properties of Metals and
    Alloys".   (Oxford University Press).

Nozieres, P.   Pines, D.   1959.   "Electron Interaction in Solids.
    Characteristic Energy Loss Spectrum".   Phys. Rev., Vol 113, pp 1254-
    1267.

Panish, M.B.   Casey Jr. H.C.   1967.   "The Solid Solubility Limits of Zinc
    in GaAs at 1000°".   J. Phys. Chem. Solids., Vol 28, pp 1673-1684.

Pines, D.   1961.   "The Many-body Problem".   (W.A. Benjamin Inc., New York,
    1961. LCCCN 61-18182).

Plunkett, J.C.   Stone, J.L.   Hyslop, A.E.   1978.   "Some Aspect of Inverse
    Bipolar Transistor Improvement through Recombination Reduction".
    Solid-State and Electron Devices, Vol 2, pp 138-148.

Popovic, R.S.   1979.   "On the Apparent Narrowing of the Bandgap in the Base
    Region of Bipolar Transistors".   Solid-State Electronics, Vol 22, pp
    348-349.

Rice, T.M.   1954.   "Selected Papers on Noise and Stochastic Processes".
    (Dover Publications Inc. N. York) Ed Wax, N. ISBN 0-486-60262-1.

Rice, T.M.   1977.   "The Electron-hole   Liquid   in   Semidonductors:
    Theoretical Aspects".   Solid State Physics, Vol 32, pp 1-86.

Samathiyakanit, V.   Sritrakool, W.   Glyde, H.R.   1982.   "Impurity-band
    Density of States in Heavily Doped Semiconductors: Numerical
    Results".   Phys. Rev. B., Vol 25, no 4, pp 2776-80.

Samathiyakanit, V.   1979.   "Electron Density of States in a Gaussian Random
    Potential: Path-Integral Approach".   Phys. Rev. B., Vol 19, pp 2266-
    2275.

Schiff, L.I.   1968.   "Quantum Mechanics".   (McGraw-Hill, 3nd Edition).

Selloni, A.   Pantelides, S.T.   1982.   "Electronic Structure and Spectra of
    Heavily Doped n-type Silicon".   Phys. Rev. Lett., Vol 49, pp 586-589.

Sernelius. B.E. Berggren. K-F. 1981. "Electron States in Heavily Doped Semiconductors". Phil. Mag. B., Vol 43, pp 115-148.

Sholl. C.A. 1967. "The Calculation of Electrostatic Energies of Metals by Plane-wise Summation". Proc. Phys. Soc., Vol 92, pp 434-445.

Slotboom. J.W. de Graaf. H.C. 1976. "Measurements of Bandgap Narrowing in Si Bipolar Transistors". Solid State Electronics, Vol 19, pp 857-862.

Sze. S.M. 1981. "Physics of Semiconductor Devices". (John Wiley and Sons. New York). 2nd Edition.

Vol'fson. A.A. Subashiev. V.K. 1967. Soviet Phys. Semiconductors Vol 1, p 327.

Wolf. H.F. 1969. "Silicon Semiconductor Data". (Pergamon Press Ltd., Oxford).

Wolff. P.A. 1962. "Theory of the Band Structure of Very Degenerate Semiconductors". Phys. Rev., Vol 126, no 2, pp 405-412.

Yang. N.T. Chou. H.K. Ragonese. L.J. 1978. "Radiation Effects on the Current Densities of Integrated Injection Logic (IIL) Devices". IEEE NS-25, pp 1652-4.

Young. J.F. van Driel. H.M. 1982. "Ambipolar Diffusion of High-density Electrons and Holes in Ge. Si and GaAs. Many-body Effects". Phys. Rev. B., Vol 26, no 4, pp 2147-2158.

Zimmermann. Rosler. M. 1976. "Theory of Electron-hole Plasma in CdS". Phys. Stat. Sol. (b), Vol 75, pp 633-645.